Building new tomorrows for humins as biorefinery by product through the design of porous materials and applications

Pierluigi Tosi

UNIVERSITÉ CÔTE D'AZUR

ÉCOLE DOCTORALE
SCIENCES FONDAMENTALES ET APPLIQUÉES

THÈSE DE DOCTORAT

Stratégies de valorisation des humines en tant que sous produits de bioraffineries grâce à l'éco conception de matériaux poreux et à leurs applications

Building new tomorrows for humins as biorefinery by-product through the design of porous materials and applications

Tosi Pierluigi

Institut de Chimie de Nice

Présentée en vue de l'obtention du grade de docteur en Chimie d'Université Côte d'Azur

Dirigée par : **Prof. Mija Alice**
Codirigée par : Dr. De Jong Ed

Soutenue le : 19 Décembre 2019

Devant le jury, composé de :

Prof. dr. ir. Erik HEERES, Univ. Groningen, Pays-Bas.
Assoc. Prof. Monika ÖSTERBERG, Univ. Aalto, Finlande.
Dr. François JEROME, Univ. Poitiers, France.
Dr. Rudy PARTON, GF Biochemicals, Italie.
Prof. Véronique MICHELET, Univ. Côte d'Azur, France.
Dr. Charlotte HUREL, Univ. Côte d'Azur, France.
Dr. Ed DE JONG, Avantium, Pays-Bas.
Prof. Alice MIJA, Univ. Côte d'Azur, France.

avantium

HORIZON 2020

cnrs

Stratégies de valorisation des humines en tant que sous produits de bioraffineries grâce à l'éco conception de matériaux poreux et à leurs applications

Building new tomorrows for humins as biorefinery by-product through the design of porous materials and applications

Juri :

Président du juri

Dr. François JEROME, Univ. Poitiers, France.

Rapporteurs

Prof. dr. ir. Erik HEERES, Univ. Groningen, Pays-Bas.
Assoc. Prof. Monika ÖSTERBERG, Univ. Aalto, Finlande.

Examinateurs

Dr. Rudy PARTON, GF Biochemicals, Italie.
Prof. Véronique MICHELET, Univ. Côte d'Azur, France.
Dr. Charlotte HUREL, Univ. Côte d'Azur, France.
Dr. Ed DE JONG, Avantium, Pays-Bas.
Prof. Alice MIJA, Univ. Côte d'Azur, France.

ABSTRACT

Developing research and markets around by-products has become indispensable not only from the environmental point of view but also for the circular economy of the industrial processes. In this context, humins constitute one of the most promising by-products. Humins are formed during the biorefinery conversion of lignocellulosic biomass derived sugars into furanic compounds. They consist in a dark-colored, highly viscous, mixture of oligomers derived from random condensations between the several intermediates (mainly HMF and derivatives) formed during the acid catalyzed process. Our group, along with many recent researches, have proven the many hidden possibilities of this furan-rich mixture, which might in turn be attractive for the interesting properties that humins can offer. In this thesis we report several studies performed in order to valorize this material, with a particular focus on humins foams, new polymeric carbon-based porous materials derived from industrial humins in a straightforward and economic attractive way.

Keywords: biorefinery, side-products, sustainable chemistry, humins, biobased thermosets, porous material, absorption

RESUME

Développer une recherche appliquée pour soutenir les marchés autour des sous-produits & déchets est devenu indispensable, non seulement du point de vue de l'environnement mais aussi pour une économie circulaire des processus industriels durables. Dans ce contexte, les humines constituent l'un des sous-produits les plus prometteurs. Les humines se forment lors de la conversion par le bioraffinage de sucres dérivés de la biomasse lignocellulosique en composés furaniques. Ils sont constitués d'un mélange d'oligomères de couleur foncée et très visqueux, dérivés de condensations aléatoires entre les différents intermédiaires (principalement le HMF et dérivés) formés au cours du processus catalysé par un acide. Notre groupe, ainsi que de nombreuses recherches récentes, a prouvé le potentiel de ce mélange riche en furanes par les propriétés intéressantes induites par les humines. Dans cette thèse, nous présentons plusieurs études réalisées afin de valoriser ce matériau, avec un accent particulier sur les mousses d'humines, nouveaux matériaux poreux polymères à base de carbone dérivés d'humines industrielles de manière simple et économique.

Mots-clés : bioraffinerie, sous-produits, chimie durable, humines, thermodurcissables biosourcés, matériaux poreux, absorption

A nonno Gigi

Index of abbreviations

Chemical compounds

ACs	activated carbon
F180-F900	humins foams (prepared at the reported temperature)
$F^2$500-$F^2$1000	humins foam (prepared at the reported temperature from F250)
FA	furfuryl alcohol
FDCA	2,5-furandicarboxylic acid
FF	furfural
HMF	5-(hydroxymethyl)furfural
HTC	hydrothermal carbon
IPA	isopropyl alcohol
LA	levulinic acid
MA	maleic anhydride
ML	methyl levulinate
PEF	polyethylene furanoate
PET	polyethylene terephthalate
RMF	5-(alkoxymethyl)furfural

Instruments and techniques

ATR	attenuated total reflection
BET	Brunauer–Emmett–Teller (BET) theory
C80	Calvet calorimeter
DFT	density functional theory
DSC	differential scanning calorimetry
DSSC	dye sensitized solar cells
FPA	fire propagation apparatus
FT-IR	Fourier transform infrared spectroscopy
GC	gas chromatography
MS	mass spectroscopy
SEM	scanning electron microscope

TGA	thermogravimetric analysis
TGA-DTA	thermogravimetric analysis combined with differential thermal analysis
TGA-MS	thermogravimetric analysis coupled with mass spectroscopy
UPLC	ultra-performance liquid chromatography
XRD	X-ray diffraction

Other abbreviations

AA	acetic acid
ACD	acid catalysed dehydration
CDG	carbon dioxide generation
CHC	complete heat of combustion
E'	Young modulus (Pa)
FF	fill factor
G'	elastic/storage modulus (Pa)
G"	viscous/loss modulus (Pa)
HHV	high heating value
HRR	heat release rate
I	electrical current
Imp	maximum power current
Isc	short circuit current
MPP	maximum power point
NHV	neat heating value
$Nl \cdot h^{-1}$	normal litters per hour
OC	oxygen consumption
P	power
PZC	point of zero charge
THC	total hydrocarbon
r.t.	room temperature
tan δ	damping factor
*T*g	glass transition temperature
V	electric potential

Vmp	maximum power voltage
Voc	open circuit voltage
wt.	weight
ρ	density
$\rho_{apparent}$	apparent density
ρ_{real}	real density
$\rho_{relative}$	relative density
φ factor	real-time equivalence ratio
Φ	porosity
σ	compressive stress (Pa)

Table of contents

1 Preface

1.1 Sustainability, Biorefinery and Valorisation – the plan B

Burning gasses, oil-based fuels and the other energetic sources on which our modern society is based have brought considerable world-scale issues. The petroleum demand is expected to increase over 30 % during the next two decades,[1] driven largely by the growing economies of India and China, while fossil resources such as crude oil, natural gases and coals are limited and generate large amounts of green-house gases. Furthermore, the pressing population growth is stressing the production efforts.[2] In the 20th century the world population increased four times, while the power consumption 16 times.[3] This is accompanied by an increases of green-houses gases emissions, especially CO_2.[4] According with the climate models data this century the emission will surpass the 550 ppm if unchecked, leading to a global warming effect which magnitude will be comparable to the Ice Age, but with opposite sign.[5]

A complete yearly report about the climate change has been published in 2019 from IPCC, the Intergovernmental Panel on Climate Change.[6] According with IPCC, in agreement with US Global Change Research Program, it seems too late to stop the increasing of the global temperatures to +1.5 °C above pre-industrial levels. It has been estimated that without social, economic and political radical actions, we will likely reach the +2 °C within the next 11 years, which is considerate the point of no return. According to these results, not only we should reduce the CO_2 emissions, but we should even find a way to take some out from the atmosphere.

As reported from Box *et al.*[7] by observation of several environmental parameters in Artic area between 1971 and 2017 (47 years), the global warming is dramatically increasing, and soon it could be out of control. During the observed period the Artic air temperatures increased of 2.7 °C, with 3.1 °C during the cold season (October-May) and 1.8 °C during the warm season (June-September). Furthermore, humidity increased along precipitations and rainfall. The Artic snow cover (which controls the terrestrial and marine ecosystem) is reducing with increasing rate. The annual duration of snow on the ground is shortening of around 2-4 days every 10 years. Not better for Artic Ocean sea ice, with a low extension recorded in summer 2012. Drying lands, warmer air and vegetation changes are leading to the developing of

uncontrolled wild fires, worsening the problem. All this is generating an ecosystem change in both land (extending the tundra) and water environment. The earth ice-mass reduction will lead, at a certain point, to a snowball effect. The ice not only controls the world temperature as climatic buffer, but also reflects the sunlight. The reduction of ice lead by global warming will increase the temperatures, which will lead to a further ice reduction, and so on. This is a loop that when out of control will evolve in snowball chain events similar to that occurs in an explosive powder once that enough energy is furnished. In the worst case scenario it will be completely out of control, without any possible coming-back strategy.[8] This will be the heredity of the Anthropocene, the era of predomination of the human society, which consequences involves environmental, geological and climate changes.

Despite the global warming and the connected problems popped up as urgency during the last decade, signals of warning form the scientific society can be found even back in the '60s.[9] Starting in '50s, the massive production of plastic signed the human society with around 300 million tons/year all over the world. The social-economic impact was huge, and doubts about the sustainability of our living standard arose. The awareness of the issues linked to the living standard reached its zenith in 1972, when the System Dynamics Groups of Massachusetts of Technology published the celebre report *The Limits to Growth.*[10]

Today it has been suggested that CO_2 emission can be controlled by economic growth and equity, since it will put an end to the industrial explosion observed during these years from the most emitting countries, but also with investments and development of new technology, distribution, conversion and production.[11]

Aware of the issues that we are facing the scientific community have re-introduced in their calendar the three Aristotle's phases: *pathos*, *logos* and *ethos*. Terms as "sustainability" became increasingly important at industrial and social level. In order to convert our technologies in a more sustainable, "green" and environmental friendly system, we need to move our studies and expectations from a linear to a circular economy mentality.

The so called "linear" economy is a model mainly exploded during the second industrial revolution of 1870 due to the introduction of petroleum, electricity and chemicals. This consumerist based model consists in the use of resources in order to produce products, which can be used and finally threw away at the end of their life-cycle. There are no plan B for them, and no use or scope for the wastes so obtained, that in the best case scenario are burnt away resulting in CO_2 emission. Due to the low sustainability of this model and to the increasing

pollution affecting the planet, during the XX century the idea a circular economy model became more and more important. The circularity is inspired by the natural biologic cycle, in which wastes are converted in new products, in a theoretical unlimited loop. Kenneth E. Boulding in 1966[12] was the first to introduce the urgency of switch the economic system from a linear (open economy) to a circular model (closed economy):

"*For the sake of picturesqueness, I am tempted to call the open economy the "cowboy economy," the cowboy being symbolic of the illimitable plains and also associated with reckless, exploitative, romantic, and violent behavior, which is characteristic of open societies. The closed economy of the future might similarly be called the "spaceman" economy, in which the earth has become a single spaceship, without unlimited reservoirs of anything, either for extraction or for pollution, and in which, therefore, man must find his place in a cyclical ecological system which is capable of continuous reproduction of material form even though it cannot escape having inputs of energy".*[12]

Therefore, according with Bouldring, the linear (open) economy is like a reckless cowboy-like society that lives on a land, exploiting it and, at the end of resources, simply moves in another land far away. Our society is more similar to a close environment, within limited space and limited resources. Without a plan B the resources will finish, while we will be literally covered by wastes.

Thanks to new approaches, including recycling, reuse and extending the life cycle of the products, the human kind made the first big step toward this paradigm change. However, as previous explained, the time available is running out, and finding new solutions that allows us to live in a more sustainable way without changing our current living standard is the only practical way to cope the problem.

We are still strictly dependent on fossil resources, especially for fuels, chemicals and polymers production.[13] For these reasons renewable and low-cost biomasses have attracted considerable interest as valid alternative. The mental scheme in this case is: converting plant into product -> dispose the product (eventually emitting CO_2) -> grow a new plant which use the equivalent CO_2 to grown. This is call "carbon neutrality", since the total CO_2 balance is zero. Therefore, in a closed cycle with CO_2 as principal combustion product of carbon-based fossil fuels, it can be fixed and converted by photosynthetic organisms into saccharides (cellulose, glucose, amylose, …) and poly-aromatics such as lignin. Thus, CO_2 is converted into biomass (complex carbon molecules), and so in new feedstock by sequestering CO_2 from air. The commitment of the European Commission set as goal the 20 % of the liquid transportation

fuels derived from biomass by the year 2020.[14] This implies a reduction in the same year of greenhouse gas emissions by 20 % compared to 1990, as stated in the Kyoto protocol.[15]
The biomass production is estimated to be 1.7 - 2.0·10^{11} tons per year, but only 6·10^{9} tons are currently used for food and non-food applications.[16] The alimentary applications are estimate to be the 96.5 - 97 %, while the remains are used in other fields, such as feedstock for the chemical industry.
For ethical reasons, the biomass feedstock should not compete with the food chain. These can be easily processed (for instance bioethanol from corn starch or sugar cane), but implies serious economic issues due to the competition with the alimentary industry. When US started using corn in the production of bioethanol, the food prices drastically increased in a narrow range of time. The food price doubled between the 2010 and the 2011, and even more in 2012, after that US legislation of 2007 approved that large volume of corn would have been converted in ethanol, leading to four-fold increasing in the production.[17,18] Furthermore, bioethanol production comports at the current stage problematics that can be solved only facing costs of the process, capital investments, valorisation of the by-products and the still quite narrow margin in profits between the product and the resources.[2]
Therefore, currently are mostly being used biomass-based fuels and chemicals derived from the not edible parts of biomass, the so called of “second generation”, in contrast with the first generation bio-based fuels and chemicals made by the same plant used for nutritional purposes. In 1994 the only terrestrial biomass growth has been estimated to around 118 billion tons/year, where around 14 billion tonnes are derived from agricultural production.[19] However, the 80 % of this is substantially considerate waste since not edible, and can be used as low cost biomass in the production of chemicals, fuels and materials.[20] During the last years also the so called “third generation” biomasses have been studied in the biofuels production.[21] In this case highly lipidic algae are used, yielding high performance biofuels with an extremely sustainable process despite several economic and technical issues are still faced at industrial level.[22,23]
The utilization of second generation biomass, developing activities and enhancing the introduction on the market of bio-based products has led to the coining of a novel term: Biorefinery.[24–26] Within it, perhaps the most prominent application is the production of the so called “biofuel”, liquid fuels obtained by the conversion of lignocellulosic biomass. The great interest is around the possibility of drastically reduce the CO_2 emission, adapted to the

circular economy principles. Biomass has proven its convertibility into fuels by using several techniques, such as fermentation (process used for bioethanol), catalytic liquefaction or gasification.[27–34] The production of biofuels are, as matter of fact, considerate a dominant sector application, especially considering that the fossil fuels reserves are becoming progressively unavailable. However, applications involving the production of bioderived carbon based-material from renewable resources are rapidly growing, due to the commercial interests around the field, the potential high-tech applications, the reduced costs and high availability of the feedstock, and the energy/chemical provision involved.[35–43]

1.2 Lignocellulosic biomass

Lignocellulosic biomass represents a deep pool of renewable resources, being convertible in bioenergy (i.e. biofuels) and chemicals.[44–47] The production of second generation lignocellulosic biomasses starts from agricultural and forestry residues, materials dedicated energy crops, waste streams, aquatic plants, wood and wood residues, animal wastes and other wastes.[48,49] Lignocellulosic material refers to plant dry matter mainly present as structural material of the plant cells wall, and its composition is strongly dependent by its source. It is composed by carbohydrate polymers (cellulose and hemicellulose), and an aromatic polymer (lignin), and is the most abundantly available raw material on Earth for the production of biofuels (Figure 1.1). Carbohydrates, in particular, are an attractive option for biomass feedstock development as natural carbon source.

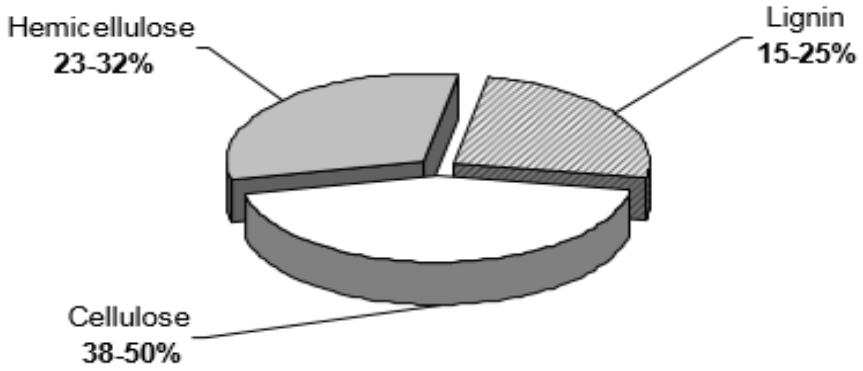

Figure 1.1 – Ratio between cellulose, hemicellulose and lignin in the composition of the lignocellulosic biomass.[48,49]

Cellulose is the most abundant biopolymer synthesised in nature, and its amount is estimated to $2 \cdot 10^9$ tons/year.[50] Cellulose is a linear polysaccharide with formula $(C_6H_{10}O_5)_n$, made by several hundred to many thousands of D-glucose monomers (Figure 1.2).

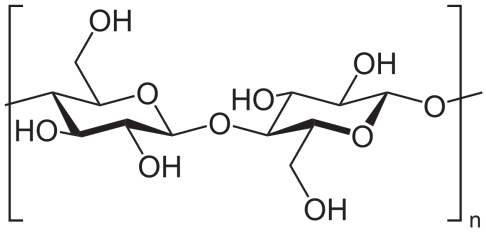

Figure 1.2 – Cellulose unit structure.

Its chain is formed by anhydroglucopyranose unit connected by β-1,4-glycosidic bonds. Thanks to glucose multiple hydroxyl groups, every chain is able to develop dense intra- or intermolecular H-bonds network. This produces microfibrils, which gives to cellulose a high crystallinity and tensile strength. Contrariwise, hemicellulose is a branched polymer with shorter chains (500–3000 sugar units), made by a mix of C6- and C5- sugars including xylan, glucuronoxylan, arabinoxylan, glucomannan and xyloglucan (Figure 1.3). Is a structural component of the plant wall cell, which cross-links together the microfibrils. Hemicellulose contains most of D-pentose sugars, and occasionally L-sugars. Also non regular sugars can be found in its structure, such as acidified forms (for instance gluconic acid and galacturonic acid). Thanks to the branched nature, if compared to cellulose, hemicellulose has a random amorphous structure with low strength, and because of the high accessible hydroxyl groups, it happens to be the most reactive part of the lignocellulosic biomass (nonetheless easier to hydrolyse).

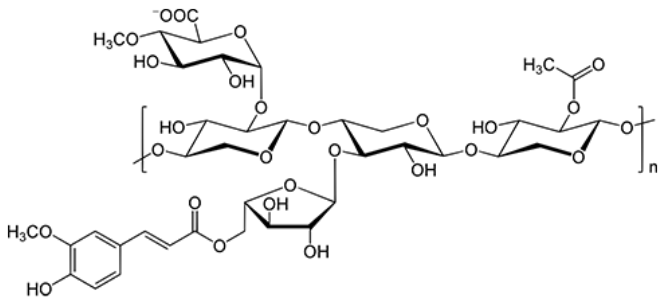

Figure 1.3 - Example of the polymeric structure in hemicellulose (xylan).[51]

Finally, lignin is an amorphous hydrophobic phenolic polymer which fills the space between cellulose and hemicellulose (Figure 1.4). The macromolecule of lignin has an average molecular mass in excess of 10000 u. Its structure is made by various type of sub-structures repeated in haphazard way, therefore its degree of polymerization is difficult to be measured due to the fragmentation occurring during the extraction. It is covalently linked to hemicellulose and thus cross-links different plant polysaccharides, conferring mechanical strength and rigidity to the cell wall and by extension to the plant as a whole.

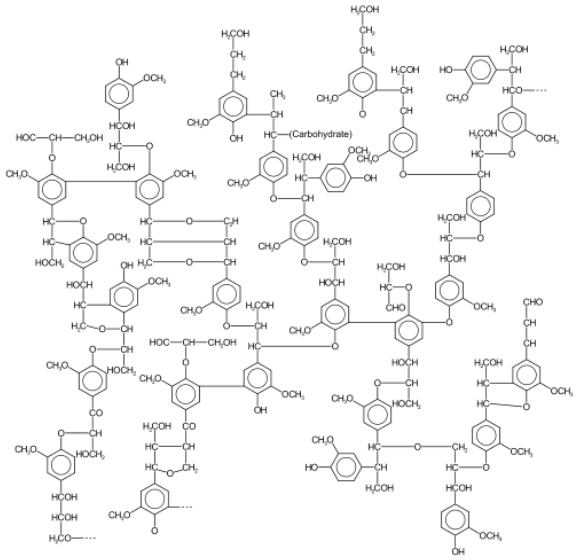

Figure 1.4 – Model of the lignin structure.[52]

Global commercial production of lignin is more than 1 million metric tons per year and is used in a wide range of low volume, niche applications.[53] However, the complete valorization of the lignin is still challenging and is being explored, but could be used as good source of aromatic chemicals and carbon fibres.[54]

Smit was the first that developed lignin technical manufacture and foreseen its possible applications.[55] The conversion of lignocellulosic biomasses could be enzymatic[56] catalytic,[57] or thermal,[27,58–60] each approach offering advantages and disadvantages. Therefore, its use represents a challenge, both technical and scientific, throughout several fields.[61,62]

The conversion of lignocellulosic biomasses can be valorised by direct conversion or multistep conversion. In the direct conversion the totality of the biomass is treated in a single process,

while in a multistep conversion is subjected to a treatment of fractioning and separation of the various components, which subsequently are individually worked up in biorefinery.

Within the direct conversion of lignocellulosic biomass, the first option is the conversion of lignocellulose with thermochemical techniques through a gasification to H_2 and CO. These can be used by Fisher-Tropsch processes to obtain alkanes and other products,[28] but require further processing of the syngas (e.g. purification, dehydrations, …); this makes this pathway more complex. Other alternative is the pyrolysis or liquefaction of the complete biomass. This is a cheap method to obtain complex bio-oil, which in the other hand happen to be not suitable for the combustion, unless is not further subjected to subsequent reactions upgrading (for instance hydrodeoxygenation).

Within a multistep strategy, instead, the preliminary treatment is the separation of the three components of lignocellulosic biomass. This allows the selective production on chemicals or fuels, depending from the matrix. Conversions on the carbohydrate fractions (cellulose and hemicellulose) are much further developed compared to the lignin fraction conversion. It starts from the hydrolysis of the polysaccharide chains yielding sugar monomers. These can be further treated to produce chemicals and bulk materials such as alkanes and polyols from hydrogenolysis,[63] ethanol by fermentation, [2] or hydroxylmethylfurfural (HMF), furfural (FF), formic acid and levulinic acid (LA) from acid-catalyzed conversion.[48] According to the US Department of Energy (DOE) the derivatives from acid-catalyzed conversion of cellulose and hemi-cellulose have high potential as platform molecules.[64]

An important example is provided by Avantium, a Dutch company which invested in the commercialization of bio-based chemicals. Avantium developed processes for the production of several furanics and levulinic esters. Furthermore, Avantium developed a large scale lignocellulosic biomass conversion process for the production of a new class of furanics building-blocs called YXY, which acted as perfect candidates for the developing of bioplastics and biofuels. With a first pilot plant able to convert sugars into HMF, Avantium was able to produce 40 tons/year of product. One of the focus is also the production of polyethylene furanoate (PEF) starting from the YXY technology, which is the homologue 100 % biobased of the poly(ethylene terephthalate) (PET), the common plastic derived by fossils.

1.3 Carbon based materials

Within the "sustainable challenge", carbon is out of doubt the most important element (Figure 1.5). Second to oxygen, it is the most abundant element that can be found in nature. Biomasses rely on CO_2 for the photosynthesis, and most of the modern hi-tech processes are based on biomass derived carbon materials, in particular porous materials (*e.g.* catalysts, separation system, electrodes, energy-storage device, purification, etc.). The necessity to achieve even more "green" versions of the classic carbon material have pushed the research toward new frontiers (such as activated carbon, graphene, carbon nanotubes or carbon aerogel).[37] This high importance of this research can be highlighted by awards won in the field, such as the Nobel Prize in chemistry for the discovery of fullerene in 1996, the Kavli Prize in Nanoscience of 2008 for nanotubes, or the Nobel Prize in Physics of 2010 for the study on graphene.[65]

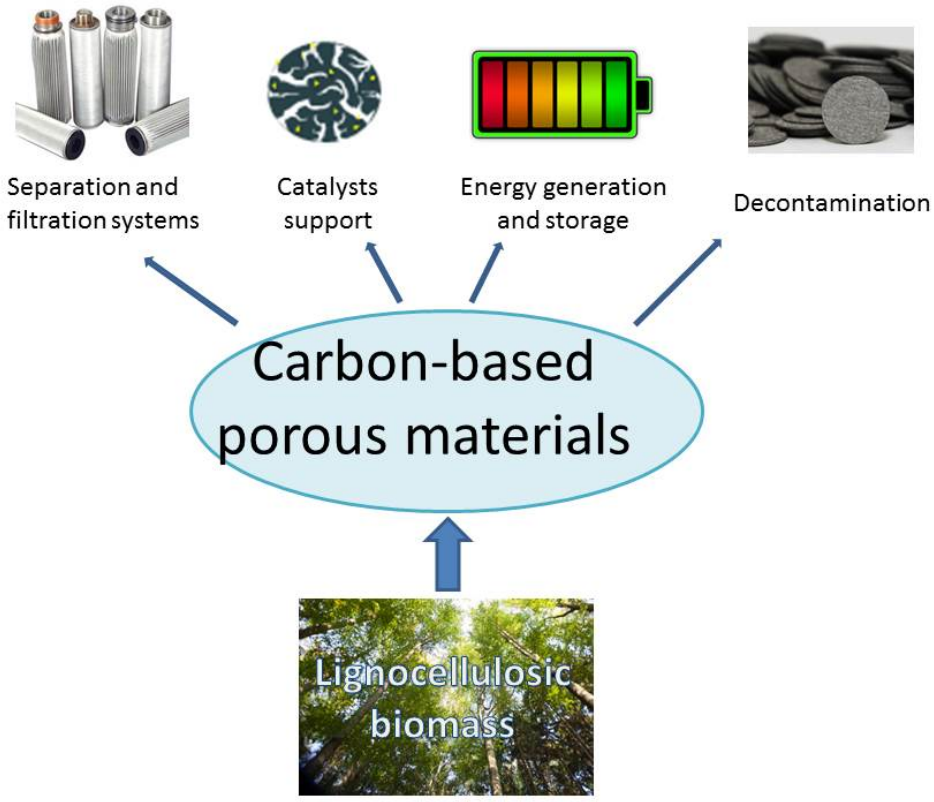

Figure 1.5 – Bioderived carbon based porous materials applications.[42,65–67]

Carbon porous materials are some of the most versatile product currently available. However, most of the common nanomaterials current used in industrial scale are generally derived by

small molecules transformations, in some applications (pharmaceutical) some synthesis is even carried out by precious metals. Most of the chemical process that deliver porosity on the material are based on harmful volatiles solvents and strong acid/base –based processes. Therefore, the research toward new greener technology must start from challenges like:

- identification of valid sustainable and globally accessible precursors;
- developing harmful chemical-free preparation protocols;
- finding alternatives to precious metals in catalysis applications or preparation;
- developing cost-effective preparation routes;
- limit the amount of wastes;
- limit the amount of CO_2 generate from the process;
- capacity of storing stable CO_2.

By converting lignocellulosic biomass, that for their nature are originating by fixating atmospheric CO_2, in other and more stable materials (activated carbon, biochar, nanomaterials, …), will lead to a stable sequestering of CO_2 and so to useful carbon-based materials with potential applications.[68–70] Since some of these applications imply the fixating of CO_2/greenhouse gases, it is even possible to achieve a combined effect in terms of CO_2 sequestering. Other carbon nanomaterials, such as catalysts that convert CO_2 and H_2 into CH_3OH, are used in mitigating the emissions. The result is an improving of the final sustainability balance of the CO_2 cycle *via* carbon materials production and applications that open the pathway to a plethora of possibilities at industrial level, with efficient costs and recycling of wastes.

Porous materials from “green” resources, such as biomass with abundant elements (C, N, O, P, …), can be produced by sustainable techniques, controlling the different elemental ratio, in particular the C %. The conversion of biomass into carbon-based materials generally implies the use of high temperatures or activation techniques in order to obtain mostly meso/micro-porous hydrophobic materials.

1.4 This thesis

In this thesis all previous introduced aspects will be discussed, with a particular focus on carbon-based materials derived from humins, the so called humins foams.

In the Chapter 2 humins will be introduced, with a complete review about these promising industrial by-products and the stat of art around them. In the past considerate a waste from the industrial-scale lignocellulosic biomass conversion, today humins, as promising furan-rich materials, have been studying and valorising in order to fully close the cycle, in agreement with the 12 principles of the green chemistry.[71–73]

In the Chapter 3 the new humins-based material called humins foam will be presented. In doing so, preliminary analysis on crude humins have been conducted. Afterwards, a complete mechanistic study of the process of foaming, along with the characterization of morphology, chemical structure, elemental content and mechanical properties of humins foams have been investigated.

In the Chapter 4 safety risk, and in particular the fire hazard related to both crude and foamed humins have been for the first time investigated.

In the Chapter 5 humins foams have been deeply characterized, reporting a screening of their physical and chemical properties along preliminary application tests, such as CO_2 adsorption at realistic operative temperatures (above 25°C) and the preparation of activated carbon monoliths.

Finally, in the Chapter 6 application studies on crude humins and humins thermoset derived materials have been presented. In particular, humins and humins derivatives have been used in the preparation of dye sensitised solar cells. Also, the preparation of composites with other sustainable materials (lignin and chitosan) have been investigated, while humins foams have been tested as sacrificial template in the preparation of alumina porous materials.

1.5 References

[1] G. Resch, A. Held, T. Faber, C. Panzer, R. Haas, *Energy Policy* **2008**, *36*, 4048–4056.

[2] Y. H. P. Zhang, *J. Ind. Microbiol. Biotechnol.* **2008**, *35*, 367–375.

[3] J. R. McNeill, *Something New Under the Sun: An Environmental History of the Twentieth Century*, Norton, New York, **2000**.

[4] M. I. Hoffert, K. Caldeira, G. Benford, D. R. Criswell, C. Green, H. Herzog, A. K. Jain, H. S. Kheshgi, K. S. Lackner, J. S. Lewis, et al., *Science (80-.).* **2002**, *298*, 981–987.

[5] M. I. Hoffert, C. Covey, *Nature* **1992**, *360*, 573.

[6] "A 2019 Climate Change Report - What's Changed Since 2014," can be found under http://mitigation2014.org/report/2019-climate-change-report/, **n.d.**

[7] J. E. Box, W. T. Colgan, T. R. Christensen, N. M. Schmidt, M. Lund, F.-J. W. Parmentier,

R. Brown, U. S. Bhatt, E. S. Euskirchen, V. E. Romanovsky, et al., *Environ. Res. Lett.* **2019**, *14*, 045010.

[8] D. H. Rothman, *Sci. Adv.* **2017**, *3*, 1–13.

[9] S. Greco, R. Bullo, *Un'onda Di Plastica*, Mediterranea, Rome, **2018**.

[10] D. H. Meadows, D. L. Meadows, J. Rgen, R. William, W. Behrens Ill, *The Limits to Growth: A Report for the Club of Rome's Project on the Predicament of Mankind*, New York, **1972**.

[11] B. Bolin, H. S. Kheshgi, *Proc. Natl. Acad. Sci.* **2001**, *98*, 4850–4854.

[12] K. E. Boulding, *E., 1966, The Economics Of The Coming Spaceship Earth*, New York, **1966**.

[13] C. E. Morrell, *Ind. Eng. Chem.* **1959**, *51*, 247–247.

[14] "Motor vehicles: use of biofuels," can be found under http://europa.eu/legislation_summaries/energy/renewable_energy/l21061_en.htm, **2003**.

[15] "EU greenhouse gas emissions and targets," can be found under http://ec.europa.eu/clima/policies/g-gas/index_en.htm, **2013**.

[16] H. Zoebelin, *Dictionary of Renewable Resources*, Wiley VCH, Weinheim, **2001**.

[17] C. Carter, G. Rausser, A. Smith, *Unpubl. Manuscr.* **2012**, *9*, 49–55.

[18] K. Bullis, "Ethanol Blamed for Record Food Prices," can be found under https://www.technologyreview.com/s/423385/ethanol-blamed-for-record-food-prices/, **2011**.

[19] O. Bobleter, *Prog. Polym. Sci.* **1994**, *19*, 797–841.

[20] S. Alfano, F. Berruti, N. Denis, A. Santagostino, "The future of second-generation biomass," **2016**.

[21] R. A. Lee, J.-M. Lavoie, *Anim. Front.* **2013**, *3*, 6–11.

[22] L. Chen, T. Liu, W. Zhang, X. Chen, J. Wang, *Bioresour. Technol.* **2012**, *111*, 208–214.

[23] A. K. Azad, M. G. Rasul, M. M. K. Khan, S. C. Sharma, **2010**, 879–888.

[24] B. Kamm, M. Kamm, *Chem. Biochem. Eng. Q.* **2004**, *18*, 1–7.

[25] B. Kamm, M. Kamm, *Appl. Microbiol. Biotechnol.* **2004**, *64*, 137–145.

[26] S. Fernando, S. Adhikari, C. Chandrapal, N. Murali, *Energy and Fuels* **2006**, *20*, 1727–1737.

[27] Z. A. B. Z. Alauddin, P. Lahijani, M. Mohammadi, A. R. Mohamed, *Renew. Sustain. Energy Rev.* **2010**, *14*, 2852–2862.

[28] D. M. Alonso, J. Q. Bond, J. A. Dumesic, *Green Chem.* **2010**, *12*, 1493–1513.

[29] T. M. C. Hoang, L. Lefferts, K. Seshan, *ChemSusChem* **2013**, *6*, 1651–1658.

[30] M. González Prieto, M. Fortunatti Montoya, P. E. Hegel, S. Pereda, *J. Supercrit. Fluids* **2018**, *134*, DOI 10.1016/j.supflu.2017.11.020.

[31] S. G. Wettstein, D. Martin Alonso, E. I. Gürbüz, J. A. Dumesic, *Curr. Opin. Chem. Eng.*

2012, *1*, 218–224.

[32] C. J. Barrett, Z. Y. Liu, J. A. Dumesic, *Nature* **2015**, *447*, 982.

[33] Y. Román-Leshkov, C. J. Barrett, Z. Y. Liu, J. A. Dumesic, *Nature* **2007**, *447*, 982–985.

[34] X. J. Ji, H. Huang, Z. K. Nie, L. Qu, Q. Xu, G. T. Tsao, *Fuels and Chemicals from Hemicellulose Sugars*, Springer, Berlin, Heidelberg, **2011**.

[35] B. Hu, K. Wang, L. Wu, S.-H. Yu, M. Antonietti, M.-M. Titirici, *Adv. Mater.* **2010**, *22*, 813–828.

[36] R. J. White, V. Budarin, R. Luque, J. H. Clark, D. J. MacQuarrie, *Chem. Soc. Rev.* **2009**, *38*, 3401–3418.

[37] M.-M. Titirici, R. J. White, N. Brun, V. L. Budarin, D. S. Su, F. del Monte, J. H. Clark, M. J. MacLachlan, *Chem. Soc. Rev.* **2015**, *44*, 250–290.

[38] A. Primo, A. Forneli, A. Corma, H. García, *ChemSusChem* **2012**, *5*, 2207–2214.

[39] M. Sevilla, M. M. Titirici, *Bol. Grup. Español Carbón* **2012**, *25*, 7–17.

[40] M. M. Titirici, N. Baccile, in *Annu. World Conf. Carbon, Clemson, USA*, **2010**, pp. 10–11.

[41] S. De, A. M. Balu, J. C. Van Der Waal, R. Luque, *ChemCatChem* **2015**, *7*, 1608–1629.

[42] M. M. Titirici, R. J. White, C. Falco, M. Sevilla, *Energy Environ. Sci.* **2012**, *5*, 6796–6822.

[43] M. M. Titirici, M. Antonietti, *Chem. Soc. Rev.* **2010**, *39*, 103–116.

[44] A. E. Farrell, R. J. Plevin, B. T. Turner, A. D. Jones, M. O'Hare, D. M. Kammen, *Science (80-.).* **2006**, *311*, 506–508.

[45] M. Galbe, G. Zacchi, *Appl. Microbiol. Biotechnol.* **2002**, *59*, 618–628.

[46] D. J. Hayes, *Catal. Today* **2009**, *145*, 138–151.

[47] M. Mascal, E. B. Nikitin, *Angew. Chemie - Int. Ed.* **2008**, *47*, 7924–7926.

[48] A. J. Ragauskas, C. K. Williams, B. H. Davison, G. Britovsek, J. Cairney, C. A. Eckert, W. J. Frederick, J. P. Hallett, D. J. Leak, C. L. Liotta, et al., *Science (80-.).* **2006**, *311*, 484–489.

[49] J. J. Bozell, G. R. Petersen, *Green Chem.* **2010**, *12*, 539–554.

[50] M. Sasaki, T. Adschiri, K. Arai, *J. Agric. Food Chem.* **2003**, *51*, 5376–5381.

[51] N. C. Carpita, *Plant Physiol.* **2011**, 171–184.

[52] E. de Jong, A. Higson, P. Walsh, M. Wellisch, *IEA Bioenergy, Task42 Biorefinery* **2012**, 33.

[53] "NNFCC renewable chemical factsheen - lignin," can be found under http://www.nnfcc.co.uk/publications/nnfcc-renewable-chemicals-factsheet-lignin, **n.d.**

[54] F. Cherubini, A. H. Strømman, *Biofuels, Bioprod. Biorefining* **2011**, 548–561.

[55] P. Smit, *Polytechn. Weekbl.* **1935**, *53*.

[56] G. W. Huber, S. Iborra, A. Corma, *Chem. Rev.* **2006**, *2*, 4044–4098.

[57] B. Girisuta, L. P. B. M. Janssen, H. J. Heeres, *Ind. Eng. Chem. Res.* **2007**, *46*, 1696–1708.

[58] K. Arai, B. Kabyemela, N. Takeda, R. Malaluan, M. Sasaki, T. Adschiri, S. Hirose, *J. Supercrit. Fluids* **2002**, *13*, 261–268.

[59] D. A. Bulushev, J. R. H. Ross, *Catal. Today* **2011**, *171*, 1–13.

[60] B. Dawoud, E. Amer, D. Gross, *Int. J. energy Res.* **2007**, *31*, 135–147.

[61] J. B. Binder, R. T. Raines, *J. Am. Chem. Soc.* **2009**, *131*, 1979–1985.

[62] J. N. Chheda, G. W. Huber, J. A. Dumesic, *Angew. Chemie - Int. Ed.* **2007**, *46*, 7164–7183.

[63] P. Gallezot, *Green Chem.* **2007**, *9*, 295–302.

[64] "Top Value Added Chemicals from Biomass Volume I — Results of Screening for Potential Candidates from Sugars and Synthesis Gas Top Value Added Chemicals From Biomass Volume I : Results of Screening for Potential Candidates," can be found under http://www1.eere.energy.gov/bioenergy/pdfs/35523.pdf, 2004, **n.d.**

[65] R. J. White, *Porous Carbon Materials from Sustainable Precursors*, The Royal Society Of Chemistry, Cambridge, **2015**.

[66] R. A. D. Arancon, C. S. K. Lin, K. M. Chan, T. H. Kwan, R. Luque, *Waste Manag. Valorization Altern. Technol.* **2017**, 23–65.

[67] L. Borchardt, Q. L. Zhu, M. E. Casco, R. Berger, X. Zhuang, S. Kaskel, X. Feng, Q. Xu, *Mater. Today* **2017**, *20*, 592–610.

[68] M. Nandi, K. Okada, A. Dutta, A. Bhaumik, J. Maruyama, D. Derks, H. Uyama, *Chem. Commun.* **2012**, *48*, 10283.

[69] J. Jagiello, J. Kenvin, A. Celzard, V. Fierro, *Carbon N. Y.* **2009**, *144*, 206–215.

[70] N. Brun, **2013**, DOI 10.1016/j.carbon.2013.05.001.

[71] A. Gałuszka, Z. Migaszewski, J. Namieśnik, *TrAC - Trends Anal. Chem.* **2013**, *50*, 78–84.

[72] S. L. Y. Tang, R. L. Smith, M. Poliakoff, *Green Chem.* **2005**, *7*, 761.

[73] P. Anastas, J. B. Zimmerman, *Environ. Sci. Technol.* **2003**, *37*, 94–101.

2 Humins – a review

2.1 Chapter content

In this review the state of art, history and researches about the humins, industrial side-products derived from the biorefinery conversion of lignocellulosic biomass, are reported. Starting from their first understanding, in over 80 years of researches focused in minimizing their production and efforts to identify their mechanism of formation, up to the recent years, where humins are finally considerate a resource to valorise and exploit.

Conditions of productions, composition, characterizations, mechanism of formation, kinetic studies, valorisation and novel applications are hence faced.

2.2 Introduction

The growing population and the living standards are increasingly requiring massive amount of energy that cannot be satisfied by the only use of the conventional energetic means.[1] Generation of heat, energy and chemicals from renewable resources over the classical fossil resources has become a priority at global scale, and is expecting to grow even more during the next 30 years.[2] The focus of the Research, Development and Deployment is on process productivities and optimization of yields, cost efficiency, feedstock availability and costs and, of course, on the reduction/valorisation of wastes/side streams and truly facilitating a circular economy.

If we take into consideration the so called "Earth Overshoot Day",[3] the index calculated by the Global Footprint Network that measures the date of the year in which the humanity have used more natural resources than the Earth can renew in one year (i.e. overfishing, overharvesting forests, over emission of CO_2 into the atmosphere, overharvesting), we can establish an impressive trend. Back in 1987 the Overshooting Day fell in December the 9th, while in 2019 we reached the unhappy result on July the 29th. Therefore, despite the incredible ecological improvement in using renewable resources over the fossil/non-renewable ones, a close look should be focused on the stabilization and reduction of the overall CO_2 emission and the reduction/valorization of wastes/side-products. This will lead to the progressive transfer from an unsustainable linear economic model[4] to a further sustainable circular model.[5,6] It has been calculated that by cutting half of the yearly CO_2 emission from fossil fuels it would be possible to move the Overshoot Day ahead 93 days in once, which is a huge improvement considering that the current target is 5 days for year.[7]

Currently, the most important renewable resource for chemicals and fuels are starch and sugars containing crops as well as to a lesser extend oil crops.[8,9] On the longer run also the abundantly available lignocellulosic biomass is a viable option.[9–11] Cellulose and hemicellulose, along with lignin, are the principal structural elements in such biomasses.[12] They are polysaccharides based biopolymers that can be used as feedstock in industrial chemical preparation (Scheme 2.1).

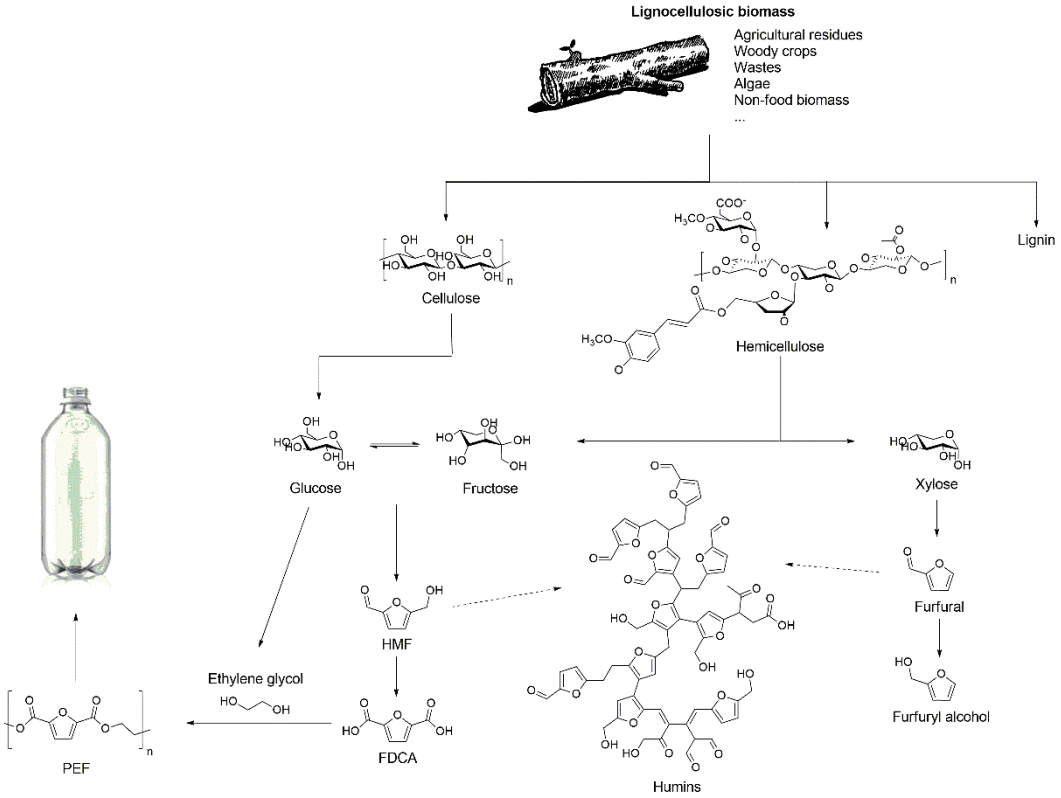

Scheme 2.1 Lignocellulosic biomass conversion.

For instance, the production of furanic building blocks involves the treatment of these sugar-containing feedstock in presence of 1-20 mol % of acids at temperatures that can vary between 175 – 225 °C for 1 - 60 min.[1] A variety of compounds are generated with mineral acid catalysts, but one of the most important reaction pathway proceeds through the 5-hydroxymethylfurfural (HMF)[14–18] and the levulinic acid (LA).[19,20] The importance of HMF can be represented in Figure 2.1, by the plethora of compounds derived by it, such as (m)ethoxymethylfurfural, 5-hydroxymethylfuroic acid, 2,5-furandicarboxylic acid, dimethylfuran, levulinic acid or adipic acid . These chemicals found promising applications in several fields such as in biofuels production, polymers, pharmaceuticals, catalysts and solvents.[21–26]

Despite the production of HMF through acid catalysed dehydration (ACD) of sugars has been extensively studied, the exact dehydration reaction mechanism is still inconclusive.[15,27,28]

Through Brønsted acid catalysis, the polysaccharide chains of the lignocellulosic biomass are subjected to depolymerization, yielding sugar monomers.[23] For instance cellulose is hydrolysed into C_6-monomers (mainly glucose and some glucose-based oligomers).[29] Hemicellulose (including xylan, glucuronoxylan, arabinoxylan), instead, produces a mix of C_5

and C_6 monomers (including xylose, mannose and galactose), with a relative composition that changes depending on its origins (e.g. hardwoods, softwoods or grasses).[11,30]

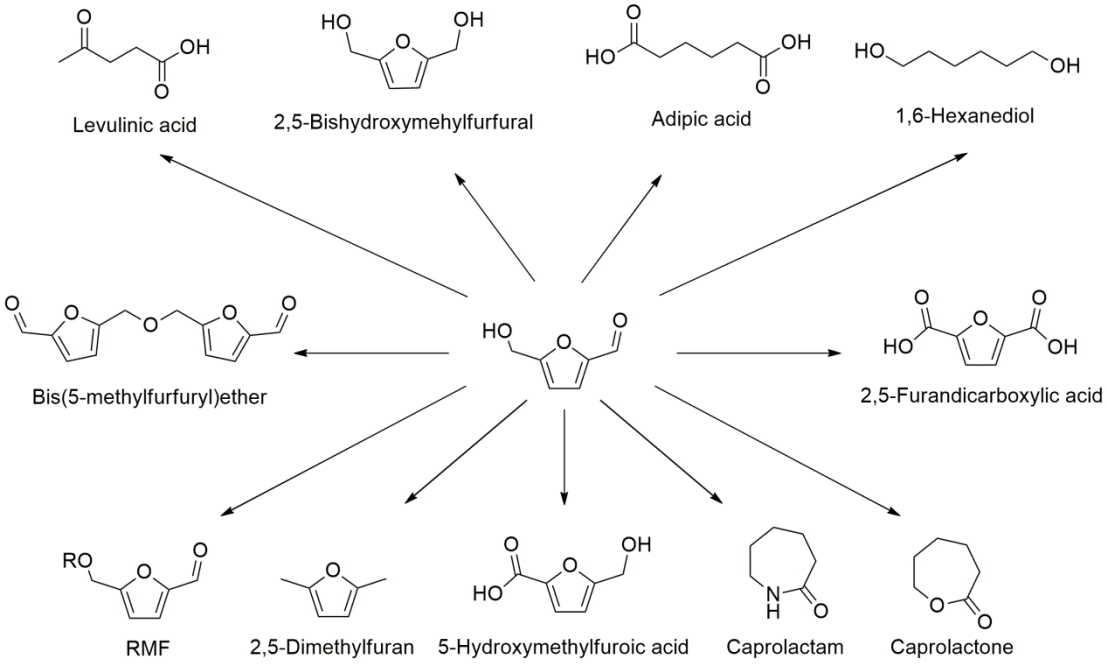

Figure 2.1 Chemical synthons derived by HMF.

While C5 sugars treated with Lewis acids eventually produce furfural (FF), the C6 ones lead to HMF at different selectivities.[15] Both FF and HMF are key intermediates for the production of further industrially relevant chemicals. However, the glucose is not directly converted into HMF, but is previously subjected to isomerization into the more active hexose, e.g. fructose.[31] This process is kinetically favoured compared to the direct conversion. Thus, under acidic conditions, it is the fructose that preferentially undergoes the dehydration into HMF and derivatives.[32,33]

Under ACD of sugars, 4-oxopentanoic acid (simply known as LA) and formic acid are also easily formed through water addition in C2 and C3 positions of the HMF furan ring. LA was for the first time prepared by the Dutch professor G. J. Mulder in 1840 by heating the sucrose in presence of a mineral acid.[34] It is classified as keto-acid, and accordingly have interesting reaction patterns.[35] LA is stable at processing conditions and has attracted a lot of interest as platform molecule for various derivatives.[26,36–38] The applications of LA and its derivatives have been reviewed extensively.[26,38–41]

The HMF was firstly reported in 1895 and has found applications as platform for chemicals.[14] Indeed, HMF can be oxidized to furandicarboxylic acid (FDCA), a replacement of *p*-terephthalic acid (PTA) derived by fossil resources and used in the production of polyethylene terephthalate (PET).[42,43] FDCA can replace PTA as building block for polyesters, and be copolymerised with ethylene glycol or derivatives to produce the polyethylene furanoate (PEF), the corresponding bioderived of PET.[44] According to the life-cycle assessment carried out by Eerhart, Faaij and Patel, replacing PTA with FDCA will conduct to important environmental benefits.[45] In a hypothesis of complete worldwide substitution of PTA with FDCA, the reduction of greenhouse gasses has been evaluated between 45 % and 55 % (20-35 Mt less of CO_2 equivalents), saving between 40 % and 50 % of non-renewable energy use a cradle to grave approach. Considering only the packaging bottles production chain, it will save between 440 and 520 PJ of non-renewable energy use. Even more importantly, compared to PET, the PEF shows higher T*g*, 10x better performance as oxygen barrier and better thermal and mechanical properties, which further justify its use.[46]

However, FDCA production is not the only application of HMF. It can be converted into 2,5-dimethylfuran, a potential biofuel with a superior energy content than the bioethanol.[47,48] HMF ether derivatives and hydrogenated products obtained from aldol condensation with acetone can also be used as fuel.[49,50]

Due to the large interest around these products, several feedstock have been examined for the production of HMF and LA, underlying economic interests and reporting the different stages of the industrial process.[51,52] Unfortunately, the ACD of carbohydrates solutions suffers by the formation of by-products, and among these a dark-coloured material with reduced solubility: the humins.[53] Humins production represents the main drawback of the ACD of sugars, since they could be related to sequestration of feedstock and catalysts, being responsible for the loss of yield in the primary products (e.g. HMF), engineering challenges and reactor working issues.[54]

The term humins was firstly used by Mulder in 1849 indicating the solid material found during the ACD of sucrose.[34] In 1880, Tollens and Grote mentioned the formation of humins as “dark-coloured caramel”, by-product of the preparation of LA.[55] The same term has been subsequently used to indicate also humins-like substances,[56] humic solids,[57–59] or in some case Biofine-char.[60] The amount of humins obtained can change depending on several factors (e.g. temperature, catalyst, feedstock, concentrations, resilience time), despite the fact that

in the first studies the yields were often not reported by the authors. According to Weingarten *et al.*, humins yield within ACD is generally around 8-20 mol% starting from HMF, 16-36 mol% starting from fructose and higher than 32 wt.% starting from glucose.[61,62] Humins formation decreases drastically the efficiency of the ACD process.[60]

An example of variability of humins yields depending from experimental conditions such as temperature used, and glucose and catalyst concentrations, is shown in Table 2.1.

Table 2.1 Comparison between acid catalyzed dehydration of glucose, reaction conditions and humins yields.

Glucose (g/L)	Temperature (°C)	Catalyst	Humins concentration (wt. %)
18	125	H_2SO_4 (0.1 M)	29[63]
50	135	$ZrPO_4$ (0.5 g/L)	29[64]
50	175	H_2SO_4 (0.5 %)	21[56]
200	170	H_2SO_4 (0.2 M)	21[65]
270	180	H_2SO_4 (0.05 M)	36[66]
360	220	H_2SO_4 (0.01 M)	35[66]

According to economic studies of biomass production, the key parameters for increasing the economic value of this conversion is the enhancement of the selectivity of the process, with elimination of the humins formation pathway.[67,68] Unfortunately, as for HMF and LA, also humins formation is an acid catalysed reaction and therefore its formation is unavoidable when complete conversion of substrate (e.g. glucose, fructose) is needed. Another more promising alternative, which starts to be explored, is the valorisation of humins as higher-value commercial product, increasing the economic viability of the ACD process.[69,70] In each case, to be able to overcome the humins challenge, a deeper understanding of their molecular structure, their formation mechanism, chemical behaviour and reactivity should be acquired.

2.3 Humins

Humins consists of oligomeric secondary products derived from the biorefinery process of conversion of sugars into HMF, FF and LA.[71–73] They are an heterogeneous and polydisperse mixture, which molecular structure is still under investigation and not univocally characterized. The degree of polymerization in humins structures is difficult to measure, since they could originated from several types of reactions, leading to subunits and structures

randomly connected and influenced by the operational parameters used during the ACD process.

The elemental composition of humins is typically found to be on the order of 55-65% carbon, 4-5% hydrogen, and 30-40% oxygen.[71,74–76] SEM revealed that humins mixture generally results in agglomerated spherical particles with a wide distribution of dimensions,[77] while NMR analysis of humins derived from cellulose hydrolysis in an ionic liquid solution showed similarities with monosaccharides[53,78]

In 1885 Conrad and Guthzeit firstly reported that the formation of humins is faster from fructose than from glucose, and even most rapid from arabinose.[79] As previous explained, within acid-catalysed conditions, the glucose is subjected to isomerization into fructose or at least the intermediate 1,2-enediol, kinetically favoured in the dehydration step to HMF.[31,53,80,81] However, glucose is converted into humins in a faster way compared to its isomerization in fructose, which explains the loss of product yield in advantage of humins formation. This isomer-dependent conversion rate was confirmed in 2011 by Kitamura, Nakahara and Mutubayasi by ^{13}C NMR observations.[82] For the same reason it has been observed that the addition of Lewis acids to glucose ACD process leads to higher HMF yields, since provides an higher isomerization rate of glucose.[14] However, it must be highlighted that humins can be formed also in other processes involving carbohydrates, such as the glucose conversion to ethylene and propylene glycol,[83,84] or the conversion of cellulose into ethanol.[85]

The ACD process requires optimizations, not only in order to reduce the formation of humins but also to maximize the desired product yield toward the selected reaction pathway. For instance, during the production of HMF its rehydration to LA must be prevented as much as possible, and therefore optimizations on concentrations, temperatures and residence time often expressed as “Combined Severity” must be taken into account. On the other hand, van Putten *et al.*[14] reported that the activation energy of humins formation from HMF is ~100 kJ mol^{-1}, while the HMF rehydration to LA is in the range 50-225 kJ mol^{-1}. These values highlight the strong influence of the temperature in the LA production. However, these results are in contrast with the kinetic studies in milder conditions in which the selectivity to the LA pathway relative to the humins pathway has a quite poor dependence from the temperature.[77]

H_2SO_4 and HCl are the most common mineral acids used in ACD of sugars into LA and HMF while, as previously explained, fructose is the best commonly available feedstock in order to

achieve HMF in high yields.[86] On the other hand, many authors report[51] that a concentration of mineral acids between 3.5 and 10 wt. % optimizes the yields of LA, while the temperature is generally set between 150 and 230 °C. Longer residence times must be avoided within HMF synthesis, since they enhance the rehydration to LA and the concomitant humins formation.[87–89] According to kinetic studies of ACD of sugars into HMF and LA, high acid concentration and lower reaction temperatures can generally reduce the production of humins.[13,62,74,77,88,90–92] Kuster et *al*.,[61,88,93] for instance, reported that at 95 °C the production of LA decreases in advantage of humins production when higher concentrations of fructose are used as starting material. Furthermore, humins formations was accelerated by the presence of oxidized compounds, and therefore in oxidizing environment, due to the increasing of the system acidity.[94] The reaction order calculated for humins formation is 1.3 when fructose is used as feedstock, while is 1.7 when HMF is used. Kuster reported also that water is the most convenient solvent for the ACD of fructose in HMF considering operational advantages, despite the lower selectivity. Anyway, whatever are the operating conditions, high selectivity was obtained using methyl isobutyl ketone as simultaneous extraction solvent in biphasic systems.[95] In a recent article this approach has been tested also in presence of carbonaceous materials, improving the liquid-liquid mass transfer of HMF in the methyl isobutyl ketone phase of around 20 % by using nanotubes (1.5 wt. % loading).[96]

Also other water-miscible solvents such ethylene glycol and alcohols showed positive effect in the conversion of fructose in HMF compared to results in pure water. The co-solvents, in this case, play on the kinetic of reaction, enhancing the HMF formation by reducing the reaction rate of LA conversion. However, the humins produced were dissolved in the ethylene glycol solution, which represents a drawback in terms of separation.[88] Also the choice of pure solvents must be considered. Sugars require very polar solvents to be solubilized, while the use of alcohols lead to HMF ethers (RMF) and LA ethers.[22] In order to improve reaction yields, biphasic reactions have been tested in order to reduce the humins formation facilitating the products solubilisation in the aqueous media.[22,97] Ion-exchange resins have been tested in water in place of the common acids, but the selectivity in HMF was not improved.[98] Also the use of microporous zeolitic materials as catalyst was tested, taking advance of their tuneable properties such as shape, adsorption selectivity, hydrophilic/hydrophobic behaviour, acid/base character.[99] Fructose dehydration using catalysts dealuminated H-form zeolites in a water/methyl isobutyl ketone (1/5 by volume) mixture was tested.[87] The best balance

between activity, selectivity and by-product amounts was found using mordenite in the protonic form (Si/Al ratio of 11) and a low mesoporous volume at 165 °C.[100] In these conditions the selectivity of HMF resulted of 91 %, and tends to decrease when Si/Al ratio increases. Higher acidity of catalysts enhances secondary reactions, increasing the formation of LA, FA and humins. The higher selectivity in literature for HMF has been reached in pure DMSO as solvent under moderate operating conditions.[86,101] DMSO partially prevents the formation of LA and humins by increasing the selectivity, but gives separations problems along other disadvantages. An enhancing of the solution acidity was observed, suggesting the formation of water and some possible toxic S-containing by-products (such H_2SO_4) derived from DMSO. However, recently Whitaker *et al.*[102] proved that DMSO is stable at the reaction conditions (120-150 °C), and that the major part of the acid species formed are confirmed to be LA, FA and humins. The author suggested that DMSO do not promote the fructose conversion into HMF working as acid catalyst but as solvation agent, while the bests reaction conditions involve a molar fraction of DMSO in water between 0.20 to 0.43.

In 2017 Gomes *et al.*[15] reached interesting results in the synthesis of HMF from water-soluble carbohydrates using a biphasic system ($NaCl_{aq}$/ THF) and a combination of Lewis acids ($ZnCl_2$ and $AlCl_3$) and Brønsted acid (HCl). With 1 h reaction time at 180 °C it was observed that HMF production increased using an extraction/reaction solvent ratio ≥ of 10. The best HMF yields achieved using glucose as feedstock were 62.7 % for $ZnCl_2$/HCl and 66.9 % for $AlCl_3$/HCl, while using sucrose as feedstock the best yields were 65.6 % for $ZnCl_2$/HCl and 54.4 % for $AlCl_3$/HCl. Good results were obtained also by using sugarcane molasses as feedstock. However, even with this set-up and despite the biphasic system, was impossible to avoid the formation of humins. Humins so formed were investigated by analytical pyrolysis, resulting to be mainly constituted by furanic species, and in particular by 2-methylfuran. In terms of humins molecular size, using $AlCl_3$/HCl were found *m/z* fragments two fold bigger than those obtained by $ZnCl_2$/HCl, showing that catalyst with stronger acid behaviour further contributes to oligomerization and condensation reaction.[15]

Better results were obtained in 2019 from Cao *et al.*[103] in HMF preparation from cellulose using hafnyl phosphates as catalysts in similar NaCl-H_2O/THF biphasic system. 69.8 % HMF yield is reported by using $HfO(PO_4)_{2.0}$ at 190 °C for 240 minutes, whit poor LA production due to the lower acidity of the catalyst. The humins formation was not avoided, however the deposition on the catalyst was extremely reduced, overcoming one of the bigger technical

issues of these by-products formation. The reduced humins deposition was suggested to be an effect of the minor adsorption of the HMF on the catalyst. Even better results were obtained by using fructose, glucose, cellobiose, sucrose and starch as feedstocks, with yields of 94.8, 90.5, 79.3, 86.6 and 75.3 % respectively. The authors suggested that hafnyl phosphates have a role in the deactivation of unselective Lewis acid sites. Furthermore, due to the biphasic system, the HMF can be easy recovered from the THF fraction of the top of the reaction pot. Despite these extremely promising results, eyes are pointed on the challenge of the process up-scaling. Another biphasic system tested involved $NaHSO_4/ZrO_2/H_2O$-THF, with a maximum HMF yield of 86.5%.[104] Here, while $NaHSO_4$ worked as acid catalyst toward HMF conversion, ZrO_2 is supposed to favour the glucose-fructose isomerization. Humins formation over the ZrO_2 catalyst was not avoided, but according to the author their production inhibit enough to allow the reuse of ZrO_2 for 6 cycles without any recover treatment.

The preparation of furfural from xylose in a greener biphasic system was reported in the same year by Millán *et al.*[105] In order to avoid the humins formation, the fast extraction of the reaction products was investigated by using an organic water-immiscible phase by isophorone, 2-methyltetrahydrofuran and cyclopentylmethylether, respectively. The maximum furfural yield reached was 78 mol % by using cyclopentylmethylether. Again, also in this study is shown that products yield decreases with the increasing of the reaction time because of humins formation. Despite the formation of humins was not avoided, this is a promising initial investigation supported by the use of greener solvents and avoiding the use of salts.

THF as co-solvent with EtOH was also studied in 2019 in the synthesis of 5-ethoxymethylfurfural (EMF) from fructose using green SO_3H-CD carbon catalyst in ultrasonic system.[106] It was observed that in the best conditions applied the catalyst was able to strongly inhibit the HMF (here as by-product), ethyl levulinate and humins formation. Furthermore, it was observed a dependence between selectivity and THF concentration. Using THF between 0 and 36 mmol it was possible to promote the selectivity for EMF, resulting in a strong suppression of the by-products, humins comprises.

Several further studies tried to optimize the process intervening on different aspects. First attempts of heterogeneous acid catalysis did not lead to better yields, and were suspected absorption of the products on the catalyst surface.[19] Better results were achieved by Zuo and Zhang with sulfonated chloromethyl polystyrene as catalyst, despite further optimizations

were required.[107] In 2019 Xu *et al.*[108] reported the synthesis of heterogeneous catalysts based on H-β zeolite $SnCl_2$-PTA/β, reaching in their bests case yields of 71 % of furfural and 30 % of HMF in biphasic systems. Still, humins were produced. Also in this case was observed that by increasing reaction times and temperatures decreases the reaction yields in favour of humins and soluble by-products formation.

Girisuta *et al.* made also kinetic models for the humins formation in the process of production of LA from several feedstocks,[13,74,109] showing that humins as by-products could not be avoided whatever the condition used. For the humins formation was calculated and activation energy of 164.7 kJ/mol,[13] which suggests that milder reaction conditions could limit the formation of this by-product. Another kinetic model from Huber *et al.* for the LA production showed that the process of glucose dehydration to HMF, HMF rehydration to LA and condensation into humins have a first order dependence with the acid concentration. As result, high temperatures and little reaction times (180 - 200 °C, less than 1 min) maximize the yield of HMF, while lower temperatures and longer reaction times maximize the LA production.[62] A kinetic model was proposed by Lund et al., which showed how acid concentration has effects on LA formation rate more than on humins formation rate.[77] Thus, high acid concentration increases the selectivity and yields of LA. In 2017 Zhang *et al*.[110] reported the impressive yield of almost 94 % HMF from glucose in Y-valerolactone using silicoaluminophosphate zeolite SAPO-34 as catalyst. Unfortunately, when high initial glucose concentrations were used, the yield decreases in favour of humins formation. On the other hand, the obtained humins resulted mainly soluble. However, up-scale studies must be conducted in order to understand the actual applicability of this process at industrial level.

Despite these researches showed limits of optimizations in terms of product yields, humins formation results still unavoidable. Therefore, in parallel to these studies aiming to reduce as much as possible their formation, humins have been subjected to deep investigations in order to reveal their nature, chemical structures, mechanism of formation and their physico-chemical properties. In 2019 Garcés et al.[111] studied the formation of HMF from glucose by a combination of homogeneous (HCl) and heterogeneous (β-zeolite) catalysts. Zeolites improved the HCl activity, and also facilitate the isomerization step of glucose into fructose. It was possible to obtain HMF with a selectivity of 41 % (140°C, 200 ppm HCl, 5 h) and a LA selectivity of 34 % (140°C, 400 ppm HCl, 24 h) in the best cases. According to the proposed kinetic model, compared to the previous cases when only mineral acids where used, the

heterogeneous/homogeneous catalysts work in combination conducted to a decreases of 30-40 % in the required activation energy of the main conversion step, and also in a reduction of humins' yield.

In 2019 Ramesh et al.[112] published an *in situ* Raman spectroscopic kinetic study about the mutarotation process for glucose inducted from metal chlorides. Among the tested metals, the rate for the glucose mutarotation follows the order $AlCl_3 < CrCl_3 < SnCl_4$. Interestingly, also the resulting humins structures appeared different, suggesting that $AlCl_3$ promotes the incorporation of furan rings and maybe HMF to DHH, while $SnCl_4$ cleaves the glucose/fructose molecules before yield HMF. On the other hand, it was found that $CrCl_3$ promotes the α-glucose anomer formation.

It must be reminded that achieving the LA as main product is also deeply investigated. In a recent work from Liu *et al*.[113] around 67.51% LA yield was achieved from cellobiose using as catalysts Brønsted-Lewis acidic ionic liquids ($[HO_3S\text{-}(CH_2)_3\text{-mim}]Cl\text{-}FeCl_3$) in hydrothermal conditions. In this reaction a synergic effect was obtained. The Lewis acid helps the isomerization from glucose to fructose, and the Brønsted-Lewis acids in synergy push the conversion toward HMF, which is the intermediate that precede the LA formation. However, also in this case large amounts of humins were produced as residual solid. Recently, Velaga *et al.*[114] reported the synthesis of LA from bamboo sawdust, cellulose, glucose and fructose reaching 61, 56, 52 and 43% of yield respectively by using Mordenite zeolites. Again, humins are formed as intermediate. The humins formation was reduced by using a biphasic system, but also the LA yields decreased.

However, must be added that humins can also be obtained in the preparation of higher value products from furanics. During the years, several reactions have been proposed in order to maximize the yields and to decrease the humins formation.[113,115–117] For instance, Piancatelli ring rearrangement is used for the preparation of cyclopentenone[118,119] from furanic compounds in aqueous phase (catalysed by acid media).[120] Cyclopentenone is a particular important compound not only because is more stable and easier to transport compared to furanics, but also because it's use in fuels preparation[118,121,122] being also an intermediate for the production of several polymers and pharmaceutical chemicals.[123,124] In 2019 Omotoso *et al.*[125] reported the synthesis of cyclopentenone and 2-cyclopentenone from furfural in vapour phase, using TiO_2 catalyst. Since it was avoided the condensed aqueous acid media which catalyses humins formation, the conversion was achieved with high selectivity.

Chemical characterization and molecular structure of humins by-products

The first study on humins structure was published by Mulder in 1840.[126] Humins were prepared by ACD of sucrose using HCl, and was found an elemental composition of 64-65 wt.% C, 5-6 wt.% H, 31-32 wt.% O. In 1937 Schweitzer proposed, starting from studies of chemical degradation, that sucrose derived humins were formed by dehydration reaction, while the pyran ring of sugar is not affected (Figure 2.2).[55,127]

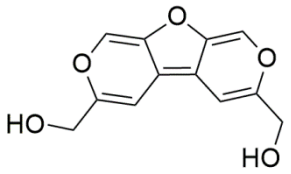

Figure 2.2 Fragment of humins structure suggested by Schweitzer by chemical degradation study and elemental analysis.

The molecular structures of ACD-derived humins are still under investigation. Separation is extremely hard to achieve, and often produces high amount of fragmentation in the humins structure. This, along with a generally high impurity level derived from the process conditions typically used in biorefinery, makes this structure hard to be identified. Furthermore, the chemical structure of humins can vary in a wide range of values, depending on the nature and amount of moieties, networks and molecular masses. For these reasons all the studies published so far show results that are hardly reproducible, and due to too many differences in the production processes, still does not exist a rigorous and specific protocol of analysis. Furthermore, when complete biomass feedstock have been used for the production of FMA or LA, an even increased complexity in the humins composition was observed. Unconverted biomass fragments were incorporated in the humins structure with new cross-links in the network or simply dispersed as impurity. In these cases FT-IR spectra of biorefinery chars indicate the presence of lignin fragment in the humins, while TGA analysis showed also the presence of limited amounts of cellulose and hemicellulose (probably as unbounded dispersed fragments).[60] Solid-state NMR studies indicate the presence of lignin residue in biorefined char derived from straw, while cellulose was identified when derived by paper. The symmetric peak pattern in the aromatic region has been associated by the authors to poly-aromatic structures condensed in the network.[128]

By studies on ACD of sugars and degradation of furanics, Baugh *et al.*[75] showed the dependence from the feedstock of the humins composition. It showed that the C content in humins derived by HMF treated at pH 2.5 was 58 wt.%, while starting from glucose it reached the 62 wt.%. When glucose was treated at pH 4, the C content decreased to 56 wt.%. Furthermore, Girisuta *et al.*[71] found a C content of 61.2 wt.% for humins formed during the production of LA from HMF. Also SEM images of humins were collected, showing agglomerated spherical particles with diameters of 5-10 µm. A higher C amount of 65.5 wt.% was found from fructose treated with phosphoric acid at high temperature.[129]

A quantification of the lignins present in the solid residues formed during acid-catalyzed hydrolysis of loblolly pinewood with different acids and at different temperatures was carried on in 2009 by Agrawal and Jones group using solid state ^{13}C NMR.[127] Moreover, the same group studied the hydrolysis in ionic liquids of several sugars, such as glucose, fructose, xylose[127] and pine wood.[78] In these studies it was shown that at high temperatures both the conversion of sugars and the yield of humins increases. The authors stated that the humins formation was due to the condensation of several water soluble products and HMF, which again plays a key role in the crosslinked network formation.

2.4 Humins formation

2.4.1 Insights on the mechanism involved

The molecular structure and the mechanism of formation of humins have not been unequivocally identified yet, despite the publication of several structural and mechanistic theories.

The self-condensation of HMF to provide humins was suggested by Daniel and Zeitsch,[130] which was then proposed also for the production of char and tar from sugars treated in (sub)-critical water.[131,132] However, while the polymerization of FF to resins was already known,[133] the HMF self-condensation pathway was criticized due to the absence of α-hydrogen.[134] However, it is generally considered that humins derived by C_6-sugars are generated from condensations between the dehydrated intermediated of the process (HMF or derivatives).[14]

In 2011 Bell and Dee reported the results of the acid catalyzed hydrolysis and dehydration of cellulose in ionic liquids using sulphuric acid.[135] The primary reaction products observed were glucose, cellobiose and HMF, while up to 30% of humins were formed as by-product. Here the humins yield was observed directly proportional to the HMF concentration, leading to the

speculation that humins were formed by condensation between glucose and HMF. A similar conclusion was drawn for xylose-derived humins, assuming a condensation between xylose and FF.[130,136,137]

Several attempts have been made to identify the mechanism of formation of humins through ACD of sugars,[138] and the most relevant insights are reported below.

2.4.2 Mechanistic pathway by Horvat

A mechanism for the ACD of HMF was suggested by Horvat in 1985[72,139] and is represented in Scheme 2.2. However, Horvat failed to come to a clear identification of the humins growth step. He simply suggested that humins are yielded by a not completely explained polymerization starting from an intermediate, the 2,5-dioxo-6-hydroxy-hexanal (DHH), which should be formed from 2,3 addition of water to HMF. Horvat was able to identify four intermediates of the ACD dehydration of sugars to humins by the use of *in situ* NMR and C^{13} labelling studies. However, DHH was never observed, and was therefore believed to be subjected to a rapid polymerization into humins. Several following studies proposed a mechanism of humins formation passing from the DHH intermediate. To report a recent example, in a study of 2019 also Velaga *et al*.[114] suggested that the humins formation involves DHH. However, this appears to be a bare speculation mostly based on the literature suggestion and only supported by unclear FTIR analyses on humins produced during the conversion of into LA using Mordenite zeolites. However, the same year Shi *et al.*[140] reported a detailed mechanistic proposal for humins formation under hydrothermal degradation of several model compounds, and again the analytical results strongly suggested the formation of DHH as one of the intermediate. Therefore, despite it has never been isolated, according to most of the reported observation DHH has been speculated as sure intermediate for humins formation.

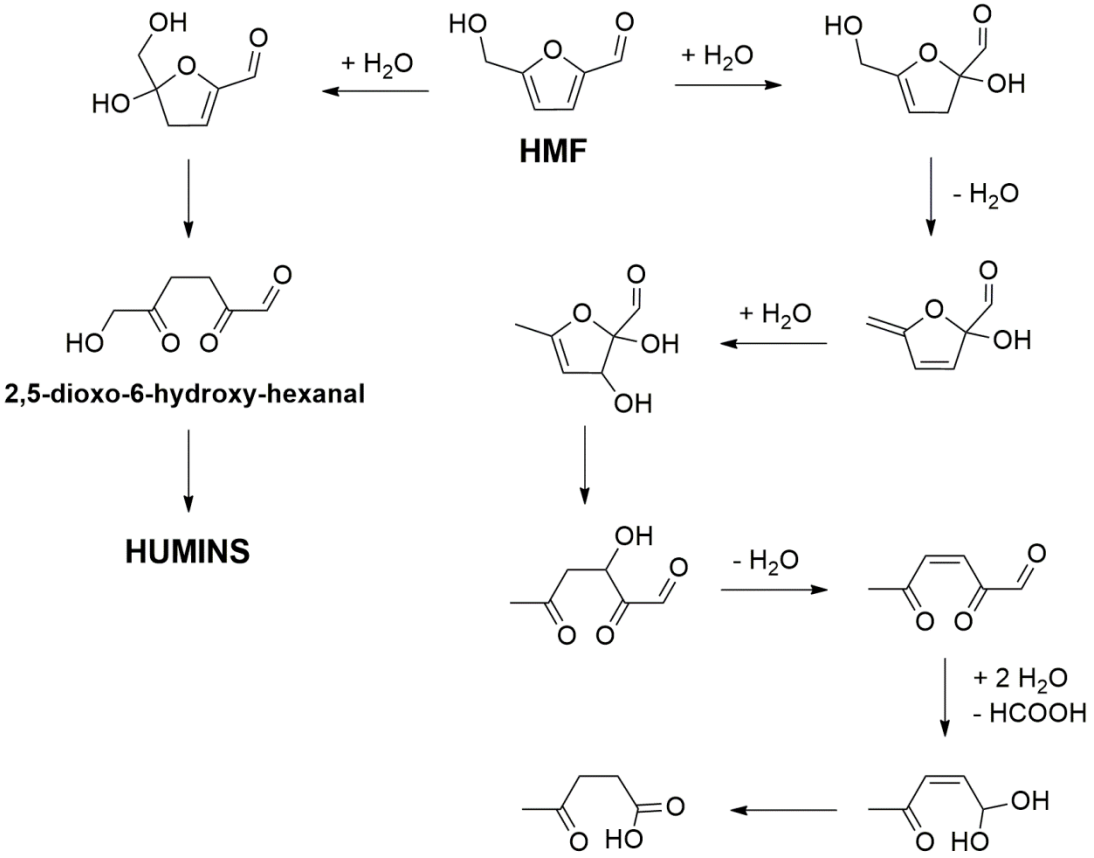

Scheme 2.2 – HMF and humins formation routes suggested by Horvat.[72,139]

This hypothesis was an important first step in the understanding of the humins mechanism of formation. Based on the NMR results a reaction pathway from fructose was developed, where the furanose form leads to HMF while the pyranose form leads to humins (Scheme 2.2).

Several follow-up propositions for the humins structure and mechanism of formation were developed by the groups of Weckhuysen,[66] Lund and Patil,[77][63] and Sumerskii.[56] Although all these proposals are extremely important for a better understanding of the mechanism of the reaction process, at present none of them can be considered to paint a complete picture.

2.4.3 Mechanistic pathway by Sumerskii and Zerubin group

In 2010 a further investigation into the molecular structure of humins was realized by Sumerskii *et al*..[56] The studied humins were derived by reactions in aqueous media with 5 wt.% carbohydrates and 0.5% H_2SO_4 at 175-180 °C for 2 h. Afterwards the solid obtained was filtrated, and the solution neutralized to let the acid-solid polymer present to precipitate. Roughly 20% of the humins could also be extracted with acetone. The soluble and insoluble humins fractions were subjected to characterization. IR analyses showed that both fractions have similar spectra, indicating that the soluble fraction is just less dense and contains shorter

oligomer chains. IR spectra revealed the presence of furanic moieties and several oxygen-rich functional groups,[56] in agreement with the ^{13}C NMR analysis on the acetone-soluble fraction. Furanics were also detected by pyrolysis-GC-MS analysis.[56] Starting from these results it was concluded that the humins structure consists of around 60% furan rings and roughly 20 % of aliphatic linkers.

A mechanism for humins formation was therefore proposed. It involves nucleophilic additions of the hydroxyl group of a first HMF molecule and the carbon aldehyde of a second HMF. This step yields acetal and hemiacetal bonds, which are present in the final humins polymer (Scheme 2.3). The process is catalyzed by Brønsted acids. Another proposed mechanism was the protonation of LA, leading to a carbocation that reacts with HMF via addition to the carbonyl or alcohol or electrophilic substitution at the furan ring (Scheme 2.3).[63,77]

Unlike the mechanism proposed by Horvat this one does not involve DHH, which molecule is not implied in the polymerization growth. Noteworthy, the final structure has a distinctly and easily discernible IR spectrum, thanks to the four fundamental vibrational mode linked to the presence of acetal group (1200-1030 cm^{-1}).

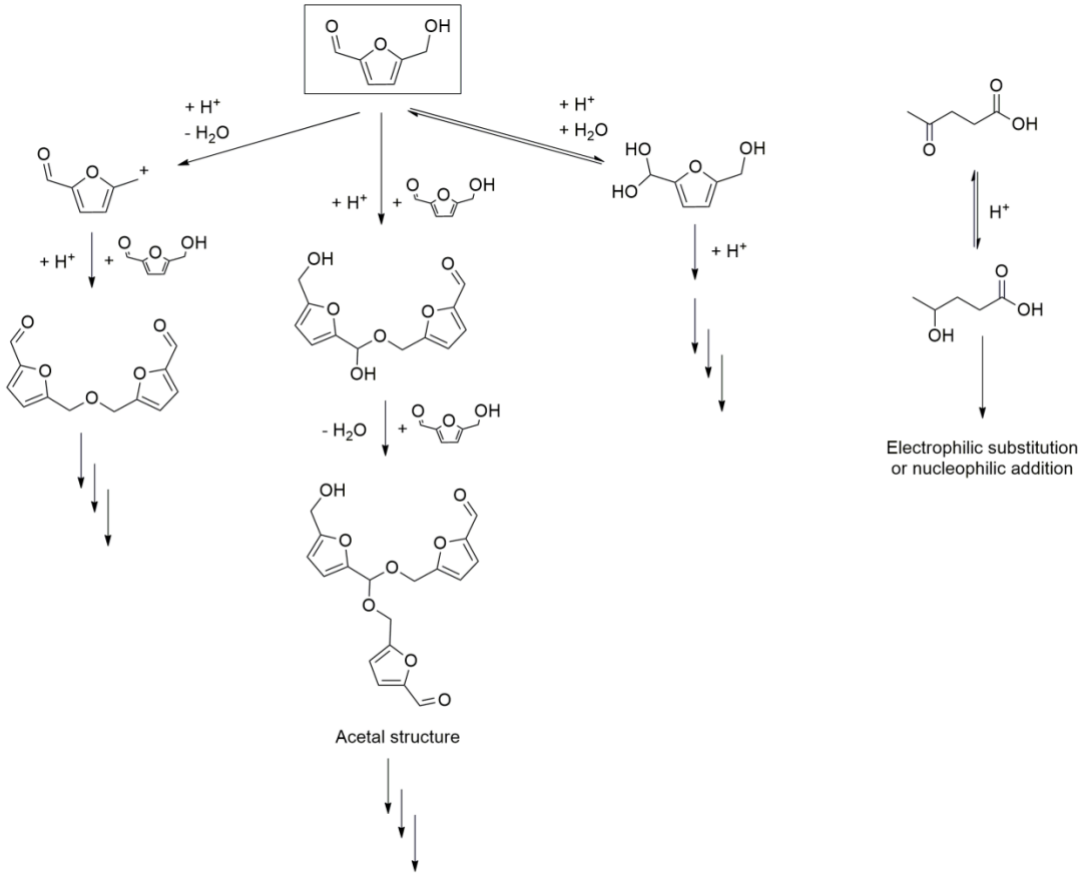

Scheme 2.3 Humins formation mechanisms suggested by Sumerskii *et al.*[63,77]

2.4.4 Mechanistic pathway by Lund group

Consistent with the mechanism proposed by Horvat, Lund *et al.*[63,77] suggested the aldol addition and condensation as main reaction steps in the acid-catalyzed growth of humins. They highlight two possible outcomes, which are similar but mechanistically different. In case the second aldol addition of HMF to DHH is just as fast as the first, the final structure should not have further enols generated. A second possibility is that the second addition is slower than the first one, resulting in a final structure which retains enols even after that all the DHH has been consumed (Scheme 2.4).

These mechanistic hypotheses, as suggested by Horvat, take into account the formation of DHH. However, the presence of DHH as intermediate was not detected, which was considered as an indication of its high reactivity.[77] The formation of DHH involves the 2,3 acid catalysed addition of water, opposed to the 4,5 addition that leads to LA. All these results strongly suggest that HMF is an important intermediate in the formation of humins. In the IR spectra humins maintain the furan ring and the hydroxymethyl group of HMF. Furthermore,

benzaldehyde (which does not form humins at the reaction condition) is incorporated in the structure if added during the acid-catalyzed conversion of HMF. Again, the IR spectrum shows the benzaldehyde ring in the humins structure, without carbonyl moiety. This study confirmed that humins growth during ACD of sugars involves the aldol addition/condensation from HMF. Following studies showed differences between humins derived by HMF, glucose, fructose and cellobiose. With longer reaction times the particles dimensions are enhanced as observed by SEM analyses, while the IR spectra did not show any change in molecular structure. Furthermore, due to its faster conversion rate, using fructose in ACD conditions would result in a minor accumulation and incorporation of HMF into the humins structure, in contrast with the high accumulation of products found in glucose- or cellobiose- derived humins.[63]

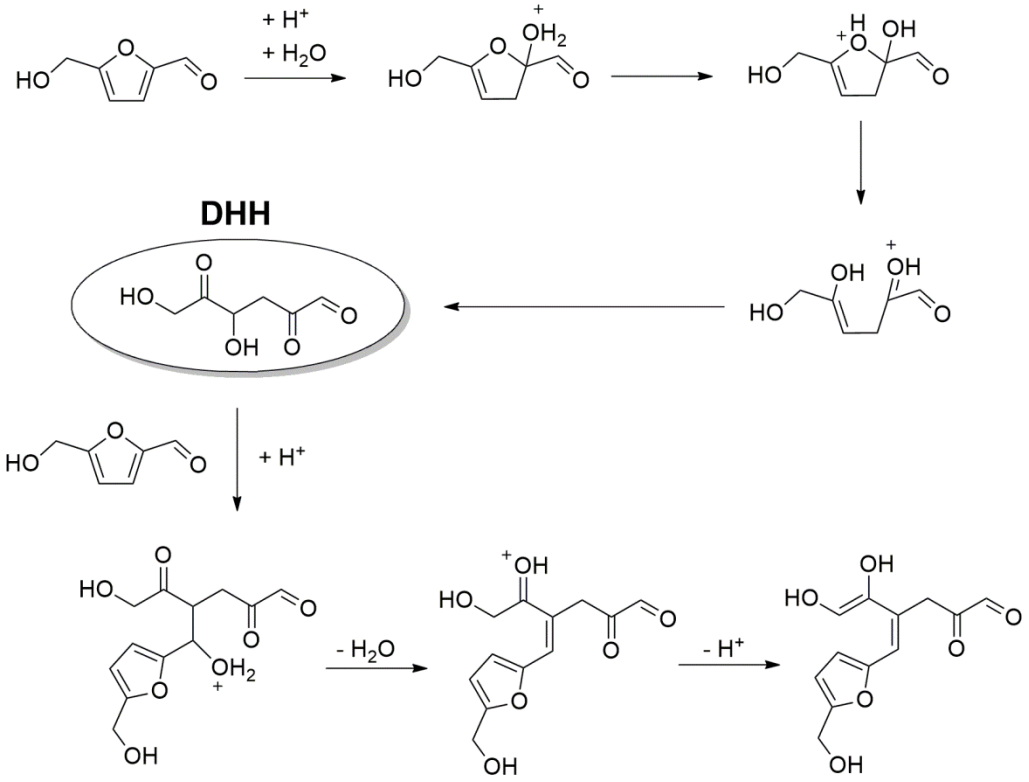

Scheme 2.4 Suggested mechanism involving DHH formation and aldol addition of HMF.[63,77]

2.4.5 Mechanistic pathway by van Zandvoort and Weckuysen

A suggestion about humins structure and the mechanism that leads to their formation was proposed in 2013 by van Zandvoort and Weckhuysen.[66] The structure here obtained appears more complex compared to the previous reports. According to the Weckhuysen's group, humins are yielded by a combination of formic acid, levulinic acid, DHH, and HMF. In the

proposed mechanism HMF is subjected to nucleophilic additions of the α and β carbons from the other intermediates, yielding humins. A model of humins structure was proposed based on extensive analytical investigations using a combination of techniques such as FTIR and solid state/standard NMR. However, since the proposed structure was mainly based on analytical results, the proposal lacks an explanation on the growth mechanism of this by-product.

Following extensive NMR studies by a combination of 1D and 2D NMR techniques the authors highlight that glucose-ACD derived humins present mainly C_{α}–$C_{aliphatic}$ and C_{α}–C_{α} linkages, and in a minor amount C_{β}–$C_{aliphatic}$ and C_{β}–C_{β} bounds.[141] The ketone moieties found could be derived by LA incorporation in the humins structure, or from intermediates of sugar dehydration/ HMF rehydration.

In 2016 Tsilomelekis reported an investigation of molecular structure, growing rate and mechanism for ACD HMF derived humins.[16] The mechanism involving the nucleophilic attach of the HMF carbonyl in α- or β-position of a second furanic ring was proven wrong. By FTIR analysis it was observed that the absorbance of C-H out of plane mode relative to the furanic hydrogens decreases after long reaction times. Also the decreasing of C=O stretching (1668 cm^{-1}) further confirms this mechanism, while does not exclude other possible pathways, such as condensation or aldol addition. Spherical humins particles have been here observed by SEM. Noteworthy, DMSO used as co-solvent seems to suppress the nucleophilic attack, leading to smaller humins particles (~ 100 nm). Inversely, using water as solvent results in bigger particles (between ~ 100 nm and 5 µm) made up by smaller ones. The humins particles growth in water has been studied under *in situ* reaction conditions using dynamic lights scattering (DLS).[16] At pH = 0 and 50 °C the initiation of the reaction, associated at the detection of the smaller particles (100 – 200 nm) was observed after 10 minutes, while using pH = 1 it was observed after 1 hour (growing rate ~ 2.1 – 2.9 nm min^{-1}). The key parameters in humins productions, as always, are temperature, reaction time and acid concentration used.[66,77] Higher temperature and higher acid concentration lead to higher growth rate and size of humins particles. According to these observations a reaction network of humins formation from HMF in presence of acid (acid catalysed degradation) has been proposed. Firstly, soluble oligomeric chains of humins are formed *via* etherification and aldol condensation.[56,63,77] Here HMF reacts with intermediates (DHH, DHH-like molecules or other HMF), and in water media, *via* nucleophilic attack, the humins particles grow.[66] By using polar aprotic co-solvents such DMSO it is possible to suppress this path, and so the particles don't

grow and stay at reduced dimensions. Finally, aggregation of the smallest particles produces largest water insoluble ones that precipitate. These reactions network give a good overview and interpolations of all the results and insight so far obtained on humins particles growth.

In addition to the previous insights, in 2017 Constant and co-workers reported[142] a quantification of the carbonyl moieties in the industrial humins obtained from ACD of fructose, using derivatization with 4-(trifluoromethyl)phenyl hydrazine and followed by ^{19}F NMR analysis. 6.6 wt .% of carbonyls, both aliphatic and conjugated, have been detected, suggesting promising applications of industrial humins following functionalization methods or a grafting pathway. Constant estimated that around 1/3 of the total amount of carbonyls presents in industrial humins were aliphatic, that could be derived by LA incorporation or from sugar/HMF derivatives of dehydration/rehydration.[16,143]

2.4.6 Mechanism pathway by Shi

In 2019 Shi *et al*.[140] reported an investigation of the humins formation pathway from hydrothermal carbonization of 37 model compounds (including carbohydrates, cyclic ketone derivatives and short oxy-organic compounds). The experimental results strongly suggest a pathway based on α-carbonyl aldehydes and α-carbonyl acids as precursors for humins formation. Experimenting reactions between two α-carbonyl aldehydes (including pyruvaldehyde and glyoxal) it was observed the aldol condensation, the subsequent acetal cyclization and dehydration as three step pathways to humins formation. Another parallel pathway suggested is the Cannizaro reaction to form α-hydroxy acids. Therefore, glucose can be also converted into 3-deoxyglucosone that then undergoes Cannizaro reaction producing α-hydroxy acid. Six different α-carbonyl aldehydes are expected forming during the hydrothermal degradation of glucose toward humins: 3-deoxyglucosone, (S)-5,6-dihydroxy-2-oxohex-3-enal, DHH, 4-hydroxy-2-oxobutanal, 2-oxobut-3-enal, and pyruvaldehyde. Furthermore, considering 14 compounds between carbohydrates and their degradation products, it has been found that rhamnose and xylose can produce more humins than 5-methylfurfulal and furfural. This effect can be explained considering that both compounds can produce α-carbonyl aldehydes by direct β-elimination and keto−enol tautomerism, and therefore producing the humins before passing from 5-methylfurfulal and furfural. In 2019 Shi et al.[144] reported a test for humins formation from carbohydrates and furfural derivatives using several solvents. It resulted that, whatever the solvents (except EtOH), all the carbohydrates tested were able to form humins. The humins formation resulted suppressed

in EtOH since it can react by acetalization with α-carbonyl aldehydes. Therefore, the condensation reaction between α-carbonyl aldehydes is suppressed. On the other hand, furfural derivatives could deliver humins only in aqueous media. Again, α-carbonyl aldehydes and α,β-unsaturated aldehydes are suggested as main humins precursors.

2.5 Humins from hydrothermal carbonization

Humins-like material can also be produced *via* hydrothermal treatment of carbohydrates or biomass derived platforms, leading to the so-called hydrothermal carbon (HTC).[145–147] HTC approach is widely employed in the production of carbonaceous compounds.[91,148] Compared to an ACD process, HTC production occurs under non-acidic conditions, and the reaction is carried out by the combined use of temperature and pressure.[149]

HTC materials are the result of cascade reactions involving dehydration, polymerization and aromatization. HTC are originated after the dehydration of C6-sugars to HMF and C5-sugars into FF, which are subsequently subjected to a combination of ring opening reactions yielding diketones. Thus, aldol-like condensations and aromatization via Diels-Alder reactions, along with polycondensations will lead to the HTC structure. This is followed by nucleation and growth of the spherical particles by the incorporation of HMF/FF derived molecules.[149] As in ACD derived humins, the so obtained HTC are mainly made by furanic cycles linked by aliphatic chains bearing hydroxyl and carbonyl moieties (Scheme 2.5). For these reasons, despite HTC materials are supposed to be different in molecular structure from ACD-derived humins, their preparation involves similar reactions and similar intermediates, and can be considerate highly related.

On the other hand, HTC treatment avoids the use of mineral acids and makes the process more environmentally friendly, while the minor amount of impurity and simplest purifications processes makes them easiest to characterize. A comparison between carbonized sugars and HTC FF- and HMF-derived was carried out.[66] The results proves that HTC from C6 are quite similar to carbonized HMF, while HTC from C5 are closer to carbonized FF.

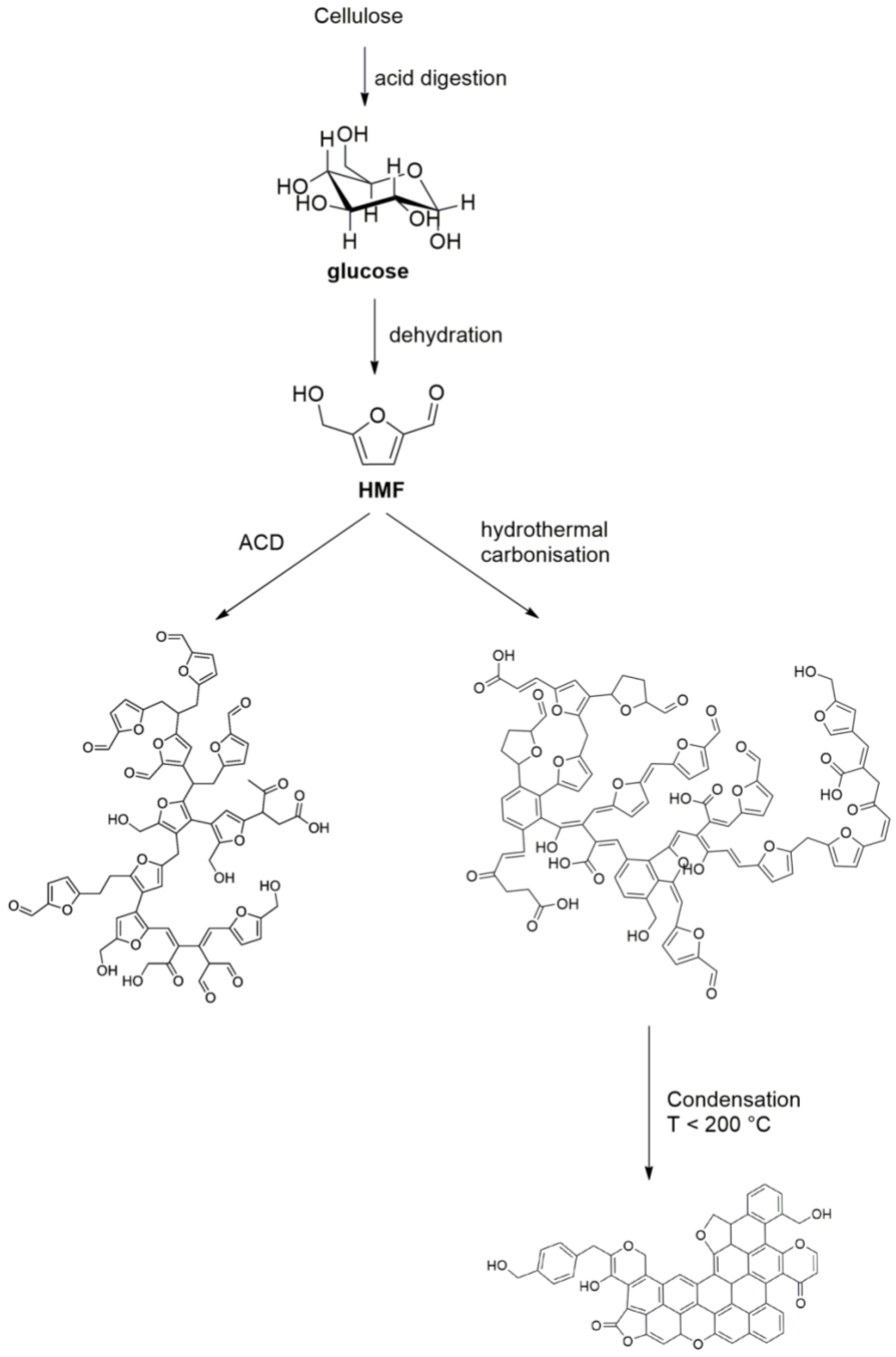

Scheme 2.5 Conversion pathways of cellulose into ACD humins (structure suggested by van Zandvoort)[66] and HTC.

This explains why HTC materials have been subjected to a more thorough characterization than humins obtained from ACD conversion, and most of the information about humins molecular structures are obtained from HTC.

Low-temperature production of HTC is carried out at temperatures lower than 250 °C[150] and can be used to functionalize and modify carbonaceous materials with straightforward reactions such as polymerization and dehydration. Using this technique it is possible to functionalize carbon microparticles or nanoparticles, but the findings are contradictory in some respects. For instance, Yao et al.[151] observed different morphologies for the surface of HTC-particles, based on the starting monosaccharide chosen (bumpy when produced from glucose, smooth when produced from fructose). On the other hand, Titirici et al.[152] highlighted that carbon derived from hexoses (including glucose and fructose) were similar to each other, but slightly different from pentose- derived HTC. Furthermore, under very similar reaction conditions, glucose derived HTC-humins had very different outcomes: i) sometimes resulted in uniform particles size,[150] ii) some others in a wide distribution of particles sizes,[152] and in one case iii) without an exact shape.[153] Same inconsistencies were found with chemical characterizations. In different studies HTC-humins were derived from fructose, glucose and HMF respectively, and in all of them the presence of aromatic compounds were detected by IR, NMR and Raman analysis.[132,151] This is in contradiction with other investigations in which hydroxylated methylenes were found in HTC derived from hexoses, while aromatic components were found in HTC derived from pentoses.[152] In their series of articles Titirici and Baccile suggested, therefore, different structures for various pentose- and hexose-derived HTC.[147,152,154] Observations by advanced solid-state ^{13}C NMR of labelled ^{13}C HTC showed that HTC-derivatives are constituted by furan-rich structures. The various subunits are linked together through aliphatic chains in α or β position, and with LA embedded in the structure.[147] Noteworthy, HTC from C5- and C6-sugars result similar to furfural (FF) and HMF, respectively. HTC from xylose (C5-sugar) resulted in a lower H/C and O/C ratio by comparison with HTC from other sugars.[152] This can be explained by the H/C and O/C ratio of the primary building blocks, e.g furfural ($C_5H_4O_2$) and HMF ($C_6H_6O_3$). By comparison with glucose-HTC, xylose-HTC in ^{13}C NMR spectra showed a minor amount of aliphatic groups, along with stronger signals associated to C=C conjugated systems. This can be associated to a higher amount of furanic groups in C5-sugars derived HTC respect to HTC from C6-sugars.[154] Together with the feedstock used, the HTC molecular structure seems also highly dependent on the preparation temperature.[154] Using ^{13}C solid-state NMR it was observed that sugars-derived HTC prepared at 180 °C consist of a furanic network with aliphatic linkers, as above reported.[147] In sugar-derived HTC calcinated at 350 °C a higher amount of conjugated

aromatic rings was found, obtained by aromatization and furan rings fusion up to polycyclic systems. Graphene-like sheets were obtained with HTC prepared above 400 °C.[154]

Also the conversion to 1,2,4-trihydroxybenzene, produced by hydrothermal treatment from HMF (27.5 MPa, 290-400 °C, 0.5 M) resulted in humins formation.[76] On the other hand, by adding 1,3,5-trihydroxybenzene (phloroglucinol) in hydrothermal treatment of monosaccharides it was recorded an increasing of the resulting spheres diameter, with around a twentyfold increasing of carbon yield.[155]. It was observed that the monosaccharides were converted into furanics during the process, which then reacted with phloroglucinol forming new networks enhancing the aggregation.

Sevilla et al.[145,146] showed that the diameter of the spherical HTC particles can be modulated in the range 0.4 - 6 µm by controlling the reaction parameters, such as temperature, reaction time, feedstock used and concentrations. Elemental analysis by XPS of HTC particles showed that the surface and the material bulk have similar O/C ratio, with the presence of several oxygen groups. Also TEM images of the HTC particles showed only slight differences between bulk and surface. The increasing temperature is associated to a decrease in the O/C and H/C ratio due to the carbonization and aromatization of the structure. This is supported by a decrease of the oxygen moieties in the IR signals. The carbon nature of HTC from sugars was also highlighted by Raman spectroscopy, and then confirmed by Shin and co-workers with the observation of the typical D and G bands of disordered graphite-like carbon at 1360 and 1587 cm^{-1}, along the presence of aromatic rings with oxygen rich functionalities.[151]

A mechanism for HTC-particles formation was proposed through condensation between glucose and furanics derived from the dehydration of cellulose, followed by aromatization. These polyaromatic spherical structures are built as a less dense hydrophilic shell and a dense hydrophobic core, and it is possible to add specific functionalities to their surfaces taking advantage of the exposed reactive moieties.[156,157] Furthermore, it has been shown that HTC can be formed around a metallic nanoparticle centre, and that HTC surfaces can be spiked by smaller metal particles (such as Ag or Pd).[150] The same behaviour can also be expected for carbonaceous humins formed by ACD.

Humins-like HTC materials have been extensively studied, and their characterization can be used as reference model for ACD-derived humins. HTC helped in better interpretation of the reaction mechanisms, yields and parameters involved during the product formation. However, these kinds of “synthetic” humins-related carbon materials are originated by well-

designed reactions in a highly controlled environment, and their "high-tech" applications are already fully defined. Furthermore, despite the HTC chemical structure is supposed to be similar to humins ACD-derived, they have different physical aspect and properties. Therefore, different considerations should be made for humins derived by ACD of sugars, where the parameters and reaction partners are more complex and varied. The challenge of finding applications for such industrial humins was unexploited for a long time, if not even considered at all. However, recently several studies have been conducted focusing on their potential applications, sometimes with encouraging results. This research area is growing fast, and the investigations around this new topic is encouraging the studies to the next stage, meaning not only focusing on avoiding humins formation but especially to valorize this interesting as well as versatile side-product.

2.6 Humins valorization

Figure 2.3 Valorization and promising applications of humins

One of the possible valorization routes for ACD derived humins involves their gasification,[23,158] leading to the production of syngas and higher value chemicals by pyrolysis.[159] In order to make these processes economically interesting, to make transportation easier or even use them as fuel, humins should be solubilized or, at least, be available in a less viscous phase.[70,160] However, the solubility of these recalcitrant by-products is quite poor. For instance, it has been reported that with 24 hours Soxhlet extraction

with acetone and ethanol only the 3-5 % of humins weight loss was achieved.[161] On the other hand, there is a growing interest in make humins more soluble and easier to be processed.[70] In 2015 van Zandvoort succeeded in obtaining reactive solubilization of humins using an alkaline pretreatments similar at those used for lignin.[141] Glucose-derived humins were solubilized in 0.5 M NaOH at 200 °C for 3.5 h, while xylose- and fructose-derived humins required a higher temperature of 240 °C. It was observed that longer treatment times and higher temperatures lead to a reduction of the average MW. 0.5 M NaOH was selected as the best concentration, since stronger alkaline environment leads to a further decreasing of the MW. Investigations performed with a combination of techniques (solid-state NMR, elemental analysis, IR, GC-MS) suggested that the alkaline treatment leads to the cleavage of C-O-C bonds, and so to the reduction of the MW. Also an increase of aromatization in the structure (presumably *via* Dies-Alder and/or dehydration reactions) was detected, that leads to polycyclic systems bearing carboxylic groups.[141] Indeed, IR signals associated to carboxyls increases at expenses of keton groups, and this structural change (along with the reduction of MW) could explain the increased solubility of humins after such treatment. The so obtained humins are soluble at pH > 7 and could find applications in the production of syngas, of hydrogen *via* water phase reforming or in catalytic hydrotreatment.[162–164]

In 2018 Cheng *et al.* studied the solubilization of humins derived from ACD of fructose using solvents with different polarities.[165] For the first time it was demonstrated that humins are not simply a polymeric product with high molecular weight molecules, but more an heterogeneous mixture of large insoluble molecules and small species easy to solubilize. This oligomeric nature was always hypothesized, but never demonstrated.[142,166,167] These molecules of different molecular weight interact with each other by weak forces and polar attractions, maximized by the polar species beard in the structures. Indeed, as observed by FT-IR analyses, dissolution of humins at room temperature does not produce breaking of covalent bonds. Cheng reported how solvents with higher donor number can dissolve larger amounts of humins, mainly the low molecular weight fractions, even at room temperature, which could be useful for humins transportation or applications. The effect of the polar solvent involves the decreasing of selectivity of the polar attraction within humins structures, which explains the higher amount of molecules dissolved. By LC-MS was detected that the molecular weight of the solubilized fraction ranged between 200-600 Da, and even < 2000 Da according to GC-MS analysis.

Liquefaction/depolymerization of synthetic and industrial ACD derived humins has been reported in 2017 *via* catalytic pyrolysis.[67,168] The obtained humins oil consisted of 5-10 wt. % of aromatics (mainly higher value/ low molecular weight compounds), while the higher heating value was estimated to be 41 $MJkg^{-1}$. This humins oil has potential use as biofuels additive, as well as source for platform chemicals and building blocks for polymers synthesis. Unfortunately, while the maximum aromatics theoretical yield from humins subjected to catalytic pyrolysis has been calculated to be around 50 wt. %, experimentally only a 9 wt. % yield was achieved.[67] According to previous quantifications of the pyrolysis oil from humins (by comparison between the volatile fractions (~ 30 % of the total oil) using GC-MS and the total oil content groups using titration and ^{31}P NMR),[169] the total phenols were estimated in the range 1.6-3.1 mmol/g, and between 85-95 % in form of oligomers. The carboxylic acid were reported as 1.1-2.1 mmol/g, with around 20 % in the oligomeric phase. Around 56% of the total oxygen-based moieties were estimated in the form of water, 20% as carboxyls, 17% as hydroxyls and 12 as acids.

Preliminary studies of spray combustion of humins as alternative to heavy fuel oil (HFO) have also been conducted.[170] In this contest, 25 % wt. of methyl levulinate (ML) was added to reduce the humins viscosity. It was reported that parameters such as stability, heating value, flashpoint, viscosity and density of the humins/ML mixture fall in the HFO limits. Furthermore, in the spray combustion tests, the mixture had ignition and combustion behavior similar to earlier observation for HFO. However, the combustion residual ash and carbon were too high, representing risks in terms engine damage, while the determination of CCAI, acid number and water was not possible to be performed.[170]

Another interesting valorization methodology involving catalytic hydrotreatment of humins has been carried out in 2016 from Wang and coworkers using ruthenium catalysts at 400 °C in presence of FA and isopropanol or H_2.[171] Up to 69 % conversion was obtained in the best case, resulting in a humins-oil mainly consistent of monomers (principally alkyl phenolics) and small oligomers. On the other hand in 2019 Pfab *et al.*[172] performed a preliminary test of extraction of 5-methoxymethylfurfural (MMF) from the humins network, followed by its hydrogenation (mainly into 5-(methoxymethyl)-2-furyl]methanol and 5-methyltetrahydrofurfuryl alcohol) in continuous flow using 5 % Ru/C and 5 % Pd/C as catalysts. Also the selective catalytic conversion of humins into short-chain carboxylic acids (e.g. FA and acetic acid) has been reported.[173] The oxidation of humins has been performed

using homogeneous polyoxometalate as catalyst in mild conditions (90-120 °C), making possible also the tuning of the conversion selectivity by tailoring the parameters. However, the isolation and purification of the products remains a challenge.

In terms of safety, thermal stability, ignitability, and combustibility of crude humins, a preliminary attempt of classification has been conducted in 2018,[54] showing that the overall fire risk associated is not significantly different from conventional woody materials. Further ecotoxicity and biodegradability tests according to the European regulation on the Registration, Evaluation, Authorisation and Restriction of Chemicals (REACH) along primary evaluation of aquatic ecosystem hazards were published in 2019.[174] The study concluded that, up to the current information gathered, humins do not bring ecotoxicological concerning and can be considerate for environmental-friendly application.

Among these valorization routes, also the degradation of humins has been taken into account. For instance, Kang *et al.*[175] studied a two-step degradation *via* alkaline-catalytic hydrothermal treatment and wet oxidation in order to produce acetic acid. Yields of 25.6-37.2% were achieved, while the purity of the product was around 46 %.

2.7 Humins-derived materials

During the last years humins have also been studied also in material science, in order to design new materials, preparing composites or as additives for improved properties.

For instance, humins can also be used as substrates in the preparation of porous carbon material (Figure 2.3).[166,176] Similar applications were reported in 2015 by Merle *et al.*[177] for the mechanical preparation of biobased macroporous foams from pulp industry, using polyphenol aqueous mixtures of tannins and lignosulfonate in presence of an additive (hardener) and a surfactant. Solid foams with average porosity of 89 % were obtained. These foams can be considered as good thermal insulators in agreement with the Federation of European Rigid Polyurethane Foams Associations[178] that fixed for these materials a conductivity in the range 0.035-0.055 $W \cdot m^{-1} \cdot K^{-1}$. Unlike the previous case, our group recently reported the preparation of fully humins based carbonaceous macroporous foams, with a single step treatment reaction and without any additive required.[179] We found that heating up industrial ACD-derived humins to a temperature higher than 180 °C, without any pretreatment or modification, , it was possible to produce a solid porous material. These humins foams have porosities and properties that can be tailored by selecting the reaction

parameters.[180] The mechanism of formation consists in a combination of phenomena: the releasing of volatiles and gasses during the heating (leading to pores formation) and the thermal-inducted auto-crosslinking (leading to polymerization of the matrix). This black-shining porous material can be produced in a straightforward and cheap way from industrial humins, where the only cost of the preparation is due to the thermal energy invested. Noteworthy, by selecting the final temperature of preparation, it is possible to control the carbon amount of these materials up to around 95 %, which opens the way to a plethora of promising applications.[181–186] Furthermore, the higher thermal stability of humins foams compared to crude humins has been highlighted, with no critical self-heating behavior and relatively safe uses.[54]

Microporous humins-based material was also prepared in 2019 by Björnerbäck and Hedin.[187] In this case, controlled porous humins were produced by ACD of sugars in concentrated sulphuric acid, then humins were washed in diethyl ether and carbonized at 400 °C. However, despite the interesting result, this process does not aim to the valorization of industrial-produced humins, but require the specific synthesis of humins following a protocol not compatible with the current Biorefinery needs.

In 2018 Kang *et al.*[188] Humins-derived activated carbon prepared at 800 °C was also studied as sorbent material. A pseudo-second-order-kinetic model was found, with a superior adsorption capacity of 1195 mg/g of methylene blue and 218 mg/g of phenol. The principal contribution of this absorption capacity was associated to pores with 1.7 – 300 nm of aperture. It was also suggested a contribution of the acid groups on the macroporous surface (> 300 nm),[189] with an interesting acid moieties amount of 3.3 meq·g^{-1}.[190–193] Furthermore, preparation of activated carbon from humins using phosphoric acid activation has been performed, reaching a BET surface area of 2375 m^2·g^{-1} in the best conditions (400 °C).[194] However, in this case a poorer Langmuir adsorption capacity of 1125 mg/g of methylene blue has been found.

Chernysheva *et al.*[195] reported the preparation of activated carbon from both physical (CO_2) and chemical activation (KOH) of previously carbonized humins, and their tests as supercapacitor electrode materials. Unfortunately, this article lacks of a good textural characterization of the activated carbon produced, while the BET surface area is quite poor compared to those commercially available[196] (only 862 m^2·g^{-1} in their best case). However, despite the electrochemical characterization of these humins-derived activated carbon was

obtained by a 3 electrodes cell (that usually gives higher capacities), this study showed a promising application route of humins valorization as supercapacitors electrodes material.

Humins have been also studied as thermoset resins and in material composite preparation. For instance, in 2014 has been reported the realization of thermosetting resins obtained by adding large quantity of humins (55 - 75 %) to PFA network.[197] The preparation was carried out by acid-induced polymerization, and the chemical interaction between the PFA and humins was observed by FT-IR analysis. This furan based resin mixture was also used in impregnation of cellulose fibers, thus to the production of the fibre-composites after curing. Noteworthy, it was found that the tensile strength of these humins/PFA composites was twofold higher compared to similar composites from PFA or PFA/lignin. Humins/PFA composites resulted in less brittle materials compared to the common furfuryl alcohol based analogues, while the interaction between resin and fiber was enhanced. Materials so obtained not only showed very interesting properties, but also reduced the costs of preparation, since minor amounts of furfural alcohol is required.

In 2017 Kang[198] reported the use of humins as low-value phenol replacement in phenol-formaldehyde adhesive for potential wood adhesion applications. Humins were previous hydrothermally treated in order to produce an alkaline soluble additive, subjected then to reaction with formaldehyde and phenol. The so obtained humins (50 % wt.)-phenol-formaldehyde adhesive shows good bonding strength and viscosity property, and met the GB/T 14732-2006 Chinese National Standard safety requirements for commercialization.

In 2018 Sangregorio *et al.*[199] reported a detailed study on the industrial humins thermo-reactivity, proving their potential application in the preparation of thermoset-like resins confirming previous results[69,166] that upon sufficient thermal treatment humins mixtures are able to react in a non-reversible way, polymerizing into a furanic based network. T_g midpont values above 65 °C were found after thermal treatments at 120-140 °C. These T_g values are close to those found for humins foams prepared at higher temperature (250 °C), proving that the completeness of the crosslinking can be approximate with a “infinite” glass transition of 70-75 °C. Following this results, in 2019 Sangregorio *et al.* reported the preparation of composites humins-flax fibers.[200] The flax/humins composites proved to have good elastic modulus of ∼1.5 GPa, while SEM showed a good adhesion between matrix and fiber. The only drawback reported is that, despite the interesting reduction of water absorption of the composite compared to the pure frax, releasing of little amount of furanic compounds in

water (mainly HMFCA) was found. Very recently Dinu and Mija[201] reported the preparation of cross-linked polyfuran resins obtained by the copolymerisation of humins with epoxide based aliphatic ethers. Noteworthy, these materials even show elastomeric behaviour, with an impressive tensile strain at break up to ≈ 60% in case of copolymerisation with poly-ethylene glycol diglycidyl ether. This has been identified as an effect of the copolymer aliphatic chain length (longer the chain, major the elastomeric effect), highlighting the possibility of tailoring the resins properties based on the foreseen applications by choosing the composition.

For applications as catalytic materials or catalyst support, humins-based iron oxide nanocomposites have been reported in 2017 by Filiciotto *et al*.[202] The catalyst was prepared by cheap and solvent-free methodologies, using both industrial ACD crude humins and humins foams. The catalysts were tested in the microwave-assisted synthesis of vanillin from isoeugenol in oxidative environment, and proved in some cases good recyclability. The authors reach yields of vanillin of 42-57 % in reaction times of only 5 minute. These yields are comparable to those reported in literature for the conversion of isoeugenol into vanillin (53-72 %) at 50 °C and long reaction times (24 h).[203,204] Indeed, the reaction times used in the study of humins/ iron oxides catalysts were quite harsh, with microwave assisted temperatures between 149–169 °C and extreme oxidizing conditions. On the other hands, this represents a promising preliminary study of application of humins based nanocomposites in this field, which open the study to further investigations and optimizations.

2.8 Conclusions

In this review the history of humins investigations and their most recent understanding, improvements and applications are reported. Humins are industrial biorefinery outcomes from the lignocellulosic biomass conversion, mainly produced in the acid catalysed dehydration of sugars into furan chemicals. In the last century the research mainly focused around the understanding of their formation mechanism, the parameters that leads to their production (e.g. feedstocks, catalysts, solvents, temperature, resilience time, concentrations) and the evaluation of yields, all aiming to the elaboration of a more selective process avoiding their formation. Despite this, humins production seems unavoidable. Several recent papers report conditions that minimize their formation, however mostly based on the only lab-scale reaction. Doubts remain about the possible upscaling, especially regarding the economy of

the process. Furthermore, several studies have been conducted during the years trying to characterize their chemical structure. Despite today we can state that most of the humins skeletons has been revealed, uncertain still remain, mostly due to high dependence on the parameters used during their production.

However, during the last decade it appears that the research aims switched, and humins gathered more and more attention as resource. Many studies focused on the valorization of these side-products. Taking advantage of their furan rich structure, the possibility to tailor their carbon amount, to exploit their direct auto-crosslink and foaming behavior, humins have been valorized and employed in several fields (production of chemicals and fuels, wood and fibers impregnation, polymer and material science, preparation of carbon-based porous materials and activated carbon, preparation of catalysts, etc.).

Today, the humins valorization research proved to be a strong and consolidate topic. Despite the fact that this just a first step toward their full exploitation, we proved that the principles of the green and circular economy can be respected, and that humins is and will be further considerate a promising and valid resource.

2.9 References

[1] J. E. Cohen, *Science (80-.).* **2003**, *302*, 1172–1175.

[2] G. Resch, A. Held, T. Faber, C. Panzer, R. Haas, *Energy Policy* **2008**, *36*, 4048–4056.

[3] E. O. Day, "Global Footprint Network.," can be found under https://www.overshootday.org/, **2017**.

[4] D. Gale, *The Theory of Linear Economic Models*, University Of Chicago Press, **1987**.

[5] P. Ghisellini, C. Cialani, S. Ulgiati, *J. Clean. Prod.* **2016**, *114*, 11–32.

[6] P. Krugman, *Econ. Policy* **1998**, *14*, 7-17.

[7] G. F. Network, "Overshoot Day - Press Release," can be found under https://www.overshootday.org/newsroom/press-release-june-2019-italian/, **2019**.

[8] E. de Jong, A. Higson, P. Walsh, M. Wellisch, *IEA Bioenergy, Task42 Biorefinery* **2012**, 33.

[9] E. de Jong, A. Higson, P. Walsh, M. Wellisch, *Biofuels, Bioprod. Biorefining* **2012**, *8*, 606–624.

[10] N. Mosier, C. Wyman, B. Dale, R. Elander, Y. Y. Lee, M. Holtzapple, M. Ladisch, *Bioresour. Technol.* **2005**, *96*, 673–686.

[11] E. de Jong, R. J. Gosselink, in *Bioenergy Res. Adv. Appl.* (Ed.: Elsevier), Elsevier, Amsterdam, The Netherlands, **2014**, pp. 277–313.

[12] J. Pérez, J. Muñoz-Dorado, T. De La Rubia, J. Martínez, *Int. Microbiol.* **2002**, *5*, 53–63.

[13] B. Girisuta, B. Danon, R. Manurung, L. P. B. M. Janssen, H. J. Heeres, *Bioresour. Technol.* **2008**, *99*, 8367–8375.

[14] R. Van Putten, J. C. Van Der Waal, E. De Jong, C. B. Rasrendra, H. J. Heeres, J. G. De Vries, R.-J. van Putten, J. C. van der Waal, E. de Jong, C. B. Rasrendra, et al., *Chem. Rev.* **2013**, *113*, 1499–1597.

[15] G. R. Gomes, D. S. Rampon, L. P. Ramos, *Appl. Catal. A Gen.* **2017**, *545*, 127–133.

[16] G. Tsilomelekis, M. J. Orella, Z. Lin, Z. Cheng, W. Zheng, V. Nikolakis, D. G. Vlachos, *Green Chem.* **2016**, *18*, 1983–1993.

[17] G. P. Perez, A. Mukherjee, M. J. Dumont, *J. Ind. Eng. Chem.* **2018**, *70*, 1–35.

[18] F. Menegazzo, E. Ghedini, M. Signoretto, *Molecules* **2018**, *23*, 1–18.

[19] B. Girisuta, Levulinic Acid from Lignocellulosic Biomass, University of Groningen, **2007**.

[20] V. Isoni, D. Kumbang, P. N. Sharratt, H. H. Khoo, *J. Environ. Manage.* **2018**, *214*, 267–275.

[21] Y. Shen, J. Sun, B. Wang, F. Xu, R. Sun, *Catalytic Approaches to the Production of Furfural and Levulinates From Lignocelluloses*, PhD Thesis. University Of Groningen, **2018**.

[22] Y. Román-Leshkov, C. J. Barrett, Z. Y. Liu, J. A. Dumesic, *Nature* **2007**, *447*, 982–985.

[23] D. J. Hayes, J. Ross, M. H. B. Hayes, S. Fitzpatrick, *Biorefineries-Industrial Process. Prod.* **2005**, *1*, DOI 10.1002/9783527619849.

[24] C. Moreau, A. Finiels, L. Vanoye, *J. Mol. Catal. A Chem.* **2006**, *253*, 165–169.

[25] M. E. Zakrzewska, E. Bogel-łukasik, R. Bogel-łukasik, *Chem. Rev.* **2011**, *111*, 397–417.

[26] J. C. van der Waal, E. de Jong, in *Ind. Biorenewables, A Pract. Viewp.* (Ed.: P.D. de María), **2016**, pp. 97–120.

[27] B. F. M. Kuster, *Starch - Stärke* **1990**, *42*, 314–321.

[28] R. J. van Putten, J. G. M. Winkelman, F. Keihan, J. C. van der Waal, E. de Jong, H. J. Heeres, *Ind. Eng. Chem. Res.* **2014**, *53*, 8285−8290.

[29] R. Rinaldi, R. Palkovits, F. Schüth, *Angew. Chemie - Int. Ed.* **2008**, *47*, 8047–8050.

[30] X. J. Ji, H. Huang, Z. K. Nie, L. Qu, Q. Xu, G. T. Tsao, *Fuels and Chemicals from Hemicellulose Sugars*, Springer, Berlin, Heidelberg, **2011**.

[31] V. Choudhary, S. H. Mushrif, C. Ho, A. Anderko, V. Nikolakis, N. S. Marinkovic, A. I. Frenkel, S. I. Sandler, D. G. Vlachos, *J. Am. Chem. Soc.* **2013**, *135*, 3997–4006.

[32] W. Deng, Q. Zhang, Y. Wang, *Sci. China Chem.* **2015**, *58*, 29–46.

[33] A. Mukherjee, M. J. Dumont, V. Raghavan, *Biomass and Bioenergy* **2015**, *72*, 143–183.

[34] G. J. Mulder, *J. für Prakt. Chemie* **1840**, *19*, 362–376.

[35] M. Sasaki, T. Adschiri, K. Arai, *J. Agric. Food Chem.* **2003**, *51*, 5376–5381.

[36] N. Brun, **2013**, DOI 10.1016/j.carbon.2013.05.001.

[37] B. V. Timokhin, V. A. Baransky, G. D. Eliseeva, *Russ. Chem. Rev.* **1999**, *68*, 73–84.

[38] R. H. Leonard, *Ind. Eng. Chem.* **1956**, *48*, 1330–1341.

[39] J. J. Bozell, L. Moens, D. C. Elliott, Y. Wang, G. G. Neuenscwander, S. W. Fitzpatrick, R. J.

Bilski, J. L. Jarnefeld, *Resour. Conserv. Recycl.* **2000**, *28*, 227–239.

[40] V. Ghorpade, H. Milford, *Industrial Applications for Levulinic Acid. In: Cereals*, Springer, Boston, MA, **1997**.

[41] X. Cao, J. Wei, H. Liu, X. Lv, X. Tang, X. Zeng, Y. Sun, T. Lei, S. Liu, L. Lin, *J. Chem. Technol. Biotechnol.* **2019**, *94*, 167–177.

[42] A. F. Sousa, C. Vilela, A. C. Fonseca, M. Matos, C. S. R. Freire, G.-J. M. Gruter, J. F. J. Coelho, A. J. D. Silvestre, *Polym. Chem.* **2015**, *6*, 5961–5983.

[43] A. C. Cardiel, B. J. Taitt, K. S. Choi, *ACS Sustain. Chem. Eng.* **2019**, *7*, 11138–11149.

[44] E. De Jong, M. A. Dam, L. Sipos, in *Biobased Monomers, Polym. Mater.*, **2012**, pp. 1–13.

[45] A. J. J. E. Eerhart, A. P. C. Faaij, M. K. Patel, *Energy Environ. Sci.* **2012**, *5*, 6407–6422.

[46] S. K. Burgess, J. E. Leisen, B. E. Kraftschik, C. R. Mubarak, R. M. Kriegel, W. J. Koros, *Macromolecules* **2014**, *47*, 1383–1391.

[47] M. Chidambaram, A. T. Bell, *Green Chem.* **2010**, *12*, 1253.

[48] S. Zhong, R. Daniel, H. Xu, J. Zhang, D. Turner, M. L. Wyszynski, P. Richards, *Energy and Fuels* **2010**, *24*, 2891–2899.

[49] A. A. Rosatella, S. P. Simeonov, R. F. M. Frade, C. A. M. Afonso, *Green Chem.* **2011**, *13*, 754.

[50] E. de Jong, T. Vijlbrief, R. Hijkoop, G. J. M. Gruter, J. C. van der Waal, *Biomass and Bioenergy* **2012**, *36*, 151–159.

[51] D. W. Rackemann, W. O. Doherty, *Biofuels, Bioprod. Biorefining* **2011**, *5*, 198–214.

[52] T. Wang, M. W. Nolte, B. H. Shanks, *Green Chem.* **2014**, *16*, 548–572.

[53] C. Sievers, I. Musin, T. Marzialetti, M. B. V. Olarte, P. K. Agrawal, C. W. Jones, *ChemSusChem* **2009**, *2*, 665–671.

[54] A. Muralidhara, P. Tosi, A. Mija, N. Sbirrazzuoli, C. Len, V. Engelen, E. de Jong, G. Marlair, *ACS Sustain. Chem. Eng.* **2018**, 16692–16701.

[55] A. Schweizer, *Recl. des Trav. Chim. des Pays-Bas* **1938**, *57*, 345–382.

[56] I. V Sumerskii, S. M. Krutov, M. Y. Zarubin, **2010**, *83*, 320–327.

[57] C. Chang, X. MA, P. CEN, *Chinese J. Chem. Eng.* **2006**, *14*, 708–712.

[58] A. Ukalska-Jaruga, A. Klimkowicz-Pawlas, B. Smreczak, *Soil Use Manag.* **2019**, 1–12.

[59] D. Zhang, H. Dang, Z. Li, C. Zhang, *Environ. Pollut.* **2019**, *252*, 296–304.

[60] D. J. Hayes, S. Fitzpatrick, M. H. B. Hayes, J. R. H. Ross, *Biorefineries-Industrial Processes and Products.*, Weinheim Wiley-VCH, **2006**.

[61] B. F. M. Kuster, H. M. G. Temmink, *Carbohydr. Res.* **1977**, *54*, 185–191.

[62] R. Weingarten, J. Cho, R. Xing, W. C. Conner, G. W. Huber, *ChemSusChem* **2012**, *5*, 1280–1290.

[63] S. K. R. Patil, J. Heltzel, C. R. F. Lund, *Energy and Fuels* **2012**, *26*, 5281–5293.

[64] V. V Ordomsky, V. L. Sushkevich, J. C. Schouten, J. Van Der Schaaf, T. A. Nijhuis, *J. Catal.* **2013**, *300*, 37–46.

[65] S. Kang, J. Yu, *Biomass and Bioenergy* **2016**, *95*, 214–220.

[66] I. Van Zandvoort, Y. Wang, C. B. Rasrendra, E. R. H. Van Eck, P. C. A. Bruijnincx, H. J. Heeres, B. M. Weckhuysen, *ChemSusChem* **2013**, *6*, 1745–1758.

[67] S. Agarwal, D. van Es, H. J. Heeres, *J. Anal. Appl. Pyrolysis* **2017**, *123*, 134–143.

[68] Z. Lin, M. Ierapetritou, N. Vladimiros, *AIChE J.* **2013**, *59*, 2079–2087.

[69] A. Mija, J. C. van der Waal, G. van Klink, E. de Jong, *Humins-Containing Foam*, **2016**, WO2017074183A8.

[70] A. Mija, J. C. van der Waal, E. de Jong, G. P. M. van Klink, *Process for the Modification of Humins*, **2018**, WO 2018/062995 A1.

[71] B. Girisuta, L. P. B. M. Janssen, H. J. Heeres, *Green Chem.* **2006**, *8*, 701–709.

[72] Horvat Jaroslav, Klaic Branimir, Metelko Biserka, Sunjic Vitomir., *Croat. Chem. Acta* **1986**, *59*, 429–438.

[73] R. Choowang, J. Lin, G. Zhao, *BioResources* **2019**, *14*, 943–953.

[74] B. Girisuta, L. P. B. M. Janssen, H. J. Heeres, *Ind. Eng. Chem. Res.* **2007**, *46*, 1696–1708.

[75] K. D. Baugh, P. L. McCarty, *Biotechnol. Bioeng.* **1988**, *31*, 50–61.

[76] G. C. A. Luijkx, F. van Rantwijk, H. van Bekkum, *Carbohydr. Res.* **1993**, *242*, 131–139.

[77] S. K. R. Patil, C. R. F. Lund, *Energy and Fuels* **2011**, *25*, 4745–4755.

[78] C. Sievers, M. B. Valenzuela-olarte, T. Marzialetti, I. Musin, P. K. Agrawal, C. W. Jones, *Ind. Eng. Chem. Res.* **2009**, *48*, 1277–1286.

[79] M. Conrad, M. Guthzeit, *Berichte der Dtsch. Chem. Gesellschaft* **1885**, *18*, 439–444.

[80] H. Zhao, J. E. Holladay, H. Brown, Z. C. Zhang, *Science (80-.).* **2007**, *316*, 1597–1600.

[81] G. Yong, Y. Zhang, J. Y. Ying, *Angew. Chemie - Int. Ed.* **2008**, *47*, 9345–9348.

[82] H. Kimura, M. Nakahara, N. Matubayasi, *J. Phys. Chem. A* **2011**, *115*, 14013–14021.

[83] P. Yazdani, B. Wang, S. Rimaz, S. Kawi, A. Borgna, *Mol. Catal.* **2019**, *466*, 138–145.

[84] J. Pang, M. Zheng, X. Li, Y. Jiang, Y. Zhao, A. Wang, J. Wang, X. Wang, T. Zhang, *Appl. Catal. B Environ.* **2018**, *239*, 300–308.

[85] C. Li, G. Xu, C. Wang, L. Ma, Y. Qiao, Y. Zhang, Y. Fu, *Green Chem.* **2019**, *21*, 2234–2239.

[86] C. Moreau, M. N. Belgacem, A. Gandini, *Top. Catal.* **2004**, *27*, 11–30.

[87] C. Moreau, R. Durand, S. Razigade, J. Duhamet, P. Faugeras, P. Rivalier, R. Pierre, G. Avignon, *Appl. Catal. A Gen.* **1996**, *145*, 211–224.

[88] B. F. M. Kuster, *Carbohydr. Res.* **1977**, *54*, 177–183.

[89] S. Amarasekara, Ananda, A. Razzaq, *Carbohydr. Res.* **2014**, *386*, 86–91.

[90] F. S. Asghari, H. Yoshida, *Ind. Eng. Chem. Res.* **2007**, *46*, 7703–7710.

[91] M.-M. Titirici, R. J. White, N. Brun, V. L. Budarin, D. S. Su, F. del Monte, J. H. Clark, M. J. MacLachlan, *Chem. Soc. Rev.* **2015**, *44*, 250–290.

[92] J. Shen, C. E. Wyman, *AIChE J.* **2012**, *58*, 236–246.

[93] B. F. M. Kuster, H. S. van der Baan, *Carbohydr. Res.* **1977**, *54*, 165–176.

[94] B. Cheng, X. Wang, Q. Lin, X. Zhang, L. Meng, R. C. Sun, F. Xin, J. Ren, *J. Agric. Food Chem.* **2018**, *66*, 11981–11989.

[95] B. F. M. Kuster, H. J. C. D. Van Steen, *Starch - Stärke* **1977**, *29*, 99–103.

[96] L. Faba, D. Garcés, E. Díaz, S. Ordóñez, *ChemSusChem* **2019**, 1–10.

[97] S. G. Wettstein, D. M. Alonso, Y. Chong, J. A. Dumesic, *Energy Environ. Sci.* **2012**, *5*, 8199–8203.

[98] D. Mercadier, L. Rigal, A. Gaset, J.-P. Gorrichon, *J. Chem. Technol. Biotechnol.* **1981**, *31*, 489–496.

[99] C. Moreau, in *Catal. Fine Chem. Synth. 4*, John Wiley & Sons Ltd, Chichester, West Sussex, **2006**, p. 141.

[100] W. Mamo, Y. Chebude, C. Márquez-Álvarez, I. Díaz, E. Sastre, *Catal. Sci. Technol.* **2016**, 2766–2774.

[101] R. M. Musau, R. M. Munavu, *Biomass* **1987**, *13*, 67–74.

[102] M. R. Whitaker, A. Parulkar, P. Ranadive, R. Joshi, N. A. Brunelli, *ChemSusChem* **2019**, *12*, 2211–2219.

[103] Z. Cao, Z. Fan, Y. Chen, M. Li, T. Shen, C. Zhu, H. Ying, *Appl. Catal. B Environ.* **2019**, *244*, 170–177.

[104] X. Fang, Z. Wang, B. Yuan, W. Song, S. Li, W. Lin, *ChemistrySelect* **2018**, *3*, 12243–12249.

[105] G. Gómez Millán, S. Hellsten, A. W. T. King, J. P. Pokki, J. Llorca, H. Sixta, *J. Ind. Eng. Chem.* **2019**, *72*, 354–363.

[106] P. Maneechakr, S. Karnjanakom, *Res. Chem. Intermed.* **2019**, *45*, 743–756.

[107] Y. Zuo, Y. Zhang, Y. Fu, *ChemCatChem* **2014**, *6*, 753–757.

[108] S. Xu, D. Pan, Y. Wu, N. Xu, H. Yang, L. Gao, W. Li, G. Xiao, *Ind. Eng. Chem. Res.* **2019**, *58*, 9276–9285.

[109] B. Girisuta, L. P. B. M. Janssen, H. J. Heeres, *Chem. Eng. Res. Des.* **2006**, *84*, 339–349.

[110] L. Zhang, G. Xi, Z. Chen, Z. Qi, X. Wang, *Chem. Eng. J.* **2017**, *307*, 877–883.

[111] D. Garcés, L. Faba, E. Díaz, S. Ordóñez, *ChemSusChem* **2019**, *12*, 924–934.

[112] P. Ramesh, A. Kritikos, G. Tsilomelekis, *React. Chem. Eng.* **2019**, *4*, 273–277.

[113] S. Liu, K. Wang, H. Yu, B. Li, S. Yu, *Sci. Rep.* **2019**, *9*, 1–9.

[114] B. Velaga, R. P. Parde, J. Soni, N. R. Peela, *Microporous Mesoporous Mater.* **2019**, *287*, 18–28.

[115] Crossley, Steven, Faria, Jimmy, Shen, Min, Resasco, Daniel E., *Science (80-.).* **2009**, *327*, 68.

[116] G. W. Huber, J. N. Chheda, C. J. Barrett, J. A. Dumesic, *Science (80-.).* **2005**, *308*, 1446–1450.

[117] C. L. Williams, C. C. Chang, P. Do, N. Nikbin, S. Caratzoulas, D. G. Vlachos, R. F. Lobo, W. Fan, P. J. Dauenhauer, *ACS Catal.* **2012**, *2*, 935–939.

[118] M. Hronec, K. Fulajtárova, T. Liptaj, M. Štolcová, N. Prónayová, T. Soták, *Biomass and Bioenergy* **2014**, *63*, 291–299.

[119] T. V. Bui, S. Crossley, D. E. Resasco, *Chem. Fuels from Bio-Based Build. Blocks* **2016**, 431–494.

[120] Y. Yang, Z. Du, Y. Huang, F. Lu, F. Wang, J. Gao, J. Xu, *Green Chem.* **2013**, *15*, 1932–1940.

[121] J. Yang, N. Li, G. Li, W. Wang, A. Wang, X. Wang, Y. Cong, T. Zhang, *Chem. Commun.* **2014**, *50*, 2572–2574.

[122] A. W. Beck, A. J. O'Brien, G. G. Zaimes, D. E. Resasco, S. P. Crossley, V. Khanna, *ACS Sustain. Chem. Eng.* **2018**, *6*, 5826–5834.

[123] J. Fischer, W. F. Hölderich, *Appl. Catal. A Gen.* **1999**, *180*, 435–443.

[124] D. T. Ngo, T. Sooknoi, D. E. Resasco, *Appl. Catal. B Environ.* **2018**, *237*, 835–843.

[125] T. Omotoso, L. V. Herrera, T. Vann, N. M. Briggs, L. A. Gomez, L. Barrett, D. Jones, T. Pham, B. Wang, S. P. Crossley, *Appl. Catal. B Environ.* **2019**, DOI 10.1016/j.apcatb.2019.04.079.

[126] G. J. Mulder, *J. Pr. Chemie* **1840**, *21*, 321–370.

[127] C. Sievers, T. Marzialetti, T. J. Hoskins, M. B. V. Olarte, P. K. Agrawal, C. W. Jones, *Bioresour. Technol.* **2009**, *100*, 4758–4765.

[128] E. H. Novotny, M. H. B. Hayes, E. R. de Azevedo, T. J. Bonagamba, S. W. Fitzpatrick, in *Int. Biochar Initiat. Conf.*, Terrigal, Australia, **2007**.

[129] F. S. Asghari, H. Yoshida, *Ind. Eng. Chem. Res.* **2006**, 2163–2173.

[130] K. J. Z. S. P. Daniel, *S. P. Daniel, K. J. Zeitsch,* **2000**, WO 0047569 A1.

[131] R. Hashaikeh, I. S. Butler, J. A. Kozinski, *Energy & fuels* **2006**, *20*, 2743–2747.

[132] A. Chuntanapum, Y. Matsumura, *Ind. Eng. Chem. Res.* **2009**, *48*, 9837–9846.

[133] A. Gandini, M. N. Belgacem, *Prog. Polym. Sci.* **1997**, *22*, 1203–1379.

[134] G. W. Huber, J. A. Dumesic, *Catal. Today* **2006**, *111*, 119–132.

[135] S. J. Dee, A. T. Bell, *ChemSusChem* **2011**, *1462*, 1166–1173.

[136] R. Weingarten, J. Cho, W. C. Conner, G. W. Huber, *Green Chem.* **2010**, *12*, 1423–1429.

[137] H. Rasmussen, H. R. Sørensen, A. S. Meyer, *Carbohydr. Res.* **2013**, DOI 10.1016/j.carres.2013.08.029.

[138] G. Yang, E. A. Pidko, E. J. M. Hensen, *J. Catal.* **2012**, *295*, 122–132.

[139] J. Horvat, B. Klaić, B. Metelko, V. Šunjić, *Tetrahedron Lett.* **1985**, *26*, 2111–2114.

[140] N. Shi, Q. Liu, R. Ju, X. He, Y. Zhang, S. Tang, L. Ma, *ACS Omega* **2019**, *4*, 7330–7343.

[141] I. Van Zandvoort, E. R. H. Van Eck, P. De Peinder, H. J. Heeres, P. C. A. Bruijnincx, B. M. Weckhuysen, *ACS Sustain. Chem. Eng.* **2015**, *3*, 533–543.

[142] S. Constant, C. S. Lancefield, B. M. Weckhuysen, P. C. A. Bruijnincx, *ACS Sustain. Chem. Eng.* **2017**, *5*, 965–972.

[143] I. van Zandvoort, E. J. Koers, M. Weingarth, P. C. A. Bruijnincx, M. Baldus, B. M. Weckhuysen, *Green Chem.* **2015**, *17*, 4383–4392.

[144] N. Shi, Q. Liu, H. Cen, R. Ju, X. He, L. Ma, *Biomass Convers. Biorefinery* **2019**, 1–11.

[145] M. Sevilla, A. B. Fuertes, *Carbon N. Y.* **2009**, *47*, 2281–2289.

[146] M. Sevilla, A. B. Fuertes, *Chem. - A Eur. J.* **2009**, *15*, 4195–4203.

[147] N. Baccile, G. Laurent, F. Babonneau, F. Fayon, M.-M. Titirici, M. Antonietti, *J. Phys. Chem. C* **2009**, *113*, 9644–9654.

[148] M.-M. Titirici, A. Thomas, M. Antonietti, *New J. Chem.* **2007**, *31*, 787.

[149] M. M. Titirici, R. J. White, C. Falco, M. Sevilla, *Energy Environ. Sci.* **2012**, *5*, 6796–6822.

[150] X. Sun, Y. Li, *Angew. Chemie Int. Ed.* **2004**, *43*, 597–601.

[151] C. Yao, Y. Shin, L. Q. Wang, C. F. Windisch, W. D. Samuels, B. W. Arey, C. Wang, W. M. Risen, G. J. Exarhos, *J. Phys. Chem. C* **2007**, *111*, 15141–15145.

[152] M.-M. Titirici, M. Antonietti, N. Baccile, *Green Chem.* **2008**, *10*, 1204.

[153] Y. Mi, W. Hu, Y. Dan, Y. Liu, *Mater. Lett.* **2008**, *62*, 1194–1196.

[154] C. Falco, N. Baccile, M.-M. Titirici, *Green Chem.* **2011**, *13*, 3273.

[155] J. Ryu, Y. W. Suh, D. J. Suh, D. J. Ahn, *Carbon N. Y.* **2010**, *48*, 1990–1998.

[156] R. Demir-cakan, N. Baccile, M. Antonietti, M. Titirici, *Chem. Mater.* **2009**, *21*, 484–490.

[157] J. Liu, P. Tian, J. Ye, L. Zhou, W. Gong, Y. Lin, G. N. Ã, *Chem. Lett.* **2009**, *38*, 948–949.

[158] T. M. C. Hoang, L. Lefferts, K. Seshan, *ChemSusChem* **2013**, *6*, 1651–1658.

[159] C. B. Rasrendra, M. Windt, Y. Wang, S. Adisasmito, I. G. B. N. Makertihartha, E. R. H. Van Eck, D. Meier, H. J. Heeres, *J. Anal. Appl. Pyrolysis* **2013**, *104*, 299–307.

[160] Y. Wang, S. Agarwal, A. Kloekhorst, H. J. Heeres, *ChemSusChem* **2016**, *9*, 2016.

[161] E. Bartels, Über Die Bildung von Huminstoffen Aus Ketosen Durch Einwirkung Konzentrierter Halogenwasserstoffsäuren, Hamburg University, **1966**.

[162] R. R. Davda, J. W. Shabaker, G. W. Huber, R. D. Cortright, J. A. Dumesic, *Appl. Catal. B Environ.* **2005**, *56*, 171–186.

[163] R. D. Cortright, R. R. Davda, J. A. Dumesic, *Mater. Sustain. Energy A Collect. Peer-Reviewed Res. Rev. Artic. from Nat. Publ. Gr.* **2011**, 289–292.

[164] J. Zakzeski, B. M. Weckhuysen, *ChemSusChem* **2011**, *4*, 369–378.

[165] Z. Cheng, J. Everhart, G. Tsilomelekis, V. Nikolakis, B. Saha, D. Vlachos, *Green Chem.* **2018**, *20*, 997–1006.

[166] P. Tosi, G. P. M. van Klink, A. Celzard, V. Fierro, L. Vincent, E. de Jong, A. Mija, *ChemSusChem* **2018**, *11*, 2797–2809.

[167] A. Mija, J. C. Van Der Waal, J. Pin, N. Guigo, E. De Jong, *Constr. Build. Mater.* **2016**, *139*, 594–601.

[168] Y. Wang, S. Agarwal, Z. Tang, H. J. Heeres, *RSC Adv.* **2017**, *7*, 5136–5147.

[169] F. Stankovikj, A. G. McDonald, G. L. Helms, M. Garcia-Perez, *Energy and Fuels* **2016**, 6505–6524.

[170] J. Feijen, G. Klink, E. Jong, A. Schmid, N. Deen, M. Boot, *SAE Tech. Pap. Ser.* **2017**, *1*, DOI 10.4271/2017-24-0119.

[171] Y. Wang, S. Agarwal, A. Kloekhorst, H. J. Heeres, *ChemSusChem* **2016**, *9*, 951–961.

[172] E. Pfab, L. Filiciotto, A. A. Romero, R. Luque, *Ind. Eng. Chem. Res.* **2019**, DOI

10.1021/acs.iecr.9b00893.

[173] S. G. Maerten, D. Voß, M. A. Liauw, J. Albert, *ChemistrySelect* **2017**, *24*, 7296–7302.

[174] A. Muralidhara, A. Bado-Nilles, G. Marlair, V. Engelen, C. Len, P. Pandard, *Biofuels, Bioprod. Biorefining* **2019**, *13*, 464–470.

[175] S. Kang, G. Zhang, Q. Yang, J. Tu, X. Guo, F. G. F. Qin, Y. Xu, *BioResources* **2016**, *11*, 9496–9505.

[176] A. Mija, E. de Jong, J. C. van der Waal, G. P. M. van Klink, *Humins-Containing Foams*, **2017**.

[177] J. Merle, M. Birot, H. Deleuze, C. Mitterer, H. Carré, F. C. El Bouhtoury, *Mater. Des.* **2016**, *91*, 186–192.

[178] BING, in *Rep. N1* (Ed.: F. of E.R.P.F. Associations), Federation Of European Rigid Polyurethane Foam Associations, **2006**, pp. 1–33.

[179] P. Tosi, G. P. van Klink, A. Celzard, V. Fierro, L. Vincent, E. de Jong, A. Mija, *ChemSusChem* **2018**, *11*, 2797-2809.

[180] A. Mija, E. de Jong, J. C. van der Waal, G. van Klink, *Humins Containing Foam*, **2017**, WO 2017074183 A1 20170504.

[181] A. Sanchez-Sanchez, M. T. Izquierdo, J. Ghanbaja, G. Medjahdi, S. Mathieu, A. Celzard, V. Fierro, *J. Power Sources* **2017**, *344*, 15–24.

[182] A. G. Pandolfo, A. F. Hollenkamp, *J. Power Sources* **2006**, *157*, 11–27.

[183] Ö. Gerçel, H. F. Gerçel, *Chem. Eng. J.* **2007**, *132*, 289–297.

[184] W. Avantium, *ChemInform Abstract : Biomass - Derived Porous Carbon Materials : Synthesis and Catalytic Applications Biomass-Derived Porous Carbon Materials : Synthesis and Catalytic Applications*, **2015**.

[185] N. P. Wickramaratne, M. Jaroniec, *ACS Appl. Mater. Interfaces* **2013**, *5*, 1849–1855.

[186] H. A. Patel, J. Byun, C. T. Yavuz, *ChemSusChem* **2017**, *10*, 1303–1317.

[187] F. Björnerbäck, N. Hedin, *ACS Sustain. Chem. Eng.* **2019**, *7*, 1018−1027.

[188] S. Kang, J. Fu, Z. Deng, S. Jiang, G. Zhong, Y. Xu, J. Guo, J. Zhou, *Sustain.* **2018**, *10*, 16–19.

[189] G. Yang, H. Chen, H. Qin, Y. Feng, *Appl. Surf. Sci.* **2014**, *293*, 299–305.

[190] N. G. Rincón-silva, J. C. Moreno-piraján, L. G. Giraldo, *J. Chem.* **2015**, *2015*, 1–12.

[191] S. Altenor, B. Carene, E. Emmanuel, J. Lambert, J. Ehrhardt, S. Gaspard, *J. Hazard. Mater.* **2009**, *165*, 1029–1039.

[192] L. Li, L. Liu, M. Gao, W. Hong, Z. Liu, L. Fan, B. Hu, *J. Mater. Chem. A* **2014**, *2*, 1795–1801.

[193] H. Sayğılı, F. Güzel, *J. Clean. Prod.* **2016**, *113*, 995–1004.

[194] S. Kang, S. Jiang, Z. Peng, Y. Lu, J. Guo, J. Li, W. Zeng, X. Lin, *Biomass Convers. Biorefinery* **2018**, *8*, 889–897.

[195] D. Chernysheva, Y. Chus, V. Klushin, T. Lastovina, L. Pudova, N. Smirnova, O. Kravchenko, V. Chernyshev, V. P. Ananikov, *ChemSusChem* **2018**, *11*, 3599–3608.

[196] M. Molina-Sabio, M. T. González, F. Rodriguez-Reinoso, A. Sepúlveda-Escribano, *Carbon*

N. Y. **1996**, *34*, 505–509.

[197] J. M. Pin, N. Guigo, A. Mija, L. Vincent, N. Sbirrazzuoli, J. C. van der Waal, E. de Jong, *ACS Sustain. Chem. Eng.* **2014**, *2*, 2182-2190.

[198] S. Kang, J. Fu, G. Zhang, W. Zhang, H. Yin, Y. Xu, *Polymers (Basel).* **2017**, *9*, 373.

[199] A. Sangregorio, N. Guigo, J. C. van der Waal, N. Sbirrazzuoli, *ChemSusChem* **2018**, DOI 10.1002/cssc.201802066.

[200] A. Sangregorio, N. Guigo, J. C. Van Der Waal, N. Sbirrazzuoli, *Compos. Sci. Technol.* **2019**, *171*, 70–77.

[201] R. Dinu, A. Mija, *Green Chem.* **2019**, DOI 10.1039/c9gc01813a.

[202] L. Filiciotto, A. M. Balu, A. A. Romero, E. Rodríguez-Castellón, J. C. Van Der Waal, R. Luque, *Green Chem.* **2017**, *19*, DOI 10.1039/c7gc01405h.

[203] A. Bohre, D. Gupta, M. I. Alam, R. K. Sharma, B. Saha, *ChemistrySelect* **2017**, *2*, 3129–3136.

[204] I. B. Adilina, T. Hara, N. Ichikuni, S. Shimazu, *J. Mol. Catal. A Chem.* **2012**, *361*, 72–79.

3 Auto-crosslinked rigid foams derived from industrial humins*

3.1 Chapter content

In this chapter a new macroporous foam-like material based on autocross-linked humins is presented. Humins foams are obtained by a simple heating process, without any kind of pre-treatment and with high control on morphology, porosity and carbon content. Untreated humins have been characterized by chromatography, elemental analysis and FT-IR, while the mechanism of foaming was elucidated by a combination of thermal and rheological analyses. A preliminary screening of conditions was conducted for identifying the parameters controlling this foaming process, by which were produced in a controlled way open and closed cells with cell diameters between 0.2 and 3.5 mm. Humins foams were characterized by Raman, FT-IR, SEM, nitrogen adsorption, pycnometry and mechanical tests. The results show that, based on humins, it is possible to obtain porous materials with controlled architectures and a range of parameters that can be tailored, depending on the foreseen applications.

*Published as: P. Tosi, G. P. M. van Klink, A. Celzard, V. Fierro, L. Vincent, E. de Jong, A. Mija, *ChemSusChem* **2018**, *11*, 2797-2809. doi.org/10.1002/cssc.201800778.

3.2 Introduction

3.2.1 Importance of porous materials

Porous materials have a number of key applications such as catalysis,[1,2] separation,[3] sensors,[4] ion-exchange,[5] etc. Depending on the expected applications important parameters, apart from the IUPAC classification on pore size, are the effective and apparent porosity, the specific surface area, the cell morphology, etc. A distinction can also be made between open and closed cells, whether the internal area of each cell is accessible or not. In particular, porous carbons derived from sustainable precursors were shown to have important applications, although these are rather limited to micro- or meso-porous activated carbons (ACs) at the industrial scale.[6,7] Purely mesoporous carbon materials are generally achieved by sacrificial templating followed by high temperatures of carbonization. Thus far, a few studies have been conducted[7–12] to achieve highly porous functional carbon materials from renewable precursors. This research topic is rapidly growing, attracting interest thanks to the clear economic advantage, the more sustainable chemistry, and the broad range of possible applications. Despite this, important drawbacks have been reported in the synthesis of biomass-based materials, mainly related to the poor control on some key characteristics such as batch-to-batch reproducibility, morphology, porosity, uniformity, surface chemistry, along with the disadvantageous use of toxic chemicals that still might be required. Therefore, biomass precursors that would be both repeatable and easy to use, as well as requiring cost-effective and sustainable synthesis routes, would be most welcome.

3.2.2 Humins

Renewable resources and low-cost biomass in particular have attracted considerable interest during the last decades as valid alternatives to the massive use of fossil resources. Among them, lignocellulosic biomass represents an appealing option, since they are one the most abundant carbon source available in nature.[13–16] Sugars can be obtained from lignocellulosic biomass[17] and subsequently converted by biorefinery methods into several platform chemicals. Industrially relevant compounds are 5-hydroxymethyl furfural (HMF) and levulinic acid (LA), derived from the acid-catalyzed dehydration (ACD) of fructose and/or glucose obtained from lignocellulosic biomass.[18] Unavoidably, during the ACD process a large amount of insoluble polymeric by-products called humins are also formed (Scheme 3.1).[19–26] Humins are dark-coloured high viscous polymeric materials, mainly derived from random and

incontrollable condensations of HMF, its precursors and its derivatives in acidic catalytic conditions. Despite several attempts for preventing the formation of humins, their production can never be avoided and represents the main drawback for an industrial scale ACD step. In terms of molecular structure, humins are influenced by the operational conditions used during the ACD process of sugars (*e.g.* the natures of solvent, feedstock and catalyst used, sugars concentration, temperature, residence time, post-treatment, etc.). Therefore, these recalcitrant organic materials are rather ill-defined and their structure is still under investigation. Very recently, Cheng *et al.*[27] identified the electron-donor–acceptor type interaction of humins fragments, indicating that a significant fraction of humins are actually made up by agglomerate of oligomers interacting by weak forces rather than real macromolecules.

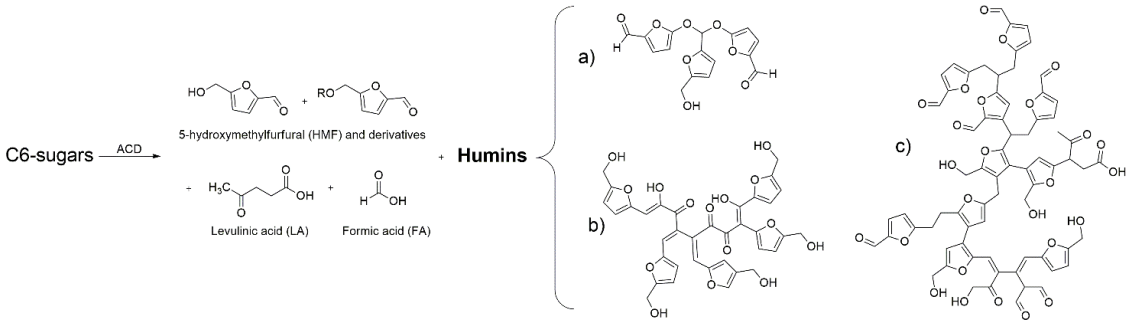

Scheme 3.1 Products of acid catalysed dehydration of sugars.[18] Examples of humins structures proposed by a) Sumerskii et al.[28], b) Patil and Lund[29] and c) Van Zandvoort *et al.*[30][31]

However, industrial scale generate humins are definitely more complicated than a collection of ideal pure humins molecules, and should rather be considered as complex mixtures. Along with humins oligomers, other chemicals that were present in the reaction medium during the ACD industrial process are indeed entrapped in the matrix (solvents, products, by-products and catalyst), thus leading to much more complex and heterogeneous materials. On the other hand, purifying such by-products before its actual use as a feedstock is not desirable since it requires time, frequently not achievable and economically not interesting on an industrial level. As a feedstock of growing interest, industrial humins are attracting the interest of the scientific community, and recently several studies have been conducted in order to modify their structure or identify potential applications.[25,32,33]

Here, a new approach for humins applications is introduced, that does not require any kind of modification or isolation, and which can be directly applied to the industrial crude material.

Taking advantage of hydroxyl, aldehyde, ketone and acid groups, we oriented our research to realize auto-crosslinking reactions leading to a thermoset porous material.[34] It is shown that, by using a simple thermal treatment, it is indeed possible to obtain porous thermosets with tunable properties, just starting from crude industrial humins. These humins foams are porous tailored structures that might play an important role in future applications in well-defined fields such as water decontamination and energy,[35] which is a clear economic advantage for a biorefinery by-product.

3.3 Results and discussion

3.3.1 Analysis of humins samples

Using the crude industrial ACD derived humins mixture, i.e., without difficult and expensive purification steps, might be the key to develop economically interesting industrial applications.

To better understand the composition, reproducibility and reactivity-property relationships, several industrial humins samples prepared by various processing conditions have been subjected to chromatographic investigations by gas chromatography (GC) and ultra-performance liquid chromatography (UPLC). As presented in Table 3.1, the amount of 5-alkoxymethyl furaldehydes (RMF), including HMF and MMF (whether encapsulated or reactively generated), has been found between 11.5 and 16.5 wt.%. Other peaks were also found by UPLC, but all were estimated below 1 wt.%, and therefore were not reported here. The LA content in the humins mixture was found by GC analysis to be less than 2 wt.%. Also methyl levulinate (ML) was generally detected, but its amount was below 0.05%.

Elemental analyses were performed on six samples, and the results are reported in Table 3.2. The main elements present in crude humins were carbon, oxygen and hydrogen, although different other elements may be present in traces. Such traces could come from the industrial processes that led to humins formation or from the source of lignocellulosic biomass, and were generally estimated below 1 wt.%. The C amount varied from 53.4 to 57.7 % for the tested samples, while H was found in the range 5.2 - 5.9 %, and O was close to 40 %.

Table 3.1 GC and UPLC analysis of 6 representatives industrial humins samples

Sample	RMF %	LA %
H1	14.13	1.19
H2	12.35	1.49
H3	13	1.4
H4	12.59	1.41
H5	16.43	1.68
H6	11.5	1.25

Table 3.2 Elemental analysis of 6 representatives industrial humins samples

Sample	C%	H%	O%	Other (%)
H1	57.71	5.25	35.7	1.34
H2	53.48	5.87	40	0.65
H3	53.59	5.88	40.2	0.33
H4	54.61	5.74	39.5	0.15
H5	53.91	5.76	39.8	0.53
H6	53.43	5.89	39.7	0.98

According to these results, the humins composition can slightly change, depending on the sample. Those variations can be associated with optimizations in the industrial ACD process in terms of temperatures and solvents used, feedstocks, residence time, concentrations of reagents, etc. Despite these differences in chemical composition, all the experiments of auto-crosslinking and foaming performed on the six samples gave similar results. Therefore, we chose to focus the crude humins characterization only on the H6 sample, since it was the most readily available.

Fourier transform infrared spectroscopy (FT-IR) analyses were performed in order to detect the modifications in the humins chemical structure during the auto-crosslinking, depending on the thermodynamic parameters of reaction. In the raw humins, the presence of -OH groups can be evidenced by a peak at 3350 cm^{-1}, with a broad shape indicative of hydrogen bonds, as presented in Figure 3.1 and in Table 3.3. Carbonyls can be found in particular at 1705 and 1664 cm^{-1}, mainly associated to humins macromolecules and partly to free unbounded monomers (such as HMF, MMF and LA). These carbonyls can belong to several functionalities (aldehydes, ketones, esters, acids), as confirmed by the variety of peaks. The presence of furanic rings can be noticed by several signals in the entire spectrum (Table 3.3). Typical peaks associated to HMF can be found at 1190 and 1664 cm^{-1}, while the presence of ethers can be attributed by peaks in the 1300-960 cm^{-1} region. Most detected groups correspond to highly reactive

moieties, which justify the thermosetting aptitude of humins through crosslinking and condensation reactions.

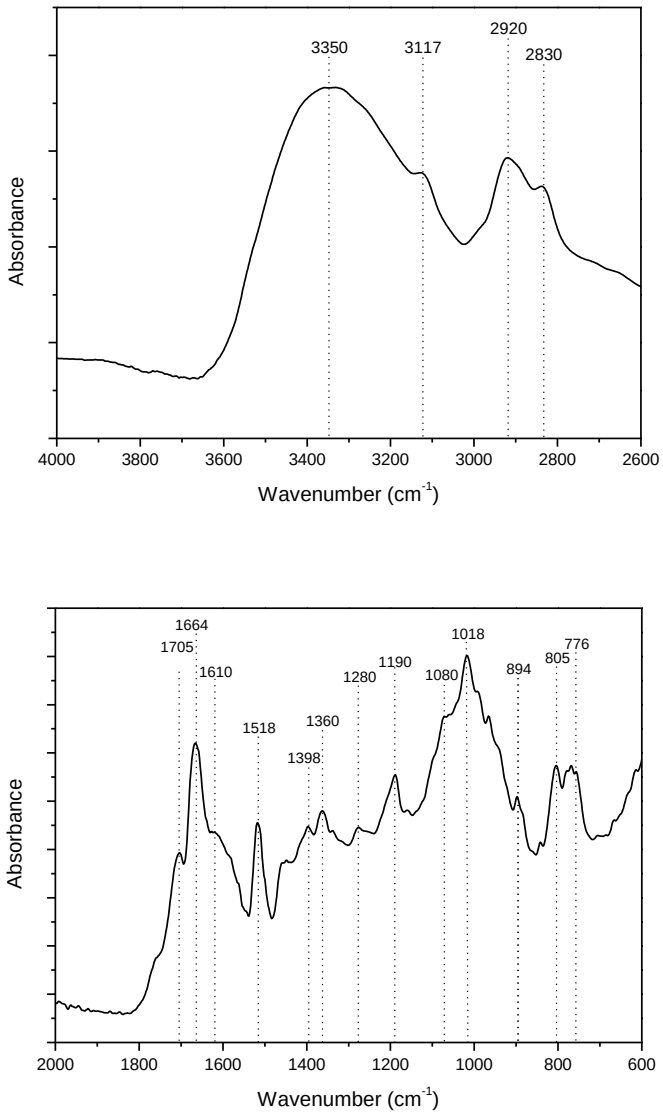

Figure 3.1 FT-IR of crude humins.

Table 3.3 Peaks assignments for FT-IR spectrum of crude humins.

cm^{-1}	**Assignment**
3350	-OH
3117	(C=C)-H
3920	C-H (sp^3)
2830	C=C
1705	conjugates C=O, COO, esters

1664	C=O, furan ring
1610, 1518	C=C, C=O, furan rings
1398	C=C in ring
1360	C-O
1280-1110	C-O, C-O-C
1190, 805, 776	furan ring
1080	(ethers, esters, furans)
1018	C-O (furan ring)
894	α-CH3 and α-CH2
850-760	=C-H, $=CH_2$, RCH=CHR (cis), C-H

3.3.2 Assessment of auto-crosslinking and foaming mechanisms

A polymeric foam can be produced from any kind of polymer, provided that the three following aspects are met: polymer in a low-viscosity state, gas release, and concomitant hardening of the material during the formation of bubbles.[36] According to this generalization, achieving foaming requires a poorly viscous material (in molten state or as unreacted mixture) that is able to solidify during a physicochemical treatment (by crosslinking), while the key factor is the formation and release of a gas accompanying the process.

As the thermal events in crude humins are hardly seen by Differential Scanning Calorimetry (DSC), the rheometric analysis was used as a proof that auto-crosslinking occurs during the heating program. The evolution of the complex viscosity of humins upon heating up to 200 °C is shown in Figure 3.2. The first critical range of temperatures is between 20 and 125 °C, as the humins viscosity drops by ~ 2.5 10^5 Pa·s. At 125 °C, the humins viscosity reaches a value as low as ~ 0.48 Pa·s, characteristic of a liquid state. Above 140 °C, fluctuations in the rheogram appear due to the onset of volatiles release, as observed by optical microscopy during heating. From then on, the changes of moduli are chaotic, and only trends are exploitable. The increase of viscosity starting at 170 °C can be associated with the initiation of auto-crosslinking reactions *via* internal condensations. For the H6-humins sample this temperature is the critical point in the process of condensation and curing, while volatiles are being generated from the sample bulk, setting the necessary conditions to obtain foams. These thermal phenomena are

subject to some small shifts in temperature when the same tests are performed on different humins samples (H1-H5). However, the aforementioned, successive, phenomena were always detected, and therefore the overall mechanism was confirmed for the whole series of samples tested.

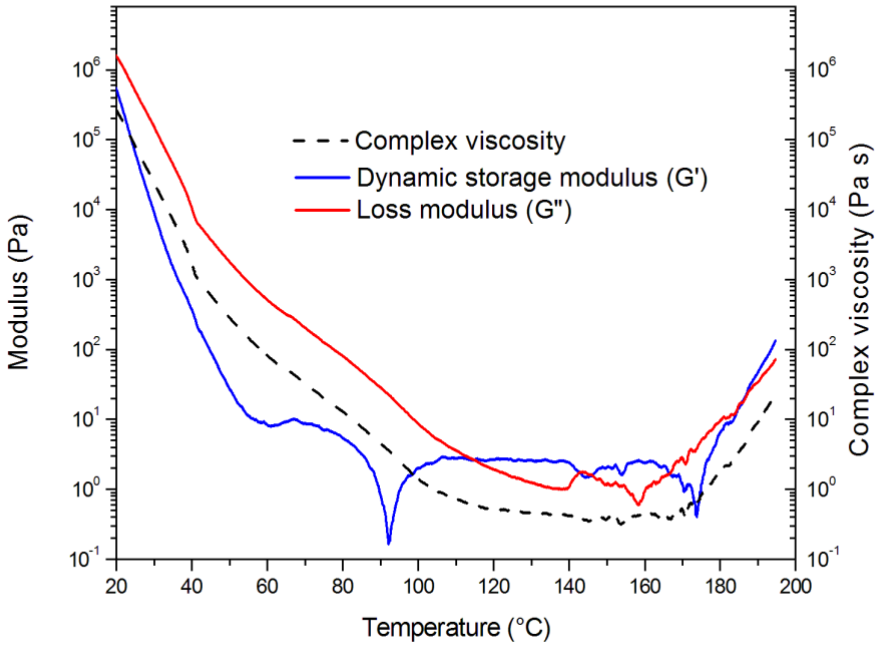

Figure 3.2 Rheometry analysis of crude humins.

The dynamic storage modulus (G') and the loss modulus (G") were plotted as function of temperature for extracting information about changes in the sample's viscoelastic state (Figure 3.2). G' measures the energy that a material stores per cycle and can be associated with the elastic contribution, while G" measures the energy dissipated or lost, and can be associated with the viscous contribution.[37] The phenomenon recorded on G' and localized at around 93° C is relative to some evaporation of adsorbed water, leading to a mass loss lower than 0.3 %, as confirmed by Thermogravimetric Analysis coupled with Mass Spectroscopy (TGA-MS). It should be mentioned that this water cannot be removed by high-vacuum treatment at moderate temperatures, nor by prolonged heat-treatments; hence this phenomenon should be taken into account also for the following tests. A first G' / G" crossover point was detected at 114.5 °C, and can be associated with the initiation of condensation reactions. The recorded fluctuations of G' and G" above 140 °C are associated with gas release, leading to bubbling at around 169 °C. A gelation point is present at around 186 °C, triggering

the formation of a giant macromolecular chain spanning the complete sample volume. Once initiated, crosslinking and condensation reactions continued and the hardening process became irreversible.

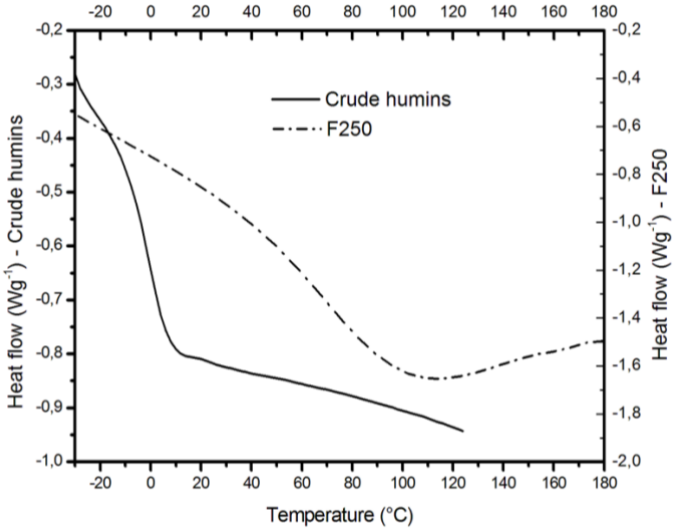

Figure 3.3 DSC comparison of *Tg* inflexions between crude and foamed humins.

In DSC analyses is possible to notice the shifting of the glass transition temperature (*Tg*) in thermal treated humins, which is related to the enhancement of the reticulation in the sample (Figure 3.3). The *Tg* midpoint (mathematically calculated) passes from -15 °C in crude humins to 66 °C in F250, leading to a rigid polymer at room temperature. Noteworthy, it is possible to note the wide range of temperature in which these transitions occur, ~40 °C for crude humins and more than 100 °C in F250, which clearly proves the heterogeneous nature of this material. As shown in FT-IR and chromatography, several species and moieties are present, and so different type of chemistry, timing and reaction temperatures are involved in the polymerization process of humins.

Thermogravimetric analysis (TGA) shows the thermal behaviour of humins and the mass loss associated with this heating process, along with information about the gases involved in the bubbling that led to the resultant macroporosity. A TGA comparison of H6 humins samples under air and N_2 is reported in Figure 3.4. In both environments, a first mass loss of 38-39 % occurred between 140 and 260 °C, with a maximum at 210-220 °C. This event can be assigned to the release of low-molecular mass species present in the humins composition or produced by condensation reactions. The polymerization between the chain fragments may also have occurred in this temperature interval. This is the range of temperatures characterizing the

foaming process, and therefore the gases here released were those directly implied in the nucleation of bubbles. The second event occurred between 280 and 340 °C, and corresponds to a mass loss of 19-20% under air and of less than 10% under nitrogen. The final event occurred only in air, up to 415 °C. It is related to the thermo-oxidative degradation of humins and led to the complete gasification of the sample at 560 °C. On the other hand, the thermogram under nitrogen showed that, at 1000 °C, ~ 26-27 % of residue was still present. This value is only slightly lower than that of pure furfuryl alcohol submitted to pyrolysis under argon (~ 40 %).[38]

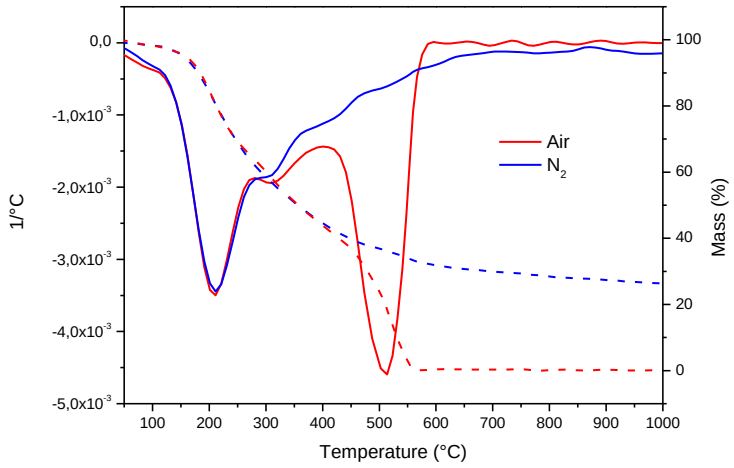

Figure 3.4 Thermogravimetric analyses comparison of H6 humins under air and under N_2: mass in % (dashed lines); differential in 1/°C (full lines).

In order to identify the species released during these mass loss steps, humins samples were subjected to investigation by TGA-MS under Ar (Figure 3.5). The first phenomenon started at 150 °C with a maximum at 203 °C, and is due to the combination of several peaks of mass loss relative to different species. CO and MeOH were detected along with CO_2, but the principal volatile species was water. Water can be released as by-product in condensation reactions (such as aldol condensation), leading to losses in oxygenated functional groups. A second mass loss started at 275 °C with a maximum at 315-340 °C and is again associated with water loss, with a contribution of CO_2 loss which had his maximum peak at 350 °C. Finally, a third mass loss step was detected with a maximum peak at 400-420 °C and was mainly associated to CO release. CH_4 was also detected with a peak at 500 °C, which overlapped the previous one.

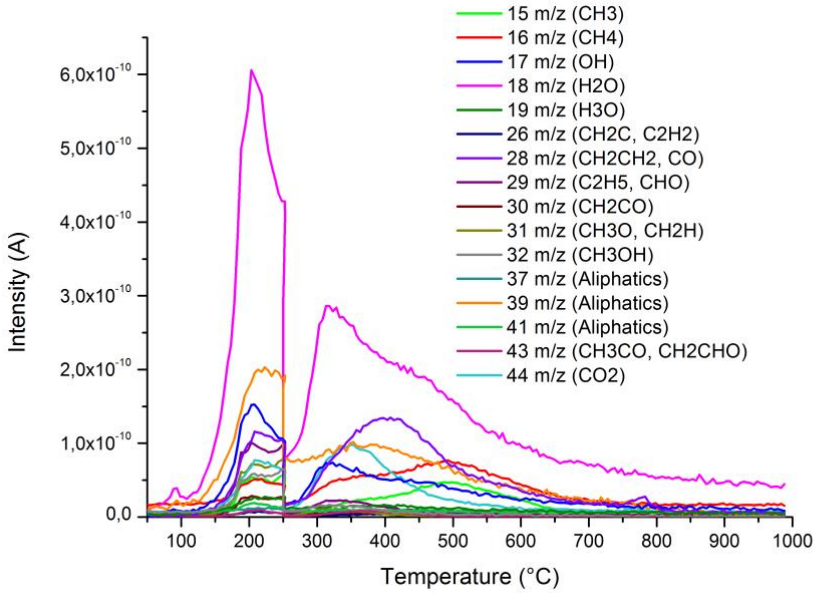

Figure 3.5 TGA-MS analyses of crude humins under Ar. Thermal program: heating from 25 to 250 °C at 5 °C·min^{-1}; 1 h isothermal step at 250 °C; heating from 250 to 1000 °C at 5 °C·min^{-1}. Gas: Ar, 50 mL·min^{-1}.

3.3.3 Foaming of humins

In order to identify which parameters govern the foaming process of crude humins under air, a preliminary screening with more than 70 experimental conditions was performed. The foams were evaluated in terms of reproducibility, homogeneity, morphology (cell dimensions), density, porosity, mechanical properties and proportion of open/closed cells as a function of the humins sample used, amount of material used, kind and dimensions of the crucible, heating ramp, residence time, gas flow and other relevant aspects.

In general, when a lower amount of humins was used, foams with smaller pores and higher homogeneity were obtained. Comparing the results obtained by using different crucibles, porcelain generally gave smaller pores and denser foams. Aluminium pans, on the other hand, tended to give foams with bigger pores and lower density.

Obviously, the thermal program is of first importance since, depending on final temperature, dynamic and / or isothermal heating, and heating rate, completely different cells morphology can be obtained. The duration of the isothermal step at the final temperature, instead, did not seem to influence the final material morphology.

Among all the thermal programs investigated, a 10 °C·min^{-1}-ramp generally led to more reproducible and uniform outcomes. All the samples tested gave comparable results, after

previous slight optimization of the parameters. Since we chose to continue the screening on one single sample, the H6 humins, which was the most readily available, all the foams preparation conditions and characterizations reported herein again refer to this sample.

Table 3.4 Screening of conditions for humins foaming (only the reproducible results are reported). Conditions A, B and C are the most reproducible. In all the experiments 1 hour isothermal step at the final temperarure was used.

Experiment	Heating rate (°C·min^{-1})	Final T (°C)	Crucible	Amount of crude humins used (g)	Minimum pore diameter (mm)	Maximum pore diameter (mm)
A01	10	175	Ceramic	5.4	0.2	0.8
A02	20	175	Ceramic	52	0.9**	2**
A03	10	175	Aluminium	5.7	0.2	0.9
A	**10**	**180**	**Ceramic**	**50**	**0.4-1.3****	**2.4-3.5****
B01	10	200	Ceramic	5	0.5	0.8
B02	0.85	220	Aluminum	21.2	0.5	1.2
B03	0.85	220	Ceramic	5	0.6	1.1
B04	2	220	Aluminum	10.4	0.4	1.1
B05	2	220	Ceramic	10.2	0.4	1
B06	5	220	Aluminium	31	*	*
B07	10	220	Aluminium	32.5	*	*
B08	10	220	Aluminium	11	0.6	2
B09	10	220	Ceramic	32.6	0.5	1.3
B10	20	220	Aluminium	32	2	3
B11	20	220	Aluminium	21.2	0.5	1.5
B12	20	220	Aluminum	21.3	0.5	1.5
B13	20	220	Ceramic	5.7	0.6	1
B14	20	220	Ceramic	5.4	0.4	1
B	**10**	**220**	**Ceramic**	**50**	**0.2**	**1**
C	**10**	**250**	**Aluminium**	**23**	**1.1**	**3**
C01	10	250	Ceramic	50	1.7	2.8
C02	20	250	Aluminium	31.7	*	*
C03	20	250	Ceramic	51	1.7	2.5
D01	2	300	Aluminium	25	0.5-1**	2-4**
D02	2	300	Ceramic	50	0.4	1
D03	10	300	Aluminium	23.8	1.4	3
D04	10	300	Ceramic	50	0.7	2
D05	20	300	Aluminium	30	*	*
D06	20	300	Ceramic	51	0.8	2
E01	10	350	Aluminium	25	0.8	2
E02	10	350	Ceramic	50	*	*
E03	20	350	Aluminium	27	0.5	2.5

E04	20	350	Ceramic	50	1.2	2.2
F01	10	400	Aluminium	20	1	2
F02	10	400	Ceramic	6	0.4	0.7

* Not homogeneous. ** Gradient observed.

Three experimental conditions/temperatures were found to be extremely reproducible for foaming humins in an oven under air (Table 3.4). Experiment "A" for foam F180 provided a vertical gradient of cell sizes. The cells were closed, and their diameter increased from top (0.4-1.3 mm) to bottom (2.4-3.5 mm). The same kind of gradients was also reported for tannin-based foams, which are other cellular materials derived from biomass.[39] Experiment "B" led to F220, being uniform foams with closed cells and lower cell diameter (0.2 - 1 mm). Compared to experiment "A", the vertical gradient was absent in experiment "B". This can be explained as follows: since bubbling started at ~ 175 °C, a progressive and moderate bubbling probably occurred in experiment "A" (180 °C). In experiment "B" (220 °C), i.e., far above this critical point, a diffusive homogeneous bubbling was generated. Furthermore, as reported in the rheological analyses, the higher temperature of experiment "B" increased the viscosity, so that bubble generation tended to be more controlled.

Experiment "C" led to the formation of foam F250 with big and uniform cells (diameters up to 3 mm). This material looked more fragile compared to other experiments because of its bigger pores, providing lower density and thinner cell walls. Unlike the previous experiment, here half of the cells were open, while the closed ones had extremely thin walls/membranes.

Other protocols gave less uniform foams and less reproducible porous structures, which are nevertheless interesting and worth to be studied. Completely open cells were obtained at temperatures higher than 300 °C. Treatments at 400 °C, depending on the conditions, could lead to thermo-oxidative degradations (as indicated also by TGA experiments on crude humins), until complete gasification. When recovered, the obtained residual material presented a loss of cells walls, yielding a completely open porous structure. The temperature, in these cases, seems to consume firstly the thin cell walls and then the thicker parts of the foam (ligaments and junctions).

Foams were also prepared at higher temperatures using a tubular furnace flushed by N_2, i.e., in an inert environment. F500 and F900 were found to be less homogeneous compared to the

foams prepared at lower temperatures, with a complex morphology and a fully open structure.

A post-treatment at 900 °C was also tested for F250. As previously mentioned, the protocol "C" used for F250 gave really homogeneous foams with big cells, among which roughly half were closed by thin polymeric membranes. The idea was to check if an additional carbonization step, inducing the expected significant weight loss seen in Figure 3.5 between 250 and 900°C, would produce a completely open structure by preferentially degrading the thinner parts of the foam. After this post-treatment, a porous networked material with fully open structure was indeed obtained (Figure 3.6). In these F250-900 materials, all the cell walls were lost, leaving only a honeycomb-like skeleton. Unlike F400, F250-900 presented a thicker architecture, meaning that the temperature affected only the cells surface and not the bulk of the structure.

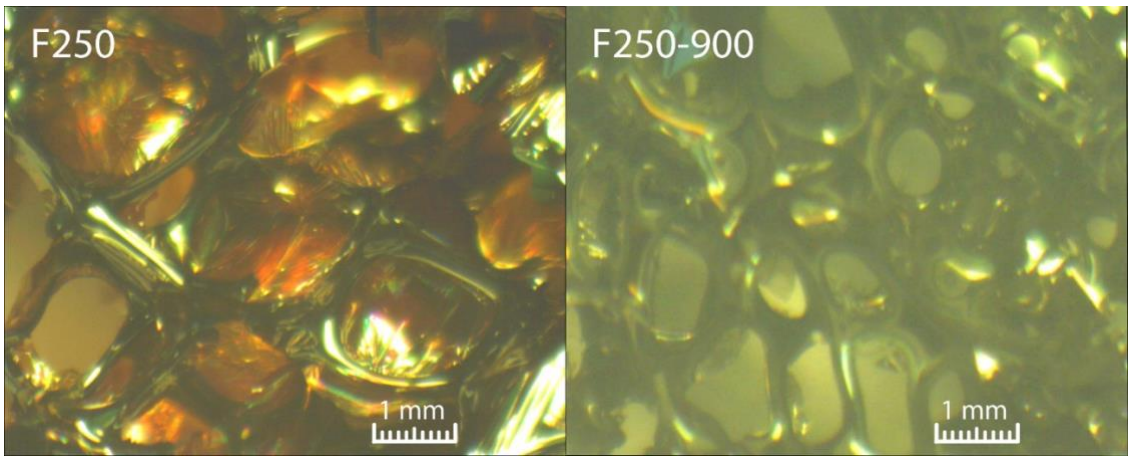

Figure 3.6 Morphology of foams F250 and F250-900.

3.3.4 Foams characterization

3.3.4.1 Elemental analysis

Elemental analysis of different foams presented in Table 3.5 shows that, as expected, the O/C ratio decreased with an increase in the final temperature. According to these results, the carbon content rose from 53.43 % in crude humins to 81.92 % in F400, while the H and O percentages decreased accordingly (Table 3.5). This is due to furanics rearrangement, volatiles loss, degradation and aromatization that occur at higher temperature, consistent with the literature reported for polyfuranic carbonization.[40] The oxygen content decreased from 39.7

% in the crude humins to 13.8 % in F400. This means that oxygen reactive moieties were mainly reduced but not completely lost at 400 °C, as already observed elsewhere for heat-treated phenolic-furanic foams.[41]

As shown in Figure 3.7 and in Table 3.5, F900 is a true carbonaceous material, since its carbon content was a high as 92.56 %. The residual hydrogen amount, < 1%, can be associated with an almost complete aromatization of the structure. The highest carbon content was found for F250-900 (94.48 %). The hydrogen ratio dropped down to ~ 0.5%, while oxygen remained at a level < 2 %. The double thermal treatment thus seemed to favour the loss of reactive moieties and to enhance the aromatization.

Table 3.5 Comparison of elemental analysis for humins and humins foams prepared with different thermal programs.

Sample	C %	H %	O %	Other (%)
Crude	53.43	5.89	39.7	0.98
F200	59.08	5.12	34.4	1.40
F250	63.12	4.52	30.9	1.46
F300	67.65	3.86	27.6	0.89
F400	81.92	3.03	13.8	1.25
F900	92.56	0.80	4.59	2.05
F250-900	94.48	0.52	1.85	3.15

As observed in the Van Krevelen diagram (Figure 3.7), H/C and O/C atomic ratios were linearly related to each other. Depending on the foreseen applications, it is therefore possible to design the composition, especially the carbon content, by controlling the thermal program during auto-crosslinking and foaming processes.

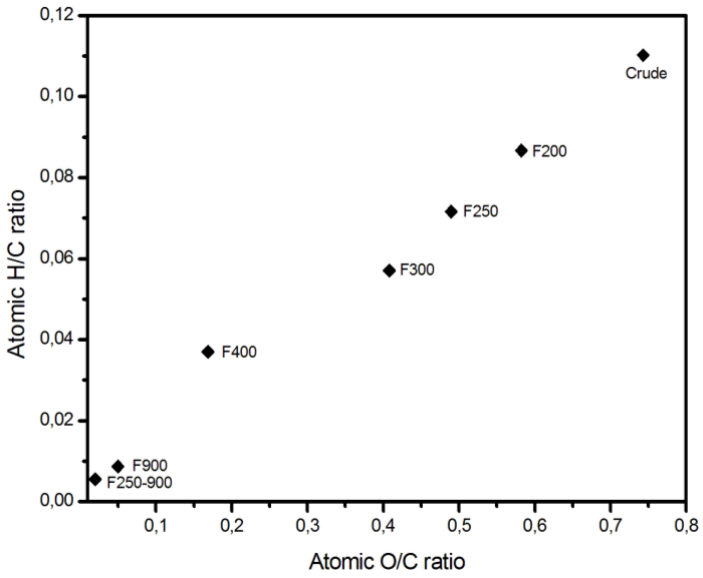

Figure 3.7 Van Krevelen diagram for humins foams.

3.3.4.2 Structural characterization

Auto-crosslinked humins foams prepared at different temperatures were characterized by FT-IR, and the results were compared with the crude humins spectrum (Figure 3.8). The signal at 3350 cm^{-1} shifted to 3421 cm^{-1} and progressively decreased in intensity when the temperature of preparation increased, showing a diminution of hydroxyls in the structure. The shifting of this signal can be related to the increase of the conjugated C=C system. The signal at 2920 cm^{-1}, associated with aliphatic C-H stretching, was still detected. It is worth noticing that the peak at 1664 cm^{-1} related to CO groups was still present in F220, but disappeared from F250. On the other hand, the peak at 1705 cm^{-1}, which was barely visible in the IR spectra of crude humins, herein clearly appeared in F220 and became the main signal up to 250 °C. This signal can be associated with CO groups within conjugated systems, and its increase confirms that reactions of aromatization and rearrangement occurred. Also a new signal appeared at 1600 cm^{-1} in F350, and can be associated with poly-aromatic formation.

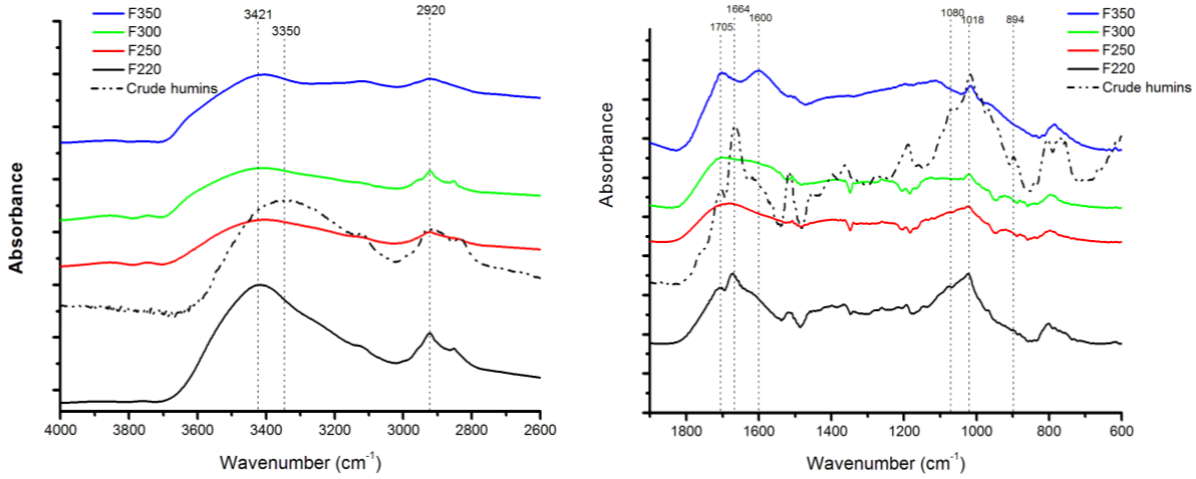

Figure 3.8 FT-IR of auto-crosslinked humins foams.

The thermal treatment manifested most of its effects in the furanic region at 1460-1362 cm^{-1}, in which the vanishing of peaks suggests rings rearrangement. In addition, the loss of the signal at 1080 cm^{-1} correlated with the release of CO found by TGA-MS confirms the breaking of furan ether ring functions. The signal at 1018 cm^{-1} assigned to α-CH_3 and α-CH_2 bending was maintained, while the peak at 894 cm^{-1} disappeared. The latter can be ascribed to =C-H and =CH_2 out-of-plane bending, and this disappearance might be linked to rearrangements and aromatization which involve firstly the external chains, or rearrangement from cis- to trans-double bonds (the less energetic stereoisomer). Observed changes in the region 850-760 cm^{-1} may correspond to ring rearrangements and hydroxyls loss due to reactions of condensation via nucleophilic attack.

Raman spectra of F300 and F900 foams are compared in Figure 3.9. The spectrum of F300 is typical of a carbonaceous material in the carbonisation regime (and not in the graphitisation regime), as it presents the classic D- and G-band at 1360 cm^{-1} and 1590 cm^{-1}, respectively, but with a broad contour and G being much more intense than D.[42] The D-band (1360 cm^{-1}) is well-known in complex carbon-based materials and is associated to breathing mode of A_{1g} symmetry of carbon rings. In highly disordered carbons, another broad band, less intense and centred around 1180 cm^{-1} overlaps the D-band, as also seen here by a shoulder at about 1200 cm^{-1}. This is characteristic of soot or coals chars,[43–45] but the interpretation of this signal is still under investigation.[46,47] The G-band (1590 cm^{-1}), instead, corresponds to Raman active vibrational $2E_{2g}$ mode of graphite single crystal, and can be associated with the degree of metallicity of the structure.

These two peaks were also detected for F900, with the D-band slightly shifted to 1345 cm^{-1} perhaps due to the effect of the sp^2/sp^3 carbon peripheral polyenes. The Raman peaks intensity height ratio I_D/I_G passed from ~ 0.75 in F300 to ~ 1 in F900. Such behaviour in the carbonisation regime is characteristic of an increased long-range order in the carbonaceous structure. This is related to a higher average crystallite size of sp^2 carbon domains, due to the higher carbon amount and higher aromatization of F900.[48] This is an important proof of the extension of the conjugated system in reticulated porous networks treated at high temperature under inert gas.

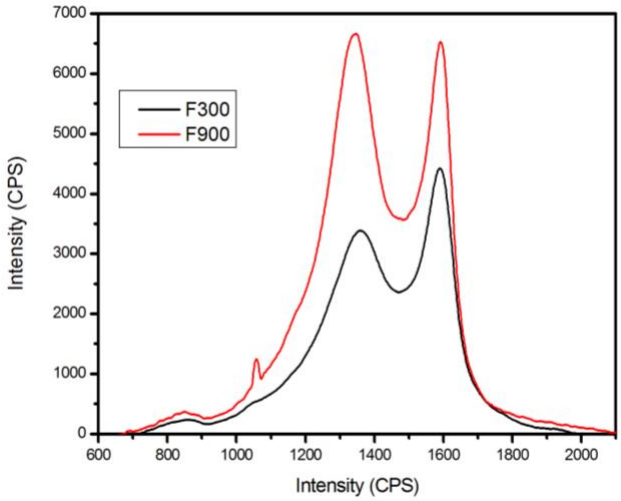

Figure 3.9 Raman spectra of humins foams F300 and F900.

3.3.4.3 Scanning electron microscopy (SEM) and Brunauer-Emmett-Teller (BET) method

In order to investigate the foams morphology, SEM images were collected for F250, F500 and F900, and are reported in Figure 3.10. In F250, well-defined spherical cells with a smooth surface can be observed (Fig. 3.10, F250 A). Those cells were connected to each other through some circular windows, making the macropores completely open and interconnected (Figure 3.10, F250 B). However, in some cases, the windows were not completely open but closed by thin, somewhat wrinkled, membranes (Figure 3.10, F250 C). The material from which the F250 foam was made looked solid, and no additional porosity could be observed at such magnification (Figure 3.10, F250 C), giving its structure to the foam backbone and making it strong. In both F500 and F900, a loss of regularity in the morphology could be noticed, the resultant structure being affected by degradation and cracking of cells wall and architecture (Figure 3.10, F500 A and F900 A). In F900 also, microcracks appeared which increased the surface area of the material. It is also possible to see that, whereas F500 did not clearly present

a secondary porosity (Figure 3.10, F500 B), a number of tiny holes could be seen at the surface of F900 (Figure 3.10, F900 B).

This result was confirmed by BET results (Table 3.6), and is consistent with the continuous release of volatiles produced at higher temperature whereas the carbonaceous structure shrinks and rigidifies at the same time, thereby developing the porosity. Similar results were also obtained by Burket et al.[40] for the pyrolysis of polyfurfuryl alcohol: these researchers observed that with thermal treatments micro and mesoporosity are obtained. In this case the effect was associated to the formation of polyaromatic domains and to the release of decomposition products.

According to BET analysis (Table 3.6), the surface area of F250 was only 0.2 $m^2 \cdot g^{-1}$. The latter rose to 2.3 $m^2 \cdot g^{-1}$ with a treatment at 500 °C, up to 74.4 with a treatment at 900 °C. This confirms the production of additional pores in F900, as displayed above in Figure 10 (F900 D). Considering that this result was obtained by a single hour of final isothermal treatment at 900 °C, and that a secondary porous network was thus created, the material might be easily converted into a monolithic activated carbon by heat-treatment in a flow of steam of CO_2 for instance, for reaching far higher surface areas.

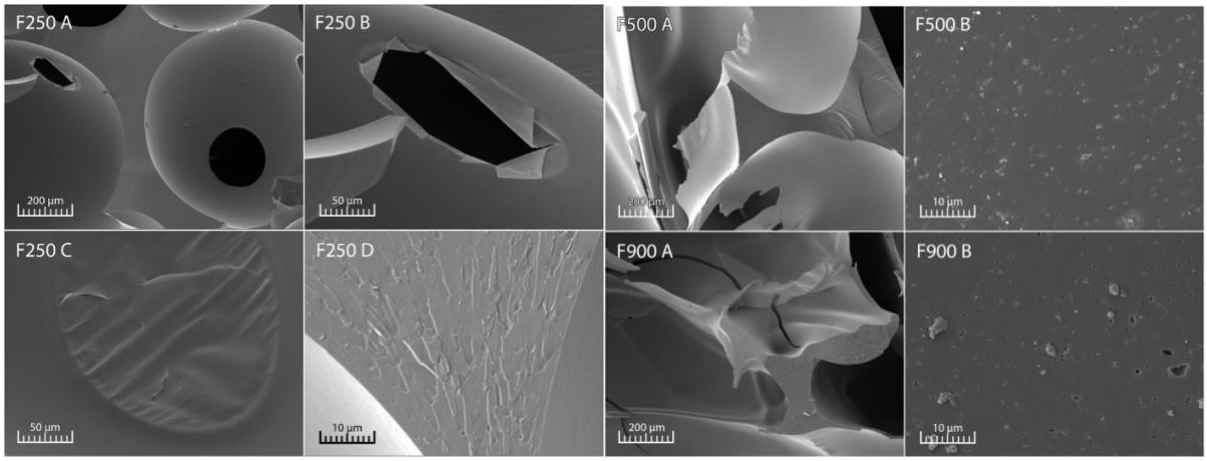

Figure 3.10 SEM images for F250, F500 and F900 foams at different magnifications.

Table 3.6 BET results for several humins foams.

Sample	BET surface area ($m^2 \cdot g^{-1}$)
F250	0.2
F500	2.3
F900	74.4
F250-900	138.9

3.3.4.4 Apparent density ($\rho_{apparent}$), real density (ρ_{real}) and porosity (Φ)

As seen in Table 3.7, $\rho_{apparent}$ of foams F180–F250 prepared in air significantly decreased when the temperature of preparation increased. This is due to the fact that higher temperatures produced bigger cells and hence a more lightweight material, as also shown by the corresponding increase of Φ. On the other hand, the real ρ_{real} of these foams remained, as expected, unaffected by the temperature of preparation. F500 and F900 did not follow this trend, giving a $\rho_{apparent}$ of 0.046 and 0.069 $g \cdot cm^{-3}$ and a relative density ($\rho_{relative}$) of 0.032 and 0.035, which are both higher than before. This is related to the dramatic shrinkage of the foam submitted to pyrolysis under inert atmosphere, and to the conversion of the furanic resin into a disordered carbon material, whose specific weight was expected to be close to 2 $g \cdot cm^{-3}$. However, the final porosity remained quite high and comparable to what was obtained when using lower temperatures in air.

Table 3.7 Apparent density, real density, relative density and porosity of humins-derived foams.

Sample	$\rho_{apparent}$ (g/cm^3)	ρ_{real} (g/cm^3)	$\rho_{relative}$	Φ (%)
F180	0.132	1.402	0.094	90.58
F220	0.045	1.407	0.032	96.80
F250	0.020	1.403	0.014	98.58
F500	0.046	1.437	0.032	96.77
F900	0.069	1.985	0.035	96.52

3.3.4.5 Mechanical properties

The results presented in Table 3.8 show that humins foams prepared under air are quite fragile materials, given their low Young's moduli and compressive strengths. Obviously, far better mechanical properties were obtained after pyrolysis at 900°C (F900), due to the intrinsic stiffness of glass-like isotropic carbon derived from furanic resins.

Table 3.8 Young's modulus E and compressive stress σ of humins foams.

Sample	E [MPa]	σ [MPa]
F180	0.60	0.006
F250	0.52	0.011
F900	12.23	0.123

3.4 Conclusions

As by-products from the industrial acid-catalysed dehydration of sugars, humins proved to be excellent precursors for producing novel rigid porous materials. Their intrinsic self-foaming and auto-crosslinking ability above 180 °C, without any kind of pre-treatment, was highlighted. The underpinning mechanism of humins foaming was identified as a combination of phenomena: melting at 120 °C, releasing of volatiles (mainly H_2O, CH_3OH, CO, CO_2) above 140 °C, auto-crosslinking above 170 °C and gelation at ~ 186 °C. From this point, bubbles were stabilised in the thermoset humins-based resin, leading to the cellular structure of the final material.

Auto-crosslinking is possible by the presence of several reactive oxygen moieties such as hydroxyls and carbonyls, which can be involved in aldol condensation, along with reactions of rearrangements and furan condensation. Indeed, FT-IR showed that –OH groups were progressively lost when increasing the foams preparation temperature, while CO groups were more and more involved in conjugated systems. New peaks appeared with temperature, associated to furanic rearrangement and aromatisation.

Humins foams could be obtained with high control on morphology and cell dimension by adjusting the parameters used during their preparation process. Foam prepared at low temperatures (between 180 and 250 °C) were quite homogeneous in terms of size and shape

of the cells, the latter being mainly closed. Foams prepared at higher temperatures (350 - 900 °C) were gradually less homogeneous, with a more open porosity, until only a reticulated structure remained. Higher temperatures of treatment increased the surface area and produced a secondary porosity, and could be converted into true vitreous carbon foams at 900°C under inert atmosphere. Besides, pyrolysis considerably improved the mechanical properties of the materials, and opened the routes towards environmental and energy applications. This will be the subject of forthcoming works.

3.5 Materials and methods

Six crude humins samples were provided by Avantium Chemicals, and produced using different times/protocols in Avantium pilot plant in Geleen (Netherlands) in 2016 during ACD of fructose and glucose into MMF. The ACD conversion of hexoses into MMF is a key step in the production of 2,5-FDCA for the formation of polyethylene-furanoate (PEF). The as-produced humins were then distilled under high vacuum to remove most of HMF and MMF content, and then used as received. These humins oligomers have molecular masses that generally range from 270 to 650 $g \cdot mol^{-1}$.[32]

Humins foams preparation

All humins foams described herein were prepared from crude humins using the following thermal program: heating from room temperature (r.t.) to final temperature at 10 $°C \cdot min^{-1}$; residence time = 1 hour. After the process, the samples were allowed to cool down to r.t.. Foam samples were named “F” followed by the final temperature used (e.g. F250 was prepared using 250 °C as final temperature).

F180, F200, F220, F250, F300, F350 and F400 were prepared in air in Nabertherm K430/75 and Nabertherm N30/85HA ovens, using Haldenwanger Evaporating Basin Porcelain Flat 888/6A, LLG-Incinerating Dish and disposable aluminium pans as crucibles.

F500 and F900 were prepared under inert atmosphere (flowing N_2, 80 $mL \cdot min^{-1}$) in a Carbolite CTF 12/100/900 Tube Oven furnace, using LLG-Incinerating Dish.

F250-900 was prepared from F250 by using a second temperature program until 900°C under N_2.

Chromatography

An external standard solution (ESS) was first prepared by dissolving saccharine (8 $g \cdot L^{-1}$) and dioxane (3 $g \cdot L^{-1}$) in acetonitrile (ACN). A sample for GC was then prepared by dissolving humins

in 4 mL ESS + 2 mL water (if required, ultra-sonic bath was used to fully dissolve the sample). Another sample for UPLC was prepared from 20 µL GC sample + 800 µL water + 180 µL ACN.

GC analyses were performed with an Interscience Trace GC device, equipped with a FID detector and VF WAXms column, id 0.25 mm, film thickness 0.25 µm, 30 m. Eluent: ACN/H_2O 50/50; injection volume: 1 µL. Dioxane was used as standard for both calibration and samples.

UPLC analyses were performed with a Waters Acquity UPLC HSS C18 column, 2.1 × 100 mm, 1.8 µm. Eluent: 0.2% trifluoroacetic acid in H_2O and ACN/MeOH 50/50. Injection volume: 3.5 µL; flow: 0.4 mL·min^{-1}; internal standard: saccharine (measured at 250 nm). Column temperature: 50 °C, equipped with detectors UV and ELSD. MMF and HMF contents were detected by UPLC-UV analysis.

Thermal analysis

TGA were performed using a Mettler Toledo TGA/SDTD 851, with a microbalance precision of ± 0.1 µg. The data were treated with STAR© software. Humins and humins foams (10-15 mg) were investigated in 70 µL alumina pans as crucibles. Humins foams were crushed before analysis in order to obtain homogeneous powder samples. The investigations were performed using dynamic thermal programs from 25 to 1000 °C at a heating rate of 10 °C·min^{-1} and under air or nitrogen flow (50 mL·min^{-1}).

TGA-MS analyses were performed on a Netzsch STA449F3 thermobalance coupled to an Aëolos QMS403D mass spectrometer equipped with a quadrupole analyser. Crude humins samples of ~ 20 mg were heated under inert gas (Ar, 50 mL·min^{-1}) in alumina pans from 25 to 1000 °C at 5 °C·min^{-1} with an isothermal plateau of 1 h at 250 °C. The transfer line was heated at 250 °C and maintained under vacuum (1·× 10^{-6} - 1·× 10^{-5} mBar). The gases were analysed in the range 1 - 300 amu. Peaks associated to flowing Ar (40, 38 and 36 m/z) were removed from the spectra.

DSC studies on crude and foamed humins were conducted on a Mettler-Toledo DSC-1 equipped with FRS5 sensor and monitored by STAR© software. The calibrations (temperature, enthalpy) were performed using indium and zinc standards. Samples of 7-11 mg were placed in 40 µL aluminium crucibles with sealed lids pierced by a single hole. The same kind of crucibles was used as reference. Humins foams were crushed before analysis. The experiments for detecting the temperature range of T_g were conducted between -60 and 125 °C for crude humins and between -60 and -300 °C for humins foams, with 30 °C·min^{-1} ramp in both cases.

Rheology

Rheological characterization of crude humins was performed with a Thermo Scientific HAAKE MARS Modular Advanced Rheometer System operated with a plate-plate geometry (1 mm gap). Experimental conditions were: sample weight ~ 10 g; temperature range from 0 to 200 °C at 1 °C·min^{-1}; 5% deformation, oscillation frequency 1 Hz.

Raman spectroscopy

Raman spectra of two samples of humins foams (F300 and F900) were acquired at room temperature using a DXR Raman Microscope AXX1606015 series, with laser depolarized at wavelength 532 nm, grating 900 lines/mm, split aperture 25 µm; acquisition time of exposition 0.25 sec, numbers of exposition 120.

Pycnometry

Four different humins foams were characterized in terms of $\rho_{apparent}$, ρ_{real} and Φ. $\rho_{apparent}$ was calculated as the weight/volume ratio of foams shaped like parallelepipeds of accurately known dimensions. ρ_{real} or skeletal density, being the density of the solid material constituting the foam, was estimated by helium pycnometry after grinding the sample, using an Accupyc II 1340 (Micromeritics, USA) apparatus. From the two aforementioned quantities, the $\rho_{relative}$ was defined as the ratio of $\rho_{apparent}$ to ρ_{real}. The overall porosity (dimensionless), was calculated as $\Phi = 1 - \rho_{relative}$. The measurements were performed on parallelepiped samples of humins foams of typical size around 3 × 3 × 1.5 cm, cut out of bigger foam blocks.

Mechanical tests

The mechanical properties of humins thermosets foams were investigated by quasi-static compression using an Instron 5944 universal testing machine equipped with a 2 kN head, and using a load rate of 2.0 mm·min^{-1}. Three samples of dimensions approximately 3 × 3 × 1.5 cm were tested in the growing direction for each formulation. Due to their brittle character, the opposite faces of parallelepiped sample of the same material were glued to poly(methyl methacrylate) (PMMA) plates with a high-resistance epoxy adhesive (Araldite®) before testing, according to a described method.[49] During the test, deformation and load were continuously recorded: the modulus was estimated from the slope of the longest linear region at strain typically lower than 10%, and the compressive strength was defined as the highest stress before densification.[50,51]

FT-IR

FT-IR analyses were performed with a PerkinElmer Spectrum BX FT-IR System (range 4000-600 cm^{-1}, 32 scans, resolution 4 cm^{-1}, interval 2 cm^{-1}). All the spectra were treated with baseline automatic correction and smoothing. Crude humins samples were analysed using attenuated total reflection (ATR) mode. Humins foams were analysed based on ground material mixed with KBr (~2/100), in order to obtain sufficient signal intensity.

Elemental Analysis

Crude humins elemental analyses were performed with Inductively Coupled Plasma ICP by Mikroanalytisches Labor Pascher, Remagen, Germany.

SEM

SEM observations on F250, F500 and F900 were carried with a Tescan Vega3 XM scanning electron microscope. Prior to observation, samples were cut and coated with platinum. A 5 kV accelerating voltage was used for imaging.

Nitrogen adsorption

The humins foams surface area was estimated by TriStar 3000 device from Micromeritics serial #470. The surface area was calculated by the regression line in the BET transform plot of nitrogen adsorption at -196 °C on crushed samples, according to the BET model equations.[52] Prior to analysis, the samples were dried at 200 °C under N_2 stream.

3.5 References

[1] R. Haag, S. Roller, *Immobilized Catalysts: Solid Phases, Immobilization and Applications*, Berlin, **2004**.

[2] S. De, A. M. Balu, J. C. Van Der Waal, R. Luque, *ChemCatChem* **2015**, *7*, 1608–1629.

[3] M. Slater, M. Snauko, F. Svec, J. M. J. Fréchet, *Anal. Chem.* **2006**, *78*, 4969–75.

[4] D. Wang, F. Li, M. Liu, G. Q. Lu, H. Cheng, *Angew. Chem. Int. Ed.* **2008**, *47*, 373–376.

[5] L. Leeb, P. Gmeiner, S. L öber, *Mol. Inform.* **2007**, *26*, 1145–1150.

[6] R. J. White, R. Luque, V. L. Budarin, J. H. Clark, D. J. Macquarrie, *Chem. Soc. Rev.* **2009**, *38*, 481–494.

[7] B. Hu, K. Wang, L. Wu, S. H. Yu, M. Antonietti, M. M. Titirici, *Adv. Mater.* **2010**, *22*, 813–828.

[8] G. Xu, J. Han, B. Ding, P. Nie, J. Pan, H. Dou, H. Li, X. Zhang, *Green Chem.* **2015**, *17*, 1668–1674.

[9] M. M. Titirici, A. Thomas, S. H. Yu, J. O. Müller, M. Antonietti, *Chem. Mater.* **2007**, *19*,

4205–4212.

[10] A. Sanchez-Sanchez, M. T. Izquierdo, J. Ghanbaja, G. Medjahdi, S. Mathieu, A. Celzard, V. Fierro, *J. Power Sources* **2017**, *344*, 15–24.

[11] A. Sanchez-Sanchez, M. T. Izquierdo, S. Mathieu, J. González-Álvarez, A. Celzard, V. Fierro, *Green Chem.* **2017**, *19*, 2653–2665.

[12] J. Encalada, K. Savaram, N. A. Travlou, W. Li, Q. Li, C. Delgado-Sánchez, V. Fierro, A. Celzard, H. He, T. J. Bandosz, *ACS Catal.* **2017**, *7*, 7466–7478.

[13] A. E. Farrell, R. J. Plevin, B. T. Turner, A. D. Jones, M. O'Hare, D. M. Kammen, *Science (80-.).* **2006**, *311*, 506–508.

[14] M. Galbe, G. Zacchi, *Appl. Microbiol. Biotechnol.* **2002**, *59*, 618–628.

[15] D. J. Hayes, *Catal. Today* **2009**, *145*, 138–151.

[16] M. Mascal, E. B. Nikitin, *Angew. Chemie - Int. Ed.* **2008**, *47*, 7924–7926.

[17] S. G. Wettstein, D. Martin Alonso, E. I. Gürbüz, J. A. Dumesic, *Curr. Opin. Chem. Eng.* **2012**, *1*, 218–224.

[18] R. Van Putten, J. C. Van Der Waal, E. De Jong, C. B. Rasrendra, H. J. Heeres, J. G. De Vries, R.-J. van Putten, J. C. van der Waal, E. de Jong, C. B. Rasrendra, et al., *Chem. Rev.* **2013**, *113*, 1499–1597.

[19] B. F.M. Kuster, L. M. Tebbens, *Carbohydr. Res.* **1977**, *54*, 158–164.

[20] B. F. M. Kuster, H. M. G. Temmink, *Carbohydr. Res.* **1977**, *54*, 185–191.

[21] B. F. M. Kuster, *Carbohydr. Res.* **1977**, *54*, 177–183.

[22] B. Girisuta, B. Danon, R. Manurung, L. P. B. M. Janssen, H. J. Heeres, *Bioresour. Technol.* **2008**, *99*, 8367–8375.

[23] B. Girisuta, L. P. B. M. Janssen, H. J. Heeres, *Green Chem.* **2006**, *8*, 701–709.

[24] B. Girisuta, L. P. B. M. Janssen, H. J. Heeres, *Ind. Eng. Chem. Res.* **2007**, *46*, 1696–1708.

[25] A. Mija, J. C. Van Der Waal, J. Pin, N. Guigo, E. De Jong, *Constr. Build. Mater.* **2016**, *139*, 594–601.

[26] L. Filiciotto, G. de Miguel, A. M. Balu, A. A. Romero, J. C. van der Waal, R. Luque, *Chem. Commun.* **2017**, *53*, 7015–7017.

[27] Z. Cheng, J. Everhart, G. Tsilomelekis, V. Nikolakis, B. Saha, D. Vlachos, *Green Chem.* **2018**, *20*, 997–1006.

[28] I. V Sumerskii, S. M. Krutov, M. Y. Zarubin, **2010**, *83*, 320–327.

[29] S. K. R. Patil, C. R. F. Lund, *Energy and Fuels* **2011**, *25*, 4745–4755.

[30] I. Van Zandvoort, E. J. Koers, M. Weingarth, P. C. A. Bruijnincx, M. Baldus, B. M. Weckhuysen, *Green Chem.* **2015**, 4383–4392.

[31] I. Van Zandvoort, Y. Wang, C. B. Rasrendra, E. R. H. Van Eck, P. C. A. Bruijnincx, H. J. Heeres, B. M. Weckhuysen, *ChemSusChem* **2013**, 1745–1758.

[32] L. Filiciotto, A. M. Balu, A. A. Romero, E. Rodríguez-Castellón, J. C. van der Waal, R. Luque, *Green Chem.* **2017**, *19*, 4423–4434.

[33] A. Mija, J. C. van der Waal, E. de Jong, G. P. M. van Klink, *Process for the Modification of Humins*, **2018**.

[34] A. Mija, E. de Jong, J. C. van der Waal, G. van Klink, *Humins Containing Foam*, **2017**, WO 2017074183 A1 20170504.

[35] L. Wei, M. Sevilla, A. B. Fuertes, R. Mokaya, G. Yushin, *Adv. Energy Mater.* **2011**, *1*, 356–361.

[36] G. Tondi, A. Pizzi, *Ind. Crops Prod.* **2009**, *29*, 356–363.

[37] J. D. Ferry, *Viscoelastic Properties of Polymers*, John Wiley & Sons, **1980**.

[38] A. Shindo, K. Izumino, *Carbon N. Y.* **1994**, *32*, 1233–1243.

[39] G. Tondi, W. Zhao, A. Pizzi, G. Du, V. Fierro, A. Celzard, *Bioresour. Technol.* **2009**, *100*, 5162–5169.

[40] C. L. Burket, R. Rajagopalan, A. P. Marencic, K. Dronvajjala, H. C. Foley, *Carbon N. Y.* **2006**, *44*, 2957–2963.

[41] G. Tondi, A. Pizzi, H. Pasch, A. Celzard, K. Rode, *Eur. Polym. J.* **2008**, *44*, 2938–2943.

[42] S. Bernard, O. Beyssac, K. Benzerara, N. Findling, G. Tzvetkov, G. E. Brown, *Carbon N. Y.* **2010**, *48*, 2506–2516.

[43] A. Sadezky, H. Muckenhuber, H. Grothe, R. Niessner, U. Pöschl, *Carbon N. Y.* **2005**, *43*, 1731–1742.

[44] T. Livneh, E. Bar-Ziv, O. Senneca, P. Salatino, *Combust. Sci. Technol.* **2000**, *153*, 65–82.

[45] A. Zaida, E. Bar-Ziv, L. R. Radovic, Y. J. Lee, *Proc. Combust. Inst.* **2007**, *31 II*, 1881–1887.

[46] B. Dippel, H. Jander, J. Heintzenberg, *Phys. Chem. Chem. Phys.* **1999**, *1*, 4707–4712.

[47] E. Bar-Ziv, A. Zaida, P. Salatino, O. Senneca, *Proc. Combust. Inst.* **2000**, *28*, 2369–2374.

[48] A. C. Ferrari, J. C. Meyer, V. Scardaci, C. Casiraghi, M. Lazzeri, F. Mauri, S. Piscanec, D. Jiang, K. S. Novoselov, S. Roth, et al., *Phys. Rev. Lett.* **2006**, *97*, 1–4.

[49] M. Letellier, C. Delgado-Sanchez, M. Khelifa, V. Fierro, A. Celzard, *Carbon N. Y.* **2017**, *116*, 562–571.

[50] A. Celzard, W. Zhao, A. Pizzi, V. Fierro, *Mater. Sci. Eng. A* **2010**, *527*, 4438–4446.

[51] G. Amaral-Labat, M. Sahimi, A. Pizzi, V. Fierro, A. Celzard, *Phys. Rev. E - Stat. Nonlinear, Soft Matter Phys.* **2013**, *87*, 1–7.

[52] P. Webb, C. Orr, *Analytical Methods in Fine Particle Technology*, Micromeritics Instrument Corp, **1997**.

4 Insights on thermal and fire hazards of humins in support of their sustainable use in advanced biorefineries*

4.1 Chapter content

The concept of circular economy is aiming at promoting innovative use of wastes, residues, or by-products into marketable chemicals and intermediates, while enhancing process economics and environmental sustainability. The current study provides characterization details necessary to establish safety information about humins on a global context. This first attempt has brought in a preliminary safety data mainly focusing on thermal and fire hazards of humins and humins foams, to ensure safe storage, handling, transportation, and processing. The obtained results show that overall fire risk of humins so far is similar to that of the conventional cellulosic fuels such as woody materials. Further consolidation of safety information shall be done with a scenario-based risk assessment approach for conditioning safe use of humins in further innovative applications. This is a dedicated research for filling the existing data gaps and developing insights on physicochemical characteristics of humins and related safety parameters (such as ignitability, flammability, or combustible behavior), that will condition inherently safer and eco-friendly processes for their sustainable valorization.

*published as: A. Muralidhara, P. Tosi, A. Mija, N. Sbirrazzuoli, C. Len, V. Engelen, E. de Jong, G. Marlair, *ACS Sustain. Chem. Eng.* **2018**, 16692–16701.

4.2 Introduction

As explained in the previous chapters, humins are heterogeneous condensation by-products produced by random polymerization processes during the ACD of sugars (Figure 4.1).[1,2] Humins formation has been known to the scientific community for almost a century through the caramelization process of sugars. Their formation, so far unpreventable, is the principle drawback of the ACD process resulting in loss of feed, reactor fouling, and other engineering challenges.[3–5]

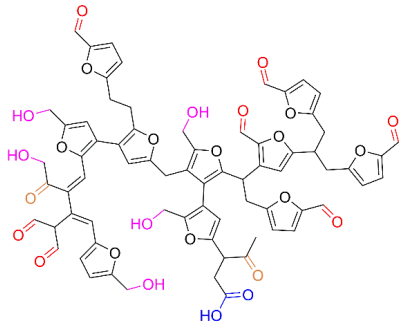

Figure 4.1 Humins molecular structure model proposed by Van Zandvoort et al. (2013).[4]

From a technical viewpoint, three strategies are possible to cope with these challenges linked to production of humins: (a) optimizing the ACD process targeting the minimization of humins production; (b) converting humins into energy to satisfy a substantial part of the energy demand of the biorefinery; (c) integrating humins as a potential valuable carbon source and additional feedstock for new biobased chemicals, biomaterials, or additives of interest. No major breakthroughs were achieved with option c;[5] therefore, for a long time, option b was the unique industrially applied strategy, while nowadays, despite remaining technical challenges, economic considerations and promising recent research advances[6–8] justify a move to option c. Considering the real industrial-scale ACD of hexoses, humins should be considered more like a mixture. The degree of branching and molecular mass of humins oligomers vary depending on the process and feedstock conditions, with subunits and structures repeated and connected in a random way. This challenging context has essentially limited industrial uses of humins to energy and/or power conversion through gasification or combustion, however clearly identifying their energy content and combustible nature.[7,9,10] Some studies have highlighted the potential of humins in catalysis, water purification, energy storage, and CO_2 sequestration,[11–13] but also as new biobased thermoset materials, a matrix

for impregnations, and in producing co-cured composite materials.[6,14,15] The last case explores the flame retardancy properties of humins (semi-protective char) that reduces the rate of thermal degradation compared to the normal unsaturated polyesters. Furthermore, has explained in Chapter 3, when crude humins are heated to a temperature superior to 180 °C, they can foam into a reticulated, rigid macroporous carbon-based material.[16] These foamed humins with versatile potential applications are emerging as a promising alternative in terms of reducing the available quantity of crude humins. Because of the complex and versatile chemical structure of humins and subsequent wide variety of physicochemical properties, the safety profiles, and accordingly the nature and intensity of risks, may significantly vary during existing and/or innovative uses. So far, as a residue used in the production site, humins' conventional hazards are not recognized by any official hazardous material classification system.[17,18] There is neither a definite description of their physicochemical properties (apart from tentative efforts of some production stakeholders), nor consensual information made available regarding precautions requested for their safe handling, use, storage, or conversion. One of the main reasons behind this is the lack of complete characterization of humins. Therefore, as a feedstock of growing interest, both crude and foamed humins (obtained by thermal curing)[16,19] must be appraised beyond legal requirements more globally in terms of physicochemical hazards for their safe utilization. In addition, accessing full characterization of physicochemical, health, and environmental hazards of these products would be a prerequisite for obtaining "end of waste status" according to the EU's waste framework directive.[20] In addition, because of intrinsic limitations of the conventional hazard rating making use of threshold values to fix regulated boundaries, substances or mixtures that are not identified as "dangerous" from hazardous materials classification systems may still induce fire or explosion risks, corrosive or oxidative environments, or trigger some toxic and ecotoxic risks depending on their context of use. Product and process safety performances must be assessed all along the value chain of humins, not only to take all types of risks (physicochemical, health, and environment) under control, but also to seek competitive advantages. In addition to addressing the conventional risks, key safety concerns shall also be appraised in humins valorization routes,[4,6,21–24] which may otherwise lead to an explosive atmosphere (ATEX) under unforeseen circumstances. Examples such as transformation requiring thermal curing of crude humins, handling or transforming foamed humins leading to dust production, pumping crude humins under

pressure, and impregnation of humins for developing composites would justify a detailed characterization of fire and explosion hazards (ease of ignition, flammability limits, dust explosion hazard profile, self-heating characteristics, and reaction to fire performance of end products). In addition, thermal stability, hot spot ignition hazard,[25] speed of combustion, type of surrounding environment, conventional methods of storage and disposal, and safety training to the employees are some of the governing factors that must also be considered in further evaluation of associated risks during the use and applications of humins. This is dedicated research for filling the existing data gaps and developing insights on physicochemical characteristics of humins and related safety parameters (such as ignitability, flammability, or combustible behavior), that will condition inherently safer and eco-friendly processes for their sustainable valorization.

4.3 Results and discussions

Crude and foamed humins underwent thermal stability tests determined by DSC, C80, and TGA, and self-heating tests using TGA/DTA. Qualitative and quantitative reaction-to-fire behavior (e.g., heat and mass release rates, yields of combustion products, duration of combustion) was examined by the Tewarson calorimeter, which instrumental details are reported in the section Materials and Methods.

4.3.1 Characterization of humins samples

Several batches of industrial humins were produced via the ACD process. Among these, two humins samples reflecting the largest variation of observed chemical composition were selected for testing. Along with humins oligomers, an amount of HMF and its alkyl derivatives in these two samples has been found between 9 % and 13 %. LA was found between 1.2 % and 1.6 %. The results discussed further are focusing on these two samples of crude humins (humins *a* and humins *b*) and another first sample of available foamed humins. Therefore, the results obtained should be considered as early information in the field of study that will require statistical consolidations in line with further process optimization.

It is worth mentioning that foamed humins (obtained by subjecting crude humins to a foaming treatment at 250 °C) differ significantly both physically and chemically from crude humins as reflected by elemental analysis results (Table 4.3) with values that are consistent with other humins compositions reported in the literature.12 The efficiency of the foaming process in terms of carbon mass intensification (17 % increase in carbon mass fraction compared to

crude humins) is obtained at the expense of 25 % of hydrogen and 24 % oxygen mass fractions, respectively. Thermal curing of crude humins to obtain foamed humins also affects the material's energy content. By using the Bioe correlation[26] to reasonably predict energy values for biomass materials,[27] the heat of complete combustion increased from 20.2 kJ g^{-1} for crude humins to 23.8 kJ g^{-1} for foamed humins.

4.3.2 Thermal hazard analysis: DSC and C80 calorimetry

Crude and foamed humins were subjected to both DSC and C80 analysis, and corresponding results were compared (Figure 4.2a and 4.2b, Table 4.1). For crude humins a wide exothermic thermal event composed of at least two peaks is observed in DSC and C80 starting at around 100–125 °C. It ends at around 300 °C in DSC and at a lower temperature in C80 which can be explained by the lower heating rate used in this case. This event could correspond to residual cross-links, self-condensation, or vaporization of monomers and is observed for both DSC and C80. The first event close to 150 °C is in good agreement with the first mass loss observed in TGA at around 150 °C. Another exothermic thermal event is observed between 300 and 400 °C in DSC. It occurs at higher temperature for humins b (300–400 °C) as compared with humins a (300–350 °C). This event is in agreement with the inflection of the TGA curve observed between 300 and 400 °C. At a temperature higher than 400 °C, the DSC curve shows the starting of an increase of the baseline that corresponds to the thermal degradation and which is confirmed by the mass loss observed in TGA at this temperature.

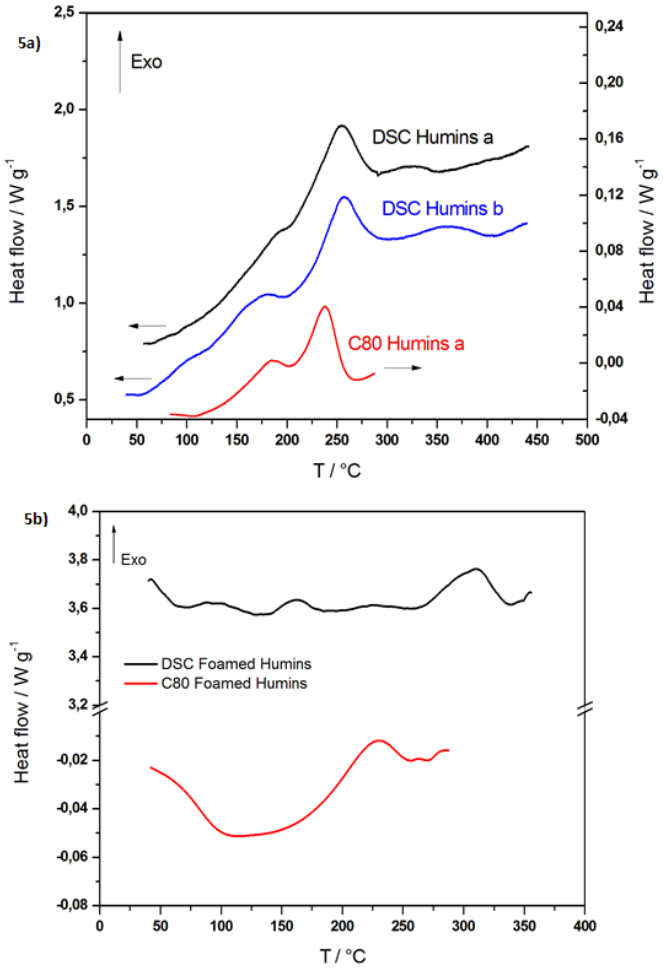

Figure 4.2 Comparison of DSC and C80 results for a) crude humins and b) foamed humins.

Foamed humins showed much less reactivity. The first baseline deviation could correspond to the glass transition, which was confirmed after careful verification of calibration tests. An exothermic thermal event is observed at around 150 °C for both DSC and C80, but ends at much higher temperature for C80. This could be explained by a higher amount of residual volatilization of organic compounds in C80 because of the higher sample mass and higher free volume in the pan. Thus, the thermal event observed in C80 could be the sum of the two thermal events observed in DSC between 140 and 270 °C, i.e., the first event starting at around 150 °C and the second one, much lower, starting at around 200 °C. Finally, a single exothermic peak between 263 and 337 °C with a T_{onset} value of 273 °C (Figure 4.2b) is observed in DSC that could correspond to the beginning of the thermal degradation of the sample.

Table 4.1 Start and onset temperatures and heats of decomposition of crude and foamed humins determined by DSC experiments.

Substrate	T_{start} (°C)	$T_{reaction}$ (°C)	T_{onset} (°C)	ΔH_d (J·g^{-1})
Crude humins *a*	143	143-352	173	-505
Crude humins *b*	132	132-318	165	-402
Foamed humins	263	263-337	273	-70

Foamed humins showed much less reactivity. The first baseline deviation could correspond to the glass transition, which was confirmed after careful verification of calibration tests. An exothermic thermal event is observed at around 150 °C for both DSC and C80, but ends at much higher temperature for C80. This could be explained by a higher amount of residual volatilization of organic compounds in C80 because of the higher sample mass and higher free volume in the pan. Thus, the thermal event observed in C80 could be the sum of the two thermal events observed in DSC between 140 and 270 °C, i.e., the first event starting at around 150 °C and the second one, much lower, starting at around 200 °C. Finally, a single exothermic peak between 263 and 337 °C with a T_{onset} value of 273 °C (Figure 4.2b) is observed in DSC that could correspond to the beginning of the thermal degradation of the sample.

For crude humins, in both test methods, (i) the decomposition reaction starts earlier because of the volatilization of lower-molecular-weight compounds, and (ii) the complexity of developing reaction mechanisms is reflected by the double peaks appearing in the thermogram. Despite their common origins, the energy levels observed from exothermic decomposition of foamed humins are significantly lower than those of crude humins.[28] Foamed humins were initially subjected to thermal curing during their preparation, where they underwent partial oxidation/transformation.[16] This initial thermal curing has contributed to self-crosslinking of humins macromolecules through the functional groups present in humins' structure. These chemical reactions contributed to a better thermal resistance and in turn better thermal stability in foams than in crude humins.

For foamed humins, the range of temperature in which thermal decomposition occurs in DSC experiments significantly exceeds the maximum operating temperature explored in C80 (300 °C). This does not render a detailed comparison between the DSC and C80 results.

C80 also operates with a larger sample mass and a smaller heat ramp than DSC. It has been observed that when solid mixtures are studied, sample size has potentially a great influence on results, and the question to be addressed is about the homogeneity of samples used from similar batches of available representative samples.[28] Heterogeneity of samples subjected to different operating conditions might slightly shift the results which are depicted by the slight variation in the range of exothermic peaks in C80 and DSC. Differences in the way pressure may build up in the closed vessels used in the experiment may also be part of the explanation of the observed differences as pressure may affect reaction kinetics. Nevertheless, these variations are not significant, and the same was also confirmed during the sample selection.

Thermal stability is not an intrinsic property of any material since its apparatus- and criteria-dependent. As a first statement relating to this aspect, our work allows to conclude that humins thermosets do not entail critical self-heating behavior. This is an early clearance for storage and transportation of such materials. End use of humins and humins-based materials deserves a more detailed evaluation of thermal stability properties depending on the context of use. Similarly, process conditions during the production of crude humins must be considered in further evaluation of thermal stability characteristics.

4.3.3 TGA and TGA/DTA

The profile of thermal stability of crude humins can be observed by TGA (Figure 4.3). Three steps of mass loss could be observed under air and only two under N_2. A first mass loss of ∼36% is observed between 120 and 270 °C in both the conditions, probably because of volatilization of low-mass molecules and products of self-condensation. Another mass loss of around 20% occurs under air in the interval 290−400 °C, while it is barely present under N_2 (∼7 %). A last mass loss of around 45 % leads to the complete thermo-oxidative degradation of humins under air between 400 and 600 °C. Under N2 the mass loss recorded between 400 and 1000 °C is only around ∼22 %, giving a final residual product of ∼26.3 %.

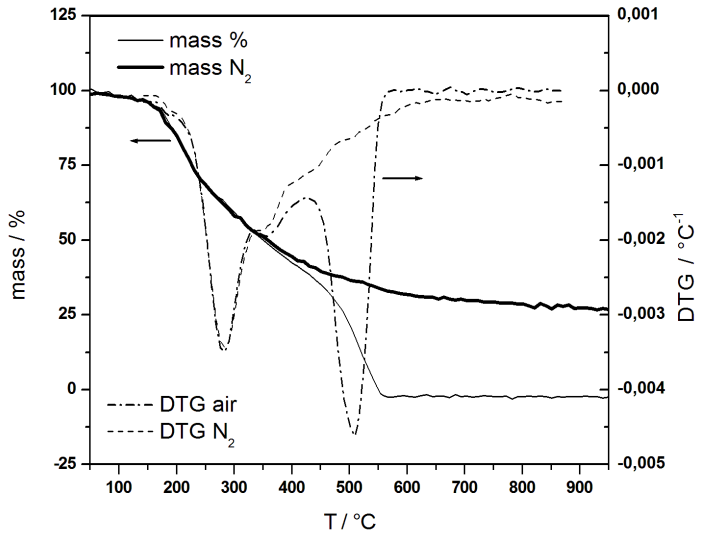

Figure 4.3 TGA and DTA results for humins in dynamic conditions between 25 and 1000 °C with a ramp of 10 °C min^{-1}. Gas flow 80 mL min^{-1}.

On the other hand, once formed by thermal curing, foamed humins gain thermal stability as a function of the temperature used during their preparation. Foams prepared at 250 °C, for instance, give a mass loss phenomenon only above 150 °C, with only 10% of mass loss at 290 °C, while thermo-oxidative degradation occurs above 450 °C, possibly leading to ignition. We can suppose that if foamed humins are prepared at temperatures higher than 250 °C, all the effects herein observed will result in further delay due to the natural increase in carbon amount. These results were compared with TGA/DTA measurements of foamed humins samples (Figure 4.4). Less than 20% mass loss was observed in the beginning of the reaction up to around 250 °C, followed by the second step of mass loss (50– 60 %) between 250 and 400 °C, and further down, foamed humins are almost completely degraded. In this case, thermal reactivity of the sample is reflected by the measured ΔT (the temperature difference between the sample and reference). A critical value of ΔT = 50 °C serves as a first-order estimation of a potential self-heating hazard based on former experiences. According to the test protocol, the material is liable to endure a high risk of self-heating if a ΔT = 50 °C is observed at a witness temperature WT $\leq$ 250 °C. Moderate self-heating risks are considered at ΔT = 50 °C between 250 and 400 °C WT, while self-heating risk is absent if ΔT = 50 °C for WT > 400 °C (or in the case that ΔT = 50 °C is never achieved).

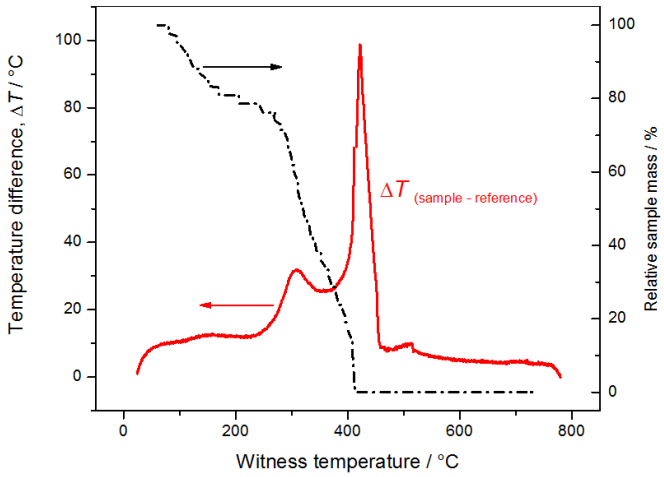

Figure 4.4 Large scale TGA/DTA results for for foamed humins (gray dotted line corresponds to the mass loss profile with its associated scale to the right.

For the foamed humins under investigation, ΔT = 50 °C was observed for WT = 421 °C, indicating that humins used in the current study do not pose any significant risk of self-heating. However, slight variation in the characteristics of humins depending on the process conditions[4,29] shall be kept in mind. Indeed, the thermal curing required to obtain foamed humins brings better thermal stability in the final material by further diminishing the effect of differences in composition compared to the pristine crude humins.

4.3.4 Fire Risk Analysis

Being a combustible feedstock by nature, for both crude and foamed humins, investigation of their behavior in fire conditions was performed. The summary of results obtained from FPA test runs and related overall analysis of mass and thermal balances are presented in Table 4.2.

Table 4.2. Burning behaviour of crude humins and foamed humins in the FPA under well-ventilated fire conditions.

Measured Parameters	Crude humins *a*	Crude humins *b*	Foamed humins
Sample mass (g)	20.4	20.8	12.6
Mass loss (%)	66.2	65.9	75.4
Ignition time (s)	88	75	22
Duration of combustion (s)	236	275	610
Average mass loss rate (g $m^{-2}{\cdot}s^{-1}$)	24.6	21.5	5.8
Max mass loss rate (g. $m^{-2}s^{-1}$)	35	40.8	11.9
Phi factor max [30]	0.19	0.22	0.16
NHV (from Boie formula in $kJ{\cdot}g^{-1}$)	20.2	20.1	23.4
Total energy release [from CDG] ($kJ{\cdot}g^{-1}$)	14.4	14.7	17
Energy efficiency conversion % (Boie Correlation)	73.5	70	54.5
Carbon mass balance (%)	95	96.3	89

4.3.5 Heat of Combustion

The theoretical heat of combustion value is a basic, very important measurement in any fire safety study. This is the theoretical maximum amount of heat that can be liberated by a product during fire, resulting from complete combustion. When the scientific validation through its actual measurement is unavailable (e.g., from oxygen bomb calorimetry), fairly accurate values of heat of combustion for solid fuels may be calculated using elemental composition of the solid alone as unique descriptors of the material, making use of well-known correlations that were initially developed for fossil fuels.[31] Two different underpinning parameters are generally used to qualify heat of combustion, the gross or high heating value (HHV), where water vapor condensation latent energy is considered, and low or net heating value (NHV), where this change in physical state is not considered.

The latter value is generally considered more appropriate in fire studies as a level of the fire location. Water is primarily released as vapor due to high fire temperature. One such empirical correlation used in this calculation is the Boie equation, which is mentioned below.[32,33]

Equation 4.1 $\Delta Hc\ (kJ\ g^{-1}) = 35.160C + 116.225H - 11.090O + 6.280N + 10.465S$

where C, H, O, N, and S are the mass fractions of carbon, hydrogen, oxygen, nitrogen, and sulfur, respectively, in the burning fuel, and ΔHc corresponds to HHV. In addition to humins produced by Synvina C.V., several other humins compositions reported in the literature[2,6,34] were also considered for calculating the Complete Heat of Combustion (CHC) values using Boie formula. Calculated values are represented in Table 4.3 together with a few reference materials like heptane, sucrose, and ethanol for a better understanding of energy intensity of humins and to predict their possible impacts.

From Table 4.3 we can observe that, irrespective of the varying origins of humins, the NHV does not vary significantly, with a standard deviation evaluated to be only ± 1.91. Irrespective of structural modifications that may result from humins' production modes, the observed differences in overall elemental composition of those carbohydrate-derived structures do not lead to significant differences in heat content. We may conclude from this simple analysis that humins would contribute to fire nearly in the same proportion as a dry wood (HHV = 19.5 $kJ{\cdot}g^{-1}$),[35] and half the proportion of more conventional hydrocarbon fuels in terms of energy release for the same mass converted in a fire event. This conclusion cannot reflect any difference in combustion kinetics which is focused in the following section.

Table 4.3 Composition and Complete Heat of Combustion (CHC) data of humins, ethanol, heptane and sucrose.

	C mass-%	H mass-%	O mass-%	NHV ΔHc ($kJ{\cdot}g^{-1}$)
Crude humins a*	53.4	5.9	39.7	20.2
Crude humins b*	53.9	5.7	39.8	20.1
Foamed humins*	63.1	4.5	30.9	23.4
Humins#[5]	60	5	32	23
Humins#[34]	64.8	4.1	31.1	24.7
Humins#[2]	66.7	3.7	29.6	23.7
Ethanol	52.2	13	34.8	26.8
Heptane	84	16	-	44.7
Sucrose	42.1	6.4	51.5	15

*Experimental humins samples; #Literature humins data

4.3.6 Ignition and Heat Release Rate in Fire Conditions

Both crude and foamed humins were submitted to piloted ignition in the Fire Propagation Apparatus (FPA). Foamed humins presented some resistance to ignition but ignited significantly faster (22 s) than crude humins *a* and *b* (88 and 75 s). The primary reason for this is the higher surface area/volume ratio in foams, where oxygen can more easily react with porous foams on the surface. Crude humins, with less surface area/volume ratio and nonporous physical state, take relatively more time for ignition. Thermal inertia of crude humins is also more important than for foamed humins, which is another potential explanation of differences observed in ignition times. Once ignited, the crude humins show a rapid increase in heat release rate which is attributed to the combustion of lower-molecular-weight hydrocarbons near the humins−fire interface. After the peak HRR (Heat Release Rate), the rate progressively decreases in 3 steps, as humins tend to swell and form residual porous char. This reflects a shift from the early diffusive flaming combustion mode taking place in the gas phase progressively to some heterogeneous combustion process involving the carbonaceous residue forming at the late stages of the studied combustion process. These results are found in correlation with TGA results discussed in the previous section.

Since lower-molecular-weight volatile compounds are partially or completely oxidized in foamed humins because of the initial thermal curing during their preparation, we may assume that the combustion of foamed humins is likely comparable with the final stage of combustion of crude humins. This is shown in the second part of the FPA combustion test, where crude humins have already turned to charring material. We have chosen to present HRR data in some unusual way for the fire test performed in a pool-like configuration (e.g., normalized values per gram of sample burnt and not per sample surface area). This is motivated by the fact that test runs (more marked with foamed humins) led to a 3D complex burning mode with a progressively undefined surface in combustion by contrast to flammable liquid pools burning in fully diffusive flaming mode in the gas phase (Figure 4.5).

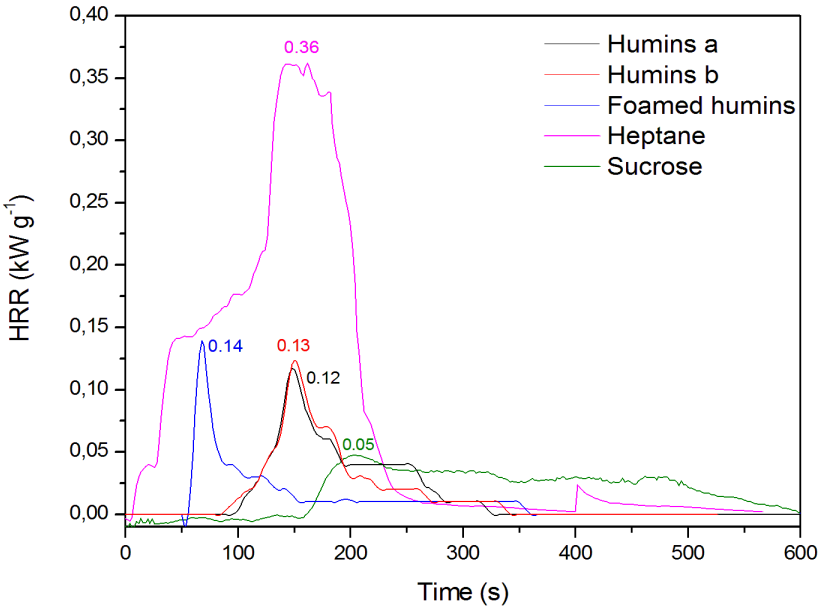

Figure 4.5. HRR (Heat Release Rate, kW g^{-1}) profiles of crude humins and foamed humins in comparison with those of heptane and sucrose as reference materials.

Peak HRR values per gram burnt of crude humins *a* and *b* and foamed humins were found to be 0.12, 0.13, and 0.15 kW·g^{-1}, respectively, and do not present any significant difference. This is likely to be due to the fact that the flaming combustion process has consumed the major part of the foamed humins sample, while in the case of crude humins a smaller fraction of the sample was consumed in the initial combustion phase. Although the comparison with heptane is not completely adequate (as a comparison between solid burning and liquid burning processes), we have tried to provide a comparison with a former test from INERIS, where heptane was burned in the Tewarson apparatus making use of the same size of sample holder, containing nearly the same amount of material (~22 g) as crude humins. In such conditions the normalized values of HRR (per unit of mass) were found to be ~ 67 % lower than that for heptane for crude humins, and ~ 59 % lower than that for heptane for foamed humins, indicating significantly lower thermal threats from humins fires compared to heptane fires. However, combustion of humins resulted in significantly higher values of HRR (60−70%) as compared to pure disaccharide sucrose in comparable fire conditions.

4.3.7 Yields of Major Combustion Products

Considering the elemental composition of humins that is essentially made of C, H, and O elements, the major gaseous combustion products expected are carbon oxides (CO and CO_2), water vapor, and unburned hydrocarbons that can be accounted for in terms of total

hydrocarbons (THCs). Release of combustion products in fire is driving the chemical threat, notably in terms of fire-induced toxicity of the fire gases and soot. This has justified the measurement of these combustion products in the FPA experiments with both crude and foamed humins. Data available so far reflects the combustion process in well-ventilated fire conditions (φ factor $\ll 1$). In these conditions, all carbon available in the crude humins structures would have preferably been converted to CO_2, reflected by the higher carbon conversion efficiency (95%) than in foamed humins (89 %) (Table 4.2).

We can further observe, from Table 4.4, a higher CO production in foamed humins than in crude humins. This statement simply finds its explanation with an easier mode of oxidation of crude humins compared to that of foamed humins in well-ventilated fire conditions, also likely to be related to enhanced thermal stability of foamed humins by initial thermal curing. Consistently, incomplete combustion of foamed humins in well-ventilated conditions is also reflected by the production of higher quantities of THC (14.9 $mg \cdot g^{-1}$). In the same combustion conditions, crude humins a and b release lower amounts of THC (1.9 $mg \cdot g^{-1}$ and 1.6 $mg \cdot g^{-1}$, respectively), as their burning process is more efficient and more favorable in the gas phase upon their release in the flame.

CO_2 is clearly the major combustion product like in any combustion process involving hydrocarbons. As there are rather limited amounts of CO and soot produced in the test, we might have expected yields of CO_2 very close to theoretical maximum values. This is not actually the case due to the charring processes taking place and leaving a significant solid residue in both crude and foamed humins. However, due to the significant toxicity of CO (known to be responsible for a majority of fire deaths from building fires for decades), it is important to notice that our tests reveal a significantly higher conversion efficiency of carbon into CO in foamed humins under well-ventilated fire conditions (~15 % of theoretical maximum yield) compared to crude humins in similar fire configurations (less than 1 %).

Table 4.4 Yields of combustion products

	Crude Humins a			Crude Humins b			Foamed Humins		
	$mg \cdot g^{-1}$ [i]	$mg \cdot g^{-1}$ [ii]	% [iii]	$mg \cdot g^{-1}$ [i]	$mg \cdot g^{-1}$ [ii]	% [iii]	$mg \cdot g^{-1}$ [i]	$mg \cdot g^{-1}$ [ii]	% [iii]
CO_2	1958	1404	72	1976	1444	73	2314	1572	68
CO	1246	8.2	0.6	1257	6.8	0.5	1473	216.1	14.6
THC	593	1.9	0.3	596	1.6	0.3	676	14.9	2.2
CH_4	234	1	0.4	226	0.7	0.3	186	11.3	6
Soot	534 [iv]	0.8	0.14	539	3.7	0.6	631 [iv]	3.3	0.5

[i]Maximum theoretical yields. [ii]Yields as measured. [iii]Related conversion efficiencies (%) of carbon content into CO_2, CO, hydrocarbon (HC) content into THC, CH_4, and soot from crude and foamed humins. [iv]In theoretical estimations, soot is assumed to be pure carbon. Note: Carbon from the sample also remained in significant quantities of solid residue.

4.3.8 Other Products of Combustion Identified from FPA

While humins were burning in the FPA, production of soot particles was one of the evident observations made both from experiments and visual observations. In a fire, soot is a carbonaceous solid matter produced in a complex way from organic hydrocarbon fragments because of significant incompleteness of the combustion process. Limited quantities of soot (mainly composed of carbon) production were observed in both crude and foamed humins samples (measured yields by optical means were 0.8 and 3.3 $mg \cdot g^{-1}$, respectively), showing not surprising values far below maximum theoretical yields (see Table 4.4). Soot is usually produced after the oxidation of burning material into CO or CO_2, in the fuel-rich region of the flame through gas−solid interactions.[32] Indeed, oxygen-containing species rarely lead to significant emission of soot when burning in fire, particularly in well-ventilated fire conditions.

4.3.9 Thermal Hazard and Induced Toxicity from Fires Involving Humins

In the current study, heat release rates and yields of major combustion products shaping the overall potential toxicity have been determined. These data can be extrapolated to any well-ventilated fire of interest for fire risk assessment purposes by the use of rather classical fire protection engineering techniques, mostly developed and published by ISO TC92 subcommittees SC3 and SC4.[36,37] From the peak value of heat release, the point source model (radiant energy fraction is supposed to dissipate isotropically into a sphere of radius R) can be used to determine the distance R from the fire source at which a given amount of humins in

fire can critically transfer energy by radiation and provoke burns on living organisms or ignite remote combustible materials.[38]

Fire-induced toxicity is far more complex,[39] and still leads in some cases to some controversial views between fire toxicity experts. However, data from two immediate previous sections can be used to build up the "source term" for fire plume dispersion simulations corresponding to a given fire scenario of interest. Certainly, according to the nature and yields of products measured, fire toxicity will not depart significantly to major cellulosic fires (woody materials) and according to our results may essentially drive an actual concern in a confined environment. Nevertheless, some precautions shall also be taken in close proximity to fire events in an open environment that would involve foamed humins, according to the increased trend to convert humins carbon content into CO.

4.4 Conclusions

Until now, industrial humins have been considered as a non-hazardous by-products, while no rigorous study has been conducted to support this classification. As crude humins are increasingly investigated as new biobased feedstock for varieties of new applications in advanced biorefineries, no longer restricting its use for in situ energy conversion, there is a need for clarification on various aspects of humins on a broader perspective. In this direction, this paper is a preliminary attempt to understand the physicochemical safety concerns such as thermal stability, ignitability, and combustibility pertaining to humins (both in crude and foamed forms). Compared to crude humins, foamed humins depicted better thermal stability properties, and do not possess critical self-heating behavior, although presenting as a highly porous structure.

As for all organic compounds, humins are to be considered as combustible materials, and they are clearly, relatively easily ignitable under the presence of an energetic ignition source. The combustion behaviour of both crude and related foamed humins was further studied, both in terms of heat impact (e.g., energy release) and chemical impact (e.g., yields of combustion products liable to drive the potential fire-induced toxicity).

From experimental data obtained and by comparison of similar data existing for other well-studied fuels, we can conclude that the overall fire risk associated with humins does not differ significantly from conventional fires that would involve more conventional cellulosic fuels (e.g., woody materials).

To our knowledge, this work is the first reported information about humins focusing on safety issues, an often underscored aspect of sustainable use of new biobased feedstocks and materials.

As a word of caution, must be drawn attention to the readers that further work is still needed to achieve a more comprehensive insight and understanding of safety issues pertaining to use of humins and humins-based derivatives. Indeed, industrial humins can vary in composition depending on their origins, and the porosity profile of foamed humins can differ depending on their preparation methods. These aspects cannot be fully accounted for in our work. Application of humins and related processing leading to endproducts from such biobased feedstocks might also significantly change the safety side, which was not considered any further in our work.

4.5 Materials and methods

Humins Samples

Crude humins were produced in 2016 in the intermediate step of the FDCA production process in the processing plant of Synvina C.V., operating in Geleen.[40] They are a highly viscous dark material (Figure 4.6a). The molecular weight of Synvina humins has been reported in another study ranging between 270 and 650 $g \cdot mol^{-1}$.[41]

Foamed humins (Figure 4.6b) were prepared in a Nabertherm K430/75 dTRON oven under air-ventilated conditions, by placing 1 kg of crude humins in a disposable aluminum pan which was heating up to 250 °C with 5 °C min^{-1} ramp, kept at 250 °C for 1 hour, then cooled down to room temperature at 10 $°C \cdot min^{-1}$. Mass loss of ∼20 % was recorded after treatment of crude humins in such conditions.

Elemental composition of both crude and foamed humins was obtained by inductively coupled plasma (ICP) by Mikroanalytisches Labor Pascher, Remagen, Germany.

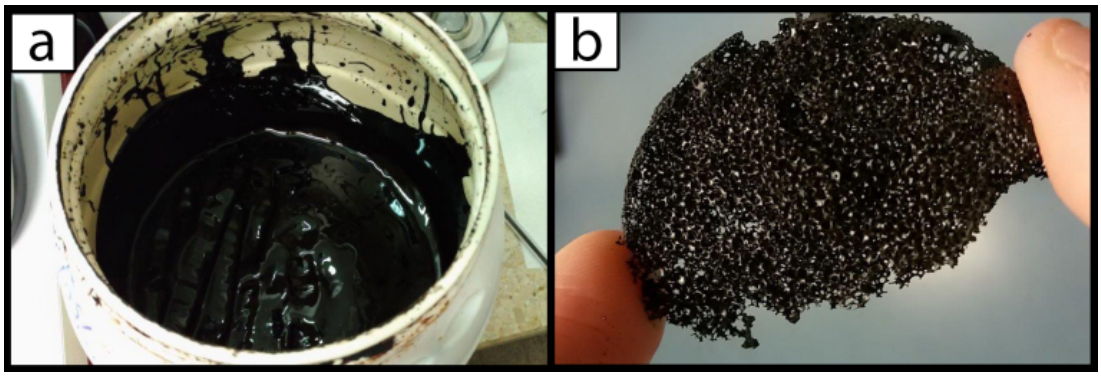

Figure 4.6 Visual aspect of a) crude and b) foamed humins used in the experiment.

Chromatographic Analysis of Raw Humins

GC analyses were performed with a TRACE GC instrument from Interscience, equipped with a FID detector and a column VF WAXms, 0.25 mm id film thickness 0.25 µm, 30 m. A 1 µL portion of a solution obtained by dissolving humins into a mixture acetonitrile/H_2O 50/50 w/w was injected and analyzed, while dioxane was used as standard in both calibration and samples. UPLC analyses were performed with a column from Waters, model Acquity UPLC HSS C18, 2.1 × 100 mm, 1.8 µm, equipped with UV and ELSD detector and maintained at 50 °C. Sample mass of 3.5 µL was injected and analyzed using 0.2% TFA in H2O and ACN/MeOH 50/50 (0.4 $mL \cdot min^{-1}$) as eluents. Saccharine was used as internal standard (measured at 250 nm).

Differential Scanning Calorimetry (DSC)

Thermal analysis was performed using the DSC apparatus from SETARAM, Model 131 evo, computer controlled by Calisto software. Temperature and enthalpy calibrations were performed by using indium, tin, lead, and zinc standards. A humins sample of 3.1 mg was prepared upstream and introduced into a high-pressure stainless-steel crucible of 30 µL volume. The crucible was then sealed under air, and introduced into the furnace of the calorimeter along with an empty crucible of the same nature serving as a reference. DSC scans were performed in the temperature range 25−500 °C with a heating ramp of 5 $°C \cdot min^{-1}$. A straight baseline has been used for thermograms. In the Results and Discussion section, T_{start} corresponds to the first integration bond, $T_{reaction}$ corresponds to the first and last integration bounds, and T_{onset} corresponds to the slope for the first part of the peak.

C80 (Calvet) Calorimeter.

A C80 CS evo instrument from SETARAM, computer controlled by Calisto software, was used as the confirmation test because of its higher sensitivity than standard, first generation DSC.

Temperature and enthalpy calibrations were performed by using indium, tin, and potassium nitrate. A 960 mg portion of crude humins and 161.8 mg of foamed humins samples were prepared upstream and introduced into a high-pressure stainless-steel cell, integrating an internal glass crucible. These quantities corresponded to the physical nature of samples with respect to the maximum available volume in the sample holder. Once closed, the crucible was introduced into the furnace of the calorimeter along with an empty crucible of the same nature that is serving as a reference. C80 scans were performed in the temperature range starting from 25 °C up to 300 °C using a heating ramp of 1 °C·min^{-1}.

Thermogravimetric Analysis (TGA)

TGA results were obtained using a Mettler Toledo TGA/SDTD 851e instrument. The microbalance has a precision of ± 0.1 µg and is kept at constant temperature (∼ 22 °C) during analyses to avoid its weight variation with temperature. A 12 mg portion of crude humins was placed in 70 µL alumina pans. The samples were heated at 10 °C·min^{-1} rate in the range 25–1000 °C under air and nitrogen gas flow of 80 mL·min^{-1} to determine the thermal behavior of humins. Foamed humins samples were subjected to TGA/DTA (DTA - differential thermal analysis) under an oxidative environment (Figure 4.7). This is a purpose-built instrument designed by INERIS (allowing application of test method ASTM E2550)[42] for further assessing the thermal hazard characteristics of solid samples. An interesting feature of this equipment[43] is the use of sample mass on the order of 1 g or more, largely over the classical milligram sample mass used in conventional laboratory-scale TGA/DTA commercial instruments. In addition to providing both mass loss and thermal decomposition, sample size also allows its use as a screening test for self-heating issues.

The test sample is placed in a small container made from wire mesh; an inert reference substance alumina is placed in an identical container. Both containers are introduced at ambient temperature into an oven and heated at a fixed rate (5 °C·min^{-1}). The variation of the mass of the sample is recorded as a function of time with an electronic balance. The temperatures of the sample and of the reference are also recorded as a function of time. An air flow of 440 Nl·h^{-1} (normal liters per hour) preheated to the oven temperature is maintained. Under these conditions, comparison of sample and reference temperatures shows, whether endothermic or exothermic, phenomena occur during the heating in a semi-quantitative way.

Figure 4.7 Large scale simultaneous TGA-DTA instrument built at INERIS.

Fire Propagation Apparatus (FPA)

The fire behavior of humins was tested using an FPA (Figure 4.8), commissioned at INERIS in 1997.[43–45] This apparatus is used as polyvalent equipment to characterize the fire behavior of various compounds under fire scenarios and associated thermal and chemical risks (e.g., fire-induced toxicity). The FPA is covered under various national and international standards, namely, FM 4910, NFPA 287,[46] ASTM E2058,[47] ISO 12136,[48] and TR 16312.[49] The apparatus is also known as the Tewarson calorimeter from name of its early designer. It is capable of measuring ignitability, fire propagation potential, and thermal and chemical characteristics of materials in fire conditions. This is a bench-scale multipurpose testing apparatus belonging to the family of fire calorimeters that has proven repeatability and reproducibility performances.[49]

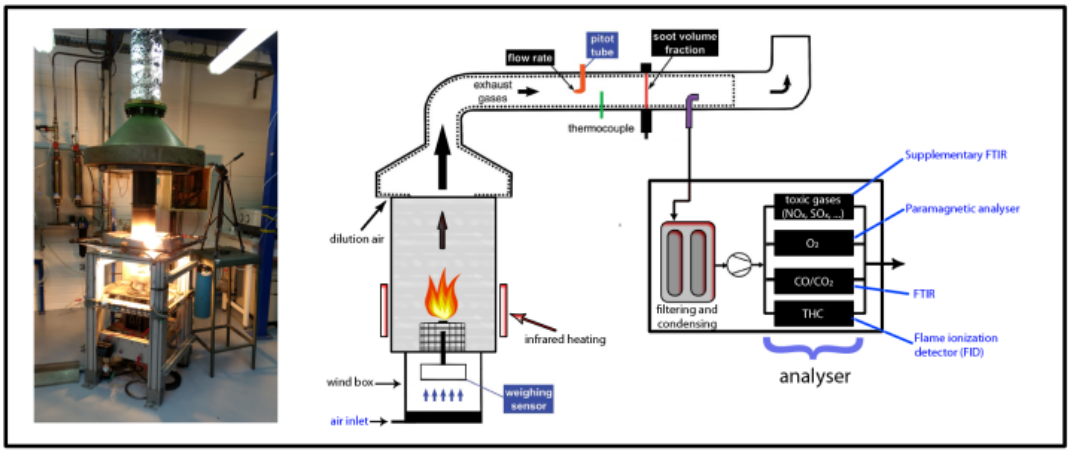

Figure 4.8 In operation and schematic view of the INERIS Fire propagation apparatus.

The INERIS FPA is fitted with a Thermo-Fisher Fourier transform infrared (FT-IR) instrument allowing the measurement of many gas species responding in the infrared spectrum. A sample mass of about 20−40 g is usually considered for testing chemicals under controlled gas flow in which characterization of the test sample (liquids, or dense or divided solids) can be made in a fuel-rich or fuel-lean environment to cover the full spectrum of fire conditions (well-ventilated to under-ventilated). Measurements such as mass loss rate, heat release rate, ease of combustion, and yields of combustion products for evaluating fire-induced toxicity are made by modern fire calorimetry relying of the assessment of oxygen consumption (OC) or carbon dioxide generation (CDG).[50] Such measurements give a broader view of the material's response to fire that facilitates a sound scientific diagnosis. Exploration of the full spectrum of ventilation conditions can be done through adjustment of inlet air flow and control of actual ventilation conditions through determination of the real-time equivalence ratio (φ factor)[43] which reflects actual fuel versus oxygen ratio normalized by the same ratio at stoichiometric conditions.

In the present study, preliminary tests were performed to choose the most suitable operating conditions for ignitability and fire propagation in well-ventilated fire conditions. Humins samples of about 20−21 g were placed in a glass sample holder. An external heat flux of 25 $kW \cdot m^{-2}$ was set in operation by four infrared heaters housed in air- and water-cooled jackets, allowing piloted ignition of the sample under calibrated heat stress by use of an electric spark or a pilot flame. Combustion gas analysis was performed by the online FTIR spectrometer calibrated over 20 gases for derivation of CO_2, CO, SO_2, NOx, HCN, and other species concentrations and relating release rates versus time. In addition, using sample mass loss data, and overall exhaust flow rate measurement, yields of related emissions may be derived.

4.6 References

[1] A. Schweizer, *Recl. des Trav. Chim. des Pays-Bas* **1938**, *57*, 345–382.

[2] A. Schweizer, **1940**, 781–784.

[3] I. Van Zandvoort, E. J. Koers, M. Weingarth, P. C. A. Bruijnincx, M. Baldus, B. M. Weckhuysen, *Green Chem.* **2015**, 4383–4392.

[4] I. Van Zandvoort, Y. Wang, C. B. Rasrendra, E. R. H. Van Eck, P. C. A. Bruijnincx, H. J. Heeres, B. M. Weckhuysen, *ChemSusChem* **2013**, 1745–1758.

[5] R. J. Van Putten, J. C. Van Der Waal, E. De Jong, C. B. Rasrendra, H. J. Heeres, J. G. De Vries, *Chem. Rev.* **2013**, *113*, 1499–1597.

[6] A. Mija, J. C. van der Waal, J. M. Pin, N. Guigo, E. de Jong, *Constr. Build. Mater.* **2017**, *139*, 594–601.

[7] T. M. C. Hoang, L. Lefferts, K. Seshan, *ChemSusChem* **2013**, *6*, 1651–1658.

[8] R. Dinu, A. Mija, *Green Chem.* **2019**, DOI 10.1039/c9gc01813a.

[9] M. Sevilla, J. A. Maciá-Agulló, A. B. Fuertes, *Biomass and Bioenergy* **2011**, *35*, 3152–3159.

[10] T. M. C. Hoang, E. R. H. van Eck, W. P. Bula, J. G. E. Gardeniers, L. Lefferts, K. Seshan, *Green Chem.* **2015**, *17*, 959–972.

[11] B. Hu, K. Wang, L. Wu, S. H. Yu, M. Antonietti, M. M. Titirici, *Adv. Mater.* **2010**, *22*, 813–828.

[12] A. Gajic, H. J. Koch, B. Marlander, *Zuckerindustrie* **2011**, *136*, 791–799.

[13] J. M. Pin, N. Guigo, A. Mija, L. Vincent, N. Sbirrazzuoli, J. C. Van Der Waal, E. De Jong, *ACS Sustain. Chem. Eng.* **2014**, *2*, 2182–2190.

[14] B. Kandola, L. Krishnan, in *Fire Saf. Sci. - Proc. 11th Int. Symp.*, **2014**, p. 769−780.

[15] B. K. Kandola, J. R. Ebdon, K. P. Chowdhury, *Polymers (Basel).* **2015**, *7*, 298–315.

[16] P. Tosi, G. P. M. van Klink, A. Celzard, V. Fierro, L. Vincent, E. de Jong, A. Mija, *ChemSusChem* **2018**, *11*, 2797–2809.

[17] ECHA, *Guidance on the Application of the CLP Criteria, Guidance to Regulation (EC) No 1272/2008 on Classification, Labelling and Packaging (CLP) of Substances and Mixtures*, **2017**.

[18] U. M. Regulations, *UN Recommendations on the Transport of Dangerous Goods - Model Regulations, 20th Revised Ed.; United Nations, New York, Geneva; ST/SG/AC10/1/Rev20 (Vol 1) and ST/SG/AC10/1 (Vol 2)*, **2017**.

[19] *Directive 2008/98/EC of the European Parliament and the Council of 19 November 2008 on Waste (Waste Framework Directive), Official Journal of European Union; European Commission*, **2008**.

[20] P. G. Urben, E. L., *Bretherick's Handbook of Reactive Chemical Hazards, 7th Ed.*, Oxford Butterworth-Heinemann, **2006**.

[21] L. Filiciotto, A. M. Balu, J. C. Van der Waal, R. Luque, *Catal. Today* **2018**, *302*, 2–15.

[22] L. Filiciotto, G. De Miguel, A. M. Balu, A. A. Romero, J. C. Van Der Waal, R. Luque, *Chem. Commun.* **2017**, *53*, 7015–7017.

[23] A. Sangregorio, N. Guigo, J. C. van der Waal, N. Sbirrazzuoli, *ChemSusChem* **2018**, DOI 10.1002/cssc.201802066.

[24] A. Sangregorio, N. Guigo, J. C. van der Waal, N. Sbirrazzuoli, *Compos. Sci. Technol.* **2019**, *171*, 70–77.

[25] J. E. Field, *Acc. Chem. Res.* **1992**, *25*, 489–496.

[26] K. Annamalai, I. K. Puri, *Combustion Science and Engineering*, CRC Press/Taylor & Francis, **2007**.

[27] W. Benaissa, D. Carson, "Comparison of the results from six calorimeters in the determination of the thermokinetics of a model reaction," can be found under https://hal-ineris.archives-ouvertes.fr/ineris-00976225/, **2011**.

[28] H. Liu, J. Y. Armand, J. Bouzon, J. M. Vergnaud, *Thermochim. Acta Elsevier Sci. Publ. B.V* **1988**, *126*, 81–92.

[29] I. van Zandvoort, E. J. Koers, M. Weingarth, P. C. A. Bruijnincx, M. Baldus, B. M. Weckhuysen, *Green Chem.* **2015**, *17*, 4383–4392.

[30] G. G. Eshetu, S. Grugeon, S. Laruelle, S. Boyanov, A. Lecocq, J.-P. Bertrand, G. Marlair, *Phys. Chem. Chem. Phys.* **2013**, *15*, 9145–55.

[31] A. O. Diallo, C. Len, A. B. Morgan, G. Marlair, *Sep. Purif. Technol.* **2012**, *97*, 228–234.

[32] M. M. Khan, A. Tewarson, M. Chaos, in *SFPE Handb. Fire Prot. Eng.*, Springer, New York, **2016**, pp. 1143–1232.

[33] G. Marlair, C. Cwiklinski, A. Tewarson, Edimbourg, **1999**.

[34] C. B. Rasrendra, M. Windt, Y. Wang, S. Adisasmito, I. G. B. N. Makertihartha, E. R. H. Van Eck, D. Meier, H. J. Heeres, *J. Anal. Appl. Pyrolysis* **2013**, *104*, 299–307.

[35] D. Drysdale, *An Introduction to Fire Dynamics, 3rd Edition*, John Wiley & Sons, Chichester, UK, **2011**.

[36] ISO, "ISO/TC 92/SC 3 - Fire threat to people and environment," **1980**.

[37] ISO, "ISO/TC 92/SC 4 - Fire safety engineering," **1991**.

[38] S. Brohez, C. Delvosalle, G. Marlair, A. Carrau, **2002**.

[39] A. A. Stec, T. R. Hull, *Fire Toxicity*, CRC Press, **2010**.

[40] Avantium, BASF, *Synvina : Joint Venture of BASF and Avantium Established*, **2016**.

[41] L. Filiciotto, A. M. Balu, A. A. Romero, E. Rodríguez-Castellón, J. C. Van Der Waal, R. Luque, *Green Chem.* **2017**, *19*, 4423–4434.

[42] Q. Kwok, B. Acheson, R. Turcotte, A. Janès, G. Marlair, *J. Therm. Anal. Calorim.* **2013**, *111*, 507–515.

[43] S. Brohez, G. Marlair, C. Delvosalle, *Fire Mater.* **2006**, *30*, 131–149.

[44] S. Brohez, G. Marlair, C. Delvosalle, *Fire Mater.* **2006**, *30*, 35–50.

[45] P. Ribière, S. Grugeon, M. Morcrette, S. Boyanov, S. Laruelle, G. Marlair, *Energy Environ. Sci.* **2012**, *5*, 5271–5280.

[46] *ASTM E2058-13a, Standard Test Methods for Measurement of Synthetic Polymer Material Flammability Using a Fire Propagation Apparatus (FPA); ASTM International, West Conshohocken, PA*, **2013**.

[47] British Standards Institution, **2011**, 1–60.

[48] ISO, "ISO/TR 16312-2:2007 - Guidance for assessing the validity of physical fire models

for obtaining fire effluent toxicity data for fire hazard and risk assessment -- Part 2: Evaluation of individual physical fire models," **2007**.

[49] G. Marlair, A. Tewarson, *Fire Saf. Sci.* **2003**, 629−642.

[50] H. Pretrel, W. Le Saux, L. Audouin, *Fire Saf. J.* **2013**, *62*, 192–205.

5 Investigating the properties of humins foams*

5.1 Chapter content

Humins as biorefineries by-product can be converted with a direct heating treatment into new rigid porous carbon materials known as humins foams. Currently, not many information about this new material are known. Here, a preparation protocol in two steps involving foaming and carbonization is reported, while the materials have been investigated in terms of morphology, elemental content, water adsorption-desorption, stability to solvents and high temperatures, and thermal conductivity. In order to evaluate their potential uses in applications such as water purification, the pH associated to the zero charge point has been identified. Foams prepared under air ventilated condition revealed an extremely negative surface, which can be used in cations exchange applications. The surface's groups have been identified by Boehm titration, showing that this behaviour can be associate to the presence of acid moieties, while the basic species result absent. The humins foams have been also tested through CO_2 adsorption tests at realistic operation conditions, revealing that their performances can compete with materials reported in literature. Finally, activated carbon monoliths from carbonized humins foams using CO_2 activation were tested, reaching a surface area of 1347 $m^2 \cdot g^{-1}$ after 20 minutes and 1482 $m^2 \cdot g^{-1}$ after 40 minutes of activation. These monoliths have been characterized in terms of morphology and elemental content. The results prove that the humins foams are very versatile materials, cost effective and easy to produce, with promising properties that can be further tailored for foreseen applications.

*Submitted to *Materials Today*.

5.2 Introduction

In Chapter 3 we have reported the preparation of a new polymeric macroporous rigid material called humins foams, which can be obtained directly from a mixture of industrial humins by a simple one-step thermal process, without any kind of modification or pre-treatment.[1] By controlling the preparation parameters, it is possible to obtain a uniform and homogeneous porosity with adjustable cell diameters of between 0.2 and 3.6 mm, or even porosity gradients. In addition, closed/open cells yield and carbon content can be tailored by choosing the conditions of preparation. The foaming mechanism has been identified as a combination of chemical reactions and physicochemical processes taking place simultaneously. The complex viscosity of the material drops from about 2.5×10^5 Pa·s to a minimum value of about 0.48 Pa·s when heated from 20 to 125 °C. At this latter temperature, the matrix is sufficiently fluid to allow an easy evolution of volatile substances. From a temperature of about 140 °C, several gases, mainly low-molecular weight species produced during the heating process (*e.g.* H_2O, CH_3OH, CO, CO_2) are released, producing bubbles in the molten humins matrix. The hardening process occurs above 170 °C, resulting in the final porosity in the thermoset humins-based material. However, it should be emphasized that the composition of raw humins may vary slightly depending on the specific parameters used in the ACD of sugars. The key steps of the foaming mechanism can be subjected to small temperature differences depending on the sample used, and in particular its viscosity. However, all the samples tested gave very similar results. Thus, in general terms, it can be assumed that this mechanism represents well the humins behaviors during the foam formation process.

Given the simple and economically attractive approach of humins foams production, as well as the current market of porous polymers and carbon-based materials, this route might represent a promising valorization of humins by-products. In order to find applications for these porous materials, their physicochemical behavior, composition, thermal stability, thermal conductivity, surface chemistry and morphology should be studied in more detail. In this work, we present the results of a series of characterizations that will help future studies to promote humins foams and optimize their parameters according to the intended application. Furthermore, a preliminary test of preparation of activated carbon monoliths from humins foams has been carried out. Activated carbon preparation is a generally inexpensive way to produce valuable materials from by-products and waste.[2,3] In 2018, Kang

et al.[4] reported the preparation of activated carbon from humins using chemical activation with KOH in a temperature range of 500 to 900 °C, reaching a BET surface area of between 428 and 1975 $m^2 \cdot g^{-1}$. Unfortunately, the material yields were quite low (15 to 39.2 %). In the same year, Chernysheva *et al.*[5] reported the preparation of activated carbon from humins using KOH activation and CO_2 physical activation, but reaching a BET area of only 862 $m^2 \cdot g^{-1}$ in the best case. We decided to test the preparation of activated carbon not directly from humins but from humins foams carbonized at 900 °C, in order to use the porous rigid carbon-based structure as a whole and to produce monoliths. Unlike the conventional powder form in which activated carbon is generally available, monoliths can be easily recovered and reused and can therefore cover a wider range of applications. Herein, we have proved that it is possible to prepare materials with high surface area that can compete with those available commercially.

5.3 Results and discussion

5.3.1 Porous structure and composition

Raw humins directly collected at the industrial plant and without any purification or modification step can be auto-crosslinked and foamed by a direct thermal activation process. However, the control of both the porosity and the morphology of the final foam requires the optimization of all the parameters involved (heating ramp, final temperature of the treatment, nature of the mold, etc.). For instance, using a heating rate of 1 $°C \cdot min^{-1}$ in a tubular oven under a flow of N_2, no foam is produced but a completely flat material is obtained instead. The chemical reactions and the gas evolution dynamics are indeed so slow that not enough bubbles are produced, and there remains after curing a quite low porosity in the material. Furthermore, ordinary tubular furnaces used for carbonization can only operate with limited amounts of material, whereas the nature of the available crucibles is generally restricted to ceramics.

To better control porosity and foaming yield, a two-step preparation is suggested. The first heating step can be carried out in air in any kind of oven using temperatures below 350 °C. Under these conditions, any type of mold, crucible, amount of humins and heating ramp can be easily applied without constraints (e.g. 1 kg of raw humins in aluminum pans). In this way, it is possible to produce large amount of humins foams in a short time, while the temperature

can be adjusted according to the desired porosity. Afterwards, the as-prepared humins foams can be carbonized at any selected temperature under N_2 and, as they have been thermoset in the previous step, the heating rate used during the carbonization does not influence the porosity.

Based on this procedure, we studied the effect of this 2-steps treatment on industrial humins and the main results concerning the synthesis yield and the characteristics of the process are presented in Table 5.1. The samples called F250 has been prepared from raw humins through a 1-step treatment at 250 °C (Figure 5.1), while F^2500 and F^2900 (2^{nd} step) have been prepared from F250 by carbonization at 1 °C·min^{-1} from 25 °C to 500 °C and to 900 °C, respectively.

Table 5.1 Data related to the preparation of humins foams, in 1 or 2 steps. The yields of the last step indicate the preparation yield for F250 (single step), and the carbonization yield for F^2500 and F^2900.

	Yield of last step (wt. %)	Total yield (wt. %)	Foaming Capacity (vol. %)	Shrinkage (from F250) (vol. %)	Bulk density (g cm^{-3})
F250	78-80	78-80	345	-	0.055
F^2500	50-52	41-43	290	17	0.070
F^2900	45.5-47.5	36-37	265	23	0.092

One hour of isothermal direct treatment at 250 °C resulted in a final foam F250 with a volume 345 % higher than that of the starting raw humins. During this process, a mass loss of about 20 % was observed, which is slightly lower than that reported in our previous work[6] due to a different thermal program (here, a direct isothermal treatment instead of a dynamic heating ramp). This method was carried out in the temperature range corresponding to the first step of mass loss deduced from the TGA of humins (140 and 260 °C). According to TGA-MS analysis, it was associated with the release of low-molecular weight species (mainly H_2O, CO_2, CO and MeOH).[6] Although TGA-MS was unable to detect any other volatile compound emitted by the material during thermal crosslinking, headspace analysis of the raw humins evidenced the presence of other species, especially furanic compounds. Head-space analyses were performed on raw humins at 170 °C (slightly below the hardening temperature), and are consistent with previously reported results.[7] During this heating process, 16 % of the total mass loss of the untreated sample was found in TGA, corresponding to the release of volatile compounds present in industrial humins. These species contribute mainly to the emission of gases during the heat treatment of humins, leading to the formation of cells in the final porous thermoset.

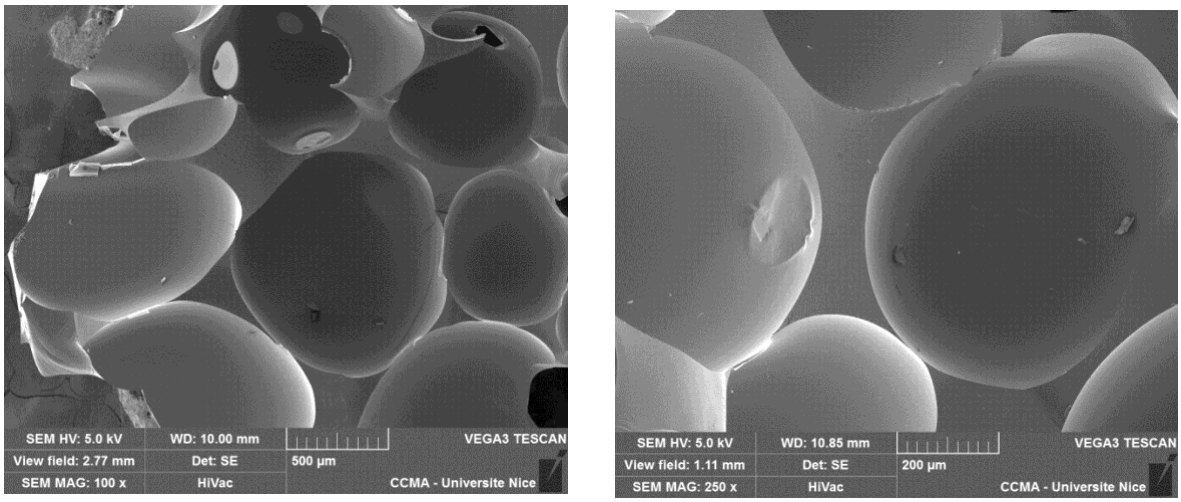

Figure 5.1 SEM images of F250 humins foam.

Despite these results derived by headspace analysis can be considered only as semi-quantitative, the values reported are interesting information for a first assessment of the species involved in the process. Accordingly, of this 16 % of mass loss, around the 49.2 % is associated to furanics (HMF, MMF and alkyl derivatives), corresponding to only around 7.9 % of the original sample mass. Around 40.5 % of this mass loss reported in **Figure 5.2** under the name "others" (corresponding to around 6.5 % of the original sample mass) includes several products such as MeOH, acetic acid, acetone, methylfoamate, formic acid and methylpuryvate.

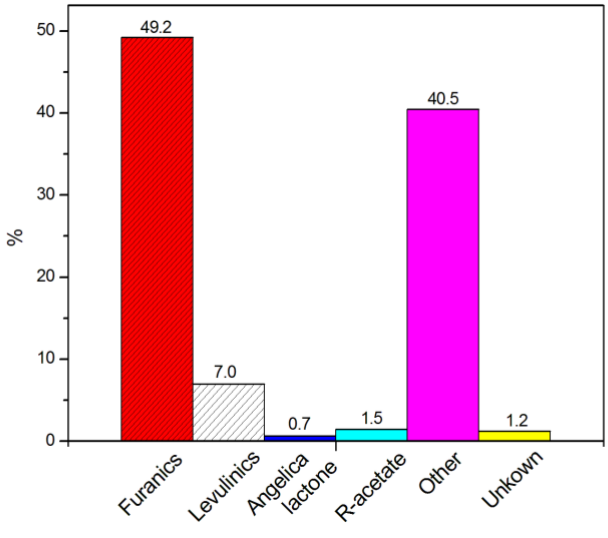

Figure 5.2 Headspace analysis of crude humins at 170 °C (total mass loss 16 %).

According to the characterization of the surface texture (BET and NLDFT) indicated in Table 5.2, the foam F250 has a negligible surface area, since the heat treatment was too mild to

produce porosity. In contrast, the foam F²500, obtained by carbonization under N_2 of F250 at 500 °C, presented a mass loss of approximately 50% during its preparation and made it possible to obtain a final yield of about 42 %. In this case, the foaming capacity was lower than that of the starting sample F250, i.e., with a volume 290 % higher than that of the initial raw humins. This is due to thermally induced rearrangements of the polymer network and the aromatization of the structure shown by the FT-IR analysis,[6] which led to a 17 % shrinkage of F²500 compared to F250, without modifying the global morphology. Again, the surface area of this foam remained little changed since the temperature was too low to produce additional porosity.

Table 5.2 Textural characterization from N_2 and CO_2 adsorption data at -196°C and 0°C, respectively, for all materials tested.

	N_2			CO_2		N_2 + CO_2				
	A_{BET} m²/g	V_{DR-N2} cm³/g	$V_{0.97}$ cm³/g	A_{BET} m²/g	V_{DR-CO2} cm³/g	S_{NLDFT} m²/g	$V_{<0.7,NLDFT}$ cm³/g	$V_{0.7-2,NLDFT}$ cm³/g	$V_{micro\ NLDFT}$ cm³/g	$V_{Total,\ NLDFT}$ cm³/g
F250	-	-	0.00		-	-	-	-	-	-
F²500	-	-	0.01	224	0.18	493	0.12	0.02	0.14	0.14
F²700	-	-	0.01	328	0.33	756	0.17	0.02	0.19	0.19
F²800	736	0.28	0.29	445	0.33	893	0.16	0.14	0.30	0.30
F²900	837	0.31	0.33	477	0.26	970	0.14	0.19	0.33	0.33
F²1000	711	0.27	0.28	481	0.28	930	0.18	0.14	0.32	0.32

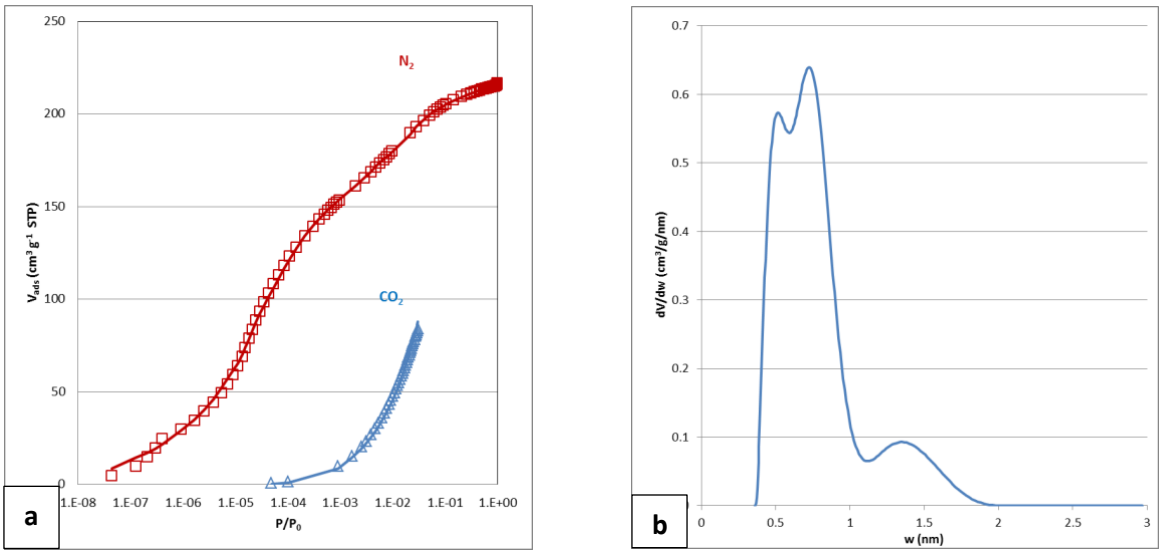

Figure 5.3 (a) Simultaneous fit of both N_2 and CO_2 isotherms of the F²900 foam by the refined 2D-NLDFT-HS method (the lines represent the predictions of the model); and (b) pore-size distribution obtained by application of the 2D-NLDFT method.

As in the previous case, the foam F^{2}900 was prepared by carbonization under N_2 of F250 at 900 °C. During this step, the material loses a mass fraction about 55 % higher than the starting F250, which gives a final yield of about 36 %. Due to the higher temperature, the shrinkage was higher than that of F500 (23 %), giving a foam volume 265 % higher than that of the starting raw humins.

In terms of BET area (A_{BET}) humins foams do not have a large surface area.[8] However, when the surface area was calculated by the 2D-NLDFT method, S_{NLDFT}, assuming slit pores, the result was higher than expected, reaching values of 756 and 970 $m^2 \cdot g^{-1}$ after carbonization at 500 and 900 °C, respectively. The surface area of F^{2}900 is thus particularly high compared to that measured for tannin-derived carbon foams, always lower than 1 $m^2 \cdot g^{-1}$.[9,10] The higher value of S_{NLDFT} when compared to A_{BET} is due to the existence of very narrow porosity, which is only accessible to CO_2 at 0 °C or in which only a monolayer of nitrogen can penetrate. In this sense, the application of the refined 2D-NLDFT model, developed for the analysis of biochars,[11] confirmed that the best simultaneous fitting of N_2 and CO_2 isotherms was obtained when the lower limit of pore width, w_{min}, of the N_2 kernel was 4.6 nm and not 3.6 nm. The adjustable value of w_{min} has a physical meaning as it provides an estimate of the minimum pore width accessible to N_2 molecules in the present conditions of measurement. Figure 5.3 shows the good simultaneous fit of N_2 and CO_2 isotherms and the corresponding pore-size distribution (PSD) obtained from this fit. The PSD showed that the carbon foam was exclusively microporous, with an average pore diameter of 0.78 nm. For F^{2}900, more than half of the microporosity corresponded to ultramicropores, $V_{0.7,NLDFT}$ = 0.16 $cm^3 \cdot g^{-1}$, while the total micropore volume was $V_{micro,\ NLDFT}$ = 0.30 $cm^3 \cdot g^{-1}$. The total volume calculated by the 2-NLDFT model was higher than that determined by N_2 adsorption, due to nitrogen diffusion limitations at -196 °C. This also agrees with the higher micropore volume of F^{2}900 determined by DR method from CO_2 adsorption data, $V_{DR\ -\ CO2}$, compared to that determined from N_2 adsorption data, $V_{DR\ -\ N2}$. Therefore, the presence of narrow ultramicropores with pore diameters of less than 0.5 nm, where diffusional resistances of nitrogen at -196 °C are important, makes $S_{NLDFT} > A_{BET}$, $V_{DR\ -\ CO2} > V_{DR\ -\ N2}$, and $V_{T,NLDFT} > V_{0.97}$.

In terms of macroporosity, according to our observations, the carbonization steps of F250 at 500 °C (in the preparation of F^2500) and 900 °C (in the preparation of F^2900) had a minor impact on the porous structure, the shape of the cells shape or the general aspect of the foams. F250 had indeed a homogeneous and uniform macroporosity, with pore diameters between 0.5 and 0.7 mm, while the cells were closed (Fig. 1). These properties were maintained in the derived foams obtained by carbonization at 500 °C and 900 °C, except for the corresponding shrinkage, which slightly reduced the pore diameters (0.3-0.5 mm in F^2900). Such shrinkage did not alter the shape of the material but only reduced its size. Indeed, carbonizing F250 parallelepipeds to 500 °C and 900 °C led to smaller final samples but maintaining exactly the same proportions.

The bulk density of the foams increases with the carbonization temperature, from 0.055 $g \cdot cm_{-}^{-3}$ for F250, to 0.070 $g \cdot cm^{-3}$ for F^2500, and 0.092 $g \cdot cm^{-3}$ for F^2900 (Table 5.1). This effect is due to both the shrinkage/aromatization and the corresponding increase of carbon content. Indeed, in terms of elemental content, as can be seen from the elemental analysis (Table 5.3) and the van Krevelen diagram (Figure 5.4), the increase in the carbonization temperature of humins foams leads to a higher and higher carbon content, while the oxygen is gradually eliminated. From a C content of 53 wt. % in raw humins, it was possible to reach about 90 % of C with a carbonization temperature of 600 °C. A maximum C content of 96 % was reached in case of carbonization at 1000 °C, which corresponds to an almost pure carbon material. In this case, the residual O is only around 1.2 wt. %. These carbon foams are electrically conductive materials that could find application in several fields (e.g., in the preparation of sacrificial electrodes, electrical devices, supercapacitators) or as microwave absorbers and shields for electromagnetic protection.

Table 5.3 Elemental analysis of humins foams.

Sample	C (wt. %)	H (wt. %)	O (wt. %)	N (wt. %)
F250	61.25	4.70	34.56	0.06
F^2400	74.45	3.50	23.02	0.08
F^2500	84.25	3.10	12.20	0.13
F^2600	89.95	2.20	6.01	0.26
F^2700	93.20	1.20	6.25	0.48
F^2900	94.28	0.75	5.60	0.39
F^21000	96.06	0.19	1.24	0.29

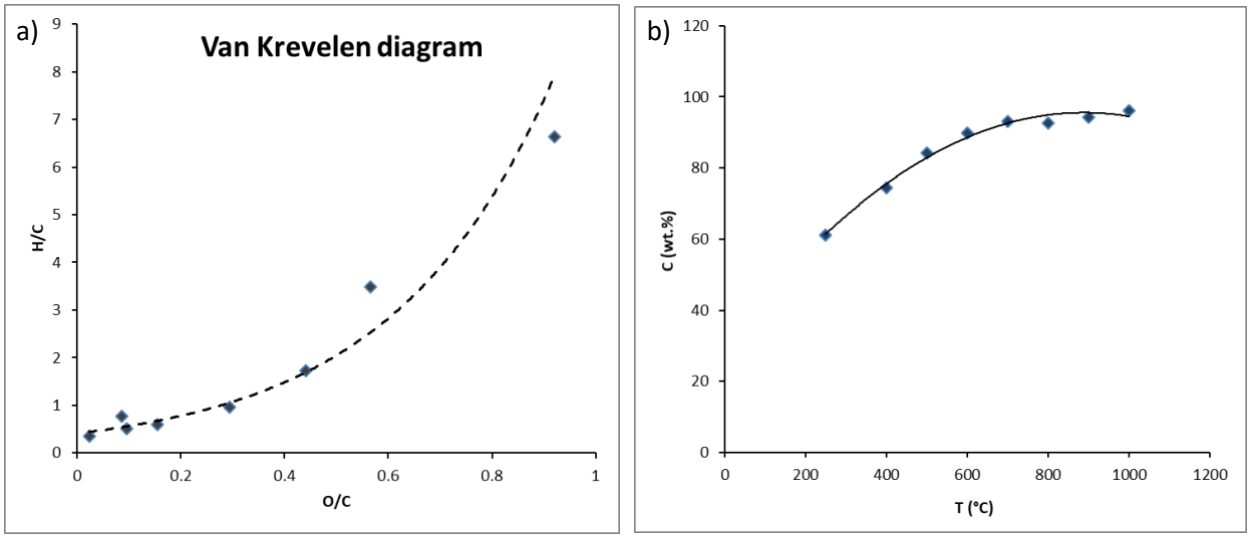

Figure 5.4 a) Van Krevelen diagram and b) evolution of carbon content as a function of temperature for the carbonization of humins foams.

The water adsorption data at 25 °C of materials F250, $F^2$500 and $F^2$900 are shown in Figure 5.5. The first part of the water adsorption isotherm, i.e., at $P/P_0 < 0.3$, reveals affinity of materials for water and is closely related to the nature and the amount of surface functional groups. The slope of the isotherm at $P/P_0 < 0.3$ decreased in the order F250 > $F^2$500 > $F^2$700 > $F^2$900, indicating the removal of oxygenated groups at increasing temperature, in agreement with the elemental analysis (Table 5.3). The second part of the water adsorption isotherm is related to the surface area, and hence the maximum amount of adsorbed water decreased in the order $F^2$900 > $F^2$700 > $F^2$250 > $F^2$500, in good agreement with the results obtained by N_2 and CO_2 adsorption already reported in Table 2. The maximum water uptake of 27.6 wt. % corresponds to $F^2$900 at $P/P_0 = 0.92$.

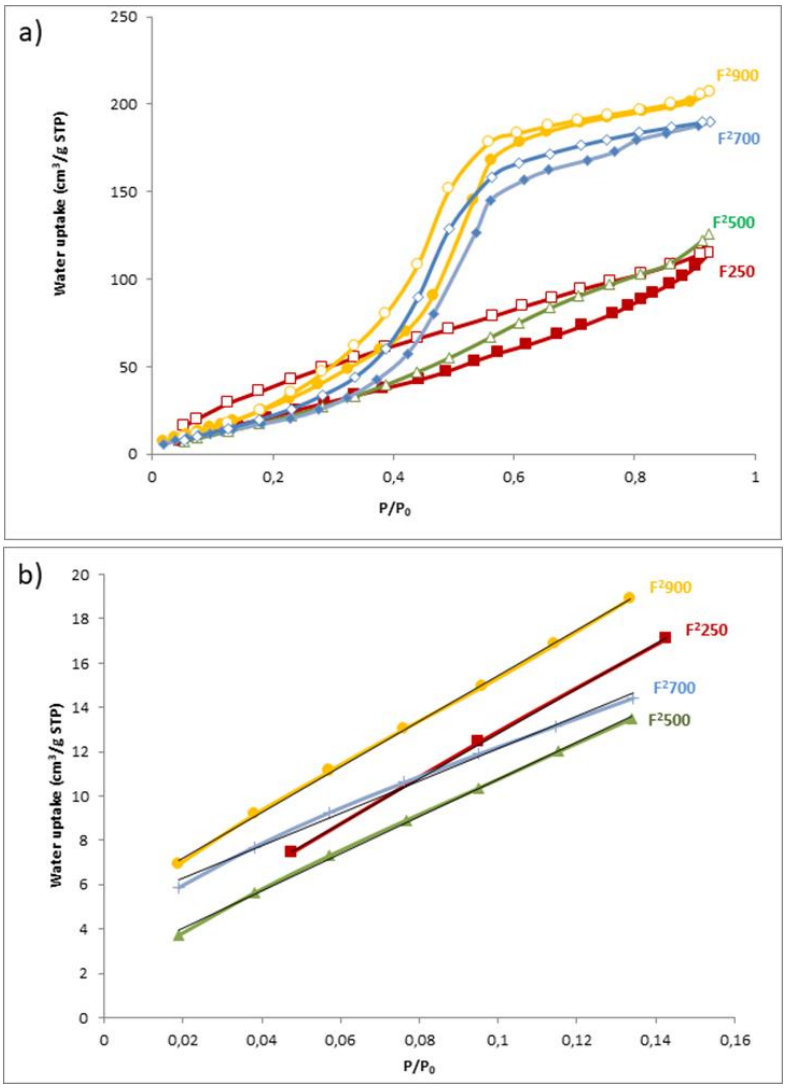

Figure 5.5 Water adsorption-desorption isotherms of humins foams F250, F2500, F2700 and F2900: a) complete data set; b) zoom on the range of low relative pressures.

5.3.2 Surface chemistry

During the foaming process of humins, the O content can be adjusted with the C content, which provides a good indication of the surface reactivity of the material. As shown in Table 5.3, the O content decreased from 34.5 wt. % in F250 to about 12 wt. % in F^2500, and even to 5.6 wt. % in F^2900. The minimum was found for F^21000, with only 1.2 wt. % of oxygen. Such a decrease in the amount of oxygen species was expected during the carbonization step. However, since some of this oxygen content can be involved in residual furan rings or in moieties of the crosslinked structure (such as ether, ester or ketone groups in the bulk), it is not possible to evaluate the surface behavior of these materials only based on this information.

By studying the oxygenated functions present on the surface of the material, useful information can be obtained concerning the possible applications of humins foams, such as adsorbents for water treatment or catalyst supports. In this context, one of the most important parameters describing the variable surface charge is the Point of Zero Charge (PZC), which is the pH that an aqueous solution in which the material is immersed must have to produce a total surface charge equal to zero (neutrality).[12] When the material is immersed in a solution whose pH is above the PZC, its surface has a net negative charge and therefore has a cation-exchange capacity (CEC). If the same material is immersed in a solution whose pH is below its PZC, it has a net positive charge with the ability to retain anions electrostatically, i.e., it has an anion-exchange capacity (AEC). To determine the PZC, several methods can be used, which may cause slight differences, depending on the technique.

The pH drift test is a method generally used to evaluate the PZC of a series of similar materials.[13,14] In this method, a certain amount of milled sample is added to an aqueous solution of known pH, and the variation of pH is recorded so that a curve of the initial pH (pH_{in}) with respect to the final pH (pH_{fin}) can be built. The PZC is thus obtained as the intersection between the resultant curve pH_{in} vs. pH_{fin} and the line $pH_{in} = pH_{fin}$. Another method is the mass titration method,[15,16] initially developed for OH-rich surfaces. The method is based on the principle that, by adding more and more solid to a solution of known pH, the latter will tend towards a pH limit value corresponding to the PZC. Therefore, starting from 3 solutions with different initial pH, and adding to each of them an increasing amount of solid, it is possible to build 3 pH curves that tend to the same value corresponding to the PZC of the solid. However, this method has some disadvantages, because the exact value associated to pH with a mass material tending to infinity is not always well defined (the curves sometimes tend toward slightly different pH), and the technique is theoretically limited to samples free of impurities. However, we used it to recheck the previous values obtained by the pH drift method. Humins foams prepared at low temperature (F180, F250 and F300, respectively prepared at 180, 250 and 300 °C under air) were also tested. Despite the good agreement found between the two techniques when using these foams, fluctuations were noted for F^2500 and F^2900.

The results obtained are reported in Table 5.4. They show that F180, F250 and F300 foams have a net negative acidic surface, with a notable value of PZC of about 2. This means that the surface of these foams is negative when immersed in water with pH values above 2, and is

positive only under extreme acidic conditions, with a water pH below 2. Since, in common aqueous applications, the pH usually ranges between 4 and 10, it can be assumed that the surfaces of F180, F250 and F300 are always negatively charged. On the other hand, the values obtained for F^2500 and F^2900 with pH drift and mass titration methods show some discrepancies, but within the limit of one pH unit. We can however approximate for both samples a PZC of around 7. According to these results, carbonization at 500 °C under inert atmosphere (N_2) is already able to produce a neutral surface by removing oxygen-based moieties from the surface, in agreement with the elemental analysis. In contrast, the PZC obtained for foams treated at lower temperatures (F180, F250 and F300) in air (oxidizing conditions) are extremely promising in CEC applications.

Table 5.4 PZC obtained from different techniques.

Sample	pH drift method	mass titration
F180	2.0	2.0
F250	2.0	2.0
F300	2.0	2.0
F^2500	6.6	7.2
F^2900	7.9	6.8

In order to better understand the nature of the remarkably low PZC values of F180, F250 and F300, the Boehm titration method[17–20] was used on a milled F250 foam. The results are reported in Table 5.5.

Table 5.5 Boehm titration results for F250 humins foam.

Sample	A_{BET}	Carboxylic groups		Lactonic groups		Hydroxyl groups		Basic groups		Total acidic groups	
	m^2/g	mmol/g	mmol/ m^2	mmol/g	mmol/ m^2	mmol/ g	mmol/ m^2	mmol/ g	mmol/ m^2	mmol/ g	mmol/ m^2
F250	0.2	0.2	0.9	0.09	0.3	0.4	1.6	0	0	0.7	2.8

Boehm's titration method is commonly used to identify and quantify oxygen-based functional groups on the surface of porous materials.[17–19,21–23] The technique is based on the assumption that bases/acids of given strengths can only neutralize stronger acids/bases. Therefore, it is assumed that $NaHCO_3$ (pK_{NaHCO3} = 6.37) can only neutralize carboxyl groups, that Na_2CO_3 (pK_{Na2CO3} = 10.25) neutralizes carbonyls and lactones, while NaOH (pK_{NaOH} = 15.74)

neutralizes all the acidic groups of the surface (carboxyls, lactones and hydroxyls). The total amount of basic surface groups can be evaluated by titration with a strong acid such as HCl. According to the results, the surface acidity of F250 can be justified by the presence of carboxylic acidic groups on the surface, accompanied by the total absence of basic sites. The main moieties present are OH-groups, while lactones are present only in the form of traces.

Since the PZC of foams prepared between 180 °C (minimum foaming temperature) and 300 °C is the same, it can be assumed that the chemical moieties on the surface of these materials are also very similar. These surprisingly low PZC values suggest their potential application to depollution of water by CEC effect.

5.3.3 Chemical stability

From the economical, practical and ecological point of view, the most interesting foam is the one that can be prepared at the lowest temperature (F180). However, since the chemical and thermal stability of such materials is influenced by the temperature of preparation itself, we must evaluate this aspect in order to identify the minimum preparation temperature of foam samples that can be applied in contact with solvents.

To evaluate the chemical stability of humins foams, samples of F180, F250 and F300 were milled and washed extensively with boiling distilled water, and the washings were analyzed by UPLC and GC-MS. While F250 and F300 wash solutions were clear and no dissolved species found inside, confirming the good stability of these foams, the resultant solution from F180 had an intense yellowish color. Furanic species were found in this solution by UPLC analysis, leading to the conclusion that F180 is not chemically stable. This can be explained by incomplete crosslinking of the structure at 180 °C, leading to the release of monomers or small oligomeric species.

Additional solubility tests were carried out by adding 0.1 g of milled humins foams to 15 mL of different solutions (water at pH 4, water at pH 9.5, EtOH, acetonitrile) and stirring the obtained suspensions for 24 h. Again, F250 and F300 demonstrated good stability, since no soluble species was found in the corresponding filtered solutions. On the other hand, the presence of furanics dissolved in F180 washing solutions was observed by UV-Visible spectroscopy (Figure 5.6). 180 °C is here confirmed to be a too low temperature to allow complete crosslinking of humins. The species released could come from either i) small

molecules released by hydrolysis from the surface of the foams, or ii) unbounded furanic species trapped in the humins mixture during the ACD process of sugars. Furthermore, according to headspace analysis, the treatment of F180 at 250 °C causes a loss of mass of 8.5 %, of which 4.2 wt. % comes from furanic compounds released in the form of volatiles. This can further justify the absence of these compounds in F250, where all volatiles are released at a higher foam preparation temperature. According to these results, it is not recommended to use F180 in applications involving immersion in solutions. However, F250 has shown good chemical stability, so the minimum temperature for preparing a stable foam for such applications can be set at 250 °C.

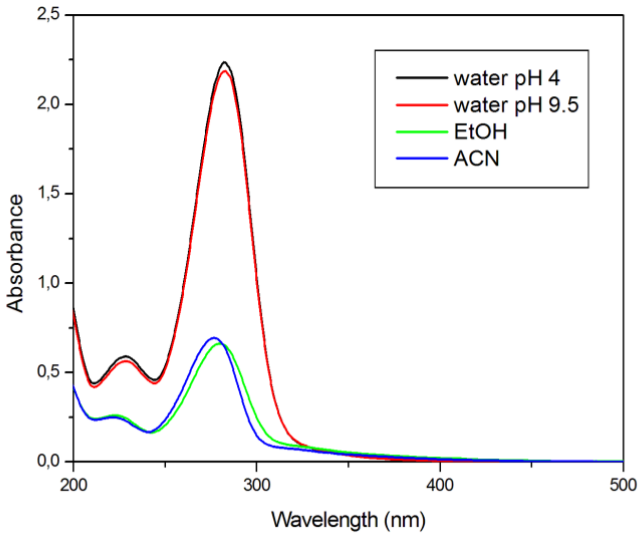

Figure 5.6 UV-Vis absorbance spectra of foam F180 washing solutions using ethanol (EtOH), acetonitrile (ACN), or water at different pH (4 and 9.5).

5.3.4 Thermal behaviour

The thermal conductivity, the bulk density (ρ) and the value of T_{10}, i.e., the temperature at which the material loses 10 % of its mass, of several humins foams are reported in Figure 5.7. It can be seen that F180 has a much higher density (0.132 $g \cdot cm^{-3}$) than that of other humins foams (below 0.1 $g \cdot cm^{-3}$). Indeed, 180 °C does not provide a sufficient mass loss (only 5.5 wt. % with a ramp of 10 $°C \cdot min^{-1}$), so that little gas is emitted during the preparation, which leads to a lower porosity in the final material. By using higher temperatures of 220 °C (mass loss of 12 wt. %) and 250 °C (mass loss of 20 wt. %), foams F220 and F250 are produced respectively with lower density and lower thermal conductivity. A further increase in the preparation temperature results in an increase in the density of the foams due to shrinkage, as well as an

increase in the thermal conductivity due to aromatization and increased C content. The maximum value of thermal conductivity was found for F^2900, 0.070 $W \cdot m^{-1} \cdot K^{-1}$, as predicted by its elemental composition (almost pure carbon) and its higher density (0.092 $g \cdot cm^3$). After optimization, foams F220, F250 and F^2500 might find interesting applications as thermal insulating materials. Indeed, according to the Federation of European Rigid Polyurethane Foams Associations, a material can be considered as good insulator if its thermal conductivity is in the range 0.035 - 0.055 $W \cdot m^{-1} \cdot K^{-1}$.[24]

On the other hand, the T_{10} value can be used to evaluate the thermal stability of humins foams. In unreacted raw humins, T_{10} was found to be around 200 °C,[6] whereas this value is higher in humins foams. With regard to the latter, T_{10} increases with the preparation temperature. This result was expected, since once a given temperature is reached during the preparation of the foam, all the possible reactions that can occur at this temperature are performed. New reactions, and therefore new loss of mass, can be observed only when the temperature is further increased. Thus, for instance, when the F300 foam is prepared at 300 °C, we assume that all the processes that could have happened at a lower temperature (e.g. 100, 150, 200, 250 °C) have already occurred, and that no mass loss can be observed below 300 °C.

The maximum value of T_{10} was reached with F^2500 (T_{10} = 500 °C), which corresponds to the value at which thermo-oxidative degradation (pyrolysis) occurs completely in air under the conditions used here. Above 500 °C, the material burnt completely. Thus, under air, no higher thermal stability can be achieved for humins foams using dynamic heating of 10 $°C \cdot min^{-1}$, as used in this work.

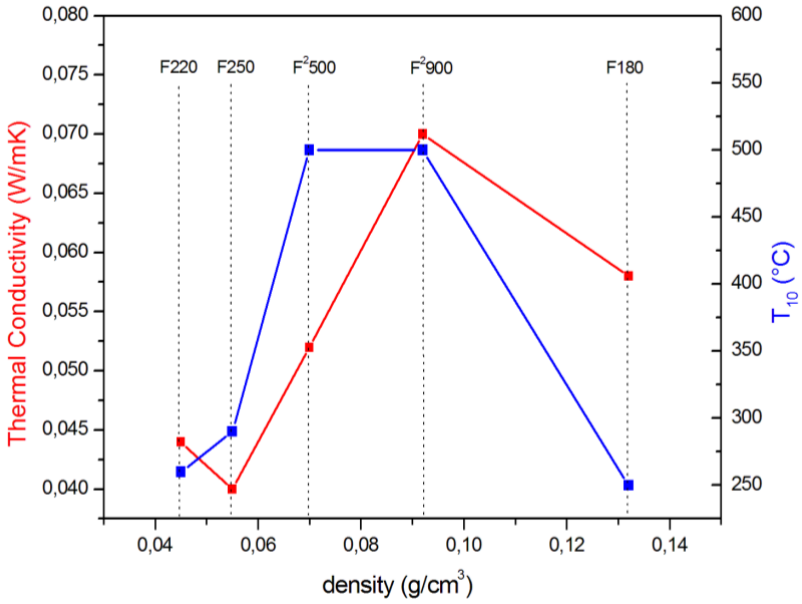

Figure 5.7 Thermal conductivity and T_{10} values (derived from TGA at 10°C·min^{-1} between 25 and 1000 °C under 50 mL·min^{-1} air flow) as a function of the bulk density (ρ) of 5 samples of humins foam.

To further evaluate the thermal stability of humins foams, headspace analyses of F180, F250 and F300 were carried out. Although these results were obtained by a qualitative analysis, we attempted to get semi-quantitative data using the total mass loss of the sample obtained by TGA and the comparisons between the areas of signals peaks in GC-MS. These results provide additional information about the nature of the gases emitted when humins foams are subjected to heating processes or thermal sources.

F180 already releases gases at 100 °C, with a mass loss of 0.5 %. Of these gases, about 70 % (corresponding to about 0.35 % of the total mass lost by F180 at 100 °C) corresponds to furanic compounds, while about 23.6 %, corresponding to 0.12 % of the total mass of F180, is associated with degradation compounds (i.e., acetone, MeOH and acetic acid).

By increasing the F180 treatment temperature, new unknown signals were found in the chromatogram. A possible candidate might be 5-methoxyfuran-2-carbaldehyde, not present in our library. As expected, the highest temperature investigated (250 °C) gave the largest amount of gas emitted by F180, which corresponds in any case to only 8.5 % of the total mass of F180. The maximum signal for F180 at 250 °C is associated with furanic compounds, which correspond to only about 4.21 % of the mass released by F180 in 2 hours. Specifically, and according to TGA, this mass loss occurs within the first 45 minutes, after which no further mass loss is detected, regardless of the duration of the thermal treatment. Therefore, we can conclude that no hazards are associated with F180 during similar thermal events.

As expected, the other foams studied (prepared at higher temperatures) showed greater thermal stability. No species were emitted and detected by treatment of F250 and F300 to 100 and 150 °C. At 200 °C, F250 had a mass loss of less than 1 %, mainly associated with degradation products. The loss of mass detected for F300 was even lower, and no furanics could be identified, suggesting their complete release during the foam preparation at 300 °C. Headspace analysis of F300 at 200 °C identified water as the main released compound, which can either be a residual by-product of condensation reactions or originate from water formerly adsorbed from the environment. Acetic acid was the main degradation product found for F300 at 250 °C. At the same temperature, traces of 2,3-butadiene and 2-butanone also appeared as degradation products, possibly associated with the higher carbon content of F300. These values are mainly relevant for describing trends. However, considering these values being the result of an overestimation, we envisage the worst possible scenario of evolution of volatiles. In the case where humins foams would be accidentally subjected to thermal sources, we can foresee an extremely limited risk for the environment and human health, in agreement with the previously reported studies.[25,26]

5.3.5 CO_2 adsorption

The application of humins foams to the adsorption of CO_2 at a temperature higher than or equal to room temperature has been tested, and the results are presented in Table 5.6. CO_2 is a molecule that can be easily adsorbed in materials having micro- and ultramicropores. Due to its low surface area (Table 5.2), F250, has the worst performance in terms of CO_2 adsorption. F^2500 and F^2700 adsorb more CO_2, and in a faster way. The fastest adsorption was observed for F^2500, where saturation was observed after only 37 minutes at 25 °C, while the largest amount of adsorbed CO_2 was found for F^2700, with 3.66 % wt. of CO_2 adsorbed. By increasing the temperature, the adsorbed molecules are less and less retained in the porous materials. F^2900 presented a quite high adsorption capacity, although less than the previous cases, its best value being 2.64 wt. % of CO_2 adsorbed at 25 °C. These results are comparable with those reported for material studied for similar application, with the advantage that humins foams are completely bioderived and that no surface activation have been performed.[27]

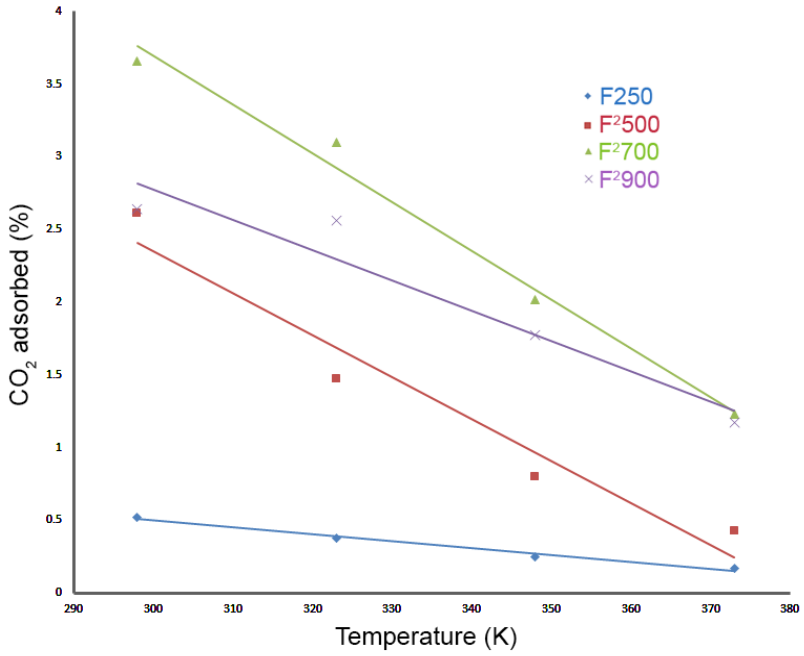

Figure 5.8 Representation of CO_2 adsorption trend at different temperatures for F250, F²500, F²700 and F²900.

Table 5.6 CO_2 adsorption capacity of humins foams F250, F²500, F²700 and F²900 at different temperatures (25, 50, 70 and 100°C). The saturation of the surface, expressed in time, is found when one reaches the plateau of the thermogram under flow of CO_2 gas.

	Temperature	**CO_2 adsorbed (wt. %)**	**Saturation (min)**
F250	25 °C / 298 K	0.52	> 60
	50 °C / 323 K	0.38	> 60
	75 °C / 348 K	0.25	> 60
	100 °C / 373 K	0.17	46
F²500	25 °C / 298 K	2.61	37
	50 °C / 323 K	1.47	25
	75 °C / 348 K	0.80	19
	100 °C / 373 K	0.43	14
F²700	25 °C / 298 K	3.66	44
	50 °C / 323 K	3.10	42
	75 °C / 348 K	2.02	36
	100 °C / 373 K	1.23	29
F²900	25 °C / 298 K	2.64	> 60
	50 °C / 323 K	2.56	> 60
	75 °C / 348 K	1.77	> 60
	100 °C / 373 K	1.17	> 60

Furthermore, we also found an almost perfect correlation between the differences in CO_2 adsorption at 50 °C and 100 °C and the volumes of micropores (< 1 nm) calculated by NLDFT (Figure 5.9). This confirms that CO_2 adsorption involves mainly pores with volumes minor than 1 nm. F250 has been neglected in this calculation because of the presence of the surface oxygen species that can influence the CO_2 adsorption as specific interaction rather than as texture effect. As observed in Figure 5.9, due to a high distribution in micropores volume, we don't find a linear relationship between values when pores < 2 nm are considerate (Figure 5.9, a). When pores < 1 nm are considered (Figure 5.9, b) we find a relation between values is almost perfect (R^2 = 0.99).

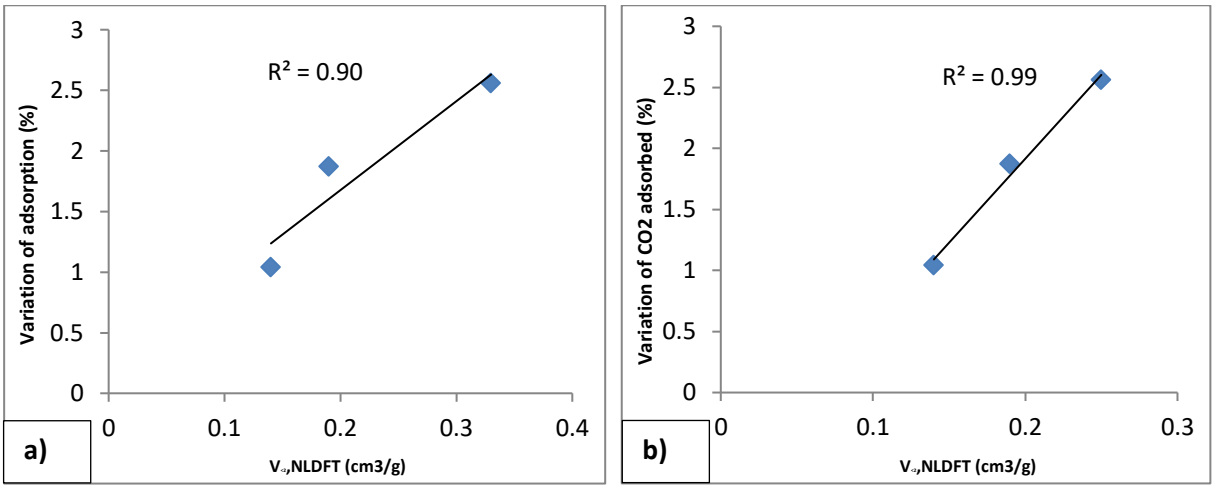

Figure 5.9 a) Volume of the pores < 2 nm (x) in function of the variation of CO_2 adsorption between 50 °C and 100 °C (y) of F²500, F²700 and F²900; b) Volume of the pores < 1nm (x) in function of the variation of CO_2 adsorption between 50 °C and 100 °C (y) of F²500, F²700 and F²900.

The capacity of storage at high temperatures (100 °C), which is relevant for combustion gases, can be compared in literature with results for similar materials. Relevant data have been recently reported about activated anthracite MSP-20X of KANSAI Coke (Japan).[28] Compared to humins foams, the latter carbon material has a higher surface area (A_{BET} = 2363 $m^2 \cdot g^{-1}$). Its CO_2 capacity passed from 2.6 $mmol \cdot g^{-1}$ (11.7 %) at 25 °C to 0.58 mmol/g (2.55 %) at 100 °C, not so far from the results here obtained for humins foams. However, humins foams have the advantage to be bioderived and sustainable, and that no activation is performed, while MSP-20X is produced from anthracite activated with KOH.

The humins foams could be competitive for CO_2 capture at relevant temperatures, even more if the apparent density of the bed is considered. Tapped density of a powder is calculated as ratio between the mass of the material and the volume it occupies after that has been tapped.

$$\text{Tap density} = \frac{\text{mass}}{\text{tapped volume}} \text{ (g/mL)}$$

Tap density can be seen as the random dense packing. Materials with high surface area generally have a low tap density, and so the needed adsorption volume (column or tank) is higher. For MSP-20X it has been calculated a tap density of 0.35 $g \cdot cm^{-3}$, while we found a much higher tap density of 1.00 $g \cdot cm^{-3}$ (Table 5.7) of grounded F^2900 humins foam. Even considering that the MSP-20X of KANSAI Coke adsorbs 2.55 % wt. of CO_2 at 100 °C, compared to 1.17 % for F^2900 we will need a taller column of MSP-20X because the bed density is much lower (2.9 times). Therefore, humins foams can compete in such applications.

Table 5.7 Tap density obtained with Autotap analyzer

	F^2900 (AUTOTAP)
Mass	4.849 g
Volume	4.85 mL
Tap density	1.00 $g \cdot cm^{-3}$

5.3.6 Activated carbon monoliths preparation

Humins foam F^2900 has been used in the preparation of activated carbon with the CO_2 activation technique. Table 5.8 presents the yields and the main textural parameters obtained by nitrogen and carbon dioxide adsorption, at -196 °C and 0 °C, respectively, for all the materials tested. The burn-off (loss of material mass) is one of the most important parameters to control in the preparation of activated carbon. As reported by Molina-Sabio *et al*., in order to maximize the porosity of the material, the burn-off should be less than 40 %.[29] Above this amount, although the material is still consumed by CO_2, no higher surface area is reached and, on the contrary, the surface area is increasingly reduced. This occurs because the pores formed during the early stages of activation increase in volume and number, and widen to melt in each other. This, along their external burning, reduces the surface area obtained during the first activation step.

Table 5.8 Yield and morphological characterization of activated carbon monoliths prepared from F^2900 humins foam at 900°C, using CO_2 flow = 60 mL/min for 10, 20, 40 and 60 min.

Time (min)	Burn off (%)	S_{BET} (m^2/g)	S_{NLDFT} (m^2/g)	$V_{DR, N2}$ (cm^3/g)	$V_{DR, CO2}$ (cm^3/g)	V_{NLDFT} (cm^3/g)	$V_{0.97}$ (cm^3/g)	V_{meso} (cm^3/g)
10	14.2	985	1151	0.37	0.33	0.40	0.41	0.01(3%)
20	36	1347	1326	0.49	0.34	0.52	0.56	0.04 (8%)
40	94.8	1482	1289	0.52	0.30	0.56	0.68	0.12 (19%)
60	100	/	/	/	/	/	/	/

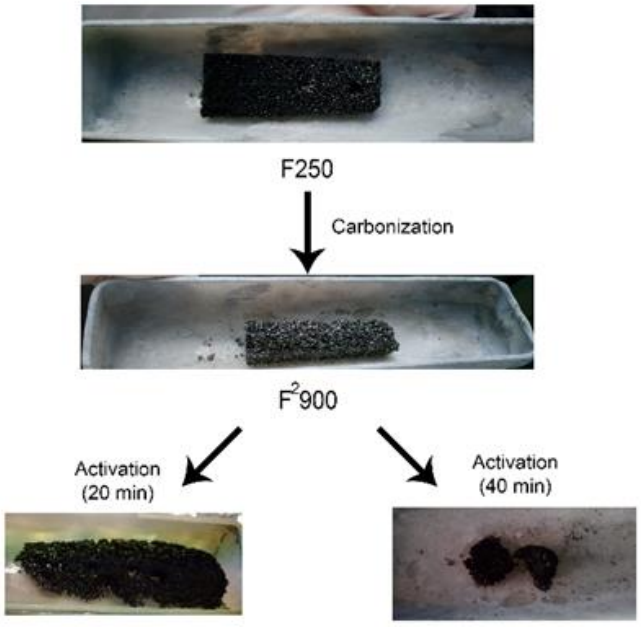

Figure 5.10 Activated carbon monoliths produced with 20 and 40 minutes of CO_2 treatment at 900°C.

The best result was obtained using an activation time of 20 minutes (Figure 5.10), with a burn-off of 36 % and a BET surface area of 1347 $m^2 \cdot g^{-1}$. Increasing the activation time to 40 minutes results in an almost complete loss of material, with a yield of only 5.2 %, while after 60 minutes the entire sample is completely consumed (Figure 5.10). The elemental analysis reported in Table 5.9 also shows how the CO_2 activation increases the O % at the expense of C %. This effect is due to the fact that during activation, CO_2 reacts with the carbon of the material, consuming it ($CO_2 + C \rightarrow 2\ CO$). As a result, C is progressively consumed, and the O/C ratio tends to increase.

F^2900 used in these preparations had an O content of 5.60 % and a C content of 94.28 %. After 10 and 20 minutes of activation, the O % increased by about 30 % while the C % decreased by 8%. This effect is even more pronounced after 40 minutes of activation, where O % reaches 14.31 %.

The BET area increased with activation time as well as the porosity in the range of micro and mesopores. Figure 5.11 shows the adsorption isotherms of nitrogen (Figure 5.11 a) and carbon dioxide adsorption (Figure 5.11 b) on non-activated F^2900 foam and activated carbon foams.

Table 5.9 Elemental analysis of activated carbon monoliths. The data are obtained as averages of two replicates.

Sample activation	C/H	%N	%C	%H	%O
10 min	61.46	0.12	90.61	1.47	8.15
20 min	53.72	0.07	86.76	1.61	7.90
40 min	72.96	0.07	76.18	1.05	14.31

By increasing the activation time, the elbow of nitrogen isotherms was widened, indicating a broadening of the microporosity and the total adsorbed volume was also higher. After 40 minutes of activation, the plateau was no longer horizontal, but a slight slope appeared, indicating the existence of mesoporosity (pores wider than 2 nm) as well as microporosity (pores narrower than 2 nm). The CO_2 adsorption isotherms give an indication of the volume of pores narrower than 1.2 nm. Activation times of up to 20 min created new pores, narrower than 1.2 nm, but higher activation times simply produced pore widening. Thus, the adsorption of CO_2 decreased and that of N_2 adsorption continued to increase. The latter was confirmed by the pore size distribution (PSD) and the cumulative pore volume (Figure 5.12) calculated by the NLDFT model.

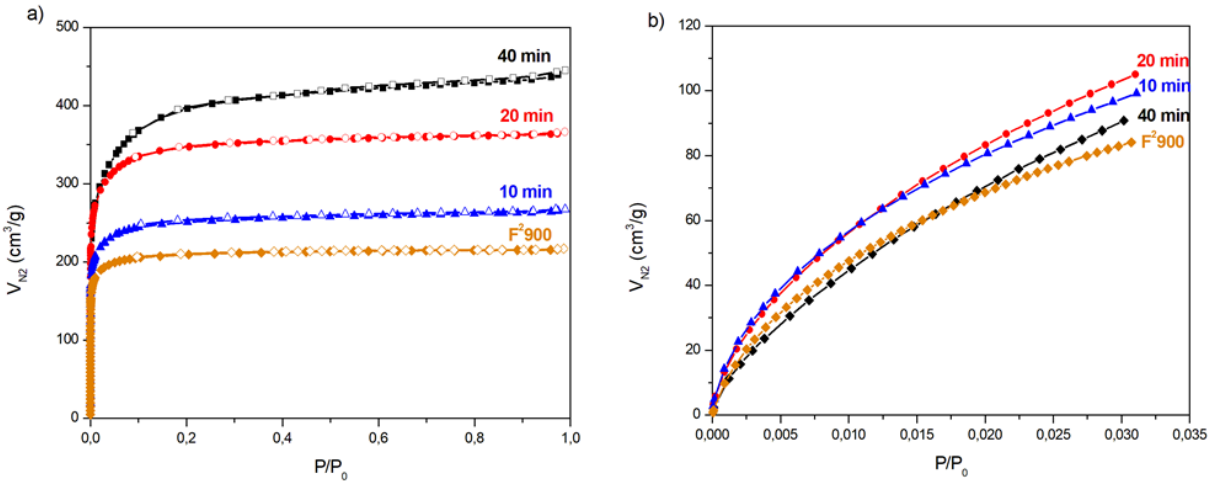

Figure 5.11 a) N_2 adsorption of F²900 and derived activated carbon monoliths produced after 20 and 40 minutes of CO_2 treatment at 900°C; b) zoom in the region 0-0-035 P/P_0.

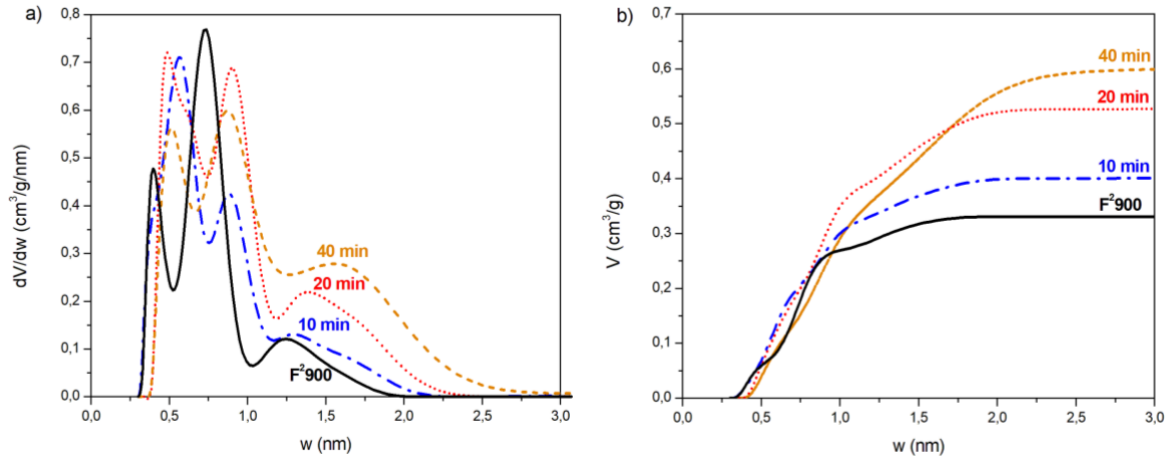

Figure 5.12 a) Pore size distribution and b) cumulated pore volume calculated by NLDFT.

5.4 Conclusions

In this work humins foams have been prepared and characterized in terms of composition, surface functionality, porosity, and thermal and chemical stability. The carbon content of humins foams can be controlled via the synthesis protocol, and can be as high as 95.4 % in the case of carbonization at 900 °C. This makes carbonized humins foams interesting for applications such as electrodes for energy storage and conversion, as catalyst supports, or as cheap adsorbents.

The surface chemistry of several humins foams has been investigated. Foams prepared at a temperature of 180 °C exhibit poor chemical stability, releasing furanic compounds in solution. These furanics might be unbound species present in the mixture of crude humins and originate

from an incomplete crosslinking, or come from the hydrolysis of the humins foams structure. Total solvent stability was obtained with foams prepared at temperatures above 250 °C. Of the foams tested, those prepared under air at a temperature below 300 °C had a net negative surface charge in water, with an impressive value of pH of zero point charge of about 2. Thanks to this low value of pH of zero point charge associated with a cation-exchange capacity, these humins foams can be applied in several fields (e.g. water depollution). In addition, thanks to their rigid and crosslinked nature, they can be prepared in blocks of indefinite dimensions (limited only by the dimensions of the crucible and the oven) and used as a whole. This aspect, as well as the cost efficiency of the raw humins, might be useful for preparing materials for the decontamination of large volumes of solvents, for which a high surface area is required.

Humins foams also have high thermal resistance, which increases with the temperature of preparation. According to headspaces analysis, all the foams tested released only a small amount of degradation gas over a period of 2 hours, thus excluding the risks of toxicity in the event of accidental presence of heat sources. The maximum amount of gas released was about 8.5 % of the total mass of the sample, obtained by heat treatment of F180 for 2 hours at 250 °C. F250 presented a higher thermal resistance, with only 0.43 % of mass loss over 2 hours. Therefore, according to the data reported here, humins foams prepared at a temperature above 250 °C exhibit the highest thermal and chemical stability, unlike those prepared at a lower crosslinking temperature. F250 also has the lowest thermal conductivity (0.04 $W \cdot m^{-1} \cdot K^{-1}$), which paves the way for new studies for applications as insulation material.

Humins foams have also been tested for CO_2 adsorption at temperatures ≥ 25 °C. The best results have been obtained at 25 °C, whereas the efficiency decreases with the increase of the adsorption temperature tested. Humins foams carbonized at 500 °C showed the fastest adsorption rate at 25 °C, reaching saturation with 2.61 wt. % of CO_2 fixed to the surface after only 37 minutes of treatment. Moreover, the largest amount of CO_2 adsorbed, 3.66 wt. %, was observed at 25 °C for foams carbonized at 700 °C, while the saturation was reached after 44 minutes of treatment.

Finally, the preparation of activated carbon monoliths from humins foams was tested. Physical (CO_2) activation was carried out at 900 °C, reaching a BET surface area of up to 1482 $m^2 \cdot g^{-1}$. The best results were obtained after 20 minutes of treatment, reaching a surface area of 1347 $m^2 \cdot g^{-1}$ with only 36 % burn-off. The textural characterization showed the presence of meso- and microporosity, as well as pores narrower than 1.2 nm. These activated carbons can

compete with those commercially available, with the advantage of great adaptability, because they can be produced in the form of monoliths easier to handle and recover, and with a favorable cost.

We can assume that all the results reported in this article, referring specifically to humins foams, could be extended (with the necessary limitations) to any material based on thermosetting humins and composites, where raw humins are used as starting material and crosslinked.

5.5 Materials and Methods

Crude materials

Humins were provided by the Avantium N.V pilot plant in Geleen (Netherlands) during the ACD of fructose into methoxymethylfurfural (MMF). This process is the key step in the production of 2,5-furandicarboxylic acid, intermediate for the production of polyethylene-furanoate (PEF).

Preparation of humins foams

The humins foams samples were designated by the letter "F" followed by the preparation temperature (e.g., F250 was prepared at 250 °C). Foams termed "F^2" were prepared with a two-step protocol (e.g., $F^2$500 was prepared by carbonizing F250 at 500 °C).

Samples F180, F220, F250 and F300 were prepared as follows: about 25 g of raw humins were installed in a rectangular flat-bottom alumina crucible and then transferred to a pre-heated Nabertherm L9/11/SKM oven for 1 h under air at temperatures of 180, 220, 250 or 300 °C, respectively. Then, the oven was set at 20 °C, and the samples were allowed to cool slowly down inside it (about 2 h required to reach room temperature).

$F^2$500, $F^2$700 and $F^2$900 were prepared by carbonization of F250 in a Carbolite GHC 12/900 tube furnace (N_2 flow ~ 80 mL·min^{-1}) with the following heat treatment: heating up at 1 °C·min^{-1}; isotherm 1 h at the final temperature (500, 700 and 900 °C, respectively); then 1 °C·min^{-1} while cooling down to room temperature.

Elemental analysis

The elemental analysis was carried out with an Elementar Vario EL Cube analyzer. Carbon, hydrogen, nitrogen and sulfur contents were first determined by combustion of the samples

at about 1700 °C (a temperature induced in a furnace, heated at 1150 °C, by a tin foil wrapping the samples and used as catalyst) in a stream of mixed oxygen and helium, the latter being used as a carrier gas. Oxygen was quantified with the same equipment in a second step, using a different procedure and another analytic column.

Headspace analysis – Headspace analyses were performed in an Agilent J&W DB624 (20 m x 0.18 mm x 1 µm) GC-MS equipped with headspace-auto-sampler and a mass-selective detector (MSD) with ionization *via* EI^+. 10 mg of humins or humins foams were weighed in a 20 mL vial and the vial was sealed. The vial was heated and shaken for 2 h (71 shakes·min^{-1} with an acceleration of 260 cm·s^{-2}) in the headspace auto-sampler, and a small amount (~ 1 mL) of the vapor was analyzed with GC-MS (inlet temperature 250 °C). The NIST library 11 was used for identification.

Density evaluation – Humins foams samples were cut into parallelepipeds and their volume determined accurately. The bulk density of each sample was evaluated as weight/volume (g/cm^3) ratio, and the average of three repetitions was calculated.

Mass titration

3 solutions of 0.2 M KCl were prepared and their pH was adjusted to either 3, 6 or 9 using 0.1 M NaOH/HCl solutions. The pH was checked at every stage using a Mettler Toledo LE pH-meter with LE438-IP67 pH electrode (calibrated every 24 h). Each of the aforementioned solutions was used to prepare 3 sets of 6 solutions (20 mL each): 6 solutions at pH 3, 6 solutions at pH 6, and 6 solutions at pH 9. In each solution of these series, an increasing amount of milled foam was added, so that each series contained 0.05, 0.1, 0.5, 1, 5 and 10 wt. % of sample, respectively. These suspensions were stirred and their pH was measured after 24 h. The final pH of each solution was plotted against the added mass of humins foam. The pH_{PZC} can be identified as the pH to which each series tends when the sample mass increases to infinity. The results have been reported as the average of three repetitions.

pH drift method

8 solutions of 0.02 M NaCl (13 mL each) were prepared by adjusting the pH in the range 2-9 with either 0.1M NaOH or 0.01 M HCl solutions. The pH was checked at each step using a Mettler Toledo LE pH-meter with LE438-IP67 electrode (calibrated every 24 h). To each solution, 0.1 g of the milled foam to be studied was added, and the mixture was stirred for 24 h. The pH shift was measured at the end of the 24 h, and the results were plotted as initial pH

(pH_{in}) vs final pH (pH_{fin}). The pH_{PZC} was identified by the point where the plotted curve crossed the line $pH_{in} = pH_{fin}$. The results were reported as the average of three repetitions.

Boehm titration

The number of surface oxygen-containing groups was calculated according to the Boehm titration method,[19,20] using the same automatic titration equipment described in the previous subsection. 20 mL of solutions of 0.05 M NaOH, 0.05 M $NaHCO_3$, 0.05 M Na_2CO_3 and 0.05 M HCl were prepared. To each solution, 0.4 g of milled humins foams were added. The flasks were sealed and the mixtures stirred with a magnetic bar for 24 h. During this time, part of the humins surface groups was neutralized by the respective solutions. The following assumptions were considered: $NaHCO_3$ neutralizes carboxyl groups; Na_2CO_3 neutralizes carbonyls and lactones; NaOH neutralizes carboxyl/lactone/hydroxyl (phenolic) groups; HCl neutralizes all basic groups. The solutions were then filtered to remove the solid material. In order to know the amount of NaOH and HCl neutralized by the surface groups of the humins foam, 2 mL of the filtered solutions were transferred to 10 mL flasks, and titrated with 0.1 M HCl and NaOH solutions respectively. On the other hand, 2 mL of the $NaHCO_3$/Na_2CO_3 filtered solutions were transferred to a 10 mL flask; to each solution, 2 mL of 0.1 M HCl were added, and the two resulting solutions were titrated back with 0.1 M NaOH. In this case, the back-titration gives results that are more accurate. The results were checked twice by a second repetition.

Solubility test

In order to identify the species released into water, 10 g of F180, F250 and F300 humins foams were thoroughly washed with boiling distilled water (550 mL) on a Büchner funnel equipped with filter paper under vacuum pumping. The filtered solutions were collected, diluted 1/3 with distilled water and saccharin (dissolved in acetonitrile (ACN)) added as an internal standard (0.2 $mg \cdot mL^{-1}$). The solutions were analyzed using a Waters Acquity UPLC HSS C18 column equipped with a UV detector, using 0.2% trifluoroacetic acid in H_2O as eluent. The column was thermostated at 50 °C.

The solubility test in different solvents was carried out by adding 0.1 g of milled F250 in 20 mL of ACN, EtOH, water at pH 4, and water at pH 9.5. The flasks were then sealed and the solutions were stirred for 24 h with a magnetic bar at room temperature. After centrifugation, 1 mL of each solution was withdrawn and was diluted 1/6 with distilled water. The absorbance of the

resultant solutions was acquired using a SHIMADZU UV-1800 spectrometer between 200 and 800 nm.

Thermal conductivity

The thermal conductivity was measured from parallelepiped-cut samples of humins foams (minimum dimensions 3 x 3 x 2 cm) using the transient plane source method with a Hot Disk TPS 2500 S thermal conductivity analyzer under fixed conditions of temperature and moisture content (20 °C and 40% relative humidity).

Thermal stability and mass loss analyses

Thermal stability and mass loss of humins foams were investigated by thermogravimetric analysis (TGA) using a Mettler Toledo TGA/SDTD 851 with a microbalance accuracy of ± 0.1 µg. The data were analyzed with STAR© software. Milled humins foams (10-12 mg) were placed in a 70 µL alumina pan and submitted to dynamic thermal programs. The thermal stability was evaluated between 25 and 1000 °C with a heating rate of 10 °C·min^{-1} (air flow = 80 mL·min^{-1}), and was reported as the T_{10} value, corresponding to the temperature at which 10 % of the mass was lost. The results were then averaged over two replicates.

Water vapor adsorption

Water vapor sorption-desorption isotherms were obtained with a Micromeritics 3Flex automatic device. Prior to analysis, the samples were outgassed under secondary vacuum at 110 °C for at least 72 h. The sorption measurements were performed by dosing water vapor at relative pressures (P/P_0) ranging from 1 to 90% at 20 °C, and measuring the equilibrium sorbed water for each value of P/P_0. Once P/P_0 = 90 % was reached, desorption was monitored, and the corresponding equilibrium sorbed water volumes were measured to build the desorption branch.

N_2 and CO_2 adsorption

Nitrogen (N_2) and carbon dioxide (CO_2) adsorption isotherms at −196 °C and 0 °C, respectively, were obtained with ASAP 2020 and ASAP 2420 (Micromeritics) automatic adsorption devices, respectively. The samples were outgassed under vacuum prior to adsorption analysis for at least 48 h at 110 °C.

Using Microactive® and SAIEUS® software provided by Micromeritics, the following parameters were calculated: (i) BET area, A_{BET} (m^2 g^{-1}), using the Brunauer–Emmet–Teller method;[30] (ii) total pore volume, $V_{0.97,N_2}$ (cm^3 g^{-1}) or Gurvitch volume, taken as adsorbed volume at the relative N_2 pressure of 0.97; (iii) Dubinin micropore volume, $V_{DR\text{-}N2}$ *or* $V_{DR\text{-}CO2}$

(cm^3 g^{-1}), from the Dubinin-Raduskevich method applied to the N_2 or CO_2 isotherms, respectively; (iv) specific surface area and micropore volume by applying the *dual gas analysis method* (2D-NLDFT) method to N_2 and CO_2 isotherms, S_{NLDFT} (m^2 g^{-1}) and $V_{\mu,NLDFT}$ (cm^3 g^{-1}), respectively.[31,32] An improved version of the 2D-NLDFT method, which takes into account the diffusion limitation in ultramicropores, was applied.[11] The pore size distribution (PSD) was also determined by applying the 2D-NLDFT to the calculation of: ultramicropore volume (pore size less than 0.7 nm) $V_{<0.7,\ NLDFT}$ (cm^3 g^{-1}), supermicropore volume (pore size between 0.7 and 2 nm) $V_{0.7\text{-}2,\ NLDFT}$ (cm^3 g^{-1}), micropore volume $V_{micro,\ NLDFT}$ (cm^3 g^{-1}), total pore volume $V_{T,\ NLDFT}$ (cm^3 g^{-1}), and average pore volume w_{av} (nm).

CO_2 adsorption above room temperature

22 mg of milled humins foams were placed in a platinum crucible with a pierced lid. The samples were analyzed with TGA under a gas flow of 80 mL·min^{-1} using the following program: from 25 to 120 °C at 30 °C·min^{-1} under N_2 (necessary to remove all gases previously adsorbed); isotherm of 30 min at 120 °C under N_2; cooling to the temperature of experiment (25/50/70/100 °C) at 30 °C·min^{-1} under N_2; equilibrium of 30 min under N_2. At this point, the gas was switched to CO_2 and the weight change was recorded for 1 h. The adsorbed CO_2 is expressed in wt. % relative to the mass of the sample. The saturation of the CO_2 adsorption, corresponding to the point where no additional CO_2 can be adsorbed on the surface of the humins foam is observed where the increase of the mass in the thermograph reaches the plateau, and is expressed in minutes.

Tap density determination

Tap and bulk density of F^2900 was measured with the tapped density analyser AUTOTAP (Quantachrome Instruments) and following the ASTM D8176-18 standard test method.[33]

Preparation of activated carbon

Approximately 250 mg of block F^2900 sample was weighted accurately and placed in an alumina crucible. Then, the sample was placed in a tubular quartz furnace. The sample was heated to 900 °C under N_2 (60 mL·min^{-1}) at 5 °C·min^{-1}. Then, the gas was switched to CO_2 (60 mL·min^{-1}) and held at 900 °C for the selected activation time (10, 20, 40 or 60 min). Finally, the gas was switched back to N_2, and the furnace was allowed to cool to room temperature.

5.6 References

[1] A. Mija, E. de Jong, J. C. van der Waal, G. van Klink, *Humins Containing Foam*, **2017**, WO 2017074183 A1 20170504.

[2] K. Kadirvelu, M. Kavipriya, C. Karthika, M. Radhika, N. Vennilamani, S. Pattabhi, *Bioresour. Technol.* **2003**, *87*, 129–132.

[3] N. Mohamad Nor, L. C. Lau, K. T. Lee, A. R. Mohamed, *J. Environ. Chem. Eng.* **2013**, *1*, 658–666.

[4] S. Kang, J. Fu, Z. Deng, S. Jiang, G. Zhong, Y. Xu, J. Guo, J. Zhou, *Sustain.* **2018**, *10*, 16–19.

[5] D. Chernysheva, Y. Chus, V. Klushin, T. Lastovina, L. Pudova, N. Smirnova, O. Kravchenko, V. Chernyshev, V. P. Ananikov, *ChemSusChem* **2018**, *11*, 3599–3608.

[6] P. Tosi, G. P. M. van Klink, A. Celzard, V. Fierro, L. Vincent, E. de Jong, A. Mija, *ChemSusChem* **2018**, *11*, 2797–2809.

[7] A. Sangregorio, N. Guigo, J. C. van der Waal, N. Sbirrazzuoli, *ChemSusChem* **2018**, DOI 10.1002/cssc.201802066.

[8] J. Encalada, K. Savaram, N. A. Travlou, W. Li, Q. Li, C. Delgado-Sánchez, V. Fierro, A. Celzard, H. He, T. J. Bandosz, *ACS Catal.* **2017**, *7*, 7466–7478.

[9] G. Tondi, V. Fierro, A. Pizzi, A. Celzard, *Carbon N. Y.* **2009**, *47*, 1480–1492.

[10] W. Zhao, A. Pizzi, V. Fierro, G. Du, A. Celzard, *Mater. Chem. Phys.* **2010**, *122*, 175–182.

[11] J. Jagiello, J. Kenvin, A. Celzard, V. Fierro, *Carbon N. Y.* **2009**, *144*, 206–215.

[12] F. I. Morais, A. L. Page, L. J. Lund, *Soil Sci. Soc. Am. J.* **1976**, *40*, 521–527.

[13] J. Rivera-Utrilla, I. Bautista-Toledo, M. A. Ferro-Garca, C. Moreno-Castilla, *J. Chem. Technol. Biotechnol.* **2001**, *76*, 1209–1215.

[14] P. C. C. Faria, J. J. M. Órfão, M. F. R. Pereira, *Water Res.* **2004**, *38*, 2043–2052.

[15] J. S. Noh, J. A. Schwarz, *J. Colloid Interface Sci.* **1989**, *130*, 157–164.

[16] S. Žalac, N. Kallay, *J. Colloid Interface Sci.* **1992**, *149*, 233–240.

[17] H.-P. H. . Boehm, *Carbon N. Y.* **2002**, *40*, 145–149.

[18] H. P. Boehm, *Adv. Catal.* **1966**, *16*, 179–274.

[19] H. P. Boehm, *Carbon N. Y.* **1994**, *32*, 759–769.

[20] H.-P. Boehm, E. Diehl, W. Heck, R. Sappok, *Angew. Chemie Int. Ed. English* **1964**, *3*, 669–677.

[21] A. Contescu, C. Contescu, K. Putyera, J. A. Schwarz, *Carbon N. Y.* **1997**, *35*, 83–94.

[22] S. L. Goertzen, K. D. Thériault, A. M. Oickle, A. C. Tarasuk, H. A. Andreas, *Carbon N. Y.* **2010**, *48*, 1252–1261.

[23] I. I. Salame, T. J. Bandosz, *J. Colloid Interface Sci.* **2001**, *240*, 252–258.

[24] BING, in *Rep. N1* (Ed.: F. of E.R.P.F. Associations), Federation Of European Rigid Polyurethane Foam Associations, **2006**, pp. 1–33.

[25] A. Muralidhara, A. R. Division, I. National, D. Environnement, *Biofuels, Bioprod. Biorefining* **2019**, 464–470.

[26] A. Muralidhara, P. Tosi, A. Mija, N. Sbirrazzuoli, C. Len, V. Engelen, E. de Jong, G. Marlair, *ACS Sustain. Chem. Eng.* **2018**, 16692–16701.

[27] E. S. Sanz-Pérez, M. Olivares-Marín, A. Arencibia, R. Sanz, G. Calleja, M. M. Maroto-Valer, *Int. J. Greenh. Gas Control* **2013**, *17*, 366–375.

[28] V. Fierro, E. García-Díez, S. Schaefer, A. Sanchez-Sanchez, M. M. Maroto-Valer, S. García, A. Celzard, in *Carbon2019*, Lexington USA, **2019**.

[29] M. Molina-Sabio, M. T. González, F. Rodriguez-Reinoso, A. Sepúlveda-Escribano, *Carbon N. Y.* **1996**, *34*, 505–509.

[30] S. Brunauer, P. H. Emmett, E. Teller, *J. Am. Chem. Soc.* **1936**, *60*, 309–319.

[31] J. Jagiello, C. Ania, J. Parra, C. Cook, *Carbon N. Y.* **2015**, *91*, 330–337.

[32] J. Jagiello, J. P. Olivier, *Adsorption* **2013**, *19*, 777–783.

[33] G. Sdanghi, V. Nicolas, K. Mozet, G. Maranzana, A. Celzard, V. Fierro, *Int. J. Hydrogen Energy* **2019**, *44*, 16811–16823.

6 Humins as bio-based template for the synthesis of alumina foams*

6.1 Chapter content

Biomass conversion strategies can improve the sustainability of the chemical industry. However, humins formation lowers the economic value of the production of chemicals from biomass. Therefore, valorisation strategies of these side-products became crucial. The peculiar foaming ability of the humins can be employed for the synthesis of inorganic foams, such as alumina. By using two different methods – one where humins foams are used as template and one where humins are foam-directing agents – this work aims to broaden the spectrum of the sustainable production of ceramic and porous materials. The as-synthesised materials were also tested in the selective oxidation of benzyl alcohol showing promising activity for catalytic applications.

*Submitted to *Journal of Material Chemistry A*

6.2 Alumina porous materials

As reported in the previous chapters, the development of a sustainable chemical industry is looking at the implementation of biomass conversion strategies to platform chemicals such as 5-hydroxymethylfurfural (HMF), furfural or levulinic acid.[1] These compounds are prepared *via* the hydrolysis of whole lignocellulosic biomass or bio-based sugars (*e.g.* glucose, xylose) catalysed by acids, either homogeneous or heterogeneous.[2] However, during the acid catalysed steps humins are formed. The implementation of a circular economy[3] is becoming imperative given the awareness of limited resources and need of environmental protection. For this, valorisation of humins through different strategies will improve the commercial value of chemical biorefineries. The several strategies studied and reported in literature include gasification/pyrolysis,[4–8] conversions to organic acids,[9,10] and (nano)composite materials.[11–14] Noteworthy, we reported in Chapter 3 the production of humins foams by direct and cheap thermal treatments (≥ 180 °C), while in Chapter 4 we deeply investigated these materials properties.[15,16] Since humins thermoset into porous material which morphology, carbon content and properties can be tailored by selecting the preparation parameters, including temperature, heating ramp and crucible material with control over the superficial oxygen functionalities, the thermal stability and the thermal conductivity, these materials are excellent candidates for porous materials templating. Furthermore, humins foams undergo complete thermo-oxidative degradation (burn-off) around 500 °C.[15] If this can be considerate a limit for many potential applications, on the other hand can be extremely useful in sacrificial templating protocols.

Inorganic (ceramic) foams have a wide range of applications thanks to their low density and thermal conductivity, thus finding applications in thermal insulations, molten metal filtration, light-weight structural components, and low-pressure drop catalyst supports.[17–21] Particularly alumina-based foams become advantageous thanks to the element's relative abundance and inexpensiveness.[22] Commonly these foams are prepared *via* the polymeric sponge replication method.[23] Other preparation methods include direct foaming of oxides dispersions by the addition of gases and surfactants, emulsion templating where the pores are given by oil droplets in a ceramic precursor sol or ceramic powder suspensions, or gel-casting.[23] However, these methods often resort to petroleum-based monomers or polymers, surfactants and solvents, thus allowing room for improvement of the process sustainability. New *green* advances in the preparation of inorganic foams look at the use of bio-based surfactants or foaming agents, such as amino acids (*e.g.* collagen)[23] or sugars (*e.g.* molten sucrose).[17–25] In a similar way, the use of

humins as renewable template/replica or as foam-directing agent is herein proposed. In this way, a cheap and environmentally-friendly product can be valorised, the mechanical stability of humins-based foams can be increased, and the sustainability of inorganic foams processes can be improved. As one of the applications of these foams would be as catalyst support, the synthesised foams were tested in the hydrogen peroxide-assisted oxidation of benzyl alcohol as model selective oxidation reaction. In particular, a protocol already described elsewhere[25–27] was employed with the difference of running the reaction under conventional heating rather than microwave. The observed activity for the alumina foams synthesised with the aid of humins endorses the development of sustainable protocols for the synthesis of inorganic foams.

6.3 Results and Discussion

Herein, humins were employed as sacrificial template/replica or as foaming agents. In the former case, foams prepared at 250 °C were employed given the higher concentration of superficial oxygen functionalities and lower thermal conductivity.[4] In particular, the presence of oxygen groups can act as anchoring points for metal precursors, such as the aluminium isopropoxide ($Al(iPrO)_3$) employed in this study. However, these foams often present fleeces blocking the pore structures, thus activation processes were investigated in order to have an open-pore structure but also modification of the superficial oxygen-containing groups. Among different oxidizers, nitric acid (5 wt. %) was found to open the cells without disrupting the macrostructure with a simple sonicator, while being also cheap and easy to do (Figure 6.1).

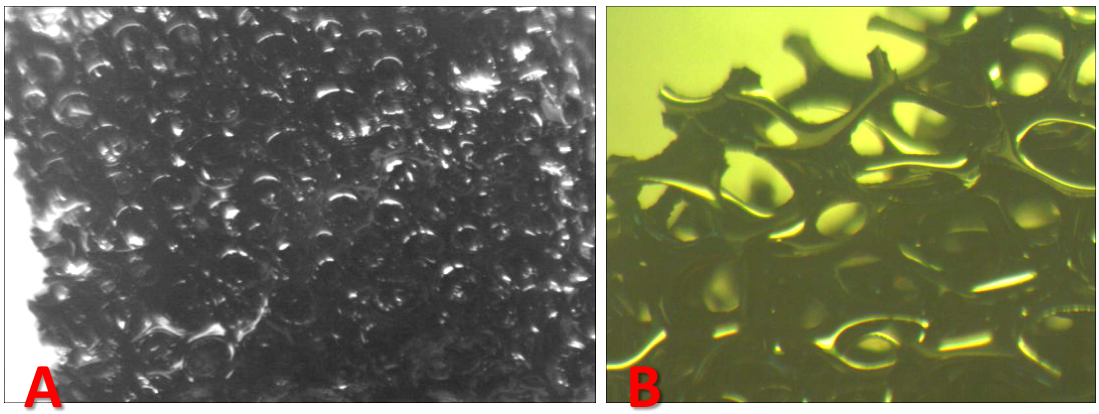

Figure 6.1 Micrographs recorded on an Optika Lite microscope of A) native foams and B) nitric acid activated foams.

On these foams, a gel-casting type of procedure with low-temperature sol-gel[28,29] synthesis of alumina from the isopropoxide precursor, $Al(iPrO)_3$, was applied in order to obtain the ceramic

foam. In particular, the sol prepared *via* hydrolysis of the isopropoxide was deposited on the humins foams by either evaporating the solvent (in our case, isopropanol) of the as-prepared sol (1.7 wt. % Al precursor), or employing a dip-coating technique by submerging the foams in the sol and repeating the procedure to achieve 50 or 100 wt. % increases of the original foams (*i.e.*, up to doubling the foam weight). Solvent evaporation would leave a lot of undeposited alumina in the vial, thus the dip-coating technique was preferred. Then the composite would be calcined at the burn-off temperature of the humins foams with 1 hour isotherms at low temperatures for solvent evaporation (50 and 80 °C) and a slow ramp (1 °C min^{-1}) to the calcination temperatures to allow a slow decomposition of the carbon template. The rationale of these experiments relies on the interaction of superficial oxygen groups of the humins foams with the $Al(OH)_3$ species formed *via* hydrolysis. In fact, the humins foams employed still would present *ca*. 30% of oxygen (based on elemental analysis) mainly as conjugated carbonyls.[15] However, an initial deposition experiment showed a tendency of pores clogging with alumina when calcined at 250 °C (Figure 6.2).

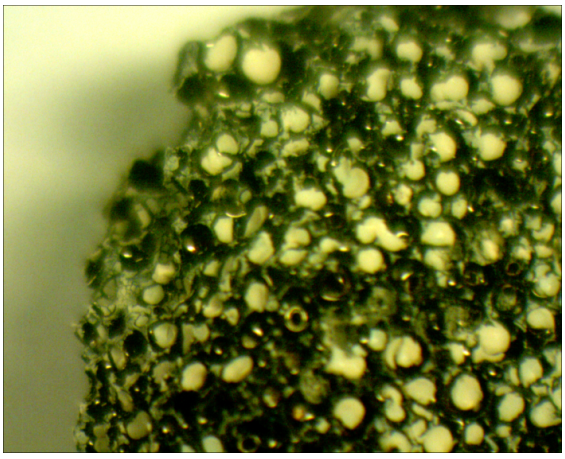

Figure 6.2 Micrograph recorded on an Optika Lite microscope of alumina deposition on a humins foam without an alkaline pretreatment.

For this, room temperature pretreatment of the foams in an alkaline media (NaOH 0.3 M, added to reach pH ~ 14) by vacuum submersion was applied in order to have higher $–COO^-$ superficial groups on the humins foams. If the foams are not dried off the excess of basic solution a gel is formed instantly upon addition of the foams; for this, the foams were allowed to dry at room temperature before being added to the sol. By doing this alkaline pretreatment and calcination at 250 °C (when the foams are still stable), it was possible to observe a better distribution of alumina on the foams structure, although still quite inhomogeneous (Figure 6.3).

Figure 6.3 Picture of alumina deposition on a humins foam with an alkaline pretreatment.

Calcinations at 500 °C allow the removal of the humins foams (based on TGA analysis),[15] and indeed an alumina foam is formed. However, the provided structure was extremely fragile and with poor mechanical properties (Figure 6.4).

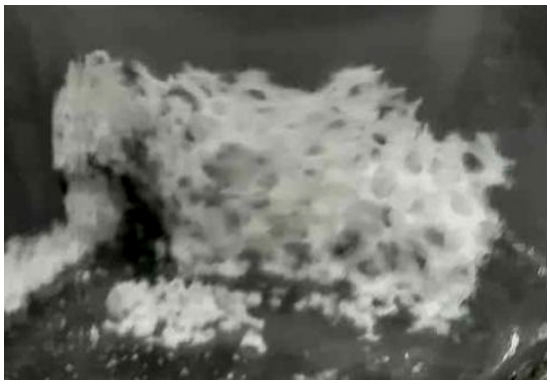

Figure 6.4 Resulting alumina foam after removal of the humins template at 500 ºC.

Even reaching a deposition up to 100 % of weight increasing did not produced foams with satisfying strength. According to XRD analysis, the alumina obtained is a γ-Al_2O_3 which is known for its catalytic or adsorbent properties (Figure 6.5).[30] Obtaining an α-Al_2O_3, on the other hand, would greatly improve the mechanical properties of the obtained foams, although its formation is given at high temperature treatments (> 1200 °C)[31] and our available equipment could only reach 1000 °C. Thus, calcination temperatures of 700 and 1000 °C were tested; although foams were formed, mechanical stability is not reached.

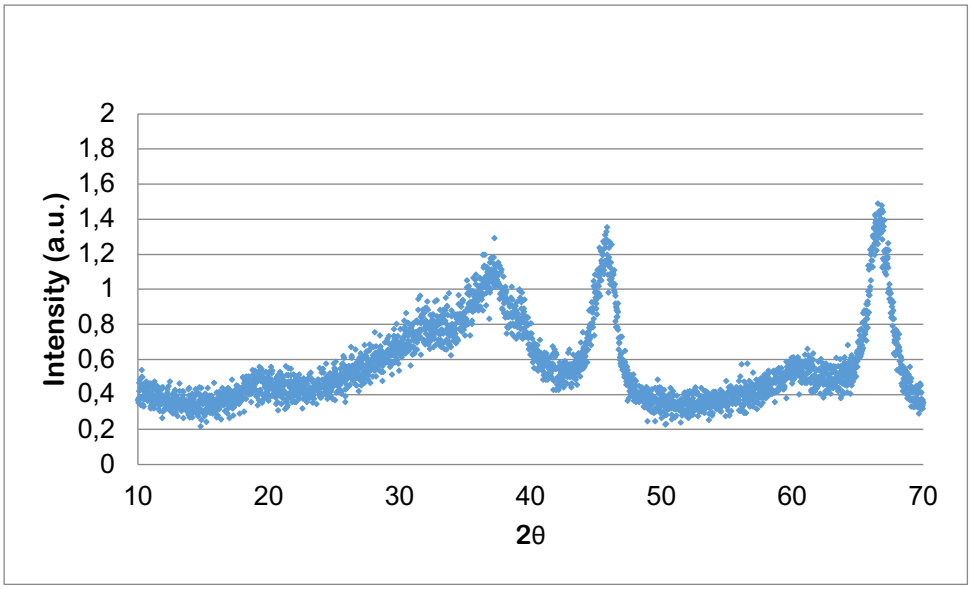

Figure 6.5 XRD pattern of an alumina foam prepared *via* dip-coating and calcinations at 500 °C.

Peptization of the Al sol with acetic acid was found to reduce the formation temperature of α-Al_2O_3 to below 1000 °C.[32,33] By keeping a molar ratio of organic solvent to acetic acid to Al isopropoxide at 40:3:1 and heating the slurry at 90 °C, a sol was prepared as described in another publication.[33] An alkaline foam (pretreated with NaOH) was then added in a dip-coating technique up to doubling the original foam weight with intermediate vacuum heating at 80 °C to speed up the process. In fact, the dip-coating technique was repeated numerous times over the course of a week given the low concentration of Al in the as-synthesised sol. The final dip-coated foam was then calcined at 700 and 1000 °C with extremely long isotherms (24 hours) at 80, 120 and 150 °C. Although an improvement of the mechanical stability was observed by small fractions, the mechanical stability is not satisfactory for the aforementioned applications. These results can be associated to the degradation of humins foams at high temperatures, releasing volatiles (*e.g.* CO, CO_2, small organic molecules) and degradation products and leading to the breaking of the scaffold. Also, during the thermal processes, the humins foams undergo shrinking, reducing greatly the strength of the scaffold.[34] Partial validation of the process described in the reference for acetic acid peptization of the alumina sol[33] is given by the observance of crystal growth and transition from the γ-Al_2O_3 to an intermediate polymorph prior to α-Al_2O_3 when increasing the temperature between 700 and 1000 °C. In fact, N_2 physisorption data showed a decrease of the BET superficial area (from 286 to 126 $m^2\ g^{-1}$) and increase of the average pores diameter (from 17 to 27 nm) with increasing the calcinations temperature, thus showing crystal growth. XRD analyses on the other hand show the transition from γ to θ-Al_2O_3,[35] although not reaching the α

form (Figure 6.6). Overall, the sol-gel procedure becomes tedious, expensive and long, and the desired mechanical strength of the foams is not reached.

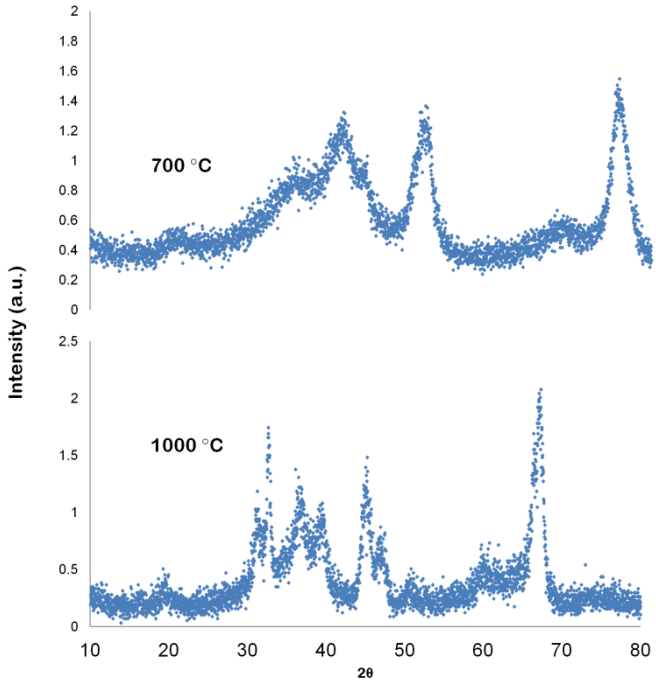

Figure 6.6 XRD patterns of the alumina foams prepared *via* dip-coating with a peptized alumina sol (acetic acid) and calcined at 700 (top) and 1000 °C (bottom).

Thus, knowing that humins can foam also in the presence of metals[14] and a similar procedure was reported elsewhere using sucrose,[17,25] a procedure were humins are employed as foaming agents has been envisioned. The idea involves the direct mixing of humins with alumina powder, the heating up of the mixture (allowing the humins to foam), and finally the burning off of the material leaving the alumina skeleton as bare structure. So, in this case, the humins foam morphology is directly transferred to the alumina, in a process that compared to the previously tested is faster, easier and solvent free. A 4 steps strategy has been designed: 1) mixing of commercial alumina with humins, 2) foaming at 220 °C, 3) carbonization at 900 °C (under N_2) and 4) burning off (600 °C in air ventilated oven). Before proceeding with the preparation, preliminary tests of mixing between humins and alumina were conducted, in order to evaluate the maximum amount of alumina that was possible to add in the humins mixture. Indeed, to achieve the expected product, the mixture should be as much concentrate on alumina as possible to give a scaffold with enough strength. For these preliminary tests, humins were heated up on a plate at 90 °C to reduce humins viscosity and allow the mechanical mixing. 35, 30, 25, 15 and 9 wt. % alumina concentrations were added respectively, and the resulting mixtures stirred. Accordingly,

it was observed that the compositions with 15 and 9 wt. % alumina can be mixed without problems on the heating plate, easily reaching a homogeneous mixture. When 25 and 30 wt. % alumina were added to the mixture, the stirring became harder to perform. A dense material was formed, but the mixing was achieved with good homogeneity by adding 0.5 mL of water, which helps reducing the mixture's viscosity. This water does not alter the morphology or the mechanical properties of the resulting foam, as we observed from preliminary tests by foaming humins with water added (up to 15 wt. %). Indeed, this water is released during the heating treatment before the cross-linking temperature is reached (170-180 °C).[15] On the other hand, it was not possible to mix when 35 wt. % alumina was added, neither after the addition of water. A tough sandy-like block was formed, and since the viscosity was too high it did not allow the humins to proper foam during the process. Noteworthy, when all these samples were subjected to foaming process (apart the 35 wt. % alumina one), the resulted foams appeared the same, and resulted in a good porous yield. Unexpectedly, also when the samples were carbonized and calcined the results were indistinguishable at sight, meaning that it is not necessary to use the higher concentration of alumina to perform this protocol.

A larger foam was thus prepared with a 30 wt. % concentration of alumina in humins along with 3 wt. % of water. Heating at 90 °C allowed stirring the slurry until homogeneity was achieved. Afterwards, the crucible was transferred in a ventilated oven and the mixture foamed for 1 hour at 250 °C. This step is necessary in order to control the kind of porosity expected. Already at 220 °C it is possible to achieve a good foam capacity with thermally stable pores morphology once the thermoset is achieved.[15] Therefore, the foam was transferred in a tubular oven and carbonized at 900 °C under N_2 for 2 hours (heating to 900 °C at 10 °C·min^{-1}, then slow cool down). During this step, the humins foams shrink of the *ca.* 20-23 % due to the rearrangement and aromatization of the chemical structure.[34] The change in chemical structure results in an increase of the C % of humins up to ~ 95 %.[15] Coupled to the shrinking of the humins scaffold, the graphene-type of thermoset increases the alumina density by compression. A final calcination step at 600 °C in a ventilated oven was then applied to remove the humins scaffold. The remaining alumina foam is rigid, although the top layer can be easily broken. Nonetheless, the interior appears sturdy and requires effort in breaking into smaller pieces.

The resulting alumina porous materials showed an average BET area of 200 $m^2 \cdot g^{-1}$ over three samples. XRD analysis showed no influence of the thermal treatments on the employed alumina nanopowder, being γ-Al_2O_3. The surface of the porous material has been investigated by SEM

analysis, and the results are reported in Figure 6.7 and Figure 6.8. According to the images, the alumina foams macroporosity resembles the one created by humins, as is possible to observe by the presence of macro-channels and cavities. On the other hand, interestingly, the surfaces appear spongy and porous, justifying the increasing of surface area (typical for humins foams is < 20 $m^2 \cdot g^{-1}$ at preparation temperatures below 400 °C).[15] The adhesion between alumina nanoparticles appears satisfactory, being able to yield compact, strong and definite structures. The surface of the obtained foam was checked from the elemental point of view by EDX, and the results are reported in Figure 6.9.

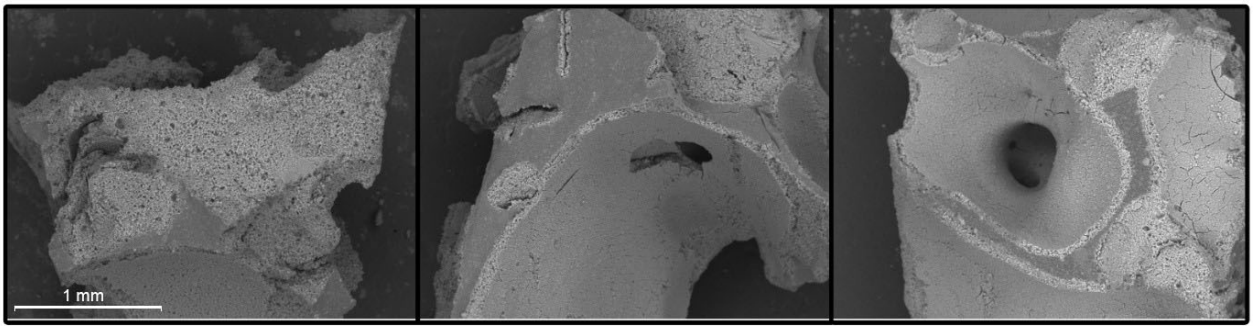

Figure 6.7 SEM images focusing 3 different positions on the alumina foam surface.

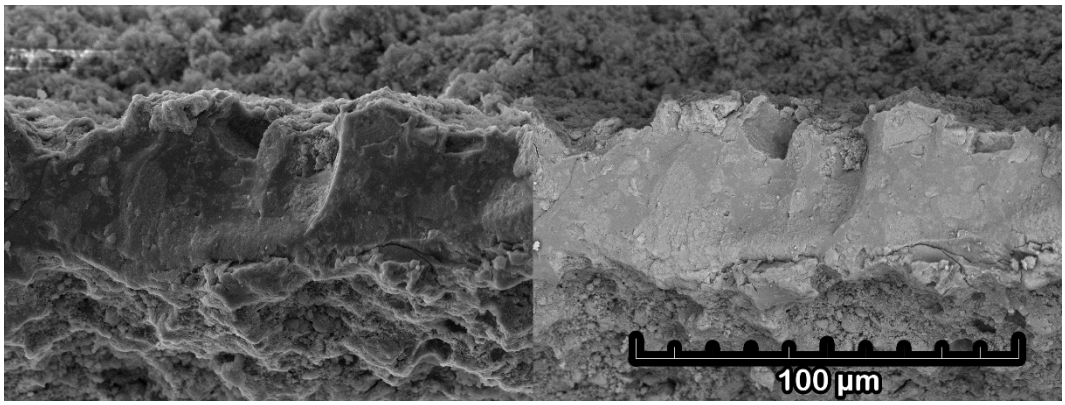

Figure 6.8 SEM observations focusing the alumina foam surface.

EDX analyses confirm that the structure is made up by alumina. Al is the maximum element detected, followed by O. The presence of carbon has still been detected, even if in small amount. However, must be highlighted that in some particular spots of the alumina surface, EDX identified a higher presence of C, indicating that an incomplete burning of the humins scaffold occurred. According to these results it seems necessary to apply higher temperatures or longer calcination treatments in order to completely get rid of all the humins residual parts. This means that the residual C % is a parameter that can be tailored. Indeed, for catalysis purposes this residual carbon can be useful, and even necessary in order to increase the eventual catalytic activity. For the other

applications, where pure alumina porous material is researched, this residual carbon should be better removed by optimizing the parameters used during the calcination step.

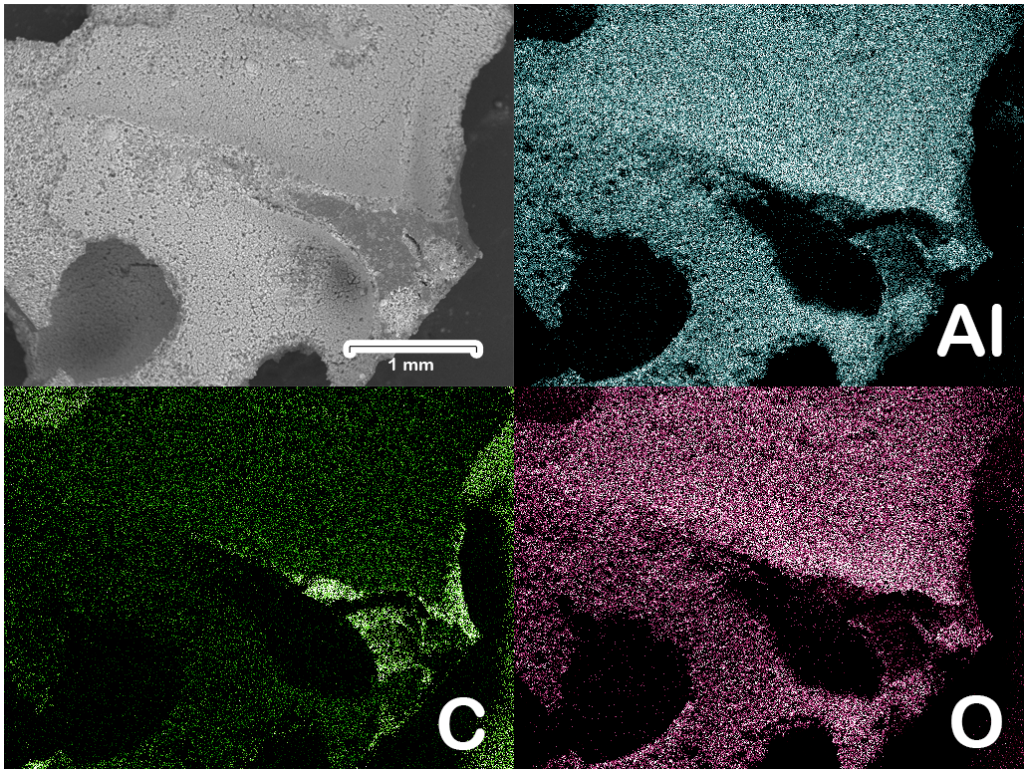

Figure 6.9 EDX of alumina foam surface. The intensity of the colour depends on the amount of element present. The colours are randomly chosen.

It should be noted that Al_2O_3 has a melting point of around 2000 °C. Despite the fact that it is not desired to reach the melting during the process, which would lead to a reduced surface area, higher temperatures would help the increasing of density and the condensation of the structure. Even if similar high temperatures are not reached in this study, an even more compact and stronger structure can be achieved by applying higher temperature treatments which will lead to the stable α-Al_2O_3.

On the other hand, γ-Al_2O_3 is traditionally preferred for catalytic purposes.[36,37] For this reason, we decided to test the commercial alumina and the alumina foams synthesised in this study in a hydrogen peroxide-assisted selective oxidation of benzyl alcohol as model compound to benzaldehyde, with a procedure described elsewhere.[25–27] The reactions were also tested against a blank in the sole presence of hydrogen peroxide in a parallel batch reactor. The mixtures were then analysed by GC for quantification and GC-MS for identification. The product of the reaction are given in Figure 6.10 and are benzaldehyde, methyl benzoate and an unknown of molecular weight of 213, signalling a similar molecule to methyl benzoate. The conversion and selectivities to the different products are given in Figure 6.11.

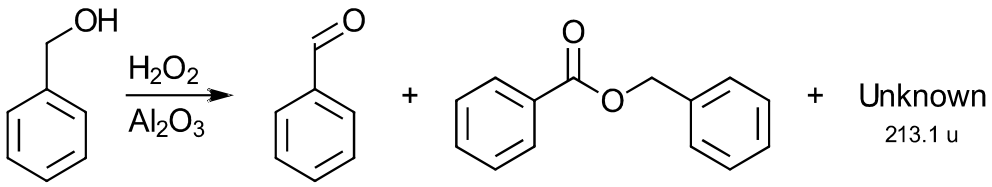

Figure 6.10 Scheme of the benzyl alcohol oxidation to benzaldehyde, methyl benzoate, and unknown by-product (in order).

The blank reaction already showed fair activity, with close to 90% of conversion, the selectivity to the desired product, benzaldehyde, was improved by both the commercial and foamed alumina. The alumina powder formed by attempting sol-gel deposition on a humins template showed a slight improvement of conversion (*ca.* 98%) but none in selectivity (*ca.* 40%) compared to the blank reaction. Both of the reactions also showed incomplete mass balances (*ca*. 90%) signalling the presence of non-volatile species.

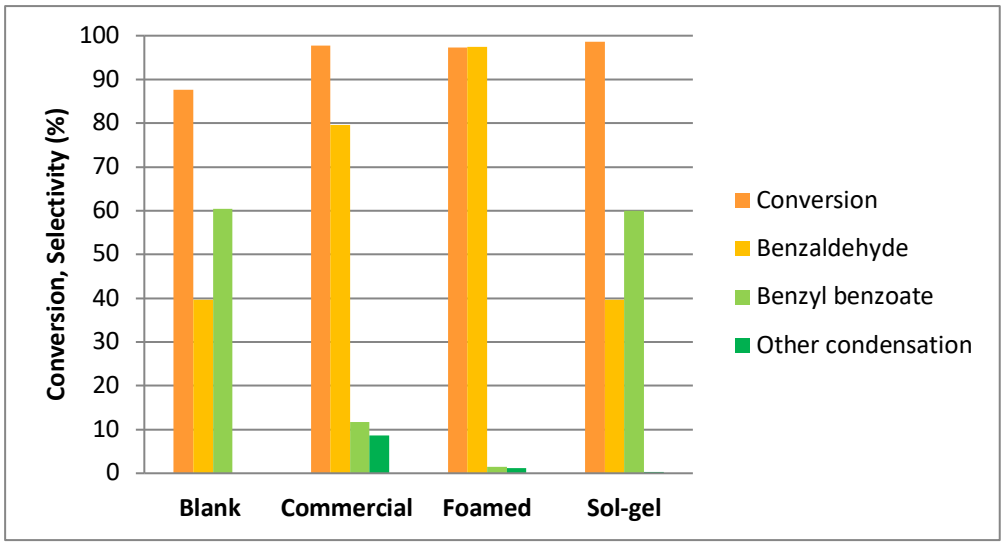

Figure 6.11 Conversion and product selectivities of the hydrogen peroxide-assisted oxidation of benzyl alcohol *i)* without a catalyst (blank), *ii)* with a commercial γ-Al_2O_3 nanopowder (commercial), *iii)* alumina foam prepared with humins as foaming-directing agent (foamed), and *iv)* alumina foam prepared with humins foams as template, acetic acid as peptization agent and 1000 °C calcination. *Reaction conditions*: 0.8 mL of benzyl alcohol, 1.2 mL of H_2O_2 50 wt. %, 8 mL of acetonitrile, 50 mg alumina catalyst, 80 °C, 1 hour.

Remarkably, the alumina foam prepared with humins as foaming agent showed a near-quantitative selectivity to benzaldehyde (*ca.* 97%), while the commercial gave a satisfactory 80% selectivity. This improvement in the catalytic performance could arise from the residual carbon species in a similar way as for the selective oxidation of allenyl compounds with humins-containing iron oxides.[14] The results of this study can thus become an incentive in the investigation of sustainable processes for the formation of inorganic foams for different

applications. In particular, the use of solventless conditions improved both the mechanical stability and catalytic activity of the formed material.

6.4 Conclusions

Concepts of sustainability and circular economy call for the valorisation of bio-derived humins to high added value applications. In this article, humins were employed as template or foam-directing agent in the preparation of inorganic foams, in particular alumina, that possess a variety of applications. Several approaches using aluminium isopropoxide sol-gels were tested. Unfortunately, all these experiment resulted expensive and long, while insufficient mechanical strength was obtained. On the other hand, the preparation of stable alumina foams was achieved with the use of humins as foam-directing agent, in a four steps protocol. As proof of concept, the as-synthesised foams were tested in the reaction of hydrogen peroxide-assisted oxidation of benzyl alcohol, along a commercial alumina sample. Noteworthy, the alumina foam prepared with humins as foam-directing agents showed a near-quantitative selectivity to benzaldehyde, proving the high applicability of the material in catalysis. In conclusion, using humins as foam-directing agents can allow the preparation of numerous inorganic foams with a new, fast, green and cost-efficient method.

6.5 Materials and methods

Humins were provided by Avantium Chemicals (Amsterdam, The Netherlands) and used as received. Nitric acid, aluminum isopropoxide (> 98%), alumina nanopowder (0.02 micron, nanopowder, γ-Al_2O_3) were purchased from Sigma-Aldrich; isopropanol (>99%) from Fisher Scientific; glacial acetic acid from Panreac Quimica SA. Isopropanol was further dried with the use of activated molecular sieves (3 Å, beads, 8-12 mesh, activated at 300 °C for 3.5 h) purchased from Acros. The humins foams employed in this study were synthesised with a procedure described elsewhere,[15,16] in particular at 250 °C (1 h isotherm and 10 °C min^{-1} ramp). All the humins foams employed in this study were activated to remove the fleeces in a 5 wt. % solution of nitric acid in a sonicator at 40 °C for 3 hours. The samples are then dried at 100 °C over night, and employed as obtained.

Humins foams as template

For the template/replica approach, sol-gels were prepared with aluminum isopropoxide [$Al(O_iPr)_3$] as precursor. In particular, 1.7 wt. % solutions of aluminum isopropoxide in dry isopropanol were prepared to which an excess of water is added (molar ratio Al isopropoxide to

water of 1:16) upon dissolution of the precursor at 60 °C and vigorous stirring. Once a clear and stable sol is formed, the stirring was stopped and the foams were added as is or with an alkaline pretreatment. When added as is, pore clogging was observed, thus the alkaline pretreatment was applied for the remaining studies. In particular, the foams were submersed under vacuum in an aqueous solution of NaOH (0.3 M) with pH 14 for 24 h, and then left drying at room temperature on an adsorbent material (*e.g.* paper). Once the excess of NaOH solution was dried, the humins foams were moved to the alumina sol. Then, either the solvent was evaporated at 80 °C until dry (typically 3 days), or the sol was used as dip-coating solution. In particular, the foams were submersed in the sol, removed and left dried at room temperature. This procedure was then repeated until either a 50 or 100% increase of the original foam weight was achieved (typically 3 and 6 times, respectively). The samples were then calcined (in air) up to 250 °C to check the distribution of the alumina on the foams, or to temperatures higher than 500 °C (500, 700 and 1000 °C) in order to remove the humins foams template. The calcinations had very slow ramp (1 °C min^{-1}) to the desired temperatures and 1-hour isotherms at 50 and 80 °C, and 4-hours isotherms at the calcination temperatures (*i.e.* 250, 500, 700 and 1000 °C) in order to have a slow evaporation of the solvent and decomposition of foams, thus allowing cross-linking of Al species and a slow release of volatiles that could disrupt the final foam.

Peptization of the alumina sol with acetic acid was also tested for the replica method, given its potential in reducing the temperature of formation of the stable ceramic α-Al_2O_3 as described in literature.[32,33] In particular, acetic acid was employed as hydrolysis agent of the aluminum isopropoxide in a molar ratio of organic solvent to acetic acid to Al isopropoxide at 40:3:1 at 90 °C until dissolution of the precursor and formation of a sol.[33] The dip-coating procedure previously described was then applied with the humins foams and calcined at high temperatures (700 and 1000 °C). Differently from the water-driven alumina sol, a procedure of 24-hours isotherms at 80, 120 and 150 °C was applied in order to slow down the solvent evaporation and the decomposition of the humins foams.

Humins as foam-directing agent

For the experiments where humins are used as foam-directing agents, the humins provided by Avantium and the commercial γ-Al_2O_3 nanopowder were employed. Mixtures of 9, 15, 25, 30, and 35 wt. % of alumina in humins were tested. In particular, 3 g of humins are heated to 90 °C on a stirring plate, and the alumina powder is added and allowed to stir until homogeneity of the slurry. The addition of water up to 15 wt. % was investigated to facilitate mixing, observing 5 wt.

% being enough. The mixture was then allowed to foam in a ventilated oven at the desired temperature (220 or 250 °C) with a 10 °C min^{-1} ramp and 1-hour isotherm. The formed carbon-containing foam was then heated under an inert atmosphere (i.e. N_2) at 900 °C to allow the formation of a strong composite. Finally, the carbon residues are removed at 600 °C in a ventilated oven (presence of air), leaving an inorganic foam.

Characterisation

Nitrogen physisorption measurements were carried out at 54 °C using an ASAP 2000 volumetric adsorption analyser from Micrometrics. Samples were degassed for 24 h at 130 °C under constant vacuum ($p < 10^{-2}$ Pa) prior to performing the measurements. Surface areas were calculated according to the BET equation, whereas average pores diameter and pores volume were obtained from the N_2 desorption branch.

X-ray Powder Diffraction (XRD) experiments were recorder on a Bruker D8 Discover diffractometer (40 kV, 40 mA), using CuKα (λ=0.15406 nm) radiation. Scans were performed over a 2θ range from 10 to 80, at step size of 0.05° with a counting time per step of 143.3 s.

Micrographs of the as-synthesised alumina foams were taken either with a normal photographic machine, a microscope or SEM-EDX. In particular, an Optika Lite microscope and Tescan Vega3 XM scanning electron microscope were used.

Catalytic testing and product analyses

The alumina foams prepared with acetic acid peptization and calcination at 1000 °C, and the foams prepared with humins as foam-directing agent were tested in the hydrogen peroxide-assisted oxidation of benzyl alcohol. A blank reaction (no catalyst) and a reaction with the commercial γ-Al_2O_3 nanopowder were also tested with the same protocol described in literature[33-35] but with larger volumes (10 mL instead of 2.5 mL). In particular, 0.8 mL of benzyl alcohol and 1.2 mL of H_2O_2 50 wt. % (2.3 equivalents) were added to 8 mL of acetonitrile for the blank reaction. For the catalysed reactions, 50 mg of the alumina nanopowder or crushed as-synthesised foams were added. The reactions were carried out in parallel in a Radleys® Carousel 12 Plus Reaction Station™ heated at 80 °C under stirring at 1000 rpm for 1 hour. The resulting solutions are then cooled down in an ice-bath and analysed by GC and GC-MS. In particular, GC analyses were run on an Agilent 7890A fitted with a Supelco column heated at 250 °C (5 min hold) from 50 °C with a 25 °C min^{-1} ramp, and to 300 °C (10 min hold) with a 20 °C min^{-1} ramp (25 min). GC-MS analyses were carried out on an Agilent 5977B MSD equipped with an HP-5 column. The

oven was set at 80 °C with a 3 °C min^{-1} ramp to 200 °C, a 10 °C min^{-1} ramp to 250 °C, and a 30 °C min^{-1} ramp to 280 °C (50 min).

6.6 References

[1] K. Kohli, R. Prajapati, B. K. Sharma, *Energies* **2019**, *12*, 233.

[2] L. Filiciotto, A. M. Balu, J. C. Van der Waal, R. Luque, *Catal. Today* **2018**, *302*, 2–15.

[3] K. E. Boulding, *Environmental Quality in a Growing Economy (H. Jarret Ed.)*, Resources For The Future/John Hopkins University Press, **1966**.

[4] Y. Wang, S. Agarwal, H. J. Heeres, *ACS Sustain. Chem. Eng.* **2017**, *5*, 469–480.

[5] S. Agarwal, D. van Es, H. J. Heeres, *J. Anal. Appl. Pyrolysis* **2017**, *123*, 134–143.

[6] Y. Wang, S. Agarwal, A. Kloekhorst, H. J. Heeres, *ChemSusChem* **2016**, *9*, 2016.

[7] T. M. C. Hoang, L. Lefferts, K. Seshan, *ChemSusChem* **2013**, *6*, 1651–1658.

[8] C. B. Rasrendra, M. Windt, Y. Wang, S. Adisasmito, I. G. B. N. Makertihartha, E. R. H. Van Eck, D. Meier, H. J. Heeres, *J. Anal. Appl. Pyrolysis* **2013**, *104*, 299–307.

[9] S. Kang, G. Zhang, Q. Yang, J. Tu, X. Guo, F. G. F. Qin, Y. Xu, *BioResources* **2016**, *11*, 9496–9505.

[10] S. G. Maerten, D. Voß, M. A. Liauw, J. Albert, *ChemistrySelect* **2017**, *24*, 7296–7302.

[11] A. Sangregorio, N. Guigo, J. C. Van Der Waal, N. Sbirrazzuoli, *Compos. Sci. Technol.* **2019**, *171*, 70–77.

[12] J. M. Pin, N. Guigo, A. Mija, L. Vincent, N. Sbirrazzuoli, J. C. Van Der Waal, E. De Jong, *ACS Sustain. Chem. Eng.* **2014**, *2*, 2182–2190.

[13] S. Kang, J. Fu, G. Zhang, W. Zhang, H. Yin, Y. Xu, *Polymers (Basel).* **2017**, *9*, 373.

[14] L. Filiciotto, A. M. Balu, A. A. Romero, E. Rodríguez-Castellón, J. C. van der Waal, R. Luque, *Green Chem.* **2017**, *19*, 4423–4434.

[15] P. Tosi, G. P. M. van Klink, A. Celzard, V. Fierro, L. Vincent, E. de Jong, A. Mija, *ChemSusChem* **2018**, *11*, 2797–2809.

[16] A. Mija, J. C. van der Waal, G. van Klink, E. de Jong, *Humins-Containing Foam*, **2016**, WO2017074183A8.

[17] S. Vijayan, P. Wilson, K. Prabhakaran, *J. Asian Ceram. Soc.* **2016**, *4*, 344–350.

[18] M. Takahashi, R. L. Menchavez, M. Fuji, H. Takegami, *J. Eur. Ceram. Soc.* **2009**, *29*, 823–828.

[19] J. Binner, H. Chang, R. Higginson, *J. Eur. Ceram. Soc.* **2009**, *29*, 837–842.

[20] W. Acchar, E. G. Ramalho, F. B. M. Souza, W. L. Torquato, V. P. Rodrigues, M. D. M. Innocentini, *J. Mater. Sci.* **2008**, *43*, 6556–6561.

[21] H. Haugen, J. Will, A. Köhler, U. Hopfner, J. Aigner, E. Wintermantel, *J. Eur. Ceram. Soc.*

2004, *24*, 661–668.

[22] A. A. Yaroshevsky, *Geochemistry Int.* **2006**, *44*, 48–55.

[23] X. Mao, *Recent Advances in Porous Ceramics (U. M. Basheer Al-Naib Ed.), Intech Open, Ch. 3*, **2017**.

[24] V. C. Colonetti, M. F. Sanches, V. C. de Souza, C. P. Fernandes, D. Hotza, M. G. N. Quadri, *Ceram. Int.* **2018**, *44*, 2436–2445.

[25] F. Mangin, P. Prinsen, A. Yepez, M. R. H. S. Gilani, G. Xu, C. Len, R. Luque, *Catal. Commun.* **2018**, *104*, 67–70.

[26] R. Hosseinpour, A. Pineda, M. Ojeda, A. Garcia, A. A. Romero, R. Luque, *Green Process. Synth.* **2014**, *3*, 133–139.

[27] A. Mariana Balu, A. Pineda, K. Yoshida, J. Manuel Campelo, P. L. Gai, R. Luque, A. Angel Romero, *Chem. Commun.* **2010**, *46*, 7825–7827.

[28] N. Yao, G. Xiong, Y. Zhang, M. He, W. Yang, *Catal. Today* **2001**, *68*, 97–109.

[29] B. E. Yoldas, *J. Mater. Sci.* **1975**, *49*, 1856–1860.

[30] M. Shayesteh, M. S. Afarani, A. Samimi, M. Khorram, *Trans. Phenom. Nano Micro Scales* **2013**, *1*, 45–52.

[31] B. Naik, N. Ghosh, *Recent Pat. Nanotechnol.* **2009**, *3*, 213–224.

[32] Y. Kobayashi, Y. Mabuchi, M. Hama, K. Inoue, Y. Yasuda, T. Morita, *J. Asian Ceram. Soc.* **2015**, *3*, 139–143.

[33] N. Bahlawane, *Thin Solid Films* **2001**, *396*, 126–130.

[34] P. Tosi, E. de Jong, A. Mija, in *ISGC2019 (The World Event Sustain. Chem. Res. Innov.*, La Rochelle, **2019**.

[35] S. H. Cai, S. N. Rashkeev, S. T. Pantelides, K. Sohlberg, *Phys. Rev. B - Condens. Matter Mater. Phys.* **2003**, *67*, 1–10.

[36] M. Trueba, S. P. Trasatti, *Eur. J. Inorg. Chem.* **2005**, *17*, 3393–3403.

[37] D. S. Maciver, H. H. Tobin, R. T. Barth, *J. Catal.* **1963**, *2*, 485–497.

7 Further valorisation routes - Appendix

7.1 Chapter content

In this chapter two further preliminary studies of industrial humins valorisation routes are reported.

Dye sensitized solar cells (DSSCs) using humins as dye have been prepared and characterized. Not only crude humins but also humins samples previously modified with maleic and succinic anhydride respectively have been employed, showing enhanced performances in DSSCs compared to the unmodified ones.

In addition, preliminary studies of preparation of all-green composite materials using humins with chitosan and in particular with lignin have been reported. Hard and compact materials were prepared by using compression moulding, while asphalt like materials were obtained by using a preparation in oven.

This chapter collects unpublished works that represent a starting point for further future researches. Herein, we prove that humins are an extremely versatile and promising material of which we just scraped the surface of all the possible applications and valorisation routes.

7.2 Humins as dye sensitizer for solar cells

7.2.1 Dye sensitized solar cells

Dye sensitized solar cells (DSSC), also know ad Grätzel cells,[1] are low-cost devices able to produce electricity through the conversion of light, in a process similar to photosynthesis.[2] This device is made up by two electrodes: the anode obtained by a porous nanocrystalline semiconductor in which a dye is adsorbed on the surface, and the counter electrode (cathode). An electrolytic solution is located between the two electrodes faces, while the dye has the key role of adsorbing photons and exchange electrons producing electrical energy.

This set-up was discovered in the late 60s.[3,4] The following researches focused in trying to overcoming the several issues of these first prototypes. The efficiency was increased with the optimization of the anode porosity by the preparation of thin oxide layers. Instead, the stability of these solar cells was a challenge non easy solved.[5] Nowadays, the DSSCs uses a porous layer of titanium dioxide nanoparticles on a transparent electrode (normal glass) with the opposite face made of fluoride-doped tin dioxide (SnO_2:F). This electrode works as anode, while a platinum-based catalyst on glass is used as cathode. A selected dye is adsorbed on the porous titanium dioxide layer, and an electrolytic (triiodide) solution is placed between the two electrode's faces. Light can be adsorbed by the dye molecules, which are excited. The electrons can be therefore release from the dye molecule and directly pass to the conduction band of TiO_2 layer, and so diffuse as effect of the electron concentration gradient to the anode above. Calling "D" a generic molecule of dye adsorbed on the titanium dioxide layer, this step can be schematized in the following way:

$$D + h\nu \rightarrow D^* \rightarrow D^+ + e^-$$

where $h\nu$ is the incident photon and D* represents the excited state of the dye molecule.

Through the anode the electrons flow *via* external circuit and are recollected at the cathode. Here it flow to the electrolytic solution with the oxidized red-ox mediator.

$$I_3^- + 2\ e^- \rightarrow 3\ I^-$$

The reduced I^- ions will close the cycle, transporting the electrons to the dye ionized molecules, refreshing their ability of adsorbing photons. 2 I^- ions will transfer their electrons to 2 D^+ molecules forming 2 elementary iodine I. These, reacting with another I^- ion, will regenerate the oxidized I_3^-, with the resulting balance:

$$3\ I^- + 2\ D^+ \rightarrow I_3^- + 2\ D$$

However, since the dye in the ionic form can quickly decompose depending on its stability, it needs to be reduced as fast as possible. Furthermore, the electrons arriving from the electrolyte are also faster than the recombination with the released electron, that would lead otherwise to a short-circuit of the DSSC.

Any kind of natural dye can be used in this application. For example, Tributsch and Calvin reported in 1971 the preliminary study of DSSC using chlorophyll extracted from spinach.[3] However, common lab experiments also involve the uses of concentred juice from red fruits (such as blueberry, strawberries or raspberries). Also natural pigments from plants, such as flower petals and leaves have been studied as easy and cheap available dyes for DSSCs.[6] Unfortunately, these dyes show low efficiency and extremely reduced life span, since they can be easily oxidized. In addition, natural dyes tend to easily degrade when exposed to UV radiations.

In terms of efficiency, the first dyes used during the 90s were mostly sensitive to the only high-frequency end of the solar spectrum.[7] Newer versions with higher frequency responses were introduced, such the triscarboxy-ruthenium terpyridine [Ru(4,4',4''-$(COOH)_3$-terpy)$(NCS)_3$]. Similar dyes were called “black dyes”, because of the dark colour due to the wider spectral response.[8] These complexed dyes can reach a theoretically efficiency as high as 90 %, meaning that theoretically they have the 90 % of chance of converting a photon into electron. Furthermore, these new dyes, unlike the natural derived pigments, proved an extremely high stability and life span. DSSCs build whit these dyes were subjected to 50 million cycles and they didn’t show any decreasing in performance. These corresponds to around 10 years of application by exposure to Switzerland sun.[8]

7.2.2 Humins and modified humins as solar cells dyes

In this optic we decided to test the humins as dyes in DSSCs preparation. Not only due to the dark-brown colour of the material, which offer wide adsorption in the spectrum, but also for the high stability and versatility of humins. Unlike common dyes, the humins show high thermal stability, which is positive for peculiar applications of DSSCs, being also stable to light. Not only unreacted humins were tested, but also 2 samples of humins previous subjected to chemical modifications by reaction with maleic anhydride or succinic anhydride (Figure 7.1).

Figure 7.1 Succinic and maleic anhydrides chemical structures.

According with the molecular structure analysis reported in the previous chapters, the humins bear several oxygen-based moieties. These can easily react with succinic anhydride toward esterification (Scheme 7.1), expecting to produce new covalent bonds and even crosslinking the humins oligomers.[9] However, must be highlighted that due to the complexity of the humins structure it is not easy to fully elucidate the final structure, and that succinic anhydride is easily hydrolysed in succinic acid in presence of water.

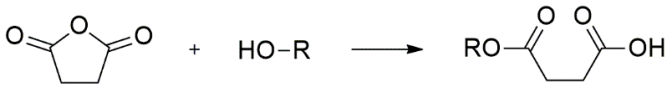

Scheme 7.1 Esterification between succinic anhydride and hydroxyl-groups.

In the case of maleic anhydride, the introduction of the double bond is expected to further increase the level of conjugation in the structure, already responsible of the dark colour associated to humins. Maleic anhydride could lead not only to the relative ester, which is the most expected reaction, but also to several possible side-reactions (Scheme 7.2). These, in agreement with the complexity and relative uncertainty around the humins structure, are far to be fully foregone.[10,11] As previously reported, the characterization of the humins structure is extremely complex to be achieved, as proved by the several decades spent in trying to characterize it. Therefore, despite we cannot fully characterize the final structures resulting from proposed reactions, the obtained results have the key role of prove of concept. The characterizations will focus on the effects of the humins modifications on the DSSC efficiency, and in the identification of a trend that could open a view to future investigations.

The reaction of humins with maleic and succinic anhydride were conducted following the protocols of 2018 from Mija *et al.*[12] reported in a patent dedicated to humins modification. Previous to the reactions, humins samples and the glassware were kept at 80 °C under high vacuum for 6 hours in order to remove as much water as possible.

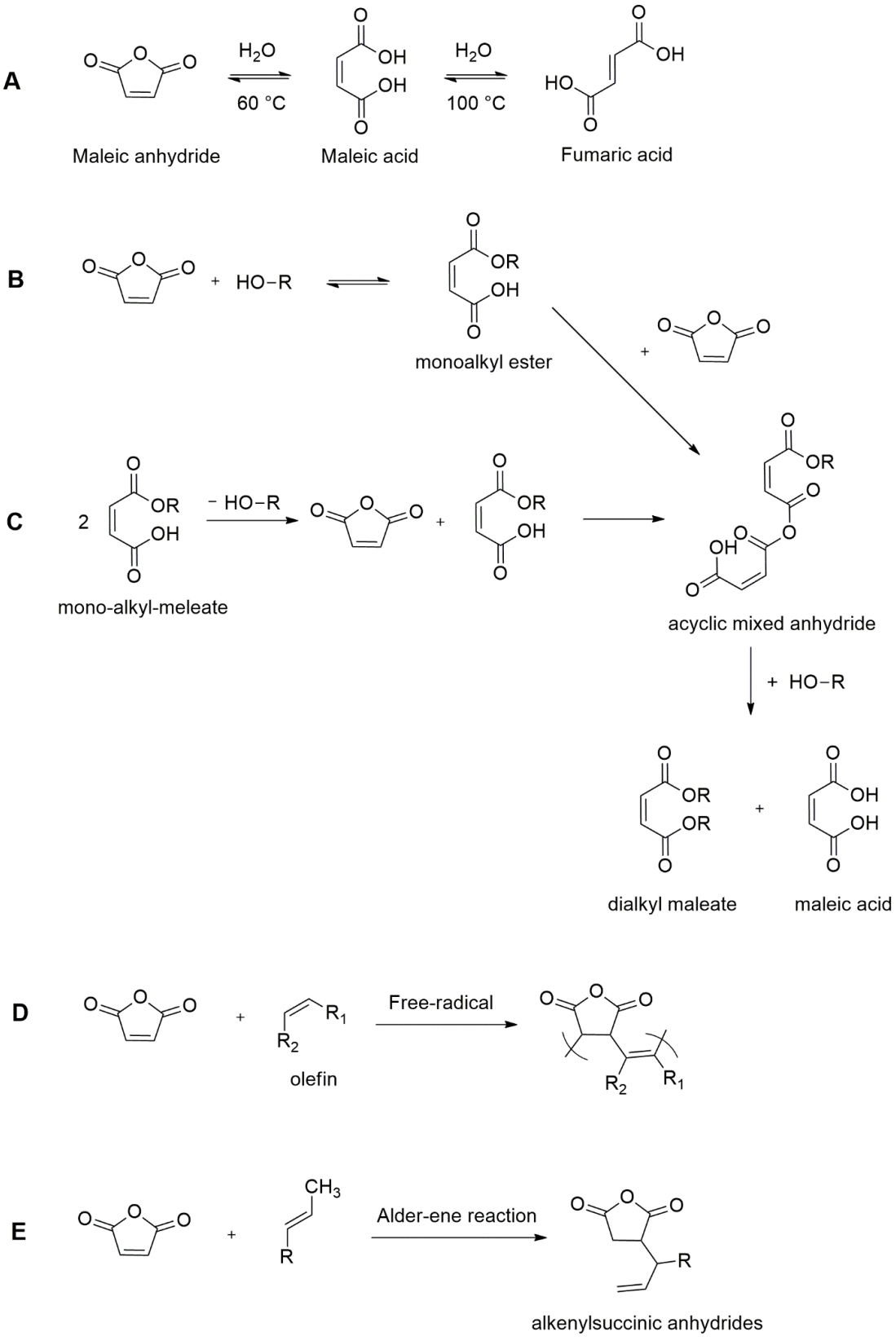

Scheme 7.2 Four possible reactions involving maleic anhydride. A) Hydrolysis in case of water contamination and isomerization to fumaric acid at 100 °C reflux; B) esterification in presence of alcohol; C) diesterification; D) polymerization with double-bonds in presence of radical initiator; Alder-ene reaction with an allylic hydrogen.[11,13,14]

7.2.3 Experimental preparation

7.2.3.1 Succinylated humins and maleated humins preparation

For this preparation it has been followed the protocols reported in 2018 from Mija *et al.*[12] 20 g of humins were placed in a round bottom flask equipped with condenser column and heated up at 90 °C. 2.2. g of 8 mL of anhydrous acetone (HPLC grade, ≥ 99.8 %) were added, and the mixture kept under reflux until the solubilization of humins was achieved (~ 1 hour). 2.2 g of succinic anhydride or maleic anhydride respectively were added, and the reflux continued for further 3 hours. Finally, the acetone was evaporated with rotavapor following by high vacuum pumping treatment.

7.2.3.2 Characterization of the modified humins

In order to have information about the modifications performed, the succinylated humins and maleated humins samples were analysed with FTIR using a Nicolet™ iS50 FTIR Spectrometer (range 4000-600 cm^{-1}, 32 scans, resolution 4 cm^{-1}, interval 2 cm^{-1}, r.t.) controlled by the program OMNIC and provided of attenuated total reflection (ATR) mode by Pike GladiATR. All the spectra were treated with baseline automatic correction and smoothing, and the results are reported in Figure 7.2.

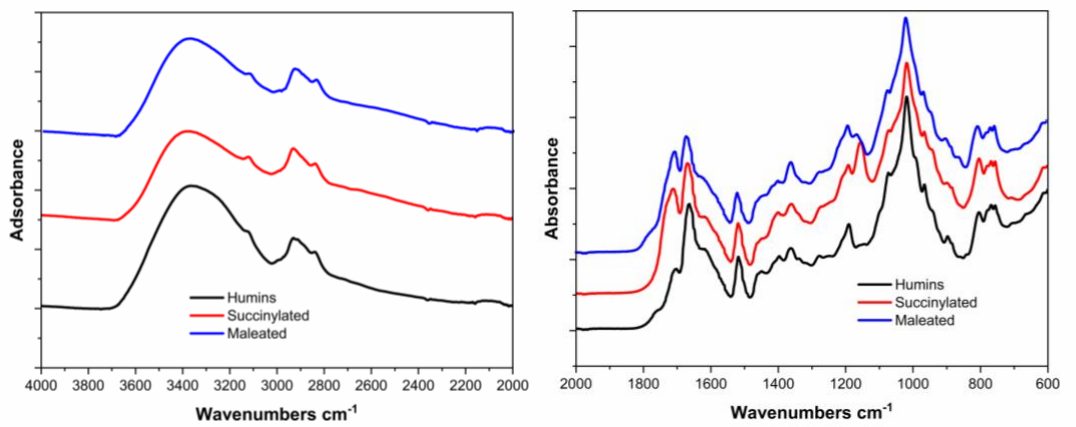

Figure 7.2 FT-IR analyses of crude humins (black line), succinylated humins (red line) and maleated humins (blue line) in the wavenumbers range 4000-600 cm^{-1}. On the left: zoom in the region 4000-2000 cm^{-1}; on the right: zoom in the region 2000-600 cm^{-1}.

The left side of the spectrum in which -OH groups can be found at 3350 cm^{-1} appears only slightly decreased in intensity after the reaction, along with the carbonyl moieties at 3117 and 2830 cm^{-1} (which were, indeed, not expected to change). This is perhaps due to the high number of hydroxyls present in the crude humins, which is probable that aren't reacted completely. We can therefore expect that only a small fraction of these groups were involved

in esterifications. On the other hand, changes can be found in the region between 2000-600 cm^{-1}. In particular it can be noticed that compared to crude humins, in succinylated and maleated humins spectra appears a strong peak at 1702 cm^{-1} that indicates the formation of esters. Furthermore, a new peak associated to C-O bond (esters and/or ethers) appears at 1155 cm^{-1} in both spectra, and is particularly intense in the succinylated humins one.

7.2.3.3 DSSC preparation

DSSCs were prepared using a commercial test kit from Solaronix with a TiO_2 electrode plate as anode and a Pt electrode as cathode, this last pierced in the canter. The anode used has a defined square porous spot of 6 x 6 mm with TiO_2 that was used to adsorb the solution of dye. The solutions of humins, succinylated humins and maleated-humins were prepared according to the following protocol: 0.55 g of sample was placed in a glass flask and heated up to 80 °C in order to decrease its viscosity. 5 mL of EtOH were added, and the mixture were stirred with a magnetic bar. The mixture was left on the heating plate for further 15 minutes, and then the flask sealed and vigorously shacked for several minutes.

In order to perform the adsorption of the sample solutions on TiO_2, the anode was placed in a watch glass with the TiO_2 layer facing the top. The humins solutions were poured on the anode until complete immersion, and left for 24 h. Afterwards, the electrode was washed with EtOH for removing the humins insoluble particles that could have been present, then partially dried out by softly tamponing with a piece of paper. Finally, the electrode was put in an oven at 80 °C under vacuum for 12 h in order to completely evaporate the solvent.

Along with the humins, succinylated humins and maleated humins deposed at the anode, other two electrodes were prepared: a white electrode and a reference, respectively. The white was prepared by performing the same adsorption protocol previously described but using only the solvent (EtOH). As reference it was used the commercial dye Ruthenizer 535-bisTBA (cis-diisothiocyanato-bis(2,2'-bipyridyl-4,4'-dicarboxylato) ruthenium(II) bis(tetrabutylammonium)), often reported in literature as N719 (Figure 7.3). Ruthenizer 535-bisTBA is a high-performance dye considerated one of the best ruthenium-based dye available for the sensitization of the titanium dioxide layer in DSSCs, and often used as standard benchmarking. It is an efficient sensitizer for a wide band-gap of oxide semiconductors like TiO_2, up to 750 nm.

The procedure of adsorption/staining on TiO_2 used in this case was followed according with the typical standard protocol reported by Solaronix.[15] A solution of Ruthenizer 535-bisTBA

(sold as powder) 0.5 mM in EtOH was prepared, and the anode was completely immersed in it for 3 h. The electrode was then washed several times with EtOH and the solvent completely evaporated for 24 hours under vacuum.

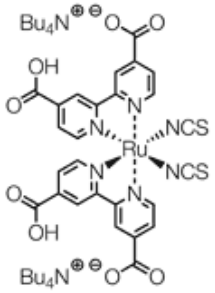

Figure 7.3 Ruthenizer 535-bisTBA

Once performed the adsorption, a gasket square mask was placed on the electrode, framing the TiO_2 spot. The counter electrode was placed on it, so that the drilled hole was fitting inside the gasket region. This sandwich-like fitting was put on a pre-heated heating plate (100 °C) for 10 minutes with a weight on it, so that a pressure was applied during the heating. This step allows the gasket to melt between cathode and anode, sealing the two electrodes but leaving the gap for the electrolyte solution.

The electrolytic solution was added through the cathode hole by using a special Vac'n'Fill Syringe from Solaronix. This syringe is necessary since the electrolytic solution must be injected through the pierced hole after the sealing with the gasket. The gap between the electrodes that must be filled is extremely limited, and the presence of air in it avoids the liquid to fully pass through. This syringe can create vacuum in the solar cell gap, and back-fill it with the electrolytic solution. The electrolytic solution used in these experiments is the Iodolyte AN-50, a ready-prepared solution based on the iodide/tri-iodide redox couple (50 mM) in acetonitrile and ionic liquid, lithium salt and pyridine derivative as additives. Once injected the electrolytic solution and the gap filled, a rectangular gasket was placed on the hole, and a glass cap placed on it. A metal plate preheated at 120 °C was placed on the cap and pressure applied, on order to melt the gasket between electrode and cap, thus sealing the hole. This prevented the electrolytic solution to evaporate. Finally, a test cell mask was applied. This mask is a black opaque adhesive that can be applied on the solar cell. It has a square-shaped opening of 8 x 8 mm that must be placed in correspondence of the TiO_2. The aim of the mask is hiding the non-active area from the light and compensate the optical loses.[16] The active area associated to this mask has been calculated as 0.36 cm^2.

Dimensions and scheme of the solar cell construction are reported below in Figure 7.4.

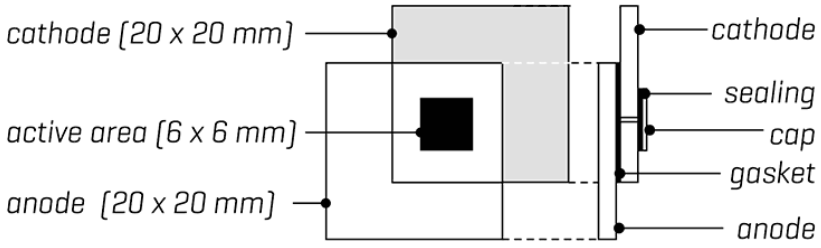

Figure 7.4 Building scheme and dimensions of the DSSC from Solaronix kit.

7.2.4 DSSCs tests: I-V curves and evaluation

In order to evaluate the performances of the previous prepared solar cells, the characteristic current-voltage (I-V) curve was plotted. This curve is acquired by applying a potential able to produce a current = 0, and then performing a screening of values manipulating the potential up to V = 0 while acquiring the I in each point. Since the power is defined by the product I x V, we can calculate the power of the solar cell for each point of potential applied.

When the solar cell is open-circuited, the current is zero while the voltage of the cell will be at is maximum. This value is known as open circuit voltage (Voc). On the other hand, when the solar cell is connected to a load (short-circuited), the voltage of the cell will be zero, but the current flowing out is at its maximum. This current is known as short circuit current (Isc). For all the voltages comprises between the short-circuit and the open-circuit conditions is possible to obtain power curves of the DSSC during illumination, associated to the kind and intensity of incident light considered.

Therefore, the I-V curve is built between V = Voc and V = 0, obtaining as two extremes of current I = 0 and I = Isc, respectively. Despite the maximum current can be achievable when the cell is short-circuited (Isc) and the maximum voltage when is open-circuited (Voc), none of these situation produces electrical power. The maximum power point (MPP) is located in a point between these two extremes and corresponds to the peak of the curve P-V (power in function of voltage, where P = I x V). At this particular condition the combination between current and voltage is set at values respectively called maximum power current (Imp) and maximum power voltage (Vmp). The ideal operational parameters for a DSSC is located in the MPP point, with Imp and Vmp as values. An example of I-V curve and relative parameters involved are reported below in Figure 7.5.

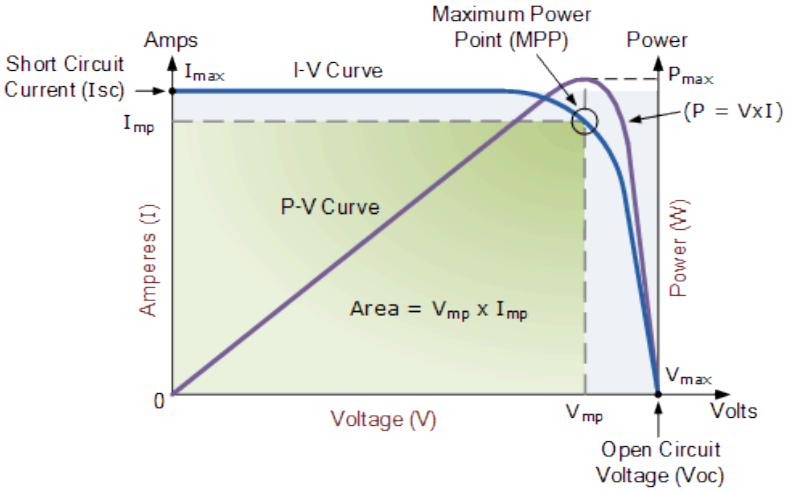

Figure 7.5 Example of I-V curve and parameters involved.

From the I-V curve it is also possible to calculate another parameter necessary to define the performance of the DSSC: the fill factor (FF).

The FF is a dimensionless value that can be associated to the quality of the array. The maximum theoretical FF of a solar cell can be calculated differentiating the power (I x V) of the solar cell with respect to the voltage, and imposing this = 0:

Equation 7.1

$$\frac{d(IV)}{dV} = 0$$

The full equation corresponds to:

Equation 7.2

$$Vmp = Voc - \frac{nkT}{q} \ln\left(\frac{Vmp}{nkT/q} + 1\right)$$

On the other hand, the empirical equation in order to calculate the FF is:

Equation 7.3

$$FF = \frac{\upsilon - \ln(\upsilon + 0.72)}{\upsilon + 1}$$

with υ corresponding to the equalized value of Voc, calculated as:

Equation 7.4

$$\upsilon = Voc \frac{q}{nkT}$$

Typical FF values found for commercial DSSCs are in the range 0.8-0.9. Closer is the FF to 1 and more power and array it provides.

These equations, since empirical, have some limitations. They show the maximum theoretical value that can be achieved from a solar cell, but since it ignores the parasitic resistive losses,

in an actual application test the FF values found will be lower. The FF can be calculated in a more practical and experimental way by the relationship between the area of the square that can be built outside the I-V curve (Voc x Isc) and the area of the biggest square that can be built inside the I-V curve (Vmp x Imp). A visual example can be found in Figure 6.12, with Voc x Isc corresponding to the blue square and Vmp x Imp corresponding to the green square. Higher is the "squareness" of the curve, closer the blue and the green areas will be, and thus their rapport will approach to 1.

FF can also be seen as the rapport between the maximum power that the device can provide under operation conditions and the Voc x Isc product. The FF value calculated in this way for commercial DSSCs is generally around 0.7-0.8, proving the differences between empirical and experimental calculations. However, these values can be even lower in case of self-built devices as those that we have used in these experiments, due to preparation flaws and materials.

Another value generally considered in order to describe a solar cell is the $\%_{eff}$. It represents the relationship between the maximum power that can be produced and the amount of irradiance (or photons) that hit the array. Depending on the type of the cell used, this value is generally calculated around 10-12% for commercial devices.

7.2.5 Experimental results

In order to acquire the I-V curves of our DSSCs it is first necessary to calculate the Voc. The DSSCs prepared with the 4 dyes (humins, succinylated humins, maleated humins, ruthenizer 535-bisTBA), along with the white, have been analysed using a Nova Autolab POTENTIOSTAT controlled by a software Nova 1.11, connected to the solar cells (Figure 7.6). The Voc values were calculated both under illumination and at dark, and the results are reported in Table 7.1 as absolute values.

Table 7.1 Open circuit voltage for dye sensitized solar cells built without dye (white sample) and with 4 different dyes. All the values are reported as absolute values.

Sample	Voc (Dark)	Voc (Light)	Gain
White	49 µV	113 µV	64 µV
Humins	3.62 mV	12.7 mV	9.08 mV
Succinylated-humins	1.26 mV	152.5 mV	151.24 mV
Maleated-humins	4.7 mV	113 mV	108.3 mV
Ruthenizer 535-bisTBA	4.2 mV	408.9 mV	404.7 mV

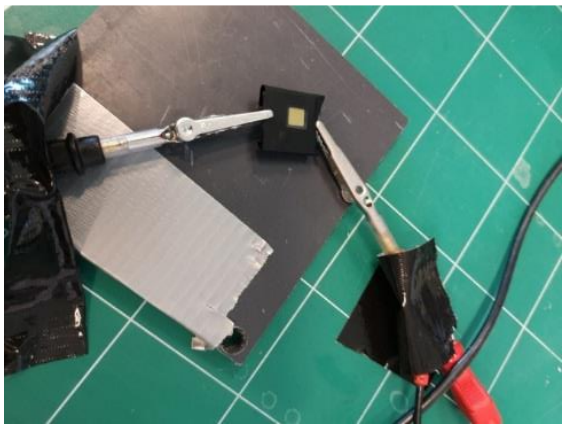

Figure 7.6 Experimental set-up.

The values of gain have been calculated as the differences between the Voc of the solar cells in conditions of dark and illumination. The illumination used was not given but natural sunlight but from artificial white light put at a fixed distance of 10 cm from the device. The presence of the reference is necessary to normalize the values accordingly. As it is possible to observe, the solar cell built with unmodified humins has the lower performances. Impressively, both the maleic and succinic modification of humins lead to a drastic increasing of the DSSC performance. What surprises is that, unlike the expectations, succinylated humins show higher Voc compared to maleated humins. The maleic-moiety, unlike the succinic one, was supposed to increase the optical absorbance of the whole structure thanks to the addition of conjugated double bounds, and therefore increase the spectral harvesting. This experiment was repeated several times, and the results confirmed. We can speculate that the succinic modification helps in some way the humins in their role of dye, participating in the stabilization of the ionic form or better helping the interactions with the molecular surrounding.

The values previous reported are necessary for the calculation of the FF and the building of the I-V curve for each device under illumination. The potential corresponding to the Voc (with a 0.01 V excess, in order to start the scanning) was applied to the solar cell, associated to a current flow ~ 0. Then, the potential was progressively manipulated (scan rate = 0.001 V) up to the voltage = 0, corresponding to the current = Isc. The values of current were plotted in function of the potential applied, and the results are shown in Figure 7.7.

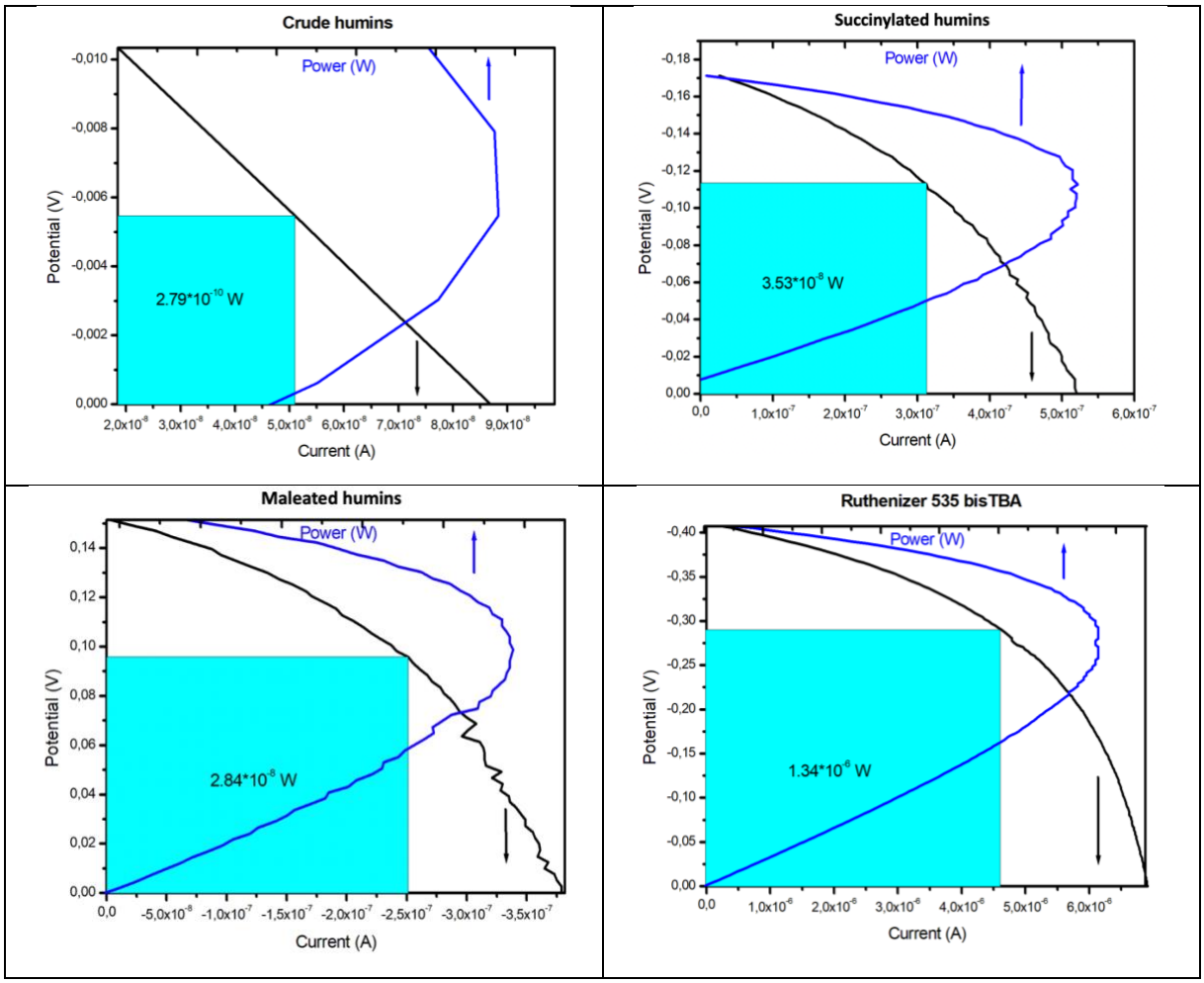

Figure 7.7 V-I curve for DSSCs using crude humins, succinylated humins, maleated humins and Ruthenizer 535-bisTBA as dyes.

As it is possible to notice from the previous V-I graphs, the "squareness" of our plottings are not comparable with the solar cells commercially available and tested in standard conditions, revealing the limits of the test cells used. Still, it is possible to observe that the lowest squareness is associated to crude humins sensitized cell, where the curve appears more like a line. Furthermore, due to the extremely low value of Voc associated to humins-derived DSSC, the scan did not allow to consider enough points. All these aspects confirmed that crude humins do not produce efficient solar cells. On the other hand, the squareness of the I-V curve is enhanced by the modification with maleic and succinic anhydrides, obtaining a shape comparable to the commercial dye.

A complete overview of the results is reported in Table 7.2.

Table 7.2 Values associated to the I-V curves of the DSSCs tested.

Sample	Isc (A)	Imp (A)	Vmp (V)	Isc*Voc (W)	Imp*Vmp (W)	FF
Humins	$4.6\ 10^{-8}$	$5.1\ 10^{-8}$	0.005	$5.8\ 10^{-10}$	$2.8\ 10^{-10}$	0.48
Succinylated-humins	$5.2\ 10^{-7}$	$3.1\ 10^{-7}$	0.11	$7.9\ 10^{-8}$	$3.5\ 10^{-8}$	0.45
Maleated-humins	$3.8\ 10^{-7}$	$2.5\ 10^{-7}$	0.096	$4.3\ 10^{-8}$	$2.8\ 10^{-8}$	0.65
Ruthenizer 535-bisTBA	$6.9\ 10^{-6}$	$4.6\ 10^{-6}$	0.29	$2.8\ 10^{-6}$	$1.3\ 10^{-6}$	0.46

As it is possible to observe from the reported values, all the FF are below the 0.5 with the only exception of the maleated modified humins one. The FF is associated to the quality of the solar cell and is strongly influenced from the building mode of the DSSCs (good injection of the electrolyte solution, good sealing of the gasket, parasitic resistive losses presence, …). We can compare the results for the different tested dye only in relation with the commercial reference (Ruthenizer 535-bisTBA). Repeating twice the preparation and the test for the maleated and succinylated humins DSSC we found the same values previous reported, which proves that the quality of the solar cells, and so the performances, correctly follow the observed trend and are influenced by the dyes used.

Despite the FF value results suggest a higher efficiency for the maleated humins derived DSSC, succinylated humins sensitized solar cell showed the best values in terms of yielded energy, with the higher current produced between all the humins-derived sample tested.

In conclusion, the modification of humins with succinic and maleic anhydride can produce efficient dyes for application in DSSCs, with performance that cannot be achieved by unreacted humins sample. This, along with the cost efficiency of the product, its stability and the interest around its valorisation, can be the key step to invest in further investigations. Despite the Voc values are not comparable with those obtained with the commercial ruthenium-based dye, the values are higher than expected. However, since only 2 modifications on the humins chemical structures were performed, we cannot trace a full

interpretation about the reason that pushed the performances of these devices, as observed with maleated and succinylated derived humins.

Considering this as a bare promising preliminary test, broad margins of optimization are expected.

7.4 Humins in preparation of all-green composites

7.4.1 The humins thermosets challenges

As reported in the previous chapters, humins have an inner thermoset nature that can be used for delivering materials. When heated up at a temperature above ~ 180 °C the material undergoes a series of reactions involving crosslinking.[17] This process is irreversible, and lead to the production of a solid rigid structure. However, due to their furanic content, alike every furanic thermoset, the resulting materials tend to be fragile and with poor mechanical strength. When this thermosetting is performed on a crude humins sample, due to secondary effects such us viscosity reduction and gas evolving through degradation/releasing of volatiles, the resulting material became porous (humins foam).[17–19]

Increasing the mechanical properties of the bare humins derived materials represents an important route in the process of valorisation up to the actual commercialization of such products. In order to do so, we should investigate strategies that allow the control over the foaming process and the mechanical properties of humins.

Avoiding or reducing the foaming would lead to a denser and more compact thermoset. Furthermore, such strategy can allow the uses of humins as resin without any additive. Such behaviour has been observed for humins heated up in a tube oven under N_2 flux, using a ramp of 1 °C·min^{-1}. This protocol was tested in the Chapter 5 about humins foams properties, when the foaming and the carbonization were tested in a one-step direct strategy. However, this product leaded to no porosity, a result opposed to what we were looking for. For example, applying as protocol the heating up of humins from r.t. to 900 °C at 1 °C·min^{-1} under N_2 it was possible to produce thick and dense monoliths (Figure 7.8) with high C %, which resulted in consequence also able to conduct electricity (how confirmed with observation of open circuit current by conductivity tester). However, during the carbonization, due to the poor elasticity of the material, in combination with the shrinking effect, it tended to break apart during the process. Therefore, no actual monoliths were produced, but mostly fragments of them. However, for the purposes of the that study, we were looking for humins foams rather than

flat materials preparation. Therefore, a two steps strategy based on the foaming at 250 °C followed by the carbonization at higher temperatures was found more appropriate for that experience. This allowed the preparation of humins foams, and afterwards their carbonization adopting the heating ramps of 1 °C·min^{-1}. Must be highlighted that, unlike the carbonized humins monoliths, humins foams did not break during the carbonization, perhaps due to the higher three-dimensional freedom.

Figure 7.8 Carbon-based conducting material with no porosity produced with a carbonization of crude humins at 900 °C using 1 °C·min^{-1} ramp.

If we want to develop new strong materials all the previous mentioned experiences and issues must be faced and overcame. We need to consider both the foaming control (in order to keep the material compact) and the material density that can increase the strength of the products. We need also to overcome the shrinking trend that provoke to breaking of the structure. Therefore, a strategy integrating strengthen humins a has been applied. In the optic of the "all green", the first strengthened selected molecule was the chitosan.

6.4.2 Humins-chitosan composites preparation

Chitosan is a natural derived randomly distributed polysaccharide. It is made up D-glucosamine (deacetylated) and N-acetyl-D-glucosamine (acetylated) bonded by β-(1→4)-link. It can be obtained by subjecting chitin from crustaceans' shells (generally shrimps) to deacetylation with alkaline treatments (Figure 7.9). The research around this material is growing, not only because of the interesting properties that chitosan shows but also because it is obtained as waste from the food industry and is one of the main sources of surface pollution in coastal areas.[20–24] Humins-chitosan, as composites, would be completely derived from by-products, in a full green chemistry design. Must be noticed that the chitosan is insoluble in water. However, humins display this double polar/apolar nature, due to the presence of both aliphatic/aromatic structures and polar species, and it is the ideal candidate to establish interactions with chitosan. Furthermore, it is possible to produce covalent bonds

between the humins hydroxyl and the amino group of chitosan, resulting in an enhancing of physical properties. Finally, the presence of amino-group increases the possibility to produce electrical-conductive materials.

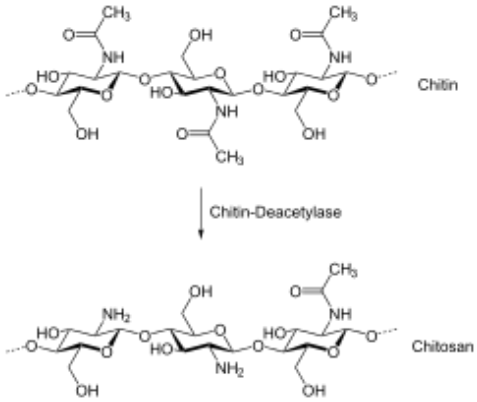

Figure 7.9 Chitosan production by partial deacetylation of chitin from crustaceans.

Chitosan from shrimp shells used in this preparation was purchased by Sigma-Aldrich (≥ 75 %, deacetylated). A preliminary test was conducted mixing humins and chitosan (15 and 20 % wt.). Around 25 g of humins were placed in an alumina crucible and heated up at 80 °C. 2 mL of water were added in order to further reduce the viscosity. 15 and 20 % wt. of chitosan were added, and the mixture kept at 100 °C for 1 hour in order to remove the excess of water. Afterwards, the highly-viscous mixture was transferred in dog-bone stamps, applying pressure on them in order to fully fill the stamp cavity. A slight excess of material was applied, so to be able to produce pressure once compressed with the mould.

The compression moulding plates were pre-heated at 220 °C. Afterwards, the samples were placed between the plates and pressure applied (around 3 tons·m^{-2}). The samples were left reacting for 1 hour, then the moulds opened and the samples slowly cooled down to room temperature.

During the moulding, part of humins flows away from the stamp, no matter of the pressure applied. This is due both to the rising of pressure due of the gas releasing from the humins, and from the reduction of viscosity due to the temperature. Because of this, an inferior amount of sample was found in the stamp. Furthermore, the shrinking effect of humins leads to samples which dimensions do not match perfectly the stamps one. In most of the experiments the sample was found broken in the narrow dog-bone part, that can be explained by a shrinking occurred after the hardening of the material, which forced the sample on the stamp walls leading to breaking (Figure 7.10). However, the material obtained resulted hard

and with an unexpected porosity due to the gas evolving (Figure 7.11), which is useful to prepare lighter materials.

The few samples fully formed were recovered and analysed with shore test, using a shore D (applied for the materials with the maximum hardness). In a scale 0-100 the samples resulted of hardness 72-82, which falls in the range classified as “extra hard materials”. This range is associated to the harder materials that can be produced. This result can be related to the hardness of the humins cross-linked resin, with a further influence of the chitosan which woks as hardener and stabilize the structure as scaffold. Chitosan increases the resistance of the bare humins thermosets, which tend to be quite fragile. Unfortunately, every attempt of realize a pure-humins dog-bone sample to use as “white reference” was impossible to achieve, since by increasing the temperature the viscosity decreases so much that the material completely flows away. Therefore, we can also observe that the presence of the chitosan as hardener increases the viscosity and the compactness of the crude material, making possible the process of preparation. However, only 2 samples were recovered intact out of 12 preparation attempts. This did not allow us to further investigate the mechanical properties of this composites. Must be highlight that this problem is only associated to the dog-bone shape, due to the presence of a narrowing. This issue can be overcome simply using a rectangular shaped stamp, or any other shapes that do not obstacle the shrinking effect while it is occurring.

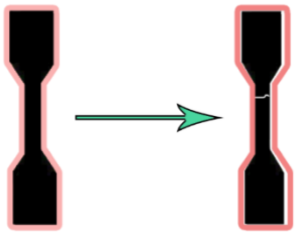

Figure 7.10 Visual example of the dog-bone sample of humins-chitosan, before and after curing. The curing, was accompanied by material flowing, gas evolving, shrinking and often breaking of the material.

Figure 7.11 Dog-bone sample of humins-chitosan (85-15%).

6.4.3 Humins-lignin composites

Despite the promising results with chitosan, we chosen to focus our effort on the preparation of another kind of composite, which composition would fulfil the lignocellulosic biomass valorisation cycle using only bioproducts of the process. During the acid-digestion step in which the cellulose and hemicellulose part of lignocellulosic biomass are depolymerised, lignin is produced as bioproduct. Lignin represents more than 25 % of the dry matter of the whole biomass, but it is still not fully exploited and currently its applications are mainly limited to energy recovery by burning. Several have been the studies trying to use and valorise this bio-derived material[25,26] (comprised the production of additive for asphalt or lignin based foams).[27,28]

Lignin represents the largest renewable resource of aromatic compounds available in nature, and its uses in new materials composition are extremely important for environmental and industrial point of views. Using lignin, exploiting its peculiar molecular structures and properties, along with the recovering/valorisation aspect that would help the whole CO_2 balance, it will meet both the ecologic and economic demand. This, merged with humins valorisation, is of great environmental and industrial interest.

For this experiment, 3 different kinds of lignin have been used: two commercially available, and one produced by Avantium.

Kraft lignin and lignosulfonate lignin were purchased by Sigma Aldrich and used as received. The same preparation previous used for humins-chitosan composites was followed. This time, samples up to 45 % wt. of lignin were prepared, since the stirring was easier to achieve, while the addition of few mL of water dramatically increased the ease of the process. The viscosity, in every case, was too low, up to be considerate a problem since once heated up the mixture tends to flow away from the stamp. Despite the several attempts, not a single sample was

fully recovered, and all the experiment failed. The few samples that were partially formed were found to be extremely fragile and friable, eve more than materials derived by pure humins (such as humins foams). Furthermore, when lignosulfonate lignin was used, the recovered residuals had a strong cabbage-like smell. We tested also the curing in disposable aluminium tray in air ventilated oven, with the same protocol used for the preparation of F250 foams. Foams were indeed produced, but their mechanical properties were even poorer than those obtained with only humins. Therefore, according with these results, the addition of lignin has a negative impact on the preparation and mechanical properties of a material so built.

On the other hand, astonishingly good results were achieved when lignin produced from Avantium (by acid treatments) was used. The material obtained with curing at temperatures between 180-250 °C was not only compact and resistant, but also reproducible. During the curing, a limited amount of the humins fraction flowed away from the stamps. This is due mainly to the viscosity reduction and to the instrumental set-up, but it did not affect the quality of the material. Samples with lignin up to 40 % wt. were produced. Noteworthy, the 35-45 % wt. lignin samples appeared wood-like in the look, but lighter. This was called “black-wood” (Figure 7.12), and can be the starting point to produce an interesting and completely green material without the use of any additive.

Figure 7.12 Humins-lignin (40 % wt.) composites – Black Wood.

With DSC analyses we calculated that the T_g midpoint of humins-thermoset prepared at 220 °C passes from 77 °C to 113 °C when 20 % lignin in added in the composition. Furthermore, according with shore tests, as well as observed in humins-chitosan composite samples, humins-lignin composites are in the range that characterizes the extra-hard materials. The results are reported in Table 7.3.

Table 7.3 Shore tests for several humins-lignin compositions using D-shore (over 3 repetitions). Extra hard materials are identified above the value of 60.

Preparation T (°C)	Lignin (%)	Shore D results
180	30	76-79
180	35	86-83
180	40	70-79
180	45	71-73
220	30	79-85
220	35	70-79
220	40	63-69
250	30	80-84
250	35	69-75
250	40	62-67

As reported in Table 7.3, the hardness of the material seems directly linked to the temperature of curing and the amount of lignin. The differences between the samples are relatively small, considering that the values range between 60 and 85 in the D-shore range. This can be associated or to a structural change in the lignin fraction during the curing process, or to an increasing of bonding between humins and lignin. The slightly decreasing of hardness by increasing the amount of lignin can also be associated to the partial increasing of elasticity, since the lignin fraction became more and more important in the composition.

Pushed by the promising results obtained in the preparation of composites with compression moulding, also the simple curing of humins-lignin mixture in air ventilate oven was tested. Several compositions, between 20 and 40 % lignin were prepared, and the samples “foamed” at 220 °C. However, no a foam was produced, but a compact coralline structure asphalt-like, extremely tough and resistant (Figure 7.13).

Figure 7.13 Asphalt-like material obtained by humins-lignin (75-25 %) composite.

Must be highlight that an interesting phenomenon occurred by stirring humins with this industrial lignin. Indeed, after the stirring, the mixture become hard sandy-stone like. When the mixtures were moved from the heating plate, and cooled down, it became tough and hard.

Still, was possible to manipulate the mixture and shape it. In the case of low lignin content, part of humins tended to foam by themselves, forming a sort of fragile separate layer on the top (~ 20 % wt. of the humins used). This layer is obtained by the bare humins that separated during the heating process due to the reduction of viscosity, that allows the lignin fraction to partially move toward the bottom. This layer, therefore, free from the lignin fraction, foams. Once recovered the sample it was possible to easily break this part, finding a compact and tough asphalt like material on the bottom, in which however the lignin concentration increased because of the phases separation. This phenomenon was observed for every composition with less than 30-35 % lignin, while above this amount the foaming process was completely absent. Therefore, the lignin controls the foaming and stabilize the mixture during the process, and this is a great advantage in the preparation of similar materials.

In terms of chemical interaction, covalent bonds between lignin and humins can easily be expected, due to the high amount of hydroxyl groups in lignin. This, along polar interactions between the two fractions, can assure a good interaction between them.

A possible reason that explains why this process works for industrial lignin and does not work for commercial ones is that the result is not only due to the chemical bonding, but also and mainly from impregnation. Indeed, the Avanium lignin are produced in the plant as block, residue of the biomass treatment, and are subsequently mechanically grinded, yielding a thicker powder with bigger particle dimensions. At this point, it is possible that the powder works as adsorbent for humins, being fortified while humins glue the several fractions together. In other words, it is a sort of lignin soaking in humins. Therefore, there is a combination of factors that allow to keep the final material structure denser and more compact, and that justify the mechanical resistance transferred from lignin to the humins-based mixture. As prove of concept, Avantium lignin used in the successful experiment was further grinded until extremely small particles were produced. By repeating the previous tests, but using this extra-grinded lignin, the preparation failed and no sample was successful recovered.

As it is possible to observe in the SEM pictures in Figure 7.14, by using bigger lignin particles in the preparation, humins-lignin (70-30 %) mixture tends to form this extremely thick sandy-like material, hard and resistant to break. The humins appeared to be completely adsorbed by the lignin particles, which however glued and stuck together. This confirms the high affinity between the humins and the lignin phases.

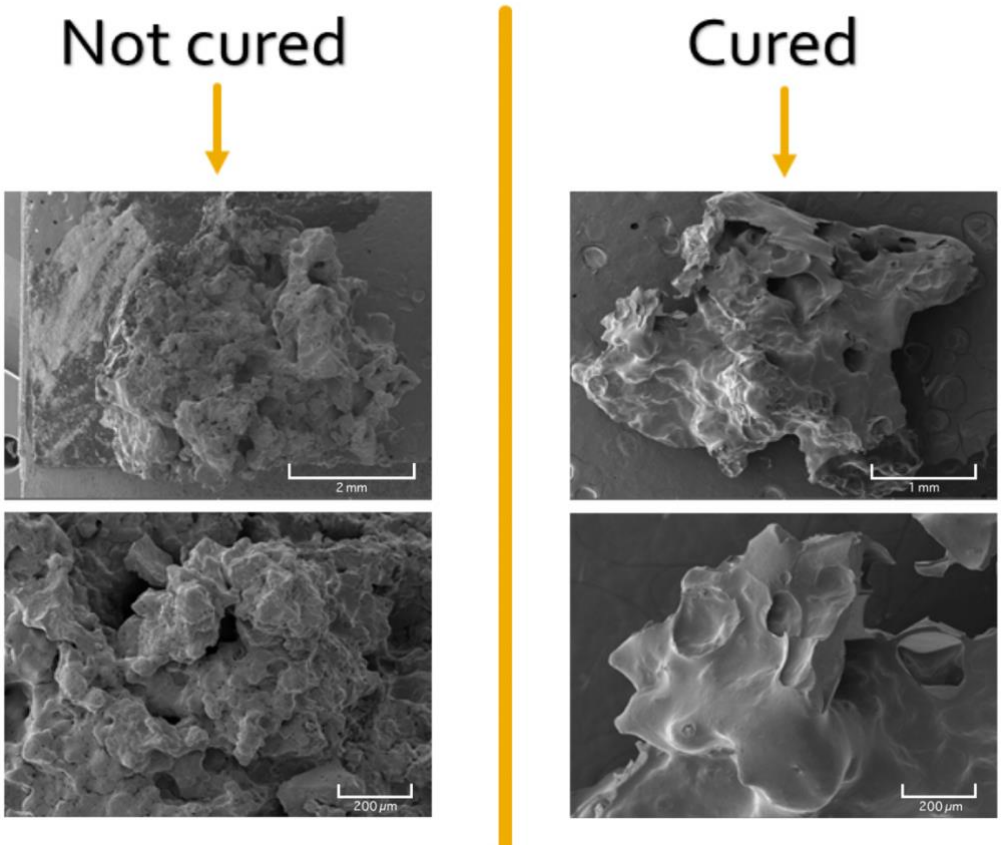

Figure 7.14 Humins-lignin (70-30 %) mixtures before and after curing at 220 °C.

Once the humins-lignin mixture is cured, it is not possible to detect anymore the presence of lignin, since completely surrounded by the humins thermoset. During the treatment it is expected an expansion in dimensions of humins, as it would be expected in foams preparation. However, in this case the humins are impregnated in the lignin, so the effect is like a humins-thermoset shield covering the particles and forming flattered surfaces. When these particles are in contact together in the mixture, the humins will behave like a binder. On the other hand, the lignin structural resistance is intact in the bulk, and transferred to the system.

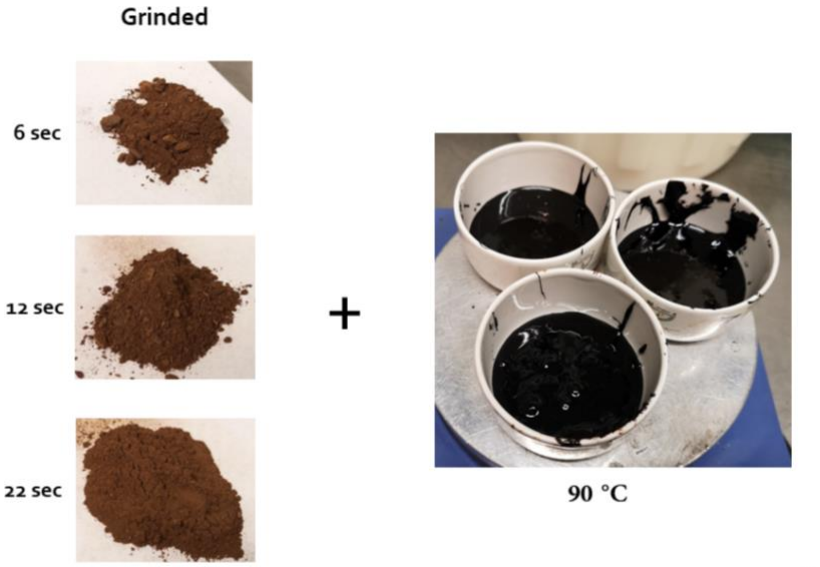

Figure 7.15 Mixing of lignin at different grinding times with humins.

In order to test the effect of grinding on the lignin in the final composite, three lignin blocks from Avantium have been subjected to mechanical grinding for 6, 12 and 22 seconds respectively (Figure 7.15). Longer is the grinding time, smaller the particles dimensions are. However, even the lignin grinded for 22 seconds were bigger in dimensions than those commercially available. Calling “big”, “medium” and “small” the particle dimensions of lignin grinded for 6, 12 and 22 seconds respectively, three series of three different samples were prepared. The first series was obtained by using the “big” lignin particles, the second by using the “medium” and the third by using the “small” ones. The samples of the series were prepared by using 10, 20 and 30 % of lignin in the final composition. Finally, the curing process was performed at 220 °C. The obtained samples are shown in Figure 7.16.

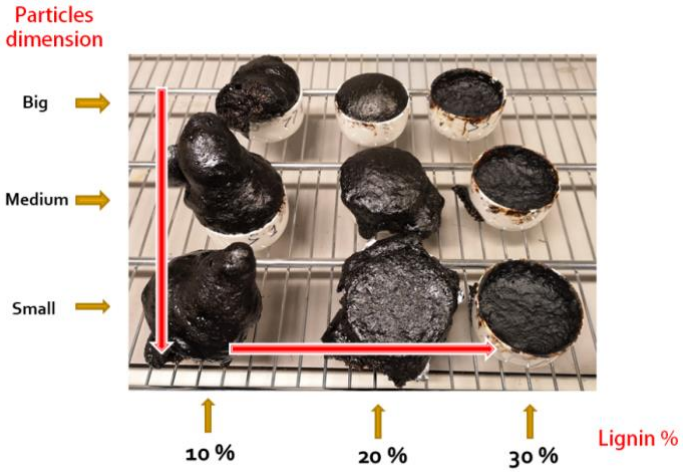

Figure 7.16 Humins-lignin composites prepared at 220 °C with different compositions and lignin granulometry.

It is possible to define a trend in the foaming control, and so in the density of the composites in function of the lignin amount and granulometry. Increasing the grinding time, so decreasing the particle dimensions, it results in an enhancing of the foam capacity compared with the commercial lignin. On the other hand, increasing the % of lignin in the composition yields more stable and denser structures, giving the possibility to control the foaming process. As expected, the foamed samples can be crushed, finding a more compacted material in the bottom side of the crucible. On the other hand, by using 30 % of lignin it was possible to obtain a completely compacted material in its entireness. Therefore, in terms of i) yields, ii) control over the preparation and iii) process economy, the use of high lignin amount is suggested.
Must be highlighted the importance of similar materials, not only in terms of valorisation of two by-products from the same spinneret, but also for the cheapness of the process and the complete absence of additives.

7.7 Conclusions

In this chapter we reported studies explored at a preliminary stage. In the first part we reported the preparation and characterization of Dye Sensitised Solar Cells (DSSCs) where humins were employed as dyes. In doing so, also modified humins obtained by reactions with succinic and maleic anhydride, respectively, were performed. Despite the reactions here used required optimization, a major level of control and deeper structural characterization of the products, these produced more efficient dyes for solar cells compared to the unmodified humins. Maleated humins-derived DSSC had the best fill factor, while the higher energy yielded with the higher current produced was achieved by using succinylated humins. The results obtained are not comparable with commercial ruthenium-based dyes, but as a preliminary study show high margins of improvement. The results are good enough to justify an economical evaluation, considering the cost effectiveness of the humins and their valorisation aims. On the other hand, investigating the correlation between the actual structural changes and enhancement of performance could bring a major consciousness about the kind of reactions and conditions to involve in similar dyes preparation. Unfortunately, due to the complex kind of mixture and extremely heterogeneous nature of humins, along with the limited amount of time available for this study, it was not possible to fully investigate the final chemical structure actually obtained. On the other hand, despite several decades of

study, humins structure itself is still under investigation, and this highlight the high level of complexity in this material characterization.

Also composites preparation of humins involving other biobased components were investigated. Chitosan was used as strengthened of the humins thermoset resin, achieving an interesting compact material. However, due to preparation problems mainly involving shrinking effects, the materials were not easily recovered from the stamps after the compression moulding preparations. Lignin-humins composites were more thoughtfully studied, considering also the major economic interest around them since both are side-products from biorefinery. A compact strong material similar to wood was prepared by using the compression moulding (180-150 °C), while a tough porous asphalt-like material was obtained by thermal treatment in oven (220 °C). We also highlighted the strong interaction between humins and lignin, not necessarily involving covalent bonding. The best results were obtained by using not commercial lignin, but lignin produced from Avantium process, and this could be the effect of the particle size used. Indeed, we hypothesized that humins have an impregnation effect on lignin, working as particles binder. On the other side, lignin allows a major control over the foaming process, keeping the mixture compact and, in some cases, completely avoiding the foaming.

These two valorisation routes can be used as starting point for future studies, giving a guideline. Furthermore, this proves the extreme versatility of humins, highlighting the fact that, up to know, we are just scratching the surface of all the possibilities that humins offer.

7.6 References

[1] Technology Academy Finland, *Professor Grätzel Wins the 2010 Millennium Technology Grand Prize for Dye-Sensitized Solar Cells*, **n.d.**

[2] H. Gerischer, M. E. Michel-Beyerle, F. Rebentrost, H. Tributsch, *Electrochim. Acta* **1968**, *13*, 1509–1515.

[3] H. Tributsch, M. Calvin, *Photochem. Photobiol.* **1971**, 95–112.

[4] H. Tributsch, *Photochem. Photobiol.* **n.d.**, 261–9.

[5] M. Matsumura, S. Matsudaira, H. Tsubomura, M. Takata, H. Yanagida, *Ind. Eng. Chem. Prod. Res. Dev.* **1980**, *19*, 415–421.

[6] M. R. Narayan, *Renew. Sustain. Energy Rev.* **2012**, *16*, 208–215.

[7] J. Gong, J. Liang, K. Sumathy, *Renew. Sustain. Energy Rev.* **2012**, *16*, 5848–5860.

[8] R. Katoh, A. Furube, M. Kasuya, N. Fuke, N. Koide, L. Han, *J. Mater. Chem.* **2007**, *17*, 3190–3196.

[9] R. G. Huber, M. A. Margreiter, J. E. Fuchs, S. Von Grafenstein, C. S. Tautermann, K. R. Liedl, T. Fox, *J. Chem. Inf. Model.* **2014**, *54*, 1371–1379.

[10] M. A. Farhan, H. B. Dheyab, A. A. Hasan, *Eur. J. Pharm. Med. Res.* **2017**, *4*, 84–90.

[11] O. M. Musa, *Handbook of Maleic Anhydride Based Materials: Syntheses, Properties and Applications*, **2016**.

[12] A. Mija, J. C. van der Waal, E. de Jong, G. P. M. van Klink, *Process for the Modification of Humins*, **2018**.

[13] J. M. Gess, D. S. Rende, *Tappi J.* **2005**, *4*, 25–30.

[14] J. J. Harrison, W. R. Ruhe Jr., *One-Step Process For The Preparation of Alkenyl Succinic Anhydride*, **1943**, U.S. Patent No. 5,319,030.

[15] Solaronix, "Ruthenizer 535-bisTBA," **n.d.**

[16] Solaronix, "Test Cell Mask - Correlation Between Mask Aperture and Efficiency," **n.d.**

[17] P. Tosi, G. P. M. Van Klink, A. Celzard, V. Fierro, L. Vincent, E. De Jong, A. Mija, P. Tosi, G. P. M. Van Klink, A. Celzard, et al., *ChemSusChem* **2018**, 2797–2809.

[18] A. Mija, E. de Jong, J. C. van der Waal, G. van Klink, *Humins Containing Foam*, **2017**, WO 2017074183 A1 20170504.

[19] A. Muralidhara, P. Tosi, A. Mija, N. Sbirrazzuoli, C. Len, V. Engelen, E. de Jong, G. Marlair, *ACS Sustain. Chem. Eng.* **2018**, 16692–16701.

[20] M. Rinaudo, *Prog. Polym. Sci.* **2006**, *31*, 603–632.

[21] C. K. S. Pillai, W. Paul, C. P. Sharma, *Prog. Polym. Sci.* **2009**, *34*, 641–678.

[22] M. N. R. Kumar, *React. Funct. Polym.* **2000**, *46*, 1–27.

[23] M. N. V. R. Kumar, R. A. A. Muzzarelli, C. Muzzarelli, H. Sashiwa, A. J. Domb, *Chem. Rev.* **2004**, *104*, 6017–6084.

[24] M. SV, M. HW., *Biomaterials* **1999**, *20*, 1133–1142.

[25] E. A. B. da Silva, M. Zabkova, J. D. Araújo, C. A. Cateto, M. F. Barreiro, M. N. Belgacem, A. E. Rodrigues, *Chem. Eng. Res. Des.* **2009**, *87*, 1276–1292.

[26] M. Alekhina, O. Ershova, A. Ebert, S. Heikkinen, H. Sixta, *Ind. Crops Prod.* **2015**, *66*, 220–228.

[27] I. John, S. Batchelder, S. S. Crump, *Asphalt Emulsion-Conditioner*, **1981**, U.S. Patent No 4,293,459.

[28] G. Tondi, M. Link, C. Kolbitsch, J. Gavino, P. Luckeneder, A. Petutschnigg, R. Herchl, C. Van Doorslaer, *BioResources* **2016**, *11*, 2972–2986.

8 Conclusions and perspectives

Toward the valorization of humins

The world's growing population, the improvement of living standard along with the increasing requirement of energy and materials are pushing the demand of natural resources utilization to its boundary. On the other, in line with the Paris agreement, the increasing of the industrial production can no longer be accompanied with the increasing of CO_2 emissions. In this optic renewable resources are gathering more and more interest over the non-renewable fossil ones.

Lignocellulosic biomass, in particular, is one of the most important renewable resource that is currently being exploited and studied. For instance, 5-hydroxymethylfurfural is a platform chemical that can be produced by the acid catalysed dehydration of sugars derived from lignocellulosic biomass digestion. It can be converted into furandicarboxylic acid, which is a bioderived replacement for the terephthalic acid currently used in the production of plastics (PET). By using the products of 5-hydroxymethylfurfural it is possible to obtain a completely bioderived plastic (PEF) with enhanced properties. Just considering the replacing of PET with PEF in the plastic bottle industry the reduction of the greenhouse gasses was estimated to 45 - 55 %.

However, one of the most challenging steps in this route is the production of furanic compounds and derivatives *via* acid catalysed dehydration of sugars. Within this step several by-products are formed, and in particular humins. Humins, the protagonists of this manuscript, are a heterogeneous mixture of oligomers derived by random condensation between the several compounds present in the acid catalysed media. In order to optimize the entire industrial process, to decrease the loss in mass and lower the production prices, applications and valorisations for humins must be investigated.

Hence, the work presented in this thesis focused on humins and humins-derived materials, trying to enhance the knowledge around these industrial side-products, highlighting their point of strength, characterizing them and directing the research toward valid valorisation routes. Giving to humins new life and commercial value will be not only an important achievement from the environmental point of view, but will push also the entire Biorefinery

chain in the competition against the “conventional” commercial chemicals derived from fossil resources.

For several decades the research focused on trying to avoid the humins formation. However, as reported in the review in Chapter 2, currently this route has not given successful results. Despite some studies found lab-scale conditions that optimized the products yields and reduced the humins formation, from an industrial-scale perspective the humins remain a constant outcome. However, as this thesis testifies, the idea of humins as unwanted by-products that requires all our efforts to avoid their formation, is almost dissolved in favour of an actual interest in their unique properties. Today several researches are conducted highlighting how we can take advance of them, in a change of focused that reminds the lignin history. We are part of this change. Of course still boundaries remain. The uncertainness around the humins chemical structures, their variability in accordance to the reaction conditions and feedstock/catalysts/solvents used, along with the complex characterization of humins and their derivatives (still under investigation), can be a limit for their commercialization. For this reason we focused our efforts in humins-derived materials that require a minimum manipulation and variables as possible. Humins foams are one of these example. Humins foams are rigid carbon-based porous materials that can be produced starting from industrial crude humins in an easy, straightforward and cost effective way. In order to prepare these materials, humins do not require any kind of pre-treatments, and the material is the same as it is collected from the industrial plant. The preparation process of humins foams only requires, depending to the properties expected, thermal treatments. Firstly, we focused the research on trying to fully identify the mechanism that lead to these outcomes. We found that the foaming process is the result of a combination of three effects: the decreasing of viscosity below 125 °C, the gas evolving above 150 °C and finally the thermosetting due to the auto-crosslinking reactions above 175 °C. All these effect are intrinsic properties of the crude humins, and can be exploited. Controlling parameters such as thermal ramp, crucible material, amount of humins or gas flow, it is possible to select the kind of porosity desired (pore size, pore opening, gradients) the carbon content and the chemical properties of the surface. We were able to reach up to around 95 % of carbon content for humins foams carbonized at 900 °C under N_2, corresponding to an almost pure carbon material fully able to conduct electricity. These materials can find applications in several fields, such as electrical devices or electrodes. For instance, they could find applications as sacrificial

electrodes, which are generally made of cheap materials in order to prevent more expensive electrode materials to corrode. Furthermore, as reported in Chapter 5, we found that using an heating ramp of 1 °C/min it was possible to completely avoid the pore formation, which can be useful if compact structural materials for electrical parts are desired. By controlling the temperature of preparation it was also possible to control the chemistry of the surface of the material. We reached a pH of zero point charge up to 2 for foams preparations between 180 °C and 300 °C, which could be further investigated in the field of decontamination and catalysts support. Furthermore, by studying the stability of the material, we found that is extremely stable when prepared at temperatures above 250 °C, with no solubility detected in the solvents tested, boiling water comprises, and a quite high thermal stability. This, associated to the thermal hazard study reported in Chapter 4 that for the first time investigated humins and humins foams safety parameters (such as ignitability, flammability, or combustible behaviour) is a valid information to justify further studies on direct crosslinking of humins. Indeed, all the results here obtained and reported can be extended on every kind of materials prepared from humins using direct crosslinking by thermal treatments. This will be especially useful in evaluating the stability limits and safety aspects regarding these materials, selecting the more adequate reaction conditions.

On the other hands further investigations are required, especially in extending the material mechanical strength. Humins foams are rigid and fragile, which is the main problem that could limit many applications. In Chapter 5 we also reported the preparation of activated carbon from humins foams, even achieving the production of monoliths. Activated carbon monoliths have the advantage, compared to the conventional powdery form, to be easier to recover and reuse. On the other hand, these are quite fragile. However, since the BET area calculated for these materials are comparable with activated carbon commercially available, and that these results are way better of those obtained for other studies of activated carbon preparation from industrial humins, this would justify their commercialization supported by further optimization of the preparation parameters. For the limited amount of time these monoliths were not tested in applications such as water decontamination or CO_2 capture, and would be interesting in future to compare their activities with those of activated carbon commercially available.

The best application currently found for humins foams involves the CO_2 capture at realistic operative temperatures (25-100 °C) reported in Chapter 5 and the direct sacrificial templating

reported in Chapter 6. For the CO_2 capture the results are not only comparable with those obtained for commercial materials, but also further optimizable. The future research should take these successful result into account, and further investigate it. On the other hand, the sacrificial templating is extremely promising and gave wonderful results. We tested this preparation for alumina, but it should be tested for more inorganic porous material preparation, perhaps in the preparation of further heterogeneous catalysts. The easiness and cost effectiveness of this preparation is, again, the major interesting point of their uses if compared with the current used methodologies.

Finally, in the Chapter 7 we reported two further studies that we didn't have time to fully investigate. The use of crude humins as dye is not interesting from a commercial point of view, especially if compared with the efficiency of the commercial dyes currently used. However, impressively, the modification of humins with maleic acid and succinic acid led to the increasing of the efficiency. Despite the activity is still lower than commercial metal-based dyes, similar humins-based dyes are extremely cheaper and safer to handle. The reason of this increased activity must be investigated in the chemical structure and in a structure/reactivity study. Unfortunately, since the chemical structure of crude humins itself is still under investigation, and that the characterization of humins and humins-derived materials is extremely hard due to the high variability, heterogeneity and complexity of the structure, such study was not fully conducted for a matter of time. It will be interesting to study the actual chemical structure associated with other modifications, trying to understand what is the reason that yield such effect. In future would be possible to target the humins modifications in order to optimize these effects. Still, unlikely it will be possible to reach the efficiency of commercial metal-based dyes, but humins-dyes could be interesting for cheap devices. More pragmatic is the uses of humins in the preparations of materials. Unlike high-tech applications, a large amount of humins would be used, with a better economic advances for the biorefinery.

In Chapter 7 we reported the preparation of several humins-based composites. Again, the aim was to find a preparation methodology as linear and direct as possible, avoiding the use of harsh chemicals or additives. Since the main problem of humins thermosets is the fragility, we used strengthen materials. In particular, we have chosen bio-derived side-products as strengthens, such as chitosan (by-product from food industry) and lignin (by-product from lignocellulosic biomass). The humins-chitosan composites were not fully investigated due to preparation problems. Indeed, due to the shrinking effect of humins during the crosslinking,

and from the narrowing of the dogbone stamps, the composites tended to break during the cooling. However, the materials recovered was promising, hard and compact, and even porous in some conditions, which is useful in order to reduce the material weight. Therefore, we expect further studies coupling chitosan and humins, by using different stamps (e.g. parallelepipeds) that allow the humins to shrink without break, and so to be able to test their mechanical properties.

However, from a practical and economical point of view, humins-lignin composites were more interesting and deserved to be studied. Indeed, both the materials derive as side-products from Biorefinery. The results are really promising, but for matter of time we could not investigate the mechanical properties of these materials, and this will be an indispensable information for further investigations. However, despite the compression moulding preparation of humins-lignin composites is promising in terms of applications, the composites prepared by curing in oven should be investigated with deep attention. This preparation lead to asphalt like materials with impressive strength, while the preparation protocol is easy, cheap and fast. The material is hard and compact, and wasn't easy to break neither by hammering it. It could be the starting point for the production of new concrete. Furthermore, depending on the relative amount of lignin used, it was possible also to create porosity, which would be interesting for many applications (such as surfaces subjected to rain or water spilling). Furthermore, based on the information here collected, we already know the chemical stability, thermal stability and safety properties of humins thermosets, information that can be used to tailor these material properties. This implies also further investigation on the composition, and the evaluation of crosslinking initiators or copolymers in order to further optimize the materials properties. Noteworthy, unlike pure humins thermosets that wan not possible to produce independently from the condition and methodology used, the strengthen gives stability to the humins resins and controls its foaming/flowing behaviour. Therefore, testing also other side-products in similar composite preparation could identify further promising partners, creating a library of materials based on humins side-products.

In conclusion, the research around humins applications is only at its start. The studies reported in this thesis must be collocated in a wider scenario. We hope that these results will be used in future for further investigations, as indication and guideline, and eventually led to the effective commercialisation of this side-product, for the sake and the success of the Biorefinery and, therefore, of our future society.

Acknowledgements

First of all, I would like to thank my thesis director Prof. Alice Mija for this amazing experience. She selected me for this project among many applicants, and I feel like this changed my life. It was an honor to work with her. I still remember the first congresses together, how I realized that it was really a friendship-like experience, and how I have felt so lucky.

Thanks also to Guy Marlair, Rafael Luque, Alina Balu, Nicolas Sbirrazzuoli, Nathanael Guigo and Johannes DeVries that, as HUGS partners, I had the honor to know and work with.

A special thanks to all the HUGS students, flat mates and friends Anna, Anitha, Layla and Fatima, the so called “HUGS angels” (cit. Jan Kees). We had so much good time together, and definitely so many experiences shared in so little time that is hard to believe. I can not wait to continue our misadventures together.

Thanks to Ed de Jong that as co-director helped me so much during the period spent in Avantium, and to Gerard van Klink for all the heads up about the laboratory work. Thanks to all the Avantium people. I will miss our lunch together, the jokes, the parties, the meetings and the laboratory life. I have loved so much working with you that I did not feel like working at all. Thanks to Carlo, Mat, Irene, Timothy, Eeles, Ilona, Annelie, Koen, Stefan, Merande, Quiona, Marian, Pablo, Andre and all the others (you are so many that It is impossible not to forgot someone). A special thanks to Jorge (now known as George) for all the crazy things that we did together and to Erica for all the support. Thanks to Jean Kees for all the good time and for the things that you unknowingly taught me. I will never forget our dance in La Rochelle.

Thanks to Alain Celzard and Vanessa Fierro for hosting me for a month in their laboratory, for all the help and all the time invested in me. And thanks to Philippe Gadonneix for all the technical help, without him I would have been lost.

Thanks also to Claire Lomenech and Charlotte Hurel for all the help and for allowing me to use their equipment!

Thanks also to all the amazing people from the University of Nice that made this experience unique. Thanks to Roxana, Chiara, Luna, Chavi, Cristina and Erol for the support and all the coffee, and thanks to Emilie, Charlotte, Angela, Marie, Emilie, Benjamin, Rime and all the others for the good time!

Thanks to all the new friends that I met during the PhD, Giorgia, Andrea, Francesco, Aurora, Elvira, Ilaria, Giuseppe, Enrico, Marco, Francesca, Valentina, Marco, Sofia e Matteo.

Thanks to all my old friend, Ciccio, Alessio, Lucio, Giampaolo, Rossella, Alessandra, Ogni, Alessio, Guido, Teresa, Isa, Erica, Karen and all the others that are still here. With most of you have been more than twenty years. We have grown, hopefully, but never got old.

Thanks to Valentina, that supported me from the start of this journey. You have changed and grow up with me. It was a nice trip, and I feel that this is also your achievement. I will always feel in debt with you.

Thanks to all my cousins and family that have followed me during these intense years.

Thanks to Claudia for all the laughs and the adventure dreams, the blind dives in this future. I can read this thesis back and remember what we were writing each other. You arrived in a dark period and made it sunny.

Grazie a chi non c'è più. Questa tesi è dedicata a nonno Gigi, che è stato sempre orgoglioso di me e sono certo che sempre lo sarà. Se avesse partecipato alla seduta di dottorato avrebbe decisamente capito poco, ma inevitabilmente avrebbe pianto.

E per ultimo, ma non per importanza, voglio ringraziare i miei genitori e mio fratello. Tutto ciò che sono lo devo a loro. Loro che non mi hanno mai fatto pressioni, che mi hanno supportato durante tutta la vita e mi hanno permesso di studiare senza mai farmi pesare un singolo minuto di ritardo. Io, e questa tesi, non saremmo qui se non fosse per voi.